DOKUZ EYLÜL UNIVERSITY

GRADUATE SCHOOL OF NATURAL AND APPLIED SCIENCES

ASSESSMENT OF THE FLUCTUATIONS OF GROUNDWATER STORAGE THROUGH GIS AND REMOTE SENSING METHODS

by

Behnam KHORRAMI

February, 2022

İZMİR

ASSESSMENT OF THE FLUCTUATIONS OF GROUNDWATER STORAGE THROUGH GIS AND REMOTE SENSING METHODS

A thesis submitted to the
Graduate School of Natural and Applied Sciences of Dokuz Eylül University
In Partial Fulfillment of The Requirements for The Degree of Doctor of Philosophy in Geographic Information Systems (GIS) Program

by

Behnam KHORRAMI

February, 2022

İZMİR

Ph.D. THESIS EXAMINATION RESULT FORM

We have read the thesis entitled "**ASSESSMENT OF THE FLUCTUATIONS OF GROUNDWATER STORAGE THROUGH GIS AND REMOTE SENSING METHODS**" completed by **Behnam KHORRAMI** under supervision of **Prof. Dr. Okan FISTIKOĞLU** and **Prof. Dr. Orhan GÜNDÜZ** and we certify that in our opinion it is fully adequate, in scope and quality, as a thesis for the degree of Doctor of Philosophy.

Prof.Dr. Okan FISTIKOĞLU Supervisor	Prof.Dr. Orhan GÜNDÜZ Co-Supervisor
Prof. Dr. Celalettin ŞİMŞEK Thesis Committee member	Assoc.Prof.Dr. Cem KINCAI Thesis Committee member
Prof. Dr. Gökmen TAYFUR Examining Committee membe	Assoc.Prof.Dr. Ebru ERİŞ Examining Committee member

Assoc.Prof.Dr. Ali GÜL
Examining Committee member

Prof.Dr.Okan FISTIKOĞLU
Director
Graduate School of Natural
and Applied Sciences

ACKNOWLEDGMENT

I would like to express my sincerest appreciation to my dear advisors; Prof. Dr. Okan FISTIKOĞLU and Prof. Dr. Orhan GÜNDÜZ, for their cooperative engagement through all the phases of my thesis project especially dear Prof. Gündüz who has played a predominant role in the successful termination of this project with his tangible support, constructive contribution and guidance throughout the work.

I am also thankful to the reverent members of the thesis advisory committee, Prof. Dr. Celalettin ŞİMŞEK and Assoc. Prof. Dr. Cem KINCAL, who supported my thesis work with their fruitful and constructive comments and suggestions.

This work was implemented and reported its findings based on the data used from a variety of data sources. I would like to express my gratitude to these agencies for providing free-access to their datasets, some of which are listed as follows:

- The National Aeronautics And Space Administration (NASA) of the United States of America remotely sensed and modeled data from GRACE, GLDAS, FLDAS and MODIS space missions.
- The European Union's Earth observation Programme (Copernicus) for simulated and reanalysis data of hydro-meteorological variables.
- The Swiss Federal Institute for Forest, Snow and Landscape Research (WSL) for the high-resolution climatic variables from Climatologies at high resolution for the earth’s land surface areas (CHELSA) mission.
- The State Hydraulic Works (SHW) and the Turkish State Meteorological Service (TSMS) for their cooperation and support by providing us with the required in-situ datasets.

I also would like to thank the Presidency for Turks Abroad and Related Communities (YTB) office for backing me up in every term either fiscally or spiritually during my Ph.D. years in Turkey.

Last but most, special thanks certainly appertain to my beloved family members especially my parents for their uninterrupted support both fiscally and spiritually without which I would not be able to cope with the hardships and challenges I encountered during my PhD studies in Turkey.

Behnam Khorrami

ASSESSMENT OF THE FLUCTUATIONS OF GROUNDWATER STORAGE THROUGH GIS AND REMOTE SENSING METHODS

ABSTRACT

Water resources in Turkey are of vital importance for the sustainable development of the country. Particularly, the groundwater aquifers make a great contribution to this development by providing the required water for different agricultural, domestic and industrial purposes. Exact country-wise monitoring of the variations of water resources is one of the priorities of Turkey. The Gravity Recovery And Climate Experiment (GRACE) mission facilitated the large-scale surveillance of groundwater storage (GWS) at regional to global scales. In this study, the spatio-temporal fluctuations of the GRACE-observed terrestrial water storage (TWS) and groundwater storage (GWS) were investigated through integrating the GRACE-derived values with the modeled data from the FLDAS, GLDAS and WGHM hydrological models. The results revealed that both the TWS and GWS manifest declining trends from 2003 to 2020. The GRACE-derived terrestrial and groundwater storages of Turkey turned out to be depleted by the annual rates of 5.16 km^3/yr and 4.02 km^3/yr, respectively which correspond to about 92.83 km3 and 72.34 km^3 of total depletion of TWS and GWS during the last 18 years. The study findings also suggest that the spatio-temporal fluctuations of these parameters agree with the fluctuations of the extreme hydrological events with more evident associations between the experienced droughts in 2007, 2008, 2014 and 2018 to 2020. In the light of the findings of this study, it seems like that there is a significant terrestrial water loss over Turkey during the specified period and more than half of this occurs in the groundwater storage component.

Keywords: GIS, GLDAS, GRACE, GWS, Remote Sensing, TWS, Turkey

YERALTISUYU DEPOLAMASINDAKİ DEĞİŞİMLERİN CBS VE UZAKTAN ALGILAMA METOTLARI İLE DEĞERLENDİRİLMESİ

ÖZ

Türkiye'deki su kaynakları, ülkenin sürdürülebilir kalkınması için hayati önem taşımaktadır. Özellikle yeraltı suyu akiferleri, farklı tarımsal, evsel ve endüstriyel amaçlar için gerekli suyu sağlayarak bu gelişmeye büyük katkıda bulunmaktadır. Su kaynaklarının değişiminin ülke bazında tam olarak izlenmesi Türkiye'nin en mühim önceliklerinden biridir. Gravity Recovery And Climate Experiment (GRACE) misyonu, bölgesel ve küresel ölçeklerde yeraltı suyu depolamasının (GWS) büyük ölçekli gözetimini kolaylaştırmıştır. Bu çalışmada, GRACE ile gözlemlenen karasal su depolaması (TWS) ve yeraltı suyu depolaması (GWS) değerlerinin mekansal-zamansal değişimleri, FLDAS, GLDAS ve WGHM hidrolojik modellerinden cıkartılan değerlerle entegre edilerek incelenmiştir. Sonuçlar hem TWS'nin hem de GWS'nin 2003'ten 2020'ye kadar düşüş eğilimleri gösterdiğini ortaya koymaktadır. Sonuçlara göre Türkiye'nin GRACE kaynaklı karasal ve yeraltı suyu depoları sırasıyla yıllık 5,16 km^3/yıl ve 4,02 km^3/yıl oranında azaldığı ortaya çıkmaktadır. Yaşanan yıllık düşüşler 18 yılda toplam yaklaşık 92.83 km^3 ve 72.34 km^3 değerine karşılık gelmektedir. Çalışma bulguları ayrıca, bu parametrelerin mekânsal-zamansal değişimlerinin aşırı hidrolojik olayların değişimleri ile uyumlu olduğunu ve 2007, 2008, 2014 ve 2018-2020 yıllarında yaşanan kuraklıklar ile de daha belirgin ilişkiler içinde olduğunu göstermektedir. Bu çalışma, belirtilen çalışma periyodunda Türkiye üzerinde önemli bir karasal su kaybı olduğunu ve bunun yarısından fazlasının yeraltı suyu depolaması bileşeninde gerçekleştiğini göstermektedir.

Anahtar kelimeler: CBS, GLDAS, GRACE, GWS, Uzaktan Algılama, TWS, Türkiye

CONTENT

Page

Ph.D. THESIS EXAMINATION RESULT FORM ii

ACKNOWLEDGMENT ii

ABSTRACT v

ÖZ vi

LIST OF FIGURES xii

LIST OF TABLES xvi

ABBREVIATIONS xvii

CHAPTER 1-INTRODUCTION 1

1.1 Motivation 1

1.2 Objectives of the study 6

1.3 Scope of the Study 7

CHAPTER 2- LITERATURE REVIEW 8

2.1 Terrestrial Water Storage 8

2.2 Groundwater Storage 10

2.3 Groundwater Monitoring Approaches 12

2.4 Hydrological applications of the GRACE estimates 14

2.5 The GRACE-based monitoring of groundwater storage 16

2.6 Downscaling of the GRACE data 18

CHAPTER 3-METHODOLOGY 22

3.1 Remote Sensing Data 22

3.1.1 GRACE/GRACE-FO 22

3.1.1.1The Basic Theory of the GRACE 22

3.1.1.2 The GRACE processing Solutions 26

3.1.2 MODIS 30

3.1.3 Hydroclimatic Models 32

3.1.3.1 GLDAS model 33

3.1.3.1.1 Noah Model 34

3.1.3.1.2 CLSM Model 34

3.1.3.2 FLDAS Model 35

3.1.3.3 WGHM Model 36

3.1.3.4 ERA-5 Model 37

3.1.3.5 CHELSA Model 37

3.1.4 Global Drought Data 38

3.1.4.1 SPEI 38

3.1.5.2 scPDSI 39

3.1.5 In-situ observations 39

3.2 Spatial Aggregation and Resampling 44

3.3 Time Series Decomposition 46

3.4 Vertical Decomposition of the GRACE TWS 47

3.5 Calculation of the Drought Indices 48

3.5.1 Enhanced Water Storage Deficit Index (EWSDI) 49

3.5.2 Standardized Precipitation Index (SPI) 50
3.6 Trend Analysis 51
3.6.1 Man-Kendall Trend Test 51
3.6.2 Sen's Slope Estimator 52
3.7 Machine Learning Statistical Downscaling 53
3.7.1 Random Forest (RF) 53
3.7.2 Designing the Downscaling Algorithm 55
3.8 Uncertainty Estimation 57
3.9 Evaluation Metrics 58
3.9.1 Coefficient of Correlation (R) 58
3.9.2 Root Mean Square Error (RMSE) 59
3.9.3 Mean Absolute Error (MAE) 59
3.9.4 Nash-Sutcliffe Efficiency Coefficient (NSE) 59

CHAPTER 4-DESCRIPTION OF THE STUDY AREA 61

4.1 Overview of Turkey 61
4.1.1 Geographic and Topographic Setting 61
4.1.2 Climate of Turkey 63
4.1.3 Water Resources of Turkey 67
4.2 Overview of the Western Anatolian Basin (WAB) 71
4.2.1 North Aegean Basin (NAB) 73
4.2.2 Gediz Basin (GB) 73
4.2.3 Kucuk Menderes Basin (KMB) 73

4.2.4 Buyuk Menderes Basin (BMB) 74

CHAPTER 5-RESULTS AND DISCUSSION 76

5.1 Fluctuations of the Simulated SMS and SWE over Turkey 76

5.2 Fluctuations of the GRACE-derived TWS over Turkey 79

5.3 Fluctuations of the GRACE-derived GWS over Turkey 84

5.4 Associations Between the GRACE- And Model-based TWS and GWS 89

5.5 Fluctuations of GWS in response to the Variations in the Meteorological Variables 94

5.6 Groundwater Response to The Hydrometeorological Extremes 98

5.6.1 TWS Decomposition 98

5.6.2 Investigating the Extreme Hydrometeorological Events over Turkey 103

5.6.3 Associations Between the Drought Indices And GWS 108

5.7 Assessment of the Agricultural Activities over Turkey 113

5.8 Downscaling Results 117

5.8.1 Model Sensitivity 117

5.8.2 Investigating the Predictive Precision of the RF Model 119

5.8.3 The Basin-scale Variations of the TWS and GWS 123

5.9. Validation 125

5.9.1 Temporal Validation Against the Simulated Groundwater Use 125

5-9.2 Validation Against the Monthly Groundwater Level Observations 126

5.10 Trend And Uncertainty Estimation 129

5.11 Spatial Variability of Trends 131

5.12 Spatial Variability of TWS and GWS over Turkey 135

CHAPTER 6 - CONCLUSIONS AND RECOMMENDATIONS 142

6.1 Main Outcomes of the Study..... 142

6.2 Recommendations 144

REFERENCES 147

APPENDICES 200

LIST OF FIGURES

Page

Figure 2.1 Graphical illustration of the Terrestrial Water Storage components 9

Figure 2.2 Distribution of world water 11

Figure 3.1 Configuration principle of the GRACE satellite mission 23

Figure 3.2 The schematic description of the GRACE measurement mechanism. The twin satellite passes over the ocean (Panel 1). Slight changes in the gravity pull don't alter the vertical position of the satellite but it changes the orbital velocity. When the satellite passes over an area of stronger gravity, the first (lead) satellite speeds up and pulls ahead of the second (trailing) satellite (Panel 2). The orbiting speed of the trailing satellite is also increased when it approaches the same spot (Panel 3). After passing over the high gravity location, the satellites decelerate (Panel 4). The consecutive set of satellite accelerations and decelerations engender a set of signals, which are recorded as the variations of gravity 25

Figure 3.3 The schematic portrayal of the routine signal processing is based on the Spherical Harmonics (SH) solution technique. The original signals are further post-processed (filtered and scaled) after going through "Destriping", "Truncation" and "Gaussian" filtering processes to come up with noise-reduced signals. 28

Figure 3.4 Spatial distribution of the scaling factor over Turkey 29

Figure 3.5 Spatial resampling process through different techniques 45

Figure 3.6 Schematic flow of the bagging ensemble Random Forest (RF) regression 55

Figure 3.7 Graphical description of the downscaling flow 57

Figure 4.1 Visual description of the geographic and topographic setting of Turkey 63

Figure 4.2 Classification of Turkey's climate based on Thorntwaite method (after Sensoy, 2012). 65

Figure 4.3 Spatial distribution of MAP (a.) and MAT (b.) values over Turkey 67

Figure 4.4 The ombrothermic diagram of Turkey is based on the long-term meteorological records (1929-2018). 68

Figure 4.5 The geographic location of the river basins of Turkey 69

Figure 4.6 The global water scarcity map in physical and economic terms 71

Figure 4.7 Illustration of the geographic position of the Western Anatolian Basin (WAB), west of Turkey. 73

Figure 5.1 Temporal variations of the simulated soil moisture storage over Turkey at monthly (a) and annual (b) time scales. 78

Figure 5.2 Temporal variations of the simulated snow water equivalent over Turkey at monthly (a) and annual (b) time scales. 79

Figure 5.3 Temporal variations of the GRACE-driven TWS over Turkey at monthly (a), annual (b), climatology (c) and seasonal (d) time scales. 82

Figure 5.4 The detected soil moisture deficit in January 2022 by the GRACE satellite harbingers a severe drought over Turkey. 84

Figure 5.5 Temporal associations of the GRACE-derived GWS by integrating different hydrological model outputs into the TWS estimates over Turkey. 86

Figure 5.6 Temporal variations of the GRACE-driven GWS over Turkey at monthly (a), annual (b), climatology (c) and seasonal (d) time scales. 88

Figure 5.7 Temporal interactions between the GRACE-derived and simulated TWS and GWS over Turkey. 92

Figure 5.8 Spatial associations between the GRACE-derived and the CLSM-derived TWS (a) and GWS (b) over Turkey. 93

Figure 5.9 Spatial associations between the GRACE-derived and the WGHM-derived TWS (a) and GWS (b) over Turkey. 94

Figure 5.10 The monthly associations of TWS with PA (a) and TA (b) over Turkey..... 96

Figure 5.11 Climatological associations between TWS and PA(a) and TA(b). 97

Figure 5.12 Annual associations between TWS and PA(a) and TA(b). 98

Figure 5.13 Decomposed GRACE-TWS over Turkey..... 101

Figure 5.14 Time series of de-trended (a) and de-seasoned (b) TWS 102

Figure 5.15 Seasonal total water storage cycle of Turkey 103

Figure 5.16 The contribution of each component of the decomposed TWS to the total variance of the time series 103

Figure 5.17 The recent monthly (a.) and annual (b) hydrometeorological status of Turkey according to the GRACE-based EWSI, SPI, SPEI and scPDSI indicators. 106

Figure 5.18 Thematic maps of the spatial distribution of drought indices over Turkey: SPI (a.), EWSDI (b.), SPEI (c.) and scPDSI (d) for the year 2008……....107

Figure 5.19 Illustration of the temporal associations between the hydrometeorological indicators and monthly groundwater storage (a), monthly groundwater storage deficit (b) and annual groundwater storage (c)…….110

Figure 5.20 Spatial correlation of the GRACE-derived GWS and hydrometeorological indices of PDSI (a.), SPEI (b.), SPI (c.) and EWSDI (d.). 112

Figure 5.21 Time series variations of the MODIS-derived Normalized Difference Vegetation Index (NDVI) over Turkey 115

Figure 5.22 Temporal associations between the variations of the NDVI and the simulated abstracted water from groundwater water (a.) and surface water (b.) over Turkey 116

Figure 5.23 Temporal associations between the fluctuations of the GRACE-derived GWS and the MODIS-derived NDVI over Turkey 117

Figure 5.24 Importance Measure Predictive (VIMP) test results for the model inputs. 119

Figure 5.25 Scatter plots and regression fits of the RF-based and GRACE-based TWS and GWS over Turkey. 121

Figure 5.26 Illustration of the annual spatial fluctuations of the GRACE-derived TWS for the year 2020 before (a.) and after downscaling (b.) practice. 122

Figure 5.27 Illustration of the annual spatial fluctuations of the GRACE-derived GWS for the year 2020 before (a.) and after downscaling (b.) practice 123

Figure 5.28 Local-scale fluctuations of terrestrial (a) and groundwater (b) storage and their interactions with soil moisture and snow water variations over the WAB 125

Figure 5.29 illustration of the monthly (a.) and seasonal (b.) interactions between the potential consumptive water use (from WGHM) and groundwater storage variations. 127

Figure 5.30 Interactions between potential groundwater use (from WGHM) and groundwater storage. 129

Figure 5.31 Illustration of the original and downscaled TWS and GWS over the WAB. 130

Figure 5.32 Validation of the original (50 km) (a) and downscaled (10 km) GWS (b) against seasonal groundwater level. 134

Figure 5.33 Spatial illustration of the annual distribution of the downscaled GRACE TWS over Turkey. 137

Figure 5.34 Spatial illustration of the annual distribution of the downscaled GRACE GWS over Turkey. 140

LIST OF TABLES

Page

Table 2.1 Summary of the groundwater depletion inferred from GRACE over different regions of the world 17

Table 3.1 The characteristics of the GRACE satellites 24

Table 3.2 Characteristics of the Land Surface Models Offered by the GLDAS 34

Table 3.3 Characteristics of the seasonal groundwater observation wells used in this study 40

Table 3.4 Specific yield values for geological materials (After Akarsu, 2019) 42

Table 3.5 Specifications of the datasets used in this study 43

Table 4.1 The zonal statistics of the long-term (1929-2018) observations of precipitation and temperature over Turkey 66

Table 4.2 Annual Average Water Potential by Basin. Source: TSHW 2020 70

Table 4.3 Groundwater potential reported for each basin 76

Table 5.1 Results of the accuracy assessment of the tried decomposition models. Mean absolute deviation (MAD), Mean Absolute Percentage Error (MAPE) and Mean Squared Deviation (MSD) metrics were used to determine the best decomposition model. 99

Table 5.2 The seasonal factors of TWS derived for each month. Seasonal factor values indicate the seasonal impact on the time series and later are used to de-season the TWS time series. 101

Table 5.3 The secular trend and uncertainty estimates of the hydrological water cycle components over Turkey. 131

Table 5.4 Volumetric trends of the hydrological water cycle components over Turkey. 132

ABBREVIATIONS

ANN	:Artificial Neural Networks
CHELSA	:Climatologies at high resolution for the earth's land surface areas
CLM	:The Community Land Model
CLSM	:Catchment Land Surface Model
CSR	:The Centre for Space Research
CWS	:Canopy Water Storage
CWSA	:Canopy Water Storage Anomalies
CWU	:Consumptive Water Use
ECMWF	:European Center for Medium-Range Weather Forecasts
ERA-5	:ECMWF Reanalysis 5th Generation
FLDAS	:the Famine Early Warning Systems Network Land Data Assimilation System
GIS	:Geographic Information Systems
GLDAS	:Global Land Data Assimilation System
GRACE	:Gravity Recovery And Climate Experiment
GRACE-FO	:Gravity Recovery And Climate Experiment Follow-On
GWA	:Groundwater Abstraction

GWS	:Groundwater Storage
GWSA	:Groundwater Storage Anomalies
LSM	:Land Surface Model
MASCON	:Mass Concentration
ML	:Machine Learning
MODIS	:Moderate Resolution Imaging Spectroradiometer
MSD	:Mean Squared Deviation
OWs	:Observation Wells
P	:Precipitation
PA	:Precipitation Anomalies
RF	:Random Forest
RS	:Remote Sensing
SDS	:Statistical Downscaling
SH	:Spherical Harmonics
SMS	:Soil Moisture Storage
SMSA	:Soil Moisture Storage Anomalies
SWE	:Snow Water Equivalent
SWEA	:Snow Water Equivalent Anomalies

SWS	:Surface Water Storage
SWSA	:Surface Water Storage Anomalies
T	:Temperature
TA	:Temperature Anomalies
TR	:Turkey
TSHW	:Turkish State Hydraulic Works
TSMS	:The Turkish State Meteorological Service
TWS	:Terrestrial Water Storage
TWSA	:Terrestrial Water Storage Anomalies
VIC	:Variable Infiltration Capacity
WAB	:Western Anatolia Bain

CHAPTER 1

INTRODUCTION

1.1 Motivation

Water resources are extremely critical for the sustainable persistence and development of different aspects of human life on the planet. Water is consumed for different purposes including agriculture, drinking, industrial production, recreation, etc. Moreover, water is of utmost importance in terms of backing up nature to procure ecosystem services. Although this critical substance plays an indisputably central role in the sustenance of both humans and wildlife, it has been being taken for granted throughout human history. Especially during the recent decades, the general status of the water (surface and subsurface) resources has become worse mainly on account of two influential factors: population growth and climate change impacts. Climate change impacts in terms of decreased precipitation and increased temperature and evapotranspiration have culminated in the diminished quantity and quality of water resources all around the world (Kamran and Khorrami, 2018). Today, we know that the climate change phenomena have affected almost all regions throughout the world by its negative, harsh and in some cases irreversible impacts on water resources and freshwater ecosystems (Abbaspour et al., 2009). It is estimated that the severity of climate change will increase during the upcoming years putting the life of more people in danger. Although climate change impacts on the variations of hydrometeorological parameters are very determining, the anthropogenic contribution to this environmental problem should not be ignored. Growing water use as a result of the population growth imposes more pressure on the world's freshwater resources. For instance, it is projected that the world population will go beyond 9.3 billion by 2050 (Pimentel and Burgess, 2013). An increase in the population number intensifies water consumption. Furthermore, the water distribution over the world is not akin to that of the population (Postel, 2000), which exacerbates the balance between water generation and water use. The increased climate change accompanied by anthropogenic drivers such

as population growth and implemented wrong policies are likely to influence different regions that are already overwhelmed by water scarcity challenges. The increased pressure on water resources has engendered major problems that limit the existence of agricultural and industrial productions, effect human health and damage environmental stability (Postel, 2000). Water scarcity, manifested in terms of the water storage shortages in either superficial or subsurface water resources, is expected to turn into a world major problem over the coming decades (Vaux, 2011) particularly over the regions with arid to semi-arid climates (Jury and Vaux, 2007).

Under this perspective of globally growing water scarcity, groundwater aquifers are likely to be the point of focus due to the fact that they act as a more reliable source of fresh and safe water (Vaux, 2011). The water stored inside the underground formations is estimated to account for 96% of the world's freshwater, guaranteeing the water needs of different water consuming sectors including household, cultivation and industry (Feng et al., 2013; Taylor et al., 2013; Ülker et al., 2018). Though water stored beneath the Earth's land surface is less exposed to threatening factors compared to surface waters, the world aquifers are dramatically stressed by overexploitation and hydrometeorological extremes. This is more tangible over arid and semiarid regions where water need is exclusively met by groundwater (Sun, 2013). Although the fast expansion of groundwater withdrawal practices may bring about some socio-economic benefits for the residents, it may also be accompanied by serious problems (Morris et al., 2003). Groundwater depletion happens when the existent hydrological balance between the groundwater abstraction and groundwater recharge is collapsed for a long time (Gleeson et al., 2010). On account of the combined natural and anthropogenic factors, the world's groundwater aquifers are crippled with uncontrolled pumping resulting in the detriment of the hydrologic balance and the depletion of groundwater whose pace has been doubled compared to the last several decades. Diminished groundwater levels may have severe and destructive ramifications for the environment affecting different aspects of human life. Groundwater depletion decreases the natural streamflow and may increase the desiccation of wetlands and ecosystems, land deformation and also salt-water intrusion. The harsh and, in most

cases, irreversible ramifications of the groundwater depletion necessitate the real-time monitoring of groundwater resources so that the managerial policies are done accurately and conveniently.

To have a quantitative understanding of the state of groundwater, monitoring is an indispensable tool to develop and implement a sound water management strategy. The quality and reliability of data determine the accuracy and applicability of the outputs of any environmental research and monitoring policy (Oyebande, 2001; Awad et al., 2009). For local scale assessment and surveillance of groundwater variations, field-based observations of groundwater wells are commonly used within the scope of the traditional (station-based) monitoring approach (Khorrami and Gunduz, 2021a). Notwithstanding their high accuracy, in-situ records suffer from poor data-gathering networks in many areas, which results in gaps in the spatio-temporal continuity of the data. The incomplete groundwater observation networks deliver insufficient and interrupted observations of water quality and quantity required for sustainable management of aquifers (UNESCO, 2009). Further, limited access to these observations, due to geopolitical issues, shackles their feasibility and applicability for especially large-scale assessment purposes. On the opposite extreme to the field monitoring methods, remote sensing generates a continuous, uninterrupted, global and affordable set of different environmental observations with acceptable to very high accuracy levels (Khorrami et al., 2019; Khorrami & Gunduz, 2020). Considering the mentioned privileges, remotely sensed data have the potentiality to be used for better monitoring and evaluation of most of the environmental issues as well as groundwater variations in particular. Therefore, the remote sensing approach is thought of as a suitable substitute to the conventional monitoring and assessment approaches compensating for the in-situ data dearth and function as a good means for the retrieval of information needed for decision-making policies (UNESCO, 2009).

The Gravity Recovery and Climate Exchange (GRACE) is one of the latest space missions run under the auspices of the National Aeronautics and Space Administration (NASA). It is a unique remote sensing program in the history of environmental remote

sensing with the feasible potentiality of delivering remote estimations of large-scale fluctuations of the Earth's water storage and mapping of regional variations of groundwater storage (Tapley et al., 2004a; Rodell et al., 2007). The GRACE mission is a combination of two sister missions. The first mission was launched in 2002 and offered its unique service for 16 years till Jun 2017. The second mission of the GRACE, called GRACE Follow-On (GRACE-FO), was placed in orbit in Jun 2018 and has been working up to date. Although the primary goal of the GRACE program was to investigate the changes of the gravity, the monthly variations of the terrestrial water storage (TWS) is done with unprecedented precision by further signal processing (Tapley et al., 2004b). TWS is a hydrological parameter of a very high importance that encompasses different critical hydrological cycle compartments including soil moisture, snow water, surface water and groundwater (Khorrami et al., 2021). TWS has a cardinal role in climatic assessments over the regional and global scales (Śliwińska et al., 2019). Accurate estimates of TWS are critical for climatological and hydrological analysis to study the occurrence of the extreme hydrometeorological events and also to investigate the interactions between climate change and water storage variations over time (Rahaman, et al., 2019a; Tangdamrongsub et al., 2020; Khorrami et al., 2021). Thanks to the inherent nature of the GRACE data, which includes the variations of different hydrological variables, spatio-temporal assessment of these variables is viable through integrating the GRACE data into hydrological models. For example, by making use of simulated variables, the groundwater storage variations can be extracted. Although the GRACE/GRACE-FO mission has been very successful in estimating large scale fluctuations of hydrological water cycle compartments, especially groundwater storage, its coarse spatio-temporal resolution has remained as one outstanding drawback of the mission, which hinders its applicability for local scales studies (Ning et al., 2014).

Though advanced remote sensing missions have so far used sophisticated and accurate data retrieval algorithms, the coarse resolution of the generated data is a issue of a variety of environmental space missions, which results in low detectability of the phenomena under study. To overcome this barrier, scientists and researchers have developed different

downscaling algorithms and techniques to fill in the spatial gaps between the large scale and local scale variability of different parameters (Sachindra et al., 2018). Downscaling is a technical term referring to a set of spatial scale reduction techniques, through which, information with a finer spatial resolution is deduced from coarse resolution data (Sahour et al., 2020). The main assumption behind the downscaling concept is that the local variations of a variable of interest are characterized or controlled by combined large-scale and local conditions (Caffrey and Farmer, 2014). Different downscaling techniques result in different levels of accuracy but the shared feature of all the downscaling approaches is that they pave the way for evaluating the fine resolution variations at local scales, which is not affordable by mere application of the original coarse resolution data.

As a rapidly developing country, Turkey's population is also growing steadily. The mean population growth rate of the country is 1.8% (Ozturk and Ozturk, 2018). The increased population in conjunction with the swift development of industry together with the side effects of climate change create multifaceted problems for Turkey's water resources. Groundwater is a key water source for Turkey due to its determining role in both the social and economic growth of the country. Therefore, better management and conservation of this resource require adequate and well-stablished monitoring networks with a focus on the continuity of underground water-bearing structures (Apaydin, 2011). However, intemperate withdrawal of groundwater in Turkey has been considered as a common problem that continues to disturb the natural hydroclimatic balance to an alarming state in some regions regarding the severely diminished water table and skyrocketed water extraction expenses. Unfortunately, due to widespread data dearth regarding the spatio-temporal characteristics of groundwater wells, a realistic portrayal of the groundwater status is very challenging and in most of the cases impossible (FAO, 2016).

1.2 Objectives of the Study

Based on this premise, an integrated methodology was organized to investigate the fluctuations of terrestrial and groundwater storage over the heterogeneous geography of Turkey. To this end, several different hydrological models, remotely sensed data, as well as field observations, were integrated to derive the spatio-temporal variations of different hydrometeorological variables. The following can be stated as the final goals to be achieved through the completion of this study:

i. Evaluation of the feasibility of the GRACE/GRACE-FO estimates for the remote monitoring of the spatio-temporal fluctuations of TWS and GWS over Turkey.

ii. Assessment of the spatio-temporal variations of different hydrological water cycle components based on the simulated data.

iii. Investigation of the hydrometeorological extremes during the recent years over Turkey by integrating different drought indices derived based on the GRACE/GRACE-FO observations, hydrological models and in-situ data.

iv. Assessment of the impacts of the experienced extreme dry events on the fluctuations of the groundwater storage over Turkey.

v. Evaluation of the basin-scale TWS and GWS changes by using spatially enhanced GRACE/GRACE-FO observations based on a machine learning downscaling algorithm.

1.3 Scope of the Study

According to the objectives given above, the general scope of this thesis is listed as follows:

i. Chapter two illustrates the scientific backgrounds of the concepts, materials and methods of the study including hydrological water cycle changes, terrestrial and groundwater variations, monitoring techniques, extreme hydrometeorological events, applications of the GRACE and hydrological models, etc. It also encompasses a literature review of the similar or related works already implemented over Turkey and other areas over the world as well.

ii. Chapter three includes the methodology of the thesis. All the details regarding the data and techniques pursued within the methodological framework of the thesis are discussed. For example, the satellite, model and field-based observations used in this study are explained. More details on the properties of the datasets and the corresponding data processing/analysis routines are discussed also discussed in this section.

iii. Chapter four is exclusively developed and organized to discuss the area of concern of this project to offer a thorough description of the study area by discussing its geographic, climatic and hydrologic characteristics in detail.

iv. Chapter five demonstrates the findings of the analysis and provides discussion of the results.

v. Chapter six includes the interpretation and conclusions and offers some recommendations by taking into account the limitations associated with this study.

CHAPTER 2

LITERATURE REVIEW

In this section, the results of the in-depth review of the pertinent literature are given to illustrate the logic behind the followed methodology and elucidate more on the motivations of conducting this thesis research. Detailed background information on the applied data and techniques are given in an organized way so that the prospective readers of the thesis are able to follow the recent developments and achievements in terms of the research material and analysis. This section of the thesis comprises different subsections as follows. In section 2.1, terrestrial water storage is discussed. In section 2.2, fluctuations of groundwater are discussed. Section 2.3 discusses the groundwater monitoring approaches. The common hydrological applications of the GRACE estimates are provided in Section 2.4. Section 2.5 casts light on the GRACE-based groundwater monitoring and eventually, the downscaling of the GRACE data is reviewed in Section 2.6.

2.1 Terrestrial Water Storage

As one of the most central and dynamic compartments of the hydrological water cycle, Terrestrial Water Storage (TWS) has a determining role in the global to regional climatic systems by exerting its control on the water and energy fluxes of the Earth (Famiglietti, 2004; Syed et al., 2008). TWS is an integrated variable consisting of water stored in different parts of the hydrological water cycle including surface water, soil water, glaciers and groundwater (Figure 2.1) (Pan et al., 2017). So, variations in the water stored on the land surface (lakes, dams, streams and snowpacks), in the soil profile and in the groundwater aquifers, result in the variations of the TWS (Long and Scanlon, 2015).

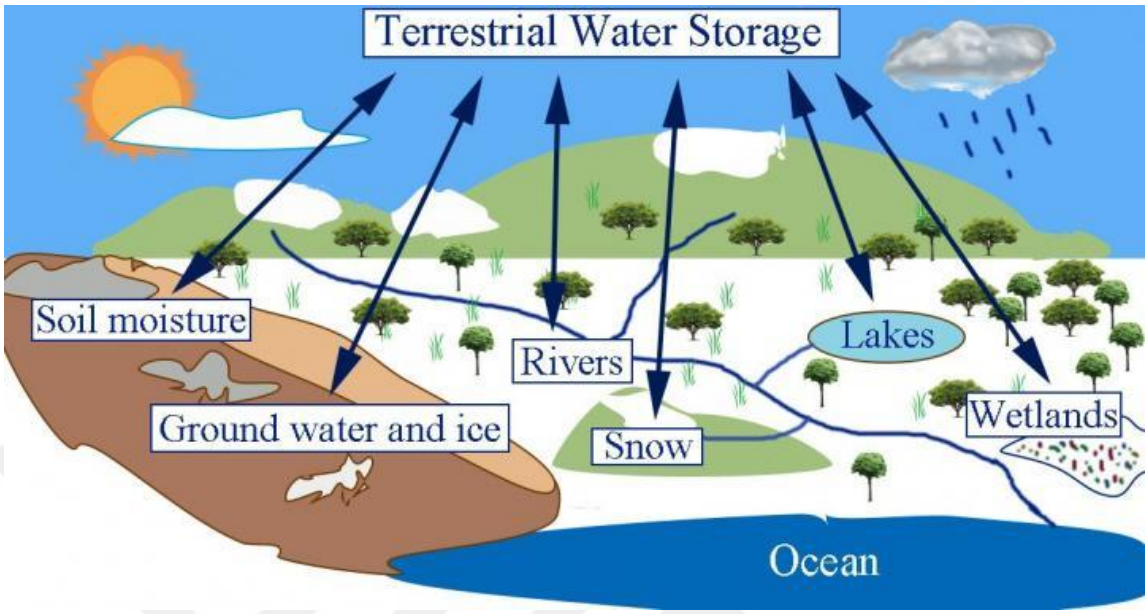


Figure 2.1 Graphical illustration of the Terrestrial Water Storage components

The variations of the TWS are traditionally investigated by integrating the observations of its components at point scales (Long et al., 2015). Hydrological models are also used to simulate the spatio-temporal variability of TWS and its compartments; however, they suffer from incomplete integration of some key components, such as groundwater storage, into the simulation. Furthermore, simulated variables by land surface models (LSMs) introduce a very large number of uncertainties in some compartments (Long et al., 2013) and thus, their reliability cannot be evaluated on account of insufficient observations available at appropriate scales.

The variations of the Earth's TWS show different characteristics according to the area of concern. For instance, over wet and tropical regions of the world such as the Amazon, surface waters control the variations of TWS. While soil moisture and groundwater compartments have a dominating role in mid-latitudes. The variations of snow water and ice packs determine the variations of TWS in polar regions (Rodell and Famiglietti, 2001). The canopy water storage changes have the least impact of the variations of TWS; thus, they are believed to be of zero impact in the TWS budget analysis. Surface water storage (SWS) is described as the volume of water stored in streams, lakes, wetlands and flooded

areas that sustain the water requirements of mostly agricultural activities. The variations in surface water alter the freshwater rates and nutrient transport (Richey et al., 2002). According to Getirana et al (2017b), SWS variations strongly affect the variations in TWS over the wet areas. However, its importance is trivial over the western US, Northern Africa, the Middle East and Central Asia. Soil Moisture Storage (SMS) is the volume of water stored in the soil profile. The variations of soil moisture content may have an influential and considerable impact on the occurrence and variations of the hydrological extreme of floods because of the fact that SMS partitions the received rainfall into surface runoff and infiltrated baseflow (Crow et al., 2005; Zehe et al., 2005). SMS variations account for most of the seasonal variations of TWS over the tropics and in the mid-latitudes. The volume of water stored in the forms of snow and icepacks is called snow water equivalent (SWE) whose variations are the primary drivers of the variations of the TWS over high latitudes and the mountainous regions in mid-latitudes as well (Rodell and Famiglietti, 2001; Getirana et al., 2017a). Snow water changes over these regions dominate the seasonal variations of TWS by the accumulation of snow during winter and melting process during spring and summer (Hallet and Allard, 1988).

2.2 Groundwater Storage

Groundwater Storage (GWS) refers to the water stored among the soil empty spaces beneath the land surface inside the underground water-bearing formations (Dong et al., 2019). It is the most important component of the Earth's TWS mainly due to its role in reserving the majority of the freshwater of the universe. Although surface waters act as the preliminary water suppliers for different sectors over the globe, groundwater resources have more importance regarding the challenges associated with the surface waters in terms of reliability and sustainability issues (Kundzewicz and Döll, 2009). Unlike surface waters, underground water resources are less exposed to pollution (Oke & Fourie, 2017). On the other hand, groundwater aquifers are known as sustained water-bearing formations with their capability to supply the required high-quality water, especially over dry periods when surface waters diminish seasonally (Naghibi et al., 2016). Groundwater aquifers

throughout the world, provide fresh water for about two billion people (Alley, 2006). Almost all (about 96.5%) of the total water of the globe is stored as saltwater in oceans and freshwater accounts for just 2.5% of it from which about 30% is reserved inside groundwater aquifers (Vallee et al., 2003). Surface waters bear a trivial share of the total freshwater of the world (1.2%). In Figure 2.2, the distribution of water is given.

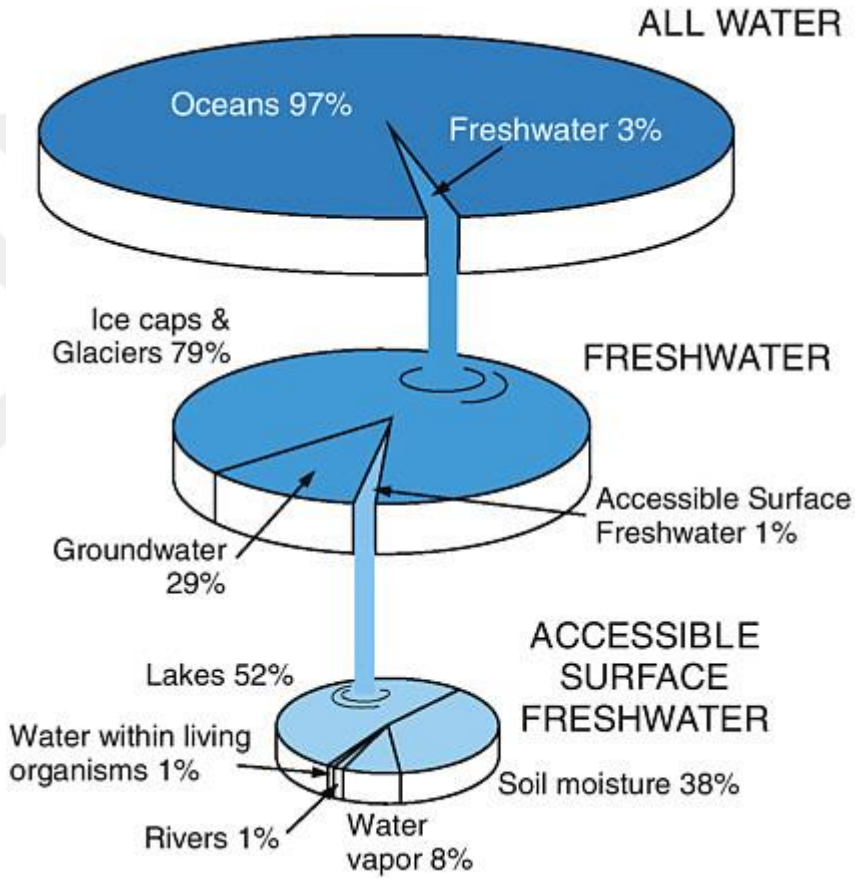


Figure 2.2 Distribution of world water

Groundwater aquifers in the mid-latitudes procure the water needed for a billion people and have an indispensable role in the Agro-industrial development of the regions (Gleeson et al., 2012). These are the only water source over regions with the harsh climatic situation (arid and semi-arid regions). Although the groundwater level fluctuates naturally on account of many natural parameters such as anomalies of the climatic parameters (precipitation and temperature), recharge patterns, streamflow anomalies and geologic

changes (Abiye et al., 2018), the increased abstraction rates during the recent decades have had a governing pressure on the status of groundwater storage all over the world. The uninterrupted shrinkage of groundwater levels (Khorrami and Gunduz, 2019) and continuous loss of its storage have resulted in a worldwide groundwater depletion (e.g., Rodell et al., 2009; Famiglietti et al., 2011; Richey et al., 2015; Girotto et al., 2017). Groundwater depletion may associate with detrimental impacts on human life from different socio-environmental perspectives. For example, it can intensify land subsidence and surface deformation, ease seawater intrusion and decrease water quality, increase water extraction costs, damage infrastructures, etc (Foster and Chilton, 2003; Galloway and Burbey, 2011;Erban et al., 2013; Shi and Jiao, 2014; Jia et al., 2019; Khorrami et al., 2021). The detrimental side effects of this phenomenon are of utmost importance due to the costs that are imposed on the natural ecosystem and human life. It is a fact that signals the importance and high priority of monitoring and assessment of the fluctuations of groundwater resources.

2.3 Groundwater Monitoring Approaches

Monitoring the status of groundwater aquifers and the variations of groundwater storage, in either temporal and spatial domain, bear cardinal importance for understanding the dynamics of freshwater, estimating depletion rate and also evaluating the associations between long-term variations of groundwater with climate variability and anthropogenic parameters (Yeh and Famiglietti, 2009). According to Bierkens and Wada (2019), the large-scale monitoring techniques for groundwater fluctuations and depletion are divided into three broad classes such as:

i. the indirect geodetic approach
ii. the water balance approach
iii. the volume-based approach

The indirect geodetic approach can be implemented using the conventional geodetic surveys or making use of remote sensing techniques/data such as GPS, radar and lidar observations (Minderhoud et al., 2017; Bierkens and Wada, 2019). Groundwater depletion is generally manifested as land surface deformations (Galloway and Burbey 2011), therefore in this approach, information on land subsidence events is used for assessing groundwater changes for regional studies.

The water balance approaches are based on the deviation between groundwater withdrawal and recharge rates. The assumption is that groundwater depletion happens when and where its abstraction rate exceeds its recharge rate. This approach suffers from some restrictions such as ignorance of water bodies and streamflow recharges and evapotranspiration impacts in the estimation process (Konikow and Leake, 2014). Since measurement of groundwater recharge and abstraction is a laborious task, the water balance approach is generally applied in large-scale hydrological models (Bierkens and Wada, 2019).

Estimation of aquifer water storage variability is of critical priority for the water resources management. The volume-based techniques estimate the rate of depletion by making use of direct estimates of groundwater storage over time. Because the water withdrawal-induced captures are taken into account, these techniques perform very well with the higher accuracy of estimates compared to the other approaches (Bierkens and Wada, 2019). Groundwater fluctuations/depletion can be evaluated and monitored through two volume-based techniques:

i. Volume changes based on in-situ observations
ii. Volume changes based on remotely sensed data

Using in-situ observations of groundwater piezometers is the traditionally applied approach for the estimation of groundwater fluctuations. This technique results in the most direct and accurate estimates of the variations of groundwater level or hydraulic heads by

processing the direct records of monitoring wells (Bierkens and Wada, 2019). By using specific yield (S_y) of the aquifer and the variations of groundwater level (Δ_H), storage variations can be estimated over regional scales (Leblanc et al., 2009) based on Equation (2.1):

$$\Delta_{GWS} = \Delta_H \times S_y \tag{2.1}$$

The accuracy of point-wise observations is high but the limited network of observation wells, as well as incomplete data, restrict the suitable application of this approach. Furthermore, the regional assessment requires the interpolated surface of the point-wise data, which brings in additional uncertainties (spatial sampling errors) into the results (Scanlon et al., 2012; MacDonald et al., 2016).

On the other hand, remote sensing techniques provide another means for the assessment of the fluctuations of groundwater based on volume estimations. Within the scope of this approach, hydrological models provide large-scale spatio-temporal estimates of groundwater depletion based on the modelled groundwater level and storage coefficients (Bierkens and Wada, 2019). The accuracy of hydrologic models significantly depends on the precision of simulations. Moreover, some additional simulated data on groundwater recharge and abstraction are required to estimate accurate estimates of the volume of storage loss (De Graaf et al., 2014; Sutanudjaja et al., 2018), that increases the uncertainty of the estimates. The GRACE mission is a relatively new satellite project, through which, the fluctuations of large-scale groundwater storage can be inferred. This approach is further discussed in detail in the following section.

2.4 Hydrological Applications of the GRACE Estimates

The time-varying data on the gravity changes increased our understanding of the mass movements of the Earth. Knowledge of the mechanism of the mass movements and their variations paved the way for a better understanding of the variations of important natural

processes such as sea-level changes, deep ocean currents and the variations in the recharge and discharge of large aquifers (Yirdaw, 2011). Since the variations of the Earth's total (terrestrial) water brings about the changes in its gravitational pull, by further processing the original gravity signals, the monthly anomalies of terrestrial water storage (TWS) are generated.

The GRACE estimates have a broad range of applications in different branches of the environmental sciences including hydrology, climatology, oceanography and geology. The literature is filled with GRACE application-oriented researches (Riley and Klemann, 2021). Since the beginning of the GRACE space program in 2002, its observations have been applied by several researchers around the world to evaluate the spatio-temporal fluctuations of TWS (e.g. Andersen et al., 2005; Han et al., 2005; Swenson et al., 2006; Syed et al., 2008; Zaitchik et al., 2008; Kim et al., 2009; Becker et al., 2011; Phillips et al., 2012; Feng et al., 2012; Lenk, 2013; Frappart et al., 2013; Moore and Williams, 2014; Jiang et al., 2014; Zhao et al., 2015; Huang et al., 2015a; Nie et al., 2016; Ndehedehe et al., 2016; Seyoum et al., 2016; Wang and Li, 2016; Yang et al., 2017; Zhang et al., 2017; Xia et al., 2017; Xie et al., 2018; Ni et al., 2018; Deng et al., 2018; Xu et al., 2019; Sliwinska et al., 2019; Jing et al., 2020; Croteau et al., 2020; Boergens et al., 2020; Fatolazadeh and Goïta, 2021; Khorrami and Gunduz, 2021a; Khaki and Hoteit, 2021; Wei et al., 2021). Through time, the GRACE-oriented research topics evolved into the integrated studies to evaluate some environmental phenomena such as extreme hydrometeorological events (Yirdaw et al., 2008; Singh et al., 2012; Thomas et al., 2014; Yi and Wen, 2016; Sinha et al., 2017; Ma et al., 2017; Zhao et al., 2017; Sun et al., 2018; Hosseini-Moghari et al., 2019; Sinha et al., 2019; Cui et al., 2021;Khorrami and Gunduz, 2021b; Xiong et al., 2021; Huang et al., 2021;Yan et al., 2021), ice sheet monitoring (Chen et al., 2006; Schrama and Wouters, 2011; Velicogna and Wahr, 2013; Schrama et al., 2014; Velicogna et al., 2020; Wang et al., 2021; Loomis et al., 2021), groundwater storage depletion (Döll et al., 2012; Chinnasamy et al., 2013; Huang et al., 2015-b; Chen et al., 2016; Humphrey et al., 2016; Castellazzi et al., 2016; Vasco et al., 2019; Bhanja et al., 2019; Frappart and Ramillien, 2018; Thomas and Famiglietti, 2019; Hu et al., 2019; Zhao

et al., 2019; Shamsudduha and Taylor, 2020; Neves et al., 2020) and land deformation and sinkhole evaluation (Tangdamrongsub and Šprlák, 2021; Khorrami et al., 2021).

2.5 The GRACE-based Monitoring of Groundwater Storage

Groundwater depletion stands for a long-term decline of water tables chiefly because of ceaseless water abstraction, climate change and inappropriate recharge practices (Gaur et al., 2011). It has been on top of the list of catastrophic environmental problems of the world and a major sustainability challenge over different parts of the world (Dangar et al., 2021). About 33% of the total water withdrawal globally appertains to abstractions from groundwater aquifers mainly for cultivation and drinking purposes (Taylor et al., 2013; Dangar et al., 2021). Groundwater is abstracted at huge rates to irrigate more than 39 million ha of agricultural lands for food production (Famiglietti, 2014; Dangar et al., 2021).

Large-scale detection of the changes of groundwater storage became viable with the advent of the GRACE mission (Yeh et al., 2006; Swenson and Wahr, 2006; Rodell et al., 2007). Hydrologists have so far well-benefited from the GRACE groundwater storage estimates over global and regional scales. These estimates were successfully used to quantify the long-term variations of groundwater storage and depletion rates in different regions (e.g. Konikow and Kendy, 2005; Rodell et al., 2009; Wada et al., 2010; Aeschbach-Hertig and Gleeson, 2012; Shen et al., 2015; Wada, 2016; Dalin et al., 2017; De Graaf et al., 2017; Castellazzi et al., 2018; Katpatal et al., 2018; Bierkens and Wada, 2019; Jia et al., 2019; Gumidyala et al., 2020; Verma and Katpatal, 2020; Jia et al., 2020; Dangar et al., 2021; Sidhu et al., 2021; Khorrami et al., 2021). Critical status was reported for vast areas in northwest India (NWI) (Rodell et al., 2009; Tiwari et al., 2009; Chen et al., 2014), the High Plains Aquifer (HPA) (Strassberg et al., 2009; Scanlon et al., 2012; Famiglietti and Rodell, 2013) and Central Valley in the USA (Famiglietti et al., 2011; Scanlon et al., 2012), the North China Plain (NCP) (Jin and Feng, 2013), the Middle East (Voss et al., 2013; Joodaki et al., 2014), southern Murray–Darling Basin (MDB) in

Australia (Leblanc et al., 2009), Songhua River Basin (Chen et al., 2019a) and the Yellow River Basin in China (Lin et al., 2019) and the Dakhla basin in Egypt (Mohamed, 2019). The depletion rate is alarming in NW India (40 mm/year), the high plains of the US (27.6 mm/year) and the North China Plain (22.0 mm/year) (Rodell et al., 2009; Scanlon et al., 2012; Feng et al., 2013; Famiglietti, 2014, Jia et al., 2020). Table 2.2 has a summary of the studies on the variations of groundwater storage based on the GRACE data over different regions of the world.

Table 2.1 Summary of the groundwater depletion inferred from GRACE over different regions of the world

Study area	**Annual Depletion**	**Temporal Window**	**Reference**
NW India	17.7 ± 4.5 (km^3)	2002 – 2008	Rodell et al. (2009)
NW and NE India	54 ± 9 (km^3)	2002 – 2008	Tiwari et al. (2009)
USA (Central Valley)	4.8 ± 0.4 (km^3)	2003 – 2010	Famiglietti et al. (2011)
Australia (Southern MDB)	18 ± 1.3 (km^3)	2002 – 2010	Leblanc et al. (2012)
USA (Central Valley)	7.7 ± 0.7 (km^3)	2006 – 2009	Scanlon et al. (2012)
Middle East (North-Central)	13 ± 1.5 (km^3)	2003 – 2009	Voss et al. (2013)
North China Plain	8.3 ± 1.1 (km^3)	2003 – 2010	Feng et al. (2013)
Arabian Middle East	15.5 (km^3)	2003 – 2013	Richey (2014)
Australia (Canning Basin)	3.5 (km^3)	2003 – 2013	
South America (Guarani)	1.0 (km^3)	2003 – 2013	
NW Sahara	2.7 (km^3)	2003 – 2013	
NW India	29.4 ± 8.5 (km^3)	2003 – 2007	Chen et al. (2014)
NW India	20.4 ± 7.1 (km^3)	2003 – 2012	
Middle East (Iran)	25 ± 3 (km^3)	2003 – 2012	Joodaki et al. (2014)

Table 2.1 Continues.

Study area	Annual Depletion	Temporal Window	Reference
High Plains Aquifer	12.5 ± 0.4 (km^3)	2003 – 2012	Brena-Naranjo et al. (2014)
Australia (Southern MDB)	17.2 ± 4.7 (km^3)	2003 – 2010	Chen et al. (2015)
China (Hai Basin)	5.5 (km^3)	2003 – 2012	Shen et al. (2015)
North China Plain	46.5 (mm)	2003 – 2013	Huang et al. (2015)
NW India Aquifer	14 (km^3)	2005 – 2010	Long et al. (2016)
China (Liao Basin)	0.92 (km^3)	2005 – 2011	Zhong et al. (2018)
World's major aquifers	60 (mm)	2004 – 2010	Frappart and Ramillien (2018)
North China Plain	1.7± 0.1 (km^3)	2004 – 2016	Zhao et al. (2019)
China (Xinjiang)	3.61 (mm)	2002 – 2017	Hu et al. (2019)
California (Central Valley)	3.1 (km^3)	2015 – 2018	Vasco et al. (2019)
China (Huang-Huai-Hai Plain)	14.1 ± 0.89 (mm)	2003 – 2015	Su et al. (2020)
India (Dehli and Uttar Pradesh)	75.2 (mm)	2003 – 2016	Sarkar et al. (2020)
SW and Central U.S Aquifers	90 (km^3)	2003 – 2014	Rateb et al. (2020)
India (Ganges-Brahmaputra Basin)	0.4 (km^3)	2003 – 2014	Bhanja et al. (2020)
Egypt (Nile Delta Aquifer)	0.083 (km^3)	2003 – 2012	Mohamed (2020)
China (Shiyang Basin)	2.2 (mm)	2011 – 2016	Liu et al. (2021a)
North China	10.9 (mm)	2003 – 2019	Liu et al. (2021b)
North China Plain	19 (mm)	2003 – 2018	Zhang et al. (2021a)
High Plains Aquifer	12.5 ± 0.4 (km^3)	2003 – 2012	Brena-Naranjo et al. (2014)

2.6 Downscaling of the GRACE Data

The GRACE mission provides the scientific community with high accuracy global estimates of TWS with a multifaceted area of applications especially in hydrology and water resources studies. The uniqueness of this mission, in delivering global TWS variations with no restrictions of location, depth and visibility, has been so impressive that it can be stated that the emergence of the GRACE revolutionized the large-scale monitoring of hydrological water cycle components, especially groundwater storage. However, its coarse resolution still remains a handicap for local studies. Although the performance of the GRACE has been confirmed over large-scale areas (Rodell and Famiglietti, 2002; Lombard et al., 2007; Landerer and Swenson, 2012; Chambers and Bonin, 2012; Jin and Feng, 2013; Famiglietti and Rodell, 2013; Castle et al., 2014; Richey et al., 2015; Scanlon et al., 2015; Chen et al., 2016; Khandu et al., 2016; Pan et al., 2017), it fails to catch the anomalies of TWS and GWS in small areas with the spatial extent of less than the GRACE footprint (~200,000 km^2) (Wang et al., 2019; Khorrami & Gunduz, 2021a). The restricting aspects of the GRACE data, which get in the way of its more suitable applications can be stated as follow:

i. Product Latency:

The GRACE estimates are not near real-time data, which is an unfavorable feature for the majority of the hydrological applications, where hourly and daily observations are of substantial priority and importance (Rodell et al., 2019).

ii. Lack of vertical information:

The GRACE doesn’t give any information regarding the vertical distribution and structure of the hydrological water cycle compartments. Thus, it's vague where these components come from. Moreover, GRACE-derived TWS data represent only the time-

dependent changes in water storage and not the water storage in itself (Joodaki et al., 2014).

iii. Coarse spatial resolution:

The GRACE estimates are offered at 1 degree (100 km) of spatial resolution, which is not an appropriate scale for local studies. (Rowlands et al., 2005; Swenson and Wahr., 2006).

The above-mentioned restrictions challenge the applications of the GRACE data. To tackle these limitations, data disintegration and downscaling techniques are used to overcome the lack of vertical information and the course spatio-temporal resolution problems, respectively.

Downscaling is a technical term referring to a set of spatial scale reduction techniques, through which, information with a finer spatial resolution is deduced from coarse resolution data (Wilby et al., 1997; Sahour et al., 2020). Downscaling techniques are divided into two approaches, namely the dynamic downscaling and statistical downscaling approaches (Liu et al., 2011). Dynamic downscaling techniques have so far been applied successfully on the GRACE/GRACE-FO data in some regions including the Mississippi River basin (Zaitchik et al., 2008), North America (Houborg et al., 2012), the Murrumbidgee catchment (Shokri et al., 2018) and the Murray-Darling basin (Shokri et al., 2019). Although dynamic techniques are of high accuracy, their feasibility is shackled by the lack of complex multisource data that is not available for many researchers (Ali et al., 2021).

The statistical downscaling techniques, on the other hand, are more straightforward that can greatly enhance the spatial resolution of hydrological variables. Within the scope of these techniques, the spatio-temporal relationships between inputs (independent variables) and outputs (dependent variables) are used to design the statistical downscaling models

(Le Roux et al., 2018). According to literature, different statistical approaches have been implemented by researchers so far to downscale GRACE products (Zaitchik et al., 2008; Yirdaw, 2011; Li et al., 2012; Schumacher, 2012; Sun, 2013; Ning et al., 2014; Kumar et al., 2016; Miro and Famiglietti, 2018; Ghasemian, 2018; Seyoum et al., 2019; Karunakalage et al., 2021). These include regression models, numerical methods such as ANN and more sophisticated data assimilation techniques, which all suggest the suitability of downscaled GRACE measurements for local-scale studies.

CHAPTER 3

METHODOLOGY

3.1 Remote Sensing Data

3.1.1 GRACE/GRACE-FO

3.1.1.1 The Basic Theory of the GRACE

The Gravity Recovery and Climate Experiment (GRACE) is a new space project operated under the auspices of the USA's NASA and the German Space Agency (DLR). The mission is based on a satellite-to-satellite tracking mechanism, which was primarily introduced in 1996 by the Center for Space Research (CSR), the German Research Centre for Geosciences (GFZ) and the Jet Propulsion Laboratories (JPL). The GRACE is a twin satellite mission (Figure 3.1) that tracks the Earth's surface with an approximated horizontal distance of 220 km and at an altitude of 500 km (Botani and Combrinck, 2012; Khorrami and Gunduz, 2021a). The two satellites are associated with a precise inter-satellite microwave ranging system, altitude sensors, accelerators and a GPS receiver (Dunn et al., 2003; Tapley et al., 2004a). Figure 3.1 shows the GRACE twin satellite mission. The onboard GPS pinpoints the geocentric-referenced spatial position of the satellites in the orbit. The accelerators control and determine the non-gravitational accelerations.

The primary and secondary scientific motivations behind the development of the GRACE project were the precise mapping of the gravitational anomalies of the Earth in spatial and temporal scales and measuring the daily profiles of temperature and humidity by using the GPS radio occultation technique (Tapley and Reigber, 2001; Tapley et al., 2004b).

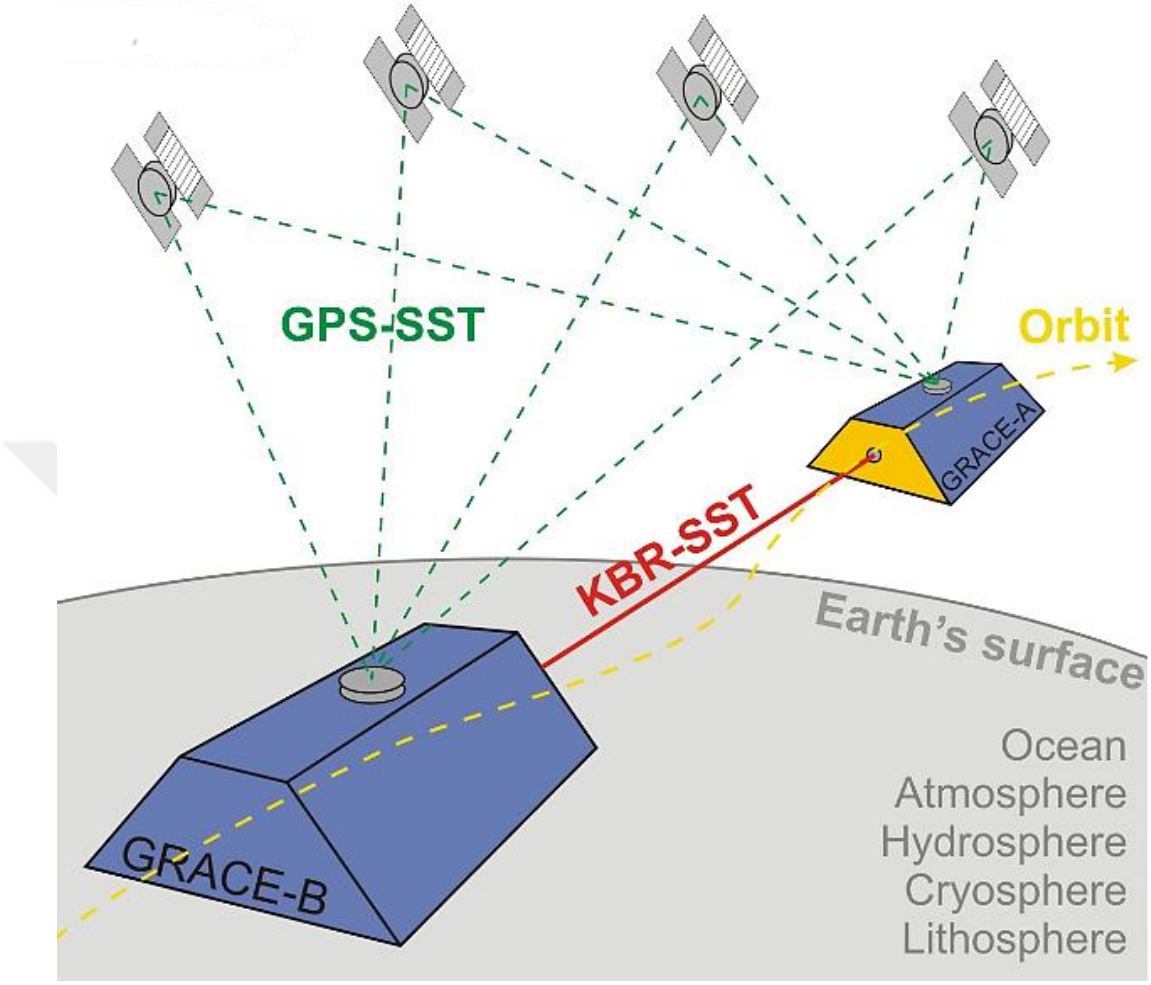


Figure 3.1 Configuration principle of the GRACE satellite program (after Schmidt et al., 2008).

The gravity signals are recorded based on Newton's gravity law (Yirdaw, 2011), which defines the interactive force between two masses as Equation 3.1.

$$F = G\frac{M \times m}{R^2} \tag{3.1}$$

where F is the gravitational force, M and m are two masses and R is the range between the two masses. G is the gravitational constant ($G = 6.673 \times 10^{-11} Nm^2/kg^2$) (Yirdaw, 2011).

Gravity exerts influence on several natural phenomena such as ocean tides and the expansion of the universe (Yirdaw, 2011). Therefore, having precise information on the Earth's gravity changes is very important for geodesy scientists. The GRACE project was developed to procure this information. The gravity signals are collected based on the variations in the horizontal distance between the two satellites. Variations of the Earth's masses such as large surface water bodies, mountains and groundwater masses, bring about the gravity changes (Feng, 2018), which are detected by the variations of the distance of the twin satellites. The gravity variations are sensed and recorded with very high sensitivity (0.1 μm/s) thanks to the K-band microwave accelerometer used to link the two satellites (Wei et al, 2008). The mechanism of signal retrieval is portrayed in Figure 3.2.

The GRACE project was started by launching the first set of satellites in March 2002. The GRACE-1 mission continued recording the gravity field for 16 years and terminated its mission in June 2017. With an 11-month delay, the second mission was started by placing the GRACE-Follow On (GRACE-FO) in the Earth's orbit in May 2018. Table 2.2. gives information on the two GRACE missions.

Table 3.1 the characteristics of the GRACE satellites (https://space.skyrocket.de/doc_sdat/ grace.htm).

Mission	**Launch date**	**Launch machine**
GRACE 1 (Tom)	17.03.2002	Rokot-KM
GRACE 2 (Jerry)	17.03.2002	Rokot-KM
GRACE-FO 1	22.05.2018	Falcon-9 v1.2(ex)
GRACE-FO 2	22.05.2018	Falcon-9 v1.2(ex)

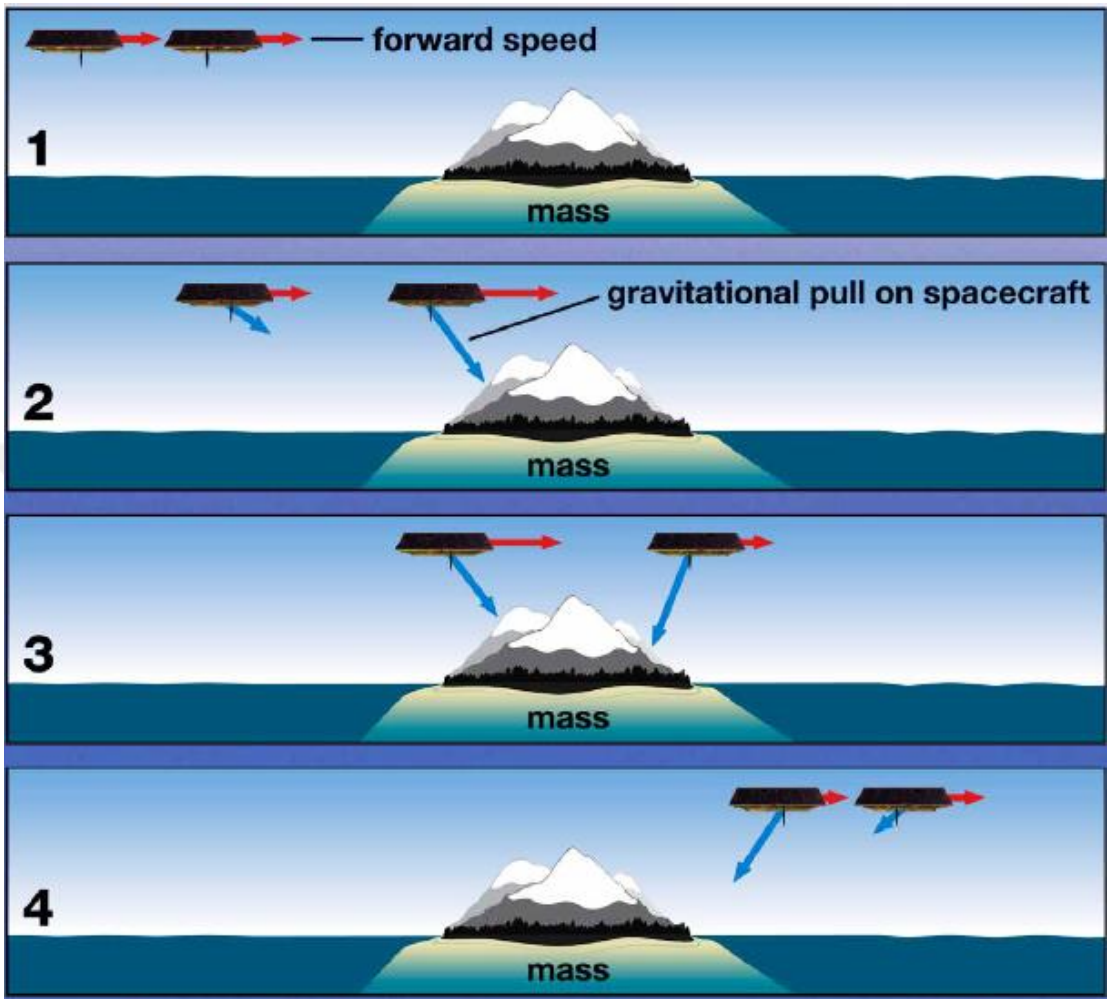


Figure 3.2 The schematic description of the GRACE measurement mechanism. The twin satellite passes over the ocean (Panel 1). Slight changes in the gravity pull don't alter the vertical position of the satellite but it changes the orbital velocity. When the satellite passes over an area of stronger gravity, the first (lead) satellite speeds up and pulls ahead of the second (trailing) satellite (Panel 2). The orbiting speed of the trailing satellite is also increased when it approaches the same spot (Panel 3). After passing over the high gravity location, the satellites decelerate (Panel 4). The consecutive set of satellite accelerations and decelerations engender a set of signals, which are recorded as the variations of gravity (Adopted from Argus et al., 2014).

3.1.1.2 The GRACE Processing Solutions

The GRACE-driven data are in three types including Level 1, Level 2 and Level 3 (Bettadpur, 2016; Karasu, 2019). The L1 data are originally sensed raw values such as the inter-satellite range rate, acceleration, sampling, etc. The GRACE original data are pure gravity signals in anomalies format (L2) showing the variations of the gravity pull of the Earth. These gravity signals are later processed and translated into suitable data of the global mass anomalies (L3) format to be fit for different environmental application purposes. The GRACE signals go through a variety of signal processes implemented by three data processing centers: The Centre for Space Research at University of Texas, Austin (CSR), GeoforschungsZentrum Potsdam (GFZ) and the Jet Propulsion Laboratory (JPL) (Jing et al., 2019). Signal to Noise (S/N) is one of the common problems in every remotely sensed data treatment. Satisfying an appropriate S/N ratio is very important depending on the type of application, in which, a trade-off practice between the volume of data (signal) and the number of errors (noises) within the data gathered by sensors is usually faced. Because the GRACE original data are noisy, the signal-to-noise ratio of the original GRACE products is relatively low (Feng, 2018), thus processing is required to suppress this noise. On the other hand, the noise suppression practice affects the signal volume. To deal with these, a series of processing techniques is required to be applied to the data before any analysis. The GRACE mission applies two different processing approaches to process the gravity signals: spherical harmonics (SP) and ii) mass concentrations (Mascons).

i. Spherical Harmonics (SH)

Spherical Harmonics is a traditional signal processing technique that has been used for the GRACE records since the commence of the project. This solution is a set of gravity parametrizing functions to generate TWS values from the original gravity anomaly signals (Wahr et al., 1998; Bettadpur, 2012). Within this processing approach, the GRACE gravity signals go through a range of processing and post-processing practices. The

processing consists of low pass filtering tasks (truncation, de-striping and gaussian). The signal filtering process is a convolution integral (Jekeli, 1981) done in two steps. First, the systematic North to South stripped form errors (Swenson and Wahr, 2006) are removed. Then, the remaining higher-order errors from the first filtering (random errors) are filtered through Gaussian smoothing (Landerer and Swenson, 2012).

Although the low pass filtering practice reduces the signal amplitude, it also attenuates some of the signal (Eicker et al., 2014). Dutt Vishwakarma et al. (2016) have reported 50% to 70% of signal attenuation over Congo-Zambezi and nearby regions in Southern Africa. To restore the lost signals, scaling is done. The scaling factors for the GRACE products are calculated based on Land Surface Models (LSMs) (Swenson and Wahr, 2002). The scaling factor minimizes the deviation between the filtered and the original signals at a 1-degree resolution (Equation 3.2).

$$M = \sum_{i=1}^{T} \left(\overline{S}_{m,i} - k\hat{S}_{m,j} \right)^2 \tag{3.2}$$

where M is the objective function to be minimized; $\overline{S}_{m,i}$ and $\hat{S}_{m,j}$ are the original and filtered simulated anomalies of TWS, respectively, in month i; k denotes the scaling factor calculated through least square's regression; T signify the number of months.

The scaling or gain factors are self-standing (independent) values derived from the Catchment Land Surface Model (CLSM). The TWS values are multiplied by the scaling factors through processing practice (Eq3.3):

$$\acute{g}(x, y, t) = g\,(x, y, t) \times SF(x, y) \tag{3.3}$$

where $g(x,y,t)$ represents the individual monthly grids, $SF(x,y)$ denotes the scaling factor at each grid and $g'(x,y,t)$ is the gain-corrected time series.

A least square regression is utilized to come up with the scaling factors which are applied to minimize the gaps (differences) between the unfiltered and filtered signals (Landerer and Swenson, 2012). The models go through the same filtering process as the GRACE. The SH processing flow and the spatial distribution of the scaling factors over Turkey are given in Figures 3.3 and 3.4, respectively.

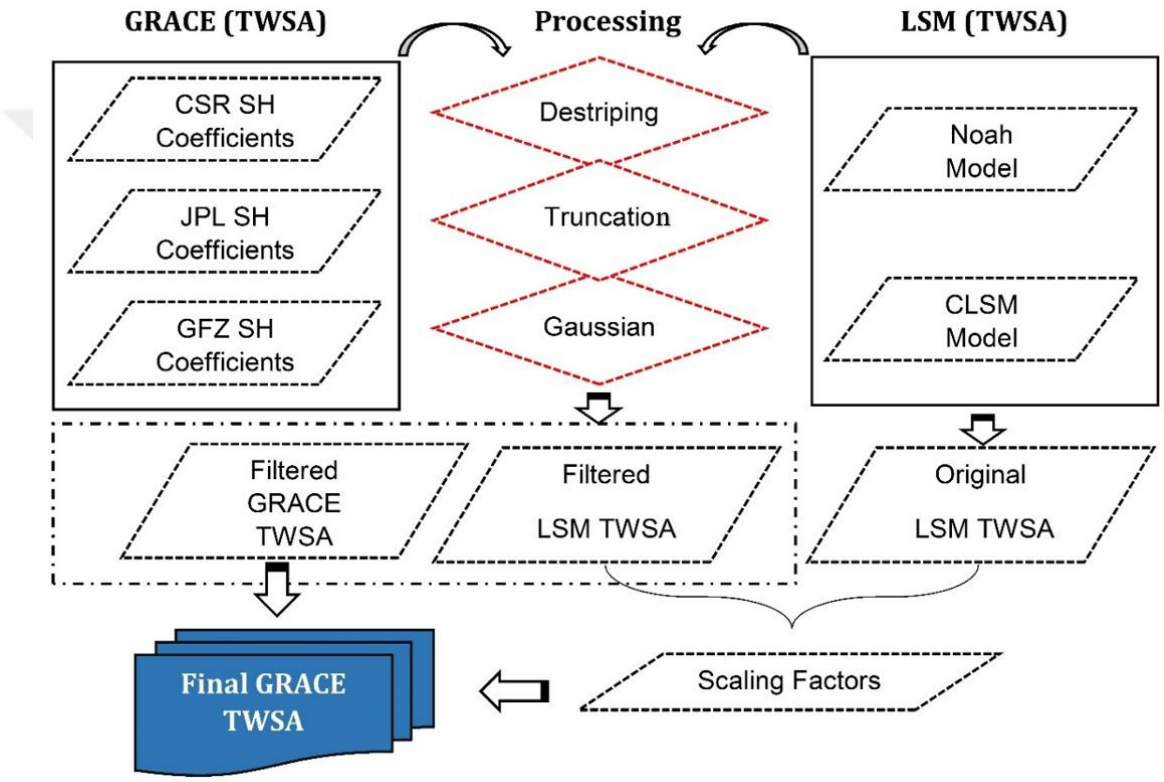


Figure 3.3 The schematic portrayal of the routine signal processing is based on the Spherical Harmonics (SH) solution technique. The original signals are further post-processed (filtered and scaled) after going through “Destriping”, “Truncation” and “Gaussian” filtering processes to come up with noise-reduced

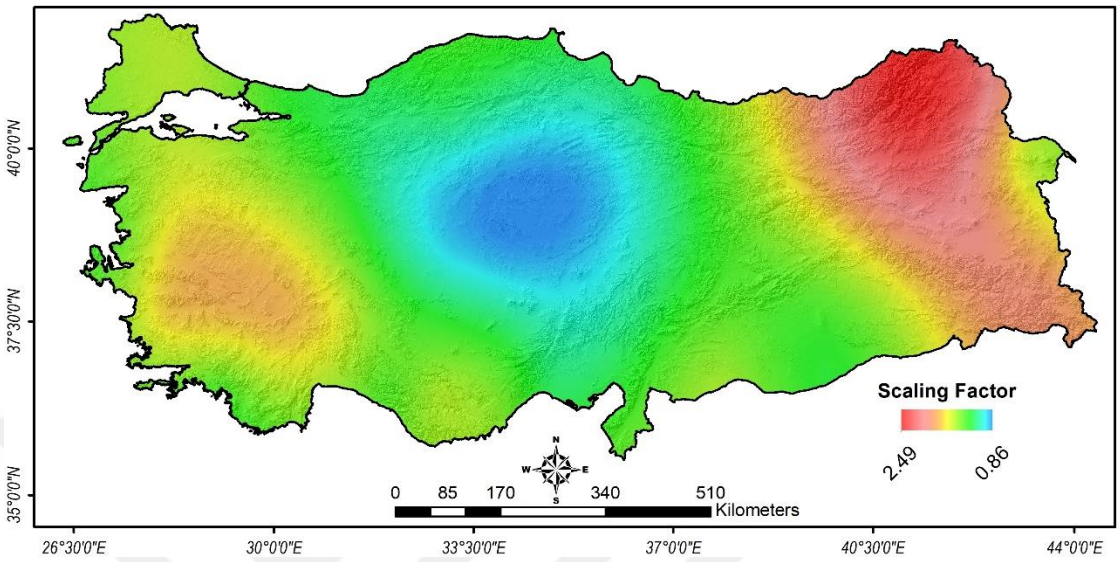


Figure 3.4 Spatial distribution of the scaling factor over Turkey

ii. Mass Concentrations (Mascon)

Mass Concentrations (Mascon) refers to a new alternative processing technique, through which the GRACE signals are parametrized with regional Mascon blocks (Luthcke et al., 2013; Watkins et al., 2015; Save et al., 2016). Mascon's technique does not apply such extent of signal processing as SH. Mascon solution data are already processed and ready to use GRACE estimates with enhanced accuracy and resolution. In this technique, to get rid of signal leakage errors across coastlines, a filter called "Coastline Resolution Improvement (CRI)" was used (Wiese et al., 2016). Through this filtering task, land and ocean signals within the same grid are separated. The combined application of scaling and CRI filters in the Mascon solution approach showed up to 30% (1.5 mm of equivalent water height) enhancement of the ratio of signal per noise over large areas (>160,000 km^2) (Wiese et al., 2016).

The SH and Mascon processing techniques are different in two significant manners. First, unlike the SH for which global parameters are used, the Mascon solution applies

regional parameters as well. Therefore, the resolution of the Mascon solutions improved to half of that of the SH solution (Scanlon et al., 2016). Furthermore, unlike the SH solution for which noise reduction and signal restoration tasks are implemented as post-processings, through which more errors (signal attenuation errors) are added to the processing errors, no post-processing is applied in the Mascons technique. In this way, the signal correlated errors (Scanlon et al., 2016) are suppressed by scaling and filtering offered by Landerer and Swenson (2012), which is more optimal than going through noise removal post-processing practices. This results in the accuracy enhancement and increased data quality for the Mascons dataset (Xu et al., 2019) and consequently more requests for the Mascon data than the SH.

In this study, the monthly estimates of TWS from the JPL processing center were used. The half-degree resolution JPL Mascons dataset was received from NASA's webpage (https://earth.gsfc.nasa.gov/geo/data/grace-mascons). The GRACE estimates suffer from gaps in its monthly records because of the repeat-orbit constellations (Jensen et al., 2020). To have a continuous time series of the GRACE data, the individual data gaps were filled in by applying the Linear Interpolation (LI) method (Long et al., 2015; Yang et al., 2017). A sample set of GRACE pixel values over Turkey and their basic statistics are given in Appendix (Table A-1 and A-2).

3.1.2 MODIS

The Moderate Resolution Imaging Spectroradiometer (MODIS) is a multispectral environmental remote sensing instrument aboard Terra and Aqua satellites. It senses the radiation changes of the Earth's surface features in 36 spectral bands with a spectral range of 0.405 to 14.385 μm (Jin et al., 2017). Several features can be retrieved based on the scanned reflectance. The Terra and Aqua satellites were put in orbit in 1999 and 2002, respectively, to collect near-daily (Salomonson et al., 1989) and monthly estimates on a variety of atmospheric, oceanic and terrestrial variables. The MODIS-derived data are very central for developing validated and globally interactive Earth system models to

support scientists and policy-makers to develop sound ideas regarding the conservation of the environment. The MODIS data are also very important for monitoring different hydrometeorological parameters at global to regional scales. In this study, NDVI values were received from the MODIS mission.

Normalized Difference Vegetation Index (NDVI) is a widely used spectral index used in various environmental studies. The satellite-derived NDVI is susceptible to the variations of the green coverages on the land surface (Goetz et al 2005; Ivanova et al., 2021) and generates very practical datasets on the qualitative and quantitative characteristics of vegetation coverage across large areas (Brown et al., 2008). The normalized difference vegetation index is calculated using near-infrared and red bands according to the following equation:

$$NDVI = \frac{Band_{NIR} - Band_{Red}}{Band_{NIR} + Band_{Red}} \tag{3.3}$$

where NIR and Red sub-indices stand for near-infrared and red band values, respectively. In this study, monthly NDVI products from MODIS satellites were used.

In light of the interactions between groundwater storage variations and that of surface water, which is manifested in terms of the soil moisture that eventually influences vegetation growth, it is said that NDVI can be used as an indicator of groundwater storage (Bhanja et al., 2019). In this study, NDVI values over Turkey were extracted using MODIS Level-3 global vegetation data (MOD13A3). MOD13A3 offers values of NDVI at 1-kilometer spatial resolution in the sinusoidal projection.

3.1.3 Hydroclimatic Models

Model data are mostly used to evaluate the spatio-temporal status of a multitude of hydrometeorological parameters and understand hydrological processes (Devia et al., 2015). The feasibility of the large-scale simulations from different hydrological models paved the way for their extended application scope in a variety of disciplines and environmental-oriented studies. Today, besides the simulated streamflow, a wide range of hydrometeorological variables such as snow cover, soil moisture, actual evapotranspiration (ET) etc. are simulated by these models worldwide (Gilfedder et al., 2012, Chen et al., 2017; Bai et al., 2018). A tremendous set of hydroclimatic models have so far been formulated to explain the global and regional status of hydrological water cycle components, such as the Famine Early Warning Systems Network (FEWS NET) Land Data Assimilation System (FLDAS), the Global Land Data Assimilation Systems (GLDAS), the Climate Prediction Center (CPC) model, the National Centers for Environmental Prediction/National Center for Atmospheric Research (NCEP/NCAR), the European Center for Medium-Range Weather Forecasts (ECMWF) model and the WaterGAP Global Hydrology Model (WGHM) (Jin and Feng, 2013; Long et al., 2017; Fatolazadeh et al., 2020; Khorrami and Gunduz, 2021a). Each model takes benefit of specific algorithms and data simulation methods, which results in different qualities and accuracy levels of the simulations. Though there is no integration of the anthropogenic conditions including the consumptive surface and groundwater, these models are deemed to delegate the actual mass anomalies (Longuevergne et al., 2013; Scanlon et al., 2012a). According to the literature, the GLDAS, the FLDAS and the WGHM models have the best precision in comparison with other hydrological models (Jin et al., 2012; Jin and Feng, 2013; McNally et al., 2017).

The scientific community has witnessed grave evolution in the applications of the hydrological models during the recent decades. These models are used not only to simulate the streamflow anomalies, but also used to model snow cover, soil moisture, actual

evapotranspiration (ET) and groundwater level (Gilfedder et al., 2012, Cai et al., 2014a, Zhang et al., 2016, Chen et al., 2017).

3.1.3.1 GLDAS Model

The Global Land Data Assimilation System (GLDAS) is a widely utilized large-scale hydrological model established by NASA and the National Centers for Environmental Prediction. Within the framework of this model, different hydrometeorological variables are simulated by integrating some in-situ and satellite observations at a higher resolution. The GLDAS utilizes advanced land surface models (LSMs), such as Community Land Model (CLM), Variable Infiltration Capacity (VIC) model, Noah model, Mosaic model and Catchment land surface model (CLSM), to simulate the land surface states and fluxes (Hu et al., 2019). The spatial resolution VIC, Mosaic and CLM is 1 degree while the Noah and the CLSM models produce 0.25-degree resolution data (Wang et al., 2016). The CLSM is the only model used by the GLDAS mission to simulate the GWS. The characteristics of different LSMs used by the GLDAS mission are given in Table 3.2. The GLDAS-derived simulations have been used for variegated purposes such as the evaluation of the terrestrial water changes, drought monitoring, soil moisture changes and groundwater storage changes in combination with the GRACE data (Yang et al., 2013; Huang et al., 2013; Hao et al., 2014; Zawadzki and Kexdzior, 2014; Yang and Chen 2015; Chen et al., 2020; Zhang et al., 2021b). In this study, the simulated variables from the Noah and CLSM models were integrated into the analysis.

Table 3.2 Characteristics of the Land Surface Models Offered by the GLDAS

Model	Hydrological Components Included				Spatial Resolution	Temporal Resolution
	Soil Moisture	Snow Water	Surface Water	Groundwater		
VIC	×	×	×	-	1˚	Monthly
Mosaic	×	×	×	-	1˚	Monthly
CLM	×	×	×	-	1˚	Monthly
Noah	×	×	×	-	0.25˚	Monthly
CLSM	×	×	×	×	0.25˚	Daily

3.1.3.1.1 Noah Model

The new Noah model was developed by improving the recent LSM physics (Ek et al., 2003) to its early version (Niu et al., 2011). The GLDAS-2.1 Noah model makes use of 36 land surface fields from January 2000 to present to simulate different parameters with a spatial and temporal resolution of 0.25 degree 3 hours, respectively. The Noah model simulates the soil moisture at 4 different depths including: 0–10 cm, 10–40 cm, 40–100 cm and 100–200 cm (Bi et al., 2016). The Noah outputs were used in this thesis in the GRACE isolation analysis.

3.1.3.1.2 CLSM Model

The Catchment Land Surface Model (CLSM) is a land model used by the GLDAS mission to provide different hydrometeorological parameters at daily resolution. The CLSM is also different from the other GLDAS-LSMs in terms of the modelling elements. Unlike the other LSMs, the CLSM benefits from a topographically derived catchment instead of a grid (Koster et al., 2000). Thanks to this modelling structure, the CLSM is

able to generate the simulated soil moisture values in more soil layers (e.g., 0–1.8 cm, 1.8–4.5 cm,4.5–9.1 cm, 9.1–16.6 cm, 16.6–28.9 cm, 28.9–49.3 cm, 49.3–82.9 cm, 82.9–138.3 cm, 138.3–229.6 cm and 229.6–343.3 cm) (Bi et al., 2016). It is also able to simulate the groundwater storage based on the catchment deficit (amount of water needed to fill a catchment), which is deemed as the main contributor for the CLSM model (Xia et al., 2017). The CLSM and the Noah models are alike from the viewpoint of the used static and forcing input data. The only difference in their outputs is the temporal resolution and the simulation of groundwater storage by the CLSM.

According to Khorrami and Gunduz (2021a), the CLSM-simulated GWS is in a moderate agreement with the GRACE-derived GWS over Turkey. On the other hand, the NASA released a new version of the CLSM model with improved spatio-temporal characteristics by assimilating it into the GRACE estimates. Since the simulations from the CLSM are thought to be enhanced through data assimilation techniques, the calibrated CLSM model was utilized in this study to evaluate its associations with the GRACE estimates.

3.1.3.2 FLDAS Model

Famine Early Warning Systems Network Land Data Assimilation System (FLDAS) is a data assimilation project being run jointly by the U.S. Geological Survey (USGS), Earth Resources Observation and Science (EROS) Center, NASA Goddard Space Flight Center (GSFC) and the University of California Santa Barbara (UCSB) Climate Hazards Group (CHG) (McNally et al., 2017). Like the commonly used GLDAS model, FLDAS also simulates different hydro-meteorological variables including rainfall, temperature, evapotranspiration, runoff, etc. by integrating remote sensed, modeled and in-situ observations at a global scale. The simulations are done under two LSMs such as the Variable Infiltration Capacity (VIC) and the Noah model (McNally et al., 2017). The spatial resolution of the VIC and Noah models are 0.25 and 0.1 degrees, respectively.

Noah is one of the well-known LSMs widely used by hydrologic modelers, by which the water and energy fluxes are simulated in four soil layers. In this project, simulated variables of soil moisture, snow water, evapotranspiration, rainfall and runoff were extracted from the latest version (version 4) of the FLDAS-Noah. The FLDAS-Noah outputs were then used to both isolate the GWS from the GRACE as well as downscaling the GRACE estimates at finer resolution.

3.1.3.3 WGHM Model

The WaterGAP Hydrology Model (WGHM) is one of the pioneering hydrological modeling missions developed with the primary motivation of quantifying large-scale (regional to global) water resources by concentrating on the anthropogenic impacts to evaluate water stress. It has also turned out to be a good-performing model for simulating the water storage status of aquifers lakes as well as wetlands (Müller Schmied et al., 2021). The WaterGAP model makes use of the available global meteorological data (e.g, air temperature, precipitation, downward shortwave radiation and downward longwave radiation) to generate 0.5-degree simulated surface of microscale terrestrial water cycle compartments (Alcamo et al., 2003; Döll et al., 2002). Waterflow and water storage values are simulated on continents by discerning the storage anomalies of snow, canopy, soil, groundwater and surface water (Döll et al., 2014). The impacts of human water consumption on terrestrial water storage are explicitly simulated (Sutanudjaja et al., 2018). The model utilizes water use models to simulate the volume of water consumption in different sectors including agriculture, livestock, domestic, industry and the water used for cooling thermal power (Flörke et al., 2013; Portmann, 2017). The grid-wise water simulations of the WaterGAP agree well with the global data (Alcamo et al., 2003). In this study, the modeled variations in the total water storage and groundwater storage of Turkey as well as its groundwater abstraction values were extracted from 0.5-degree resolution WaterGAP model outputs.

3.1.3.4 ERA-5 Model

The ERA5 is the latest version (5th generation) of the European Centre for Medium-Range Weather Forecasts (ECMWF) model, which provides data from the atmosphere, ocean and land surface. It benefits from a sophisticated Land Data Assimilation System to analyze land surface variables (Hersbach et al., 2020). By simulating a wide range of hydrometeorological variables from 1979 onward, the ERA-5 has so far backed up the scientific community. The ERA5-Land is a high-resolution ERA5 model, which is derived by atmospheric forcing based on the near-surface meteorology state and flux fields. ERA5-Land generates global estimates of up to 50 parameters describing the water and energy cycles over land with the spatial and temporal resolutions of 10 km and 1-hour, respectively (Cao et al., 2020). The fine resolution data from the ERA-5 model were used to assess the uncertainties of the simulated soil moisture and snow water from the FLDAS model.

3.1.3.5 CHELSA Model

The Climatologies at High Resolution for The Earth's Land Surface Areas (CHELSA) is a new global climatic model, hosted by the Swiss Federal Institute for Forest, Snow and Landscape Research WSL, which offers high-resolution monthly climatic parameters. It applies a quasi-statistical downscaling algorithm (Karger et al., 2017) to downscale the ERA-Interim variables from 10 km to 1 km spatial resolution. The CHELSA takes the benefit of orographic predictors such as wind fields, valley exposition and boundary layer height with a bias correction to generate high-resolution precipitation estimates (Karger and Zimmermann, 2019). The CHELSA model supplies monthly-downscaled temperatures and precipitation products in two types including "CHELSAcruts" and "Timeseries". While the CHELSAcruts range from 1979 to 2016 (Khorrami and Gunduz, 2021a), the Timeseries products cover data from 1979 to 2018. In this study, the CHELSAcurts grided precipitation data was used.

3.1.4 Global Drought Data

3.1.4.1 SPEI

The Standardized Precipitation-Evapotranspiration Index (SPEI) is a multiscale drought index calculated based on monthly climatic water balance (Beguería et al., 2010) where the deviation of precipitation and evapotranspiration records are used instead of mere precipitation as done in Standardized Precipitation Index (SPI) calculation (Khorrami and Gunduz, 2021b). The integration of evapotranspiration into the calculation process is the unique aspect of the SPEI, through which the evaporative demand is applied to better describe the global hydrometeorological extremes (Beguería et al., 2010).

Currently, for global SPEI data, two available datasets are offering ready-to-use data. These databases are "SPEI Global Drought Monitor (SGDM)" (https://spei.csic.es/map/maps.html#months=1#month=9#year=2021) and the "SPEIbase" (https://spei.csic.es/database.html). Both of the datasets are in 0.5-degree resolution and grid format. The major difference between them lies in the way the Potential Evapotranspiration (PET) is calculated. Unlike the SGDM, which is based on the Thornthwaite PET estimation, the SPEIbase applies PET estimated based on the FAO-56 Penman-Monteith method. Because the Penman-Monteith method is considered a premium technique for deriving drought indices, the Penmann-Monteith derived SPEIbase dataset is highly recommended for most uses especially for the long-term climatological evaluation and monitoring. The SPEIbase supplies the scientific community as well as the public sector with the monthly grided multiscale (1- 48 months) SPEI data in a temporal window ranging from 1901 to 2018. The SPEI data were used for drought evaluation over Turkey.

3.1.5.2 scPDSI

The Palmer Drought Severity Index (PDSI) is a water balance-based indicator of soil moisture availability (Briffa et al., 2009). The PDSI is calculated by using historical precipitation and temperature data integrated into the soil characteristics of the area of concern (Briffa et al., 2009). The hydrometeorological condition is defined according to 11 classes depicting the relative soil moisture status over a given area determined by Palmer (1965). The PDSI has been used for analyzing and monitoring hydrometeorological events all over the world (van der Schrier et al., 2013). However, it is associated with specific restrictions. Well et al. (2004) casted doubt on the efficacy of the original PDSI metric for drought analysis stating that the index is lame in defining the climatic status over diverse climatological regions. They also suggested that the PDSI suffers from a bimodal distribution where maxima in the distribution fall outside the near-normal category (Briffa et al., 2009). Intending to make the PDSI results more comparable over regions with climatic diversity, Wells et al. (2004) developed an improved PDSI called the Self-calibrating Palmer Drought Severity Index (scPDSI). In this thesis, the monthly scPDSI values of Turkey were received from the Climatic Research Unit (CRU) at the University of East Anglia, which generates an open to public 0.5-degree global gridded scPDSI dataset (https://www.uea.ac.uk/web/groups-and-centres/climatic-research-unit/data).

3.1.5 In-Situ Observations

Field-based observations of precipitation and depth to groundwater were received from the Turkish Meteorological Service (TMS) and The State Hydraulic Works (TSHW), respectively. The monthly precipitation records were received from 108 meteorological stations over Turkey with a temporal window of 2003-2017. Characteristics of the used 108 main meteorological stations of Turkey are given in the Appendix (Table A-3).

For groundwater data, the seasonal records of the Western Anatolian Basins (WAB) from 2003 to 2016 were used. The characteristics of the groundwater observation wells (GOW) utilized in this study are given in Table 3.3.

Table 3.3 Characteristics of the seasonal groundwater observation wells used in this study

Basin ID	**Basin Name**	**Total number of the GOWs**	**Temporal Resolution**	**Temporal Window**
04	North Aegean	15	Seasonal	2003-2016
05	Gediz	10		
06	Kucuk Menderes	57		

The GRACE mission gives the monthly variations of GWS. To validate the GRACE-derived GWS with in-situ observations of depth-to-GW (DTG), the latter should go through a statistical process to be converted into field-based GWS. To this end, first, the DTG data of each observation well was changes to the groundwater level (GWL) based on the surface elevation (Z) of each corresponding well (Eq 3-12).

$$GWL = Z - DTG \tag{3.12}$$

Then the variations of GWL (ΔGWL) were extracted by subtracting the same baseline as the GRACE mission (mean of 2004-2009) (Moghim, 2020). Finally, the in-situ GWS values were calculated by using the specific yield (Sy) of each well (Eq 3-13). The GWL values were converted into GWS by being multiplied with specific yield (Sy) for the unconfined aquifers or storativity for the confined aquifers.

Specific Yield (Sy) is the prospective volume of liquid water that is drained from an unconfined aquifer under gravity. It is a unitless hydrological parameter calculated as the

ratio of the volume of water to the unit change in the water table height. The GWS change for each well can be calculated as:

$$\Delta GWS = S_y \times \Delta GWL \tag{3.13}$$

Specific yield changes according to the aquifer properties and geological structures (Karasu, 2019). The accurate estimation of this parameter requires implementation of pumping tests. Unfortunately, there is no reliable information on the estimated Sy over the WAB. Therefore, the Sy of the seasonal observation wells, used for validation purpose, was estimated based on the values reported by Akarsu (2019) for each lithological structure of the wells in the study area (Table 3.4.). The Sy estimates used in this study are ranged from 0.17 to 0.26. Concise information on the datasets used in this study is given in Table 3.5.

Table 3.4 Specific yield values for geological materials (After Akarsu, 2019)

Aquifer Material		(Morris & Johnson, 1967)		(Johnson, 1967)	(Health, 1983)
		S_y Range (%)	S_y Mean (%)		
Siltstone		0.9 – 32.7	12	-	-
Clay		1.1 – 17.6	6	2	2
Silt		1.1 – 38.6	20	8	-
Loess		-	18	-	-
Tuff		2.0 – 47.0	21	-	-
Limestone		0.2 – 35.8	14	-	18
Schist		-	26	-	-
Basalt		-	-	-	8
Fine	Sand	1.0 – 45.9	33	21	22
Medium		16.2 – 46.2	32	26	
Coarse		18.4 – 42.9	30	27	
Fine	Sandstone	2.1 – 39.6	21	-	6
Medium		11.9 – 41.1	27	-	
Fine	Gravel	12.6 – 39.9	28	25	19
Medium		16.9 – 43.5	24	23	
Coarse		13.2 – 25.2	21	22	

Table 3.5 Specifications of the datasets used in this study

Mission	Resolution		Data Link
	Temporal	Spatial	
GRACE/GRACE-FO JPL	Monthly [2002-present]	0.5º	https://earth.gsfc.nasa.gov/geo/data/ grace-mascons
GLDAS-Noah	Monthly [2000- present]	0.25º	https://disc.gsfc.nasa.gov/datasets?keywords=GLDAS
GLDAS-CLSM	Daily [2003- present]	0.25º	https://disc.sci.gsfc.nasa.gov/datasets/GLDAS_CLSM025_DA1_D_2.2/summary?keywords=GRACEDA
FLDAS-Noah	Monthly [1982-present]	0.25º	https://disc.gsfc.nasa.gov/datasets/FLDAS_NOAH01_C_GL_MA_001/summary
FLDAS-Noah	Monthly [1982- present]	0.1º	https://disc.gsfc.nasa.gov/datasets/FLDAS_NOAH01_C_GL_M_001/summary
WGHM-WaterGAP2.2	Monthly [1901-2016]	0.5º	https://www.uni-frankfurt.de/77679007/9__GW_Stress_Indicators
ERA5-Land	Monthly [1950- present]	0.1º	https://cds.climate.copernicus.eu/cdsapp#!/dataset/reanalysis-era5-land-monthly-means?tab=overview
CHELSA	Monthly [1901-2016]	0.0083º	http://chelsa-climate.org
MODIS-MOD13C2	Monthly [2003- present]	0.05º	https://lpdaac.usgs.gov/products/mod13c2v006/
Field Observations (P)	[2003-2016]	-	Turkish State Meteorological Service (TSMS)

Table 3.5 Continues

Mission	Resolution		Data Link
	Temporal	Spatial	
Field Observations (GW)	[2003-2016]	-	Turkish State Hydraulic Works (TSHW)

3.2 Spatial Aggregation and Resampling

Spatial aggregation and resampling are two technical GIS and remote sensing terms referring to the manipulation of gridded datasets to derive a new set of spatial information. Through the aggregation process, grid information of the different spatial thematic layers (Gómez et al., 2009) are aggregated to come up with a single layer representing the unit characteristics of the variable of interest over the area of concern. Spatial resampling, on the other hand, is an interpolation technique and a set of mathematical functions for changing the geometric characteristics of spatial data to transform them to a particular new scale and projection. Resampling practice can be implemented on gridded data via three techniques namely Nearest Neighbor, Bilinear and Cubic Convolution (Parker et al., 1983; Baboo and Devi, 2010).

- The nearest neighbor is the simplest resampling technique, which makes use of the closest sample points to the target location in the original raster (Baboo and Devi, 2010). The output raster of this method bears the original point values as the original layer; however, it may have duplicated or lost pixel values.

- The Bilinear technique applies the pixel values of the four weighted points around (generally in the center or upper left of the pixel) the target location (Baboo and Devi, 2010). The new pixel values are altered due to the averaging process. The bilinear algorithm performs the calculations in both directions.

- The cubic convolution is similar to the Bilinear technique in terms of pixel averaging practice. The only difference is that, in Cubic convolution, an average of 16 pixels are used to resample them to the new location. As a result, it requires more processing time approximately 10 times more than the Bilinear method (Baboo and Devi, 2010). Although through cubic convolution results have better visual quality, the over-smoothing of the original raster may result in unrealistic values, which go beyond the range of the selected pixels for averaging. In Figure 3.5 the schematic description of the resampling techniques is given.

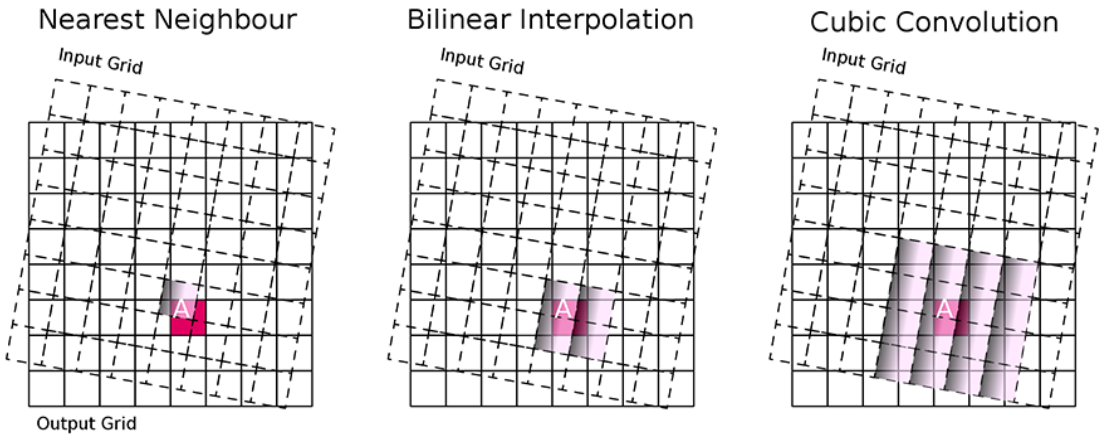


Figure 3.5 Spatial resampling process through different techniques

In this study, the spatial aggregation of the SMS layers simulated by the Noah model from GLDAS and FLDAS missions in various vertical layers of the soil [0-10, 10-40, 40-100 and 100-200 cm] was implemented to come up with a single representative layer of the soil moisture status of the study area. Furthermore, on account of the mismatches of the used datasets in this study from the viewpoint of their spatial resolution, Bilinear resampling was utilized to bring all the analysis data into the resolution of the GRACE JPL Mascons (0.5-degree) in an attempt to ensure the spatial consistency of the layers. The spatial aggregation (re-griding) has the unique merit of bringing all the study layers (data) from different spatial characteristics to the same, comparable scale to guarantee the

accuracy of the comparisons reducing the influences of finer-scale noises (Ljungqvist et al., 2019).

3.3 Time Series Decomposition

The time series of the GRACE-driven TWS can be partitioned into three components such as trend, seasonal pattern and residual pattern (Equation 3.4). The GRACE time series are generally decomposed for different reasons particularly for better description of the role and impact of each component of the GRACE time series on the temporal variability of the GRACE-derived TWS (Barletta et al., 2012; Frappart et al., 2013; Humphrey et al., 2016).

$$\Delta TWS_{\,Total} = \Delta TWS_{\,Trend} + \Delta TWS_{\,Seasonal} + \Delta TWS_{\,Residual} \quad (3.4)$$

In statistics, partitioning time series into its components is central to the statistical analysis of data, through which secular and seasonal trends are unearthed (Dokumentov and Hyndman, 2020). Different decomposition techniques are generally divided into two time series decomposition approaches: i) additive and ii) multiplicative approaches (Dokumentov and Hyndman, 2020). Eq. 3.5 and 3.6 define these two models, respectively:

$$Y_t = S_t + T_t + R_t \quad (3.5)$$

$$Y_t = S_t \times T_t \times R_t \quad (3.6)$$

where. Y_t delegates the actual time series data and S_t, T_t and R_t signify the seasonal trend, long-term trend and sub-seasonal residual parts of each time series data, respectively (Adenomon and Ojehomon, 2014; Humphrey et al., 2016).

The suitability of these techniques is evaluated through statistical metrics and the most commonly used metrics are Mean Absolute Deviation (MAD), Mean Absolute Percentage

Error (MAPE) and Mean Squared Deviation (MSD) (Karmaker et al., 2017). These parameters are defined in Eq. 3.7, 3.8 and 3.9, respectively.

$$MAD = \frac{\sum_{i=1}^{n} |e_t|}{n} \tag{3.7}$$

$$MAPE = \frac{\sum_{i=1}^{n} \left|\frac{e_t}{x_t}\right|}{n} \times 100 \tag{3.8}$$

$$MSD = \frac{\sum_{i=1}^{n} |e_t|^2}{n} \tag{3.9}$$

where e and n denote the deviation of the actual time series values (x) from the predicted and the number of data points respectively. Lower values demonstrate a better fit of the model (Cooray, 2008).

3.4 Vertical Decomposition of the GRACE TWS

The GRACE gives vertically integrated estimates of the Earth's TWS. To investigate the variations of groundwater storage using the GRACE-derived TWS, vertical decomposition of the TWS values has to be implemented. To this end, the simulated hydrological cycle parameters should be integrated into the TWS data. Different hydrological model outputs can be used but the simulation of the GLDAS model is among the most preferred and popular data sources for this purpose. The GRACE-derived TWS represents the storage variations of different hydrological cycle compartments such as soil moisture, snow water, surface water and groundwater (Equation 3.10).

$$\Delta TWS = \Delta GWS + \Delta SWE + \Delta SMS + \Delta SWS \tag{3.10}$$

where GWS, SWE, SMS and SWS denote groundwater storage, snow water equivalent, soil moisture storage and surface water storage, respectively.

The variations in GWS can be retrieved from the vertically integrated TWS using the Equation (3.11).

$$\Delta GWS = \Delta TWS - [\Delta SWE + \Delta SMS + \Delta SWS] \quad (3.11)$$

The monthly estimates of the SWE, SMS and SWS are mandatory to be integrated into the GRACE-derived TWS to extract the GWS values. According to Rodell et al. (2005), the seasonal and inter-annual changes in biomass are very trivial that the GRACE satellite cannot detect them. Moreover, excluding the humid tropical regions of the world, the impact of the variations of surface water is typically insignificant relative to that of the remaining compartments (SMS, GWS and SWE) (Rodell and Famiglietti 2001; Rodell et al., 2009). In light of the mentioned facts and according to the previously published studies, the GWS component of Turkey is decomposed from GRACE TWS based on the simplified equation (Equation 3.12) by integrating only the SWE and SMS variables (Yang et al., 2015; Deng and Chen, 2017; Hu et al., 2019; Khorrami and Gunduz, 2021a).

$$\Delta GWS = \Delta TWS - [\Delta SWE + \Delta SMS] \quad (3.12)$$

3.5 Calculation of the Drought Indices

The GRACE-derived indices are widely used for the assessment and monitoring of hydrogeological events. The GRACE-derived Enhanced Water Storage Deficit Index (EWSDI) was defined and used here in this study by using the decomposed TWS values from the GRACE for drought assessment. In addition, Standardized Precipitation Index (SPI) based on the in-situ observations of precipitation, the modeled Standardized Precipitation-Evapotranspiration Index (SPEI) and the Self-Calibrated Palmer Drought Severity Index (scPDSI) were also used to have a comprehensive evaluation of the experienced extreme events in Turkey on the variations of its groundwater storage.

3.5.1 Enhanced Water Storage Deficit Index (EWSDI)

Developed by Khorrami and Gunduz (2021b), the Enhanced Water Storage Deficit Index (EWSDI) is an enhanced form of the commonly used WSDI index, for which the mean and standard deviation of the time series of The Water Storage Deficit (WSD) concept that was originally developed by Thomas et al. (2014). The deviations of the water storage from the monthly climatology values (Eq. 3.13) given by WSD showcase the water storage deficit and surplus in terms of negative and positive values, respectively. GRACE-based WSDI (Sinha et al., 2017; Yu et al., 2019) is calculated based on WSD values as follows:

$$WSD_{ij} = TWSA_{ij} - \overline{TWSA_j} \tag{3.13}$$

$$WSDI_{ij} = \frac{WSD_{ij} - \mu}{\sigma} \tag{3.14}$$

where WSD_{ij} and $WSDI_{ij}$ represent water storage deficit and its index for the month j of the year i, respectively. $\overline{TWSA_j}$ is the climatology value of month j. μ and σ denote the mean and standard deviation of the water storage deficit (WSD) time series, respectively.

Khorrami and Gunduz (2021b) proposed the EWSDI as a new grid-based enhanced approach to boost the accuracy of WSDI by making use of the grided mean and standard deviation of WSDI (Eq 3.15):

$$EWSDI_{ij} = \frac{WSD_{ij} - \left|\bar{X}_{ij}\right|}{\sigma_{ij}} \tag{3.15}$$

3.5.2 Standardized Precipitation Index (SPI)

Standardized Precipitation Index (SPI) is among the most interesting and widely used hydrometeorological indices recommended by the "Lincoln declaration on drought indices" (Stagge et al., 2015). The application of SPI is quite common within the scientific and governmental institutions for the detection and surveillance of extreme dry and wet periods (Hayes et al., 2011). It is computed through fitting a gamma distribution (Hosseini-Moghari et al., 2019) to the raw observations of precipitation and then changing it to a normal distribution. Gamma distribution defines the variability of precipitation and is calculated by its probability density function (Abeysingha and Rajapaksha, 2020):

$$g\,(x) = \frac{1}{\beta^{a}\Gamma(a)} x^{a-1} e^{-(\frac{x}{\beta})}, \qquad for\ x > 0, \tag{3.16}$$

$$a = \frac{1}{4a}\left[1 + \sqrt{1 + \frac{4A}{3}}\right] \tag{3.17}$$

$$\beta = \frac{\bar{x}}{a} \qquad where\ A = (\bar{x}) - \frac{\sum \ln(x)}{n} \tag{3.18}$$

where, x represents precipitation records, a , β and $\Gamma(a)$ denote the shape parameter, scale parameter and gamma distribution respectively, n is the number of observations.

The cumulative probability of precipitation is defined by using the subsequent parameters. At x=0, the gamma function is undefined, therefore, the cumulative probability is computed as:

$$H(x) = q + (1 - q)G(x), \tag{3.19}$$

where q and G (x) signify the zero-precipitation probability and the cumulative probability of the incomplete gamma function, respectively. H (x) is then transformed to the standard normal distribution, which defines the SPI values (Tigkas et al., 2015; Abeysingha and Rajapaksha, 2020; Dikici and Aksel, 2021).

3.6 Trend Analysis

The trend analysis methods for the detection of the significance downward and upward trends of different hydroclimatic parameters are classified into two broad classes of parametric and non-parametric techniques. While the parametric techniques make use independent data with normal distribution, in the non-parametric techniques the normal distribution is not required for the used data (Gocic and Trajkovic, 2013). In this study, the spatio-temporal trends of the data were investigated based on the two well-known non-parametric trend analysis tests of Mann-Kendall and Sen's slope estimator.

3.6.1 Man-Kendall Trend Test

The Man-Kendall (MK) trend test (Mann, 1945; Kendall, 1975) was utilized to unearth the trend of the time series. MK is a non-parametric statistical test, for which no particular distribution of the input variables is required (Alhaji et al., 2018) therefore, it is commonly utilized for trend analysis of the time series of hydrometeorological variables (Yue et al., 2002; Modarres and Silva, 2007; Tabari and Morafi, 2011; Wang et al., 2020). The MK tend test is done through the following equations:

$$S = \sum_{i=1}^{SS-1} \sum_{j=i+1}^{SS} sgn(x_i - xi) \dots for\ j > I \qquad (3.20)$$

$$V(S) = \frac{SS(SS-1)(2SS+5) - \sum_{m=1}^{SS} ti(m-1)(2m+5)m}{18} \qquad (3.21)$$

$$Z = \begin{cases} \frac{S-1}{\sqrt{V(S)}} & S > 0 \\ 0 & S = 0 \\ \frac{S+1}{\sqrt{V(S)}} & S < 0 \end{cases} \quad (3.22)$$

where SS is the sample size, x is the variable, V(S) is the variance of S, t_i is the number of ties of length m and Z is the standardized S (Blain, 2013).

In the MK test, the null hypothesis (H_0) says that there is no trend in the time series whose authenticity can be checked according to Z value. H_0 is rejected if $|Z| > Z_{1-(\alpha/2)}$. In this case, H_0 is rejected so it can be stated that there is a trend in the time series. The tendency of trend is also determined according to the value of Z. Positive Z indicates an ascending trend while negative Z denotes a descending trend (Gocic and Trajkovic, 2013). In this study, the significance of each tiemseries trend was evaluated at the significance levels (α) of 0.05.

3.6.2 Sen's Slope Estimator

The Sen's slope estimator technique was established by Sen (1968) as a non-parametric test to approximate the trend slope. It has been widely applied for trend analysis of a variety of hydrometeorological variables (Yue and Hashino, 2003; Yunling and Yiping, 2005; Partal and Kahya, 2006; Tabari and Marofi, 2011; Gocic and Trajkovic, 2013; Dawood, 2017; Mohsin and Lone, 2021). In its calculation process, the Sen's Slope estimator goes through the following steps:

$$Q_i = \frac{X_j - X_k}{j - k} \quad for\ i = 1, \dots, N, \quad (3.23)$$

where, X_j and X_k represent the data values at times j and k (j>k) respectively (Gocic and Trajkovic, 2013). The Sen's slope is calculated as the median of the slope:

$$Q_{med} = \begin{cases} Q_{[(N+1)/2],} & for\ odd\ N \\ \dfrac{Q_{[N/2]} + Q_{[(N+2)/2]}}{2} & for\ even\ N \end{cases} \quad (3.24)$$

The calculated Q_{med} determines the reflection and the steepness of the existing trend via its sign and value (Gocic and Trajkovic, 2013). The sen's slope method was used to define the trends' magnitude.

3.7 Machine Learning Statistical Downscaling

Statistical downscaling is the most preferred downscaling approach because of its convenience of application. It is based on the statistical interrelations between the input data and the predictand. There are different techniques developed to statistically enhance the resolution of remote sensing data. These techniques are the water balance equation method (Ning et al., 2014; Yin et al., 2018), Markov chains (Hou et al., 2017), regression kriging (Jin et al., 2018), Machine learning algorithms (Miro et al., 2018; Li et al 2019; Ali et al., 2021) and stochastic models (So et al., 2017). In this study, Random Forest Machine Learning (RFML) algorithm was utilized as a statistical downscaling (SD) technique to derive basin-scale finer resolution TWS and GWS from coarse resolution GRACE estimates.

3.7.1 Random Forest (RF)

As one of the commonly applied bagging or bootstrap aggregating ensemble algorithms (Jyolsna et al., 2021; Zounemat-Kermani et al., 2021), Random Forest (RF) is a nonlinear machine learning model (Rahaman et al., 2019b) proposed by Breiman (2001), which can be applied for both classification and regression problems. Bagging or bootstrap aggregating refers to the method of selecting random training samples from the original training data for model training with replacement. A combination of the models' outputs

is done according to the majority vote (Zounemat-Kermani et al., 2021). Consisting of a combination of multiple classifications and regression trees (CART), RF generates a regression tree based on the bagging method and uses the average results of each decision tree (Rahaman et al., 2019b). The RF algorithm is used for both classification purposes and developing regressive models (Zounemat-Kermani et al., 2021). Averaging the outcomes of several models used in the RF prediction process results in the decreased over-fitting of the predictions. Therefore, this model is preferred over the single decision tree models (Zounemat-Kermani et al., 2021).

In light of its unique advantages, such as the feasibility of working with numerous inputs, high precision and detection of the significance of the variables (Rahaman et al., 2019b; Chen et al., 2019b), the RF model has a widespread application in remote sensing and hydrology (Hua et al., 2018). The RF model was designed as follows: at the first step, two-third of the input variables were used to extract the model training samples based on the Bootstrap technique (Ali et al., 2021). Then, the remaining data (also known as the Out of Bag (OOB) dataset) were used to test the accuracy of the model. Afterward, for each sample, a decision tree is constructed and all of the sample decision trees are combined into a random forest model. Figure 3.6 describes how RF functions in forecasting values.

The predictive power of each variable was evaluated using a variable importance measure predictive (VIMP) test (Ali et al., 2021). The greater the VIMP, the stronger the variable. Eventually, the predicted values were compared with the dependent variable to compute residuals at a coarse resolution and the model was run on the independent variable at a finer resolution (10 km). The fine resolution TWS estimates were generated after residual correction.

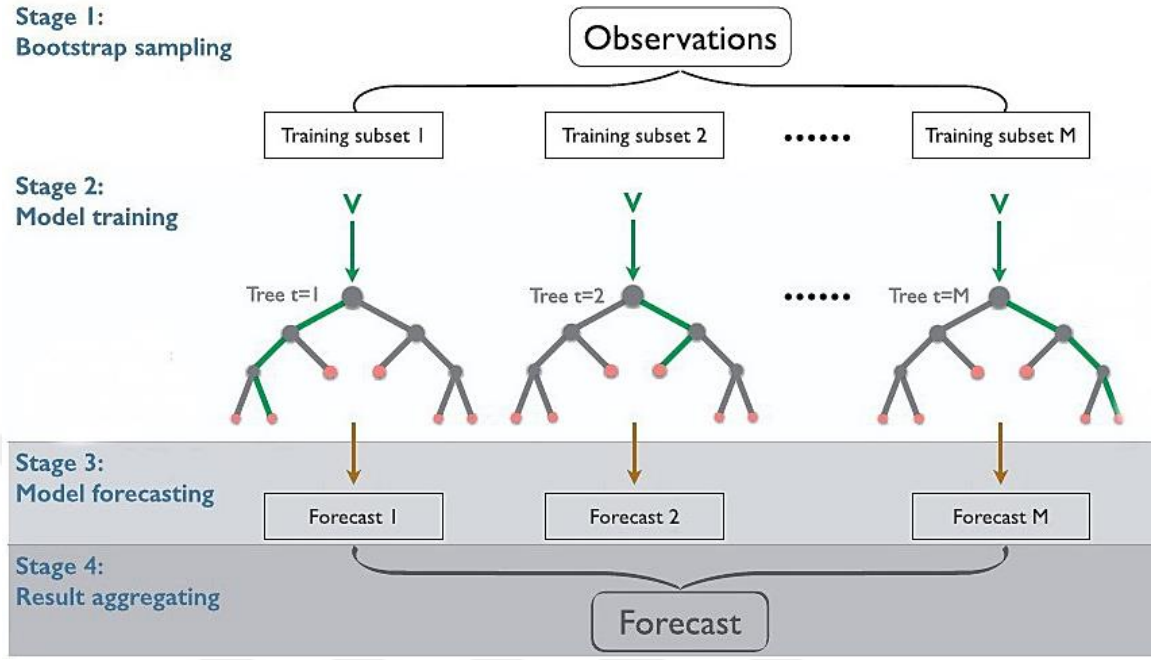


Figure 3.6 Schematic flow of the bagging ensemble Random Forest (RF) regression (After He et al., 2016)

3.7.2 Designing the Downscaling Algorithm

The model designation to downscale the GRACE-TWS estimates from 50 km to 10 km resolution are shown in Figure 3.7 and are implemented as follows:

i. All the input variables were aggregated to the spatial resolution of the GRACE-JPL Mascon (50 km) and then the statistical associations between the TWS, geospatial variable (elevation) and hydrometeorological variables (soil moisture, snow water, rainfall, surface runoff, evapotranspiration) at 50 km resolution were investigated.
ii. The residual values were calculated by deducing the model-derived TWS from the original GRACE-TWS.
iii. The developed model was applied to the hydrometeorological and geospatial parameters in the resolution of 10 km to attain the estimated 10 km TWS. Subsequently, the residuals were added to the simulated TWS at 10 km to obtain

the downscaled TWS. This residual correction is performed through the following steps: i) first, the 10-km predictor parameters are resampled to the 50-km of the original GRACE-TWS resolution, ii) then, the 50-km residual TWS values are calculated by taking the simulated and the actual TWS data and iii) and finally, the computed coarse resolution residuals were regirded through cubic convolution method to generate 10-km residual TWS and added to the fine resolution simulated TWS which yields the final downscaled TWS. The residual correction guarantees the spatio-temporal harmony between the downscaled and the original TWS and also corrects for a prediction bias that might result from omitted variables.

iv. Eventually, the downscaled GWS values were extracted by subtracting the FLDAS-derived SMS and SWE from the downscaled TWS.

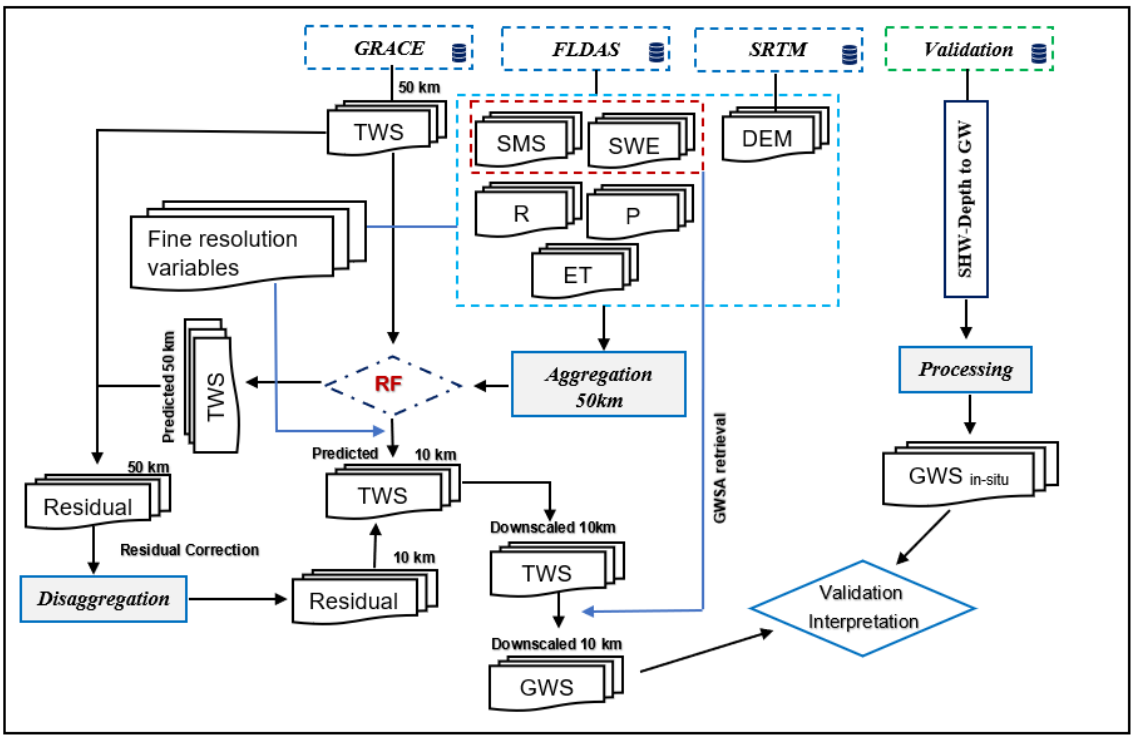


Figure 3.7 Graphical description of the downscaling flow

3.8 Uncertainty Estimation

The gravity signals detected and recorded by the GRACE satellites, suffer from a variety of uncertainties imposed during either signal gathering or during signal processing tasks (Landerer and Swenson, 2012; Wahr et al., 2006; Karasu, 2019). The actual errors associated with the GRACE data are added to the final GRACE TWS estimates from the following sources:

i. Leakage errors imposed during the truncation and spatial filtering of the gravity fields
ii. The other geophysical signal errors required to be excluded from the GRACE estimates
iii. Uncertainty of GRACE low-degree Stokes coefficients and geocenter series (Chen et al., 2021).

These errors are the gravity residuals of the post-processing and rescaling the SH values to get the TWS signals. The errors associated with the GRACE records affect the performance of the mission. They have an important role in a better description of the datasets and therefore, uncertainty estimation is a central part of the GRACE-related studies.

The standard method for estimating the GRACE errors is to compare its observations with independent data from other sources (Argus et al., 2020; Chen et al., 2021). Since the GRACE JPL Mascons are released with the estimated uncertainties of TWS values, in this thesis, the uncertainty values were used from the NASA's uncertainty report for the GRACE TWS. The estimated uncertainties of the GRACE-TWS data are calculated by taking the quadrature sum of the error components (Karasu, 2019). The TWS error is calculated through Equation 3.25.

$$TWS_{error} = \sqrt{(ME)^2 + (LE)^2} \tag{3.25}$$

where ME and LE represent the measurement and leakage errors, respectively.

Because some extra errors may be added to the original TWS values through the model integrated GRACE decomposition process, the uncertainty of the extracted GWS has to be calculated. Here, the GRACE-derived GWS uncertainties were estimated based on the error propagation theory, according to which, the estimated errors in the TWS (achieved from the data provider) and in the land surface model outputs culminate into the uncertainties of the resulting GWS (Sahour et al., 2020). The GWS errors were calculated according to the following equation (Eq 3.26).

$$\sigma_{GWS} = \sqrt{(\sigma_{TWS})^2 + (\sigma_{SMS})^2 + (\sigma_{SWE})^2} \quad (3.26)$$

where σ values stand for the standard deviation values of the corresponding parameter.

3.9 Evaluation Metrics

The performance of the RF model was assessed through application of different statistical metrics to verify the accuracy of the downscaled TWS. The metrics utilized in this study are; the Pearson's correlation (R), Root Mean Square Error (RMSE), Mean Average Error (MAE) and Nash-Sutcliffe Efficiency Coefficient (NSE). A brief explanation of each evaluation metric alongside their computation formulas is given in the following sections.

3.9.1 Coefficient of Correlation (R)

The coefficient of correlation demonstrates the extent or degree of the existing linear relationship between two parameters. Higher R means better performance of the constructed model, which means the model of interest performs better in simulating the variable. R is calculated through the following equation.

$$R = \frac{\sum_{i=1}^{N}(X_i - \bar{X})(Y_i - \bar{Y})}{\sqrt{\sum_{i=1}^{N}(X_i - \bar{X})^2}\sqrt{\sum_{i=1}^{N}(Y_i - \bar{Y})^2}} \quad (3.27)$$

3.9.2 Root Mean Square Error (RMSE)

The Root Mean Square Error (RMSE) shows the deviation of the actual observations from the simulated values. Smaller RMSE indicates better performance for the model.

$$RMSE = \sqrt{\frac{\sum_{i=1}^{N}(X_i - Y_i)^2}{N}} \quad (3.28)$$

3.9.3 Mean Absolute Error (MAE)

The Mean Absolute Error (MAE) represents the arithmetic mean of the absolute deviations of the actual observations and the simulated values. MAE can give a better measurement of simulation errors because of its computational nature where the problem of error canceling each other is avoided (Chen et al., 2019b).

$$MAE = \frac{1}{N}\left(\sum_{i=1}^{N}|Y_i - X_i|\right) \quad (3.29)$$

3.9.4 Nash-Sutcliffe Efficiency Coefficient (NSE)

The Nash-Sutcliffe Efficiency (NSE) evaluates the performance of a model, generally hydrologic models. The NSE ranges from -1 to +1 in value where higher values imply better accuracy for the model simulations and vice versa. The NSE values closer to zero indicate that the simulated values are closer to the mean of the actual observations, which

express an overall credible result for the model but are associated with the large simulation errors (Chen et al., 2019-b). The NSE value is calculated as follows:

$$NSE = 1 - \frac{\sum_{i=1}^{N}(Y_i - X_i)^2}{\sum_{i=1}^{N}(X_i - \bar{X})^2} \tag{3.30}$$

Where, for all the mentioned metric equations, X_i and Y_i represent the original GRACE-TWS and the RF-simulated TWS respectively. $\bar{X}$, $\bar{Y}$ and N denote the average values of the Xi and Yi and the total number of samples respectively.

CHAPTER 4

DESCRIPTION OF THE STUDY AREA

In this chapter, brief information on the general situation of Turkey is given with particular reference to its geographic, topographic and climatic situation as well as its hydro-meteorological characteristics.

4.1 Overview of Turkey

4.1.1 Geographic and Topographic Setting

Turkey is located between the geographic coordinates of 25°38’ to 44°48’ East and 35°48’ to 42°6’ North (Figure 4.1). With the geographical extension of 1650 km from west to the east and 650 km from north to the south, Turkey’s total surface area reaches about 78 million ha. Geographic neighbors of the country are Iran, Georgia, Armenia, Syria, Iraq, Bulgaria and Greece. (Altinbilek and Hatipoglu, 2020). As a transcontinental country, Turkey’s territory encompasses both Asian and European soils so that it makes a bridge between these two continents, which runs from the Black Sea to the strait of Bosphorus through Marmara Sea and the Dardanelles Strait to the Aegean Sea and the Mediterranean Sea to the south (Kuzucuoğlu, 2019). Turkey is internally divided into seven regions according to their different climatic, geographic and topographic characteristics such as climate type, location, flora and fauna, habitat and agricultural diversities. The regions of Turkey are listed as the Black Sea region in the north, Marmara and Aegean regions in the west, Mediterranean region in the south, Eastern Anatolia region in the east, Southeast Anatolia region in the south-east and the Central Anatolian region in the middle of the country. These regions are named according to their geographic location. While four regions (the Aegean, Black Sea, Marmara and Mediterranean regions) carry the name of the seas bordering them, the remaining three regions (Central, Eastern and South-Eastern Anatolia regions) are named in accordance with their location in the Anatolian peninsula.

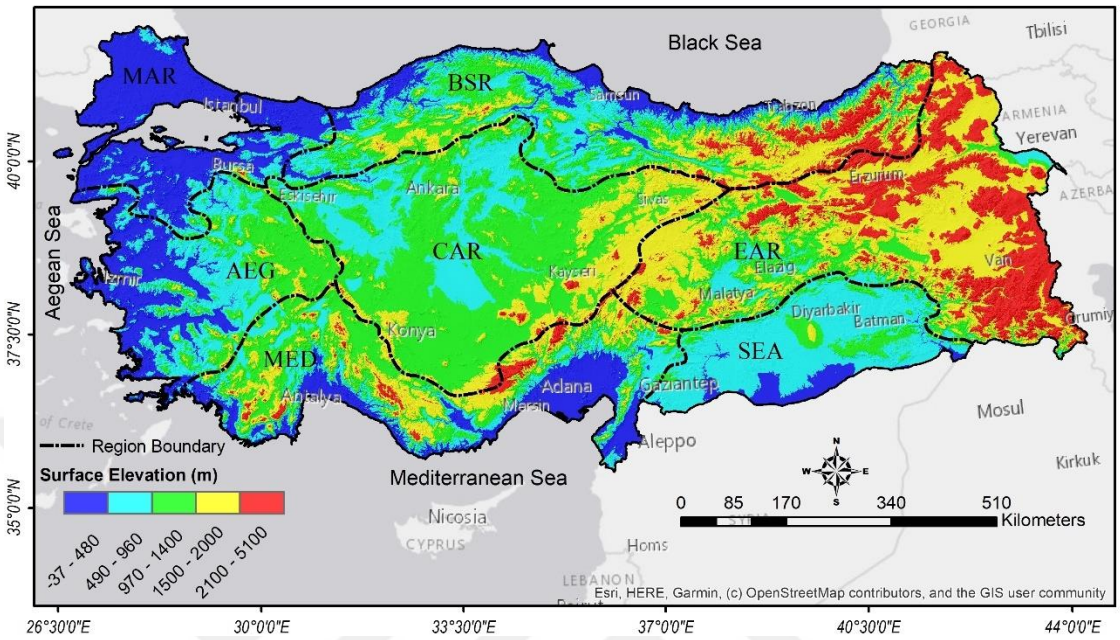


Figure 4.1 Visual description of the geographic and topographic setting of Turkey. The seven geographic regions: Marmara region (MAR), Black Sea region (BSR), Aegean region (AEG), Mediterranean region (MED), Central Anatolian region (CAR), Eastern Anatolian region (EAR) and South-East Anatolian region (SEA) are separated by a dashed line. The surface altitude ranges from -37 m (below the sea level) in the coastal areas to over 5000 m in the East.

From a morphological perspective, Turkey is a topographically diverse country with a variety of terrain features e.g., plains and mountains. The surface topography tends to increase from the west to the east of the country. This rising trend of the surface altitude (Kuzucuoğlu, 2019) poses the eastern parts to more topographic heterogeneity where the tallest mountains exist. Turkey's territory is basically covered by mountains; East Anatolian Highlands in the East, Black Sea Mountain Range in the North, the Taurus Mountains in the South and the Anatolian Plateau in the center (Nistor and Man, 2019). This geographic and topographic diversity of the country engender different situations in terms of climatic, hydrological and meteorological conditions. The climatic and hydrometeorological characteristics of Turkey are discussed in detail in the following sections.

4.1.2 Climate of Turkey

Being located on the arid belt of the world, Turkey demonstrates generic semi-arid climate characteristics (Apaydin, 2011). The Thornthwaite-based classification map (Figure 4.2) illustrates the classified climate of Turkey according to this method. According to the map, the dominant climate of the inland Anatolia, Iğdır and Şanlıurfa is of semi-arid type, while the Eastern Black Sea is the very wet region. The Black Sea and the peripheries of Bitlis and Muğla have a humid climate. Other large areas of Turkey are semi-dry and semi-humid climatic regions (Sensoy et al., 2012).

However, the geographic position of Turkey (adjacency to vast water bodies; the Black Sea in the north, the Marmara and Aegean seas in the west and the Mediterranean Sea in the south) accompanied by its regional topographic heterogeneity engender diversified climatic situations all over the geographic regions of Turkey (Khorrami and Gunduz, 2021b). The coastal areas in the Aegean and Mediterranean regions experience Mediterranean cyclonic tracks (Kuzucuoğlu, 2019). The Back Sea coasts, on the other hand, take the benefit of humidity tracks that originated from the Black Sea and Siberian High System (Türkeş and Erlat 2003; Şahin and Çığızoğlu 2012; Kuzucuoğlu, 2019). These weather patterns bring about a mild climate for the coastal areas of the country (Sensoy et al., 2008). The Central plateau is besieged with highlands, which results in considerable depletion of humidity. This low humidity together with the high-temperatures defines the dry climatic condition of the region.

Briefly, the orographic impacts of the diverse topography in addition to the origin of precipitation and humidity (Atlantic and Mediterranean (West and Southwest), Pontic and Siberian (North and Northeast), Mesopotamian (Southeast), characterize the climatic situations of different regions over Turkey (Kuzucuoğlu, 2019). These combined factors pose the country to climatic variance within short distances. Consequently, precipitation and temperature vary significantly over different geographic regions.

In Table 4.1 and Figure 4.3, the long-term zonal values and country-wise spatial maps of precipitation and temperature are given. The 90-year (1929-2018) country-wise mean annual precipitation and temperature in Turkey are calculated as 639.34 mm and 13.14°C respectively (TSMS, 2020). According to Figure 4.3, the eastern BSR receives the maximum precipitation (1300 mm/yr) while the minimum precipitation (370 mm/yr) occurs over the CAR. The temperature ranges from 3.9°C in the East Anatolia region, to 20°C in the coastal regions of Aegean, the Mediterranean and a small part in the Southeast Anatolia regions.

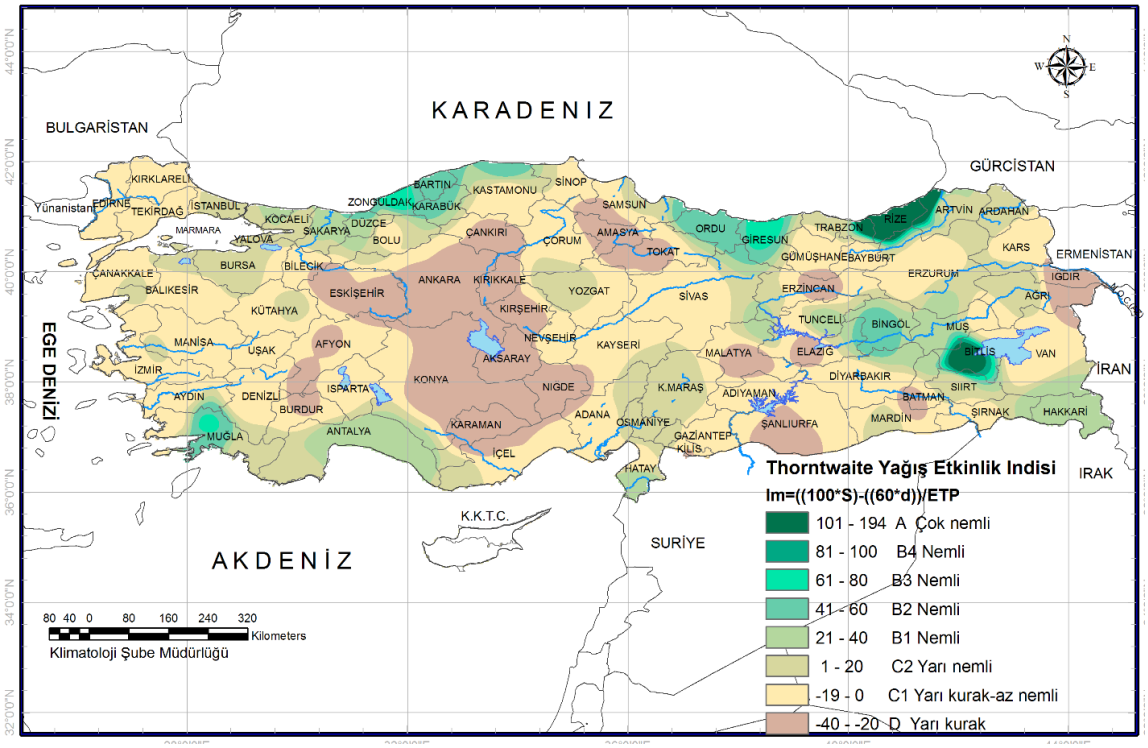


Figure 4.2 Classification of Turkey's climate based on Thorntwaite method (after Sensoy, 2012)

Table 4.1 The zonal statistics of the long-term (1929-2018) observations of precipitation and temperature over Turkey.

Variable		Zone	Avg.	Min.	Max.	Std. Dev.
Monthly statistics	Precipitation	Black Sea Region (BSR)	66.56	35.60	192.63	38.75
		Eastern Anatolia Region (EAR)	50.30	21.43	101.42	22.04
		South-East Anatolia Region (SEA)	47.56	37	59.52	9.13
		Central Anatolia Region (CAR)	32.50	26.94	46.87	5.12
		Aegean Region (AEG)	56	36.70	99.63	19.22
		Marmara Region (MAR)	55.50	37.82	70.50	10.50
		Mediterranean Region (MED)	62.20	35.5	93.75	20.30
	Temperature	Black Sea Region (BSR)	12.58	7.01	14.70	2.15
		Eastern Anatolia Region (EAR)	9.96	3.90	15.10	3.42
		South-East Anatolia Region (SEA)	16.50	14.90	18.30	1.05
		Central Anatolia Region (CAR)	11.14	9.10	12.27	1.09
		Aegean Region (AEG)	14.77	10.70	18	2.89
		Marmara Region (MAR)	14.22	12.50	15.10	0.80
		Mediterranean Region (MED)	17.02	12.20	19.20	2.75

To give an insight into the monthly variations of precipitation and temperature over Turkey, the ombrothermic diagram of Turkey (Figure 4.4) was generated based on the long-term averages. The diagram indicates that the highest precipitation occurs in December and January, while during July and August, it reaches its lowest amounts. The temperature turns out to precede the precipitation from June to September, which signals a dry period for the country during this period.

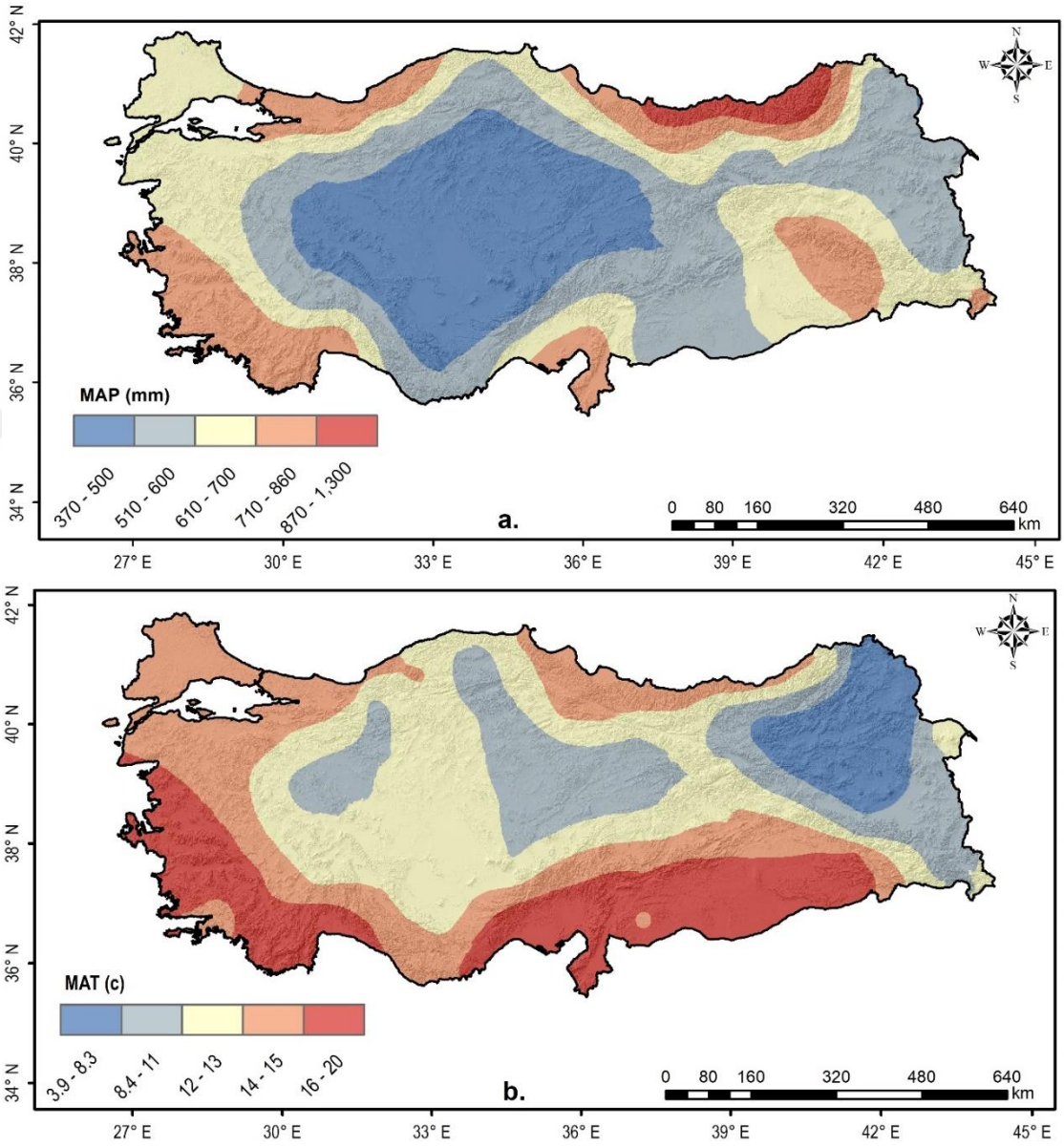


Figure 4.3 Illustration of the spatial dispersion pattern of Mean Annual Precipitation (a.) and Mean Annual Temperature (b.) values over Turkey

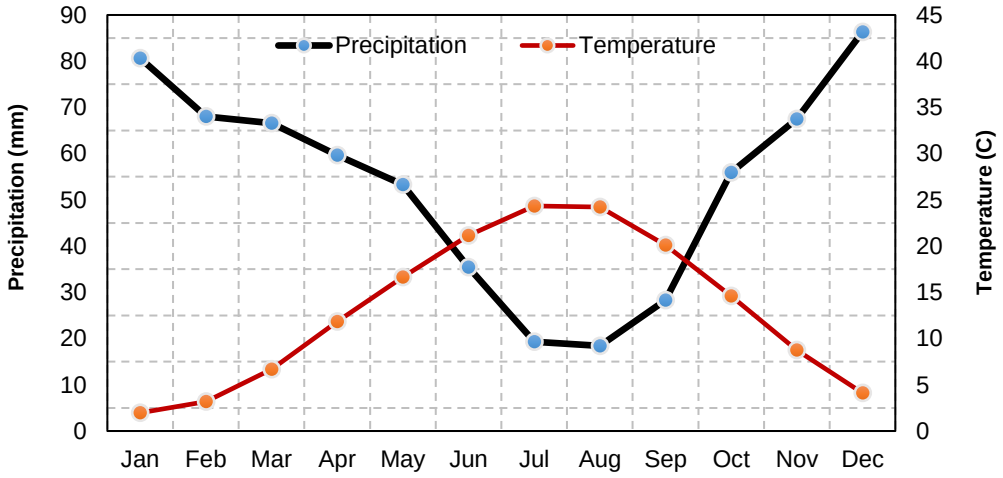


Figure 4.4 The ombrothermic diagram of Turkey based on the long-term meteorological records (1929-2018)

4.1.3 Water Resources of Turkey

There are more than 120 natural lakes, 293 dams and 1,000 small reservoirs which over all contribute to the surface water resources of Turkey. These surface water resources are geographically shared among 25 river basins (Figure 4.5) and overall account for about 80% of the country's total water potential (Harmancioglu, 2020). The drainage area of the river basins ranges from 6306.2 km^2 (Lake Burdur basin) to 176142.7 km^2 (Euphrates-Tigris River basins), which correspond to about 0.81% and 22.55% of the total drainage area of Turkey, respectively. Table 4.2 gives information on the surface area and discharge of each river basin of the country.

Groundwater contributes to approximately 18% of the country's water potential but this amount is not available due to some technical and economic limitations (Yazicigil and Ekmekci, 2020). Groundwater aquifers feed a considerable portion of the streamflow of the stream network through springs and baseflow. The agricultural sector consumes most of the water available in Turkey, from which groundwater accounts for about 20%

to 25 % (Kibaroglu et al., 2011). According to the master plan of the country's water resources (TSHW, 2020), the following statistics have been reported for the year 2020:

- The total annual water flow is 185 billion m^3.
- The useable water potential is 112 billion m^3, from which surface water accounts for 94 billion m^3 and groundwater is about 18 billion m^3.
- The country's total water use for the year 2020 is 57.44 billion m^3, which is used for different purposes, 44.25 billion m3 (77%) for irrigation and 13.19 billion m3 (23%) for drinking-domestic and industrial water (TSHW, 2020).

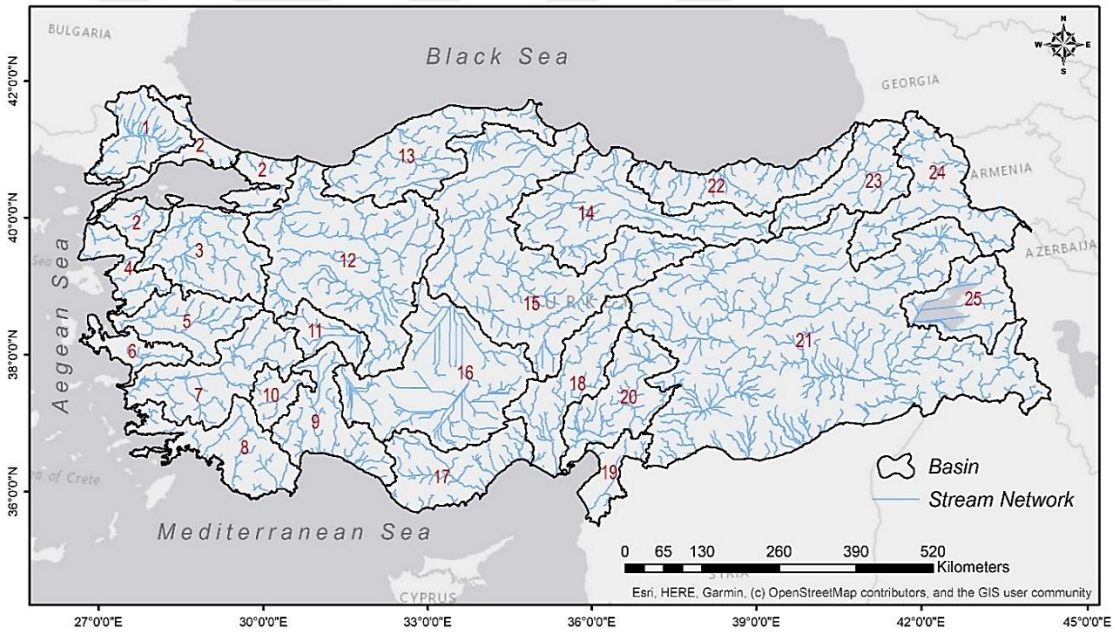


Figure 4.5 The geographic location of the hydrologic basins of Turkey (basin names are given in Table 4.2)

Table 4.2 Annual Average Water Potential by Basin. Source: TSHW 2020

ID	Basin Name	Area (km^2)	Mean Natural Flow (hm^3)	Mean Annual discharge ($L/s/km^2$)
1	Meric - Ergene	14,560	1657	3.6
2	Marmara	24,100	7442	10.2
3	Susurluk	22,399	4963	6.5
4	North Aegean	10,003	1985	6.4
5	Gediz	18,000	1776	3.3
6	Kucuk Menderes	6,907	624	2.8
7	Buyuk Menderes	24,976	3047	3.7
8	West Mediterranean	20,953	6499	9.8
9	Antalya	19,577	12944	20.3
10	Burdur Lake	6374	234	1.2
11	Akarcay	7,605	375	1.5
12	Sakarya	58,160	6487	3.2
13	West Black Sea	29,598	10797	11.9
14	Yesilirmak	36,114	7046	5.6
15	Kizilirmak	78,180	7004	2.7
16	Konya	53,850	2407	1.5
17	East Mediterranean	22,048	7559	11.3
18	Seyhan	20,450	6183	8.9
19	Asi	7,796	1782	7.2
20	Ceyhan	21,982	7734	11.5
21	Euphrates - Tigris	184,918	56316	22.8
22	East Black Sea	24,077	16426	22.8
23	Coruh	19,872	6981	10.9
24	Aras	27,548	4480	5.1
25	Van Lake	19,405	2602	4.6
TOTAL		779,452	185352	7.66

In light of the geographic and topographic diversity of the country, Turkey's water resources are distributed unevenly over different regions of the country. The irregular flow of the streams renders these surface water resources an unusable water source (Cakmak, 1997). Although in the past Turkey was known as a water-rich country, currently there is tremendous pressure on its water resources. Turkey's water resources are heavily under the control of two major effective parameters: the swift growth of population and the harsh impacts of climate change (Yazicigil and Ekmekci, 2020). Taking into account the international standards regarding the minimum values of per capita water availability, Turkey can be categorized as a water-crisis-beaten country. While the water scarcity threshold for water-rich countries is 8,000 to 10,000 m^3 per capita, the per capita water availability for Turkey is only 1,700 m^3 and it is projected to even decrease to less than 1,300 m^3 per capita by the end of 2030 (Yazicigil and Ekmekci, 2020). According to Paul et al. (2016), Turkey is classified as countries approaching physical water scarcity (Figure 4.6). From the figure 4.6, it is understood that being located in the Middle East, one of the arid zones of the world, Turley faces the greatest challenges regarding its water resources. Therefore, it is expected to suffer more from the water scarcity crisis in the near future, which will add up to the currently experienced socio-environmental problems over the country.

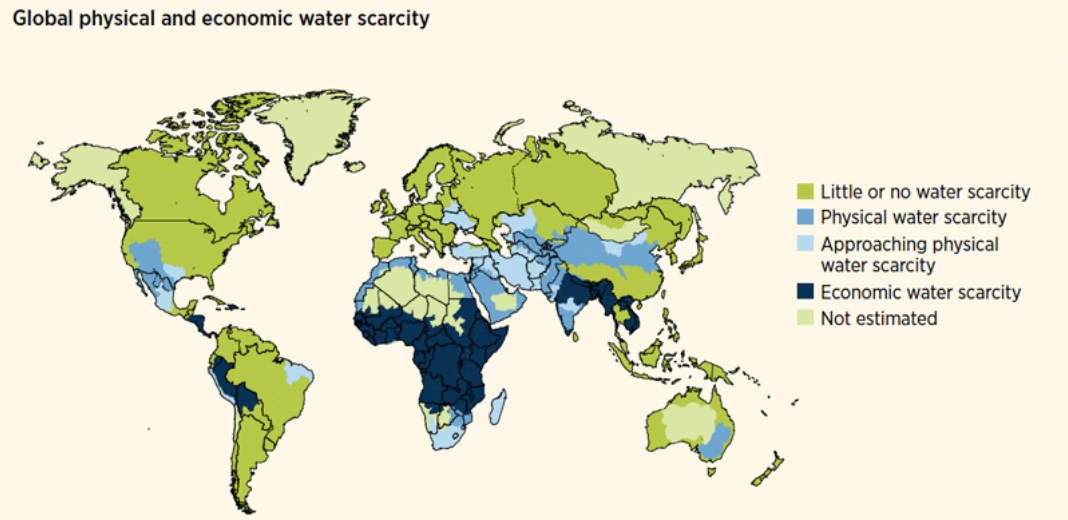


Figure 4.6 The global water scarcity map (after Paul et al., 2016).

4.2 Overview of the Western Anatolian Basin (WAB)

The Western Anatolian Basin (WAB) is situated between 37.00º- 40.00º N and 26.00º-30.30º E and is a geographical combination of 4 hydrological river basins namely Küçük Menderes, Büyük Menderes, Gediz and Kuzey Ege in the Aegean region, western Turkey (Figure 4.7). With an estimated area of 60,000 km^2, the WAB covers the majority (71%) of western Anatolia. The Mediterranean climate typically characterizes the climatic situation of the WAB where summer months are dry and warm while it is cold and rainy in winter (Ay, 2021). The mean annual precipitation of the region ranges from 450 to 1200 mm (Asikoglu and Benzeden, 2014). The following gives brief information on each river basin of the study area.

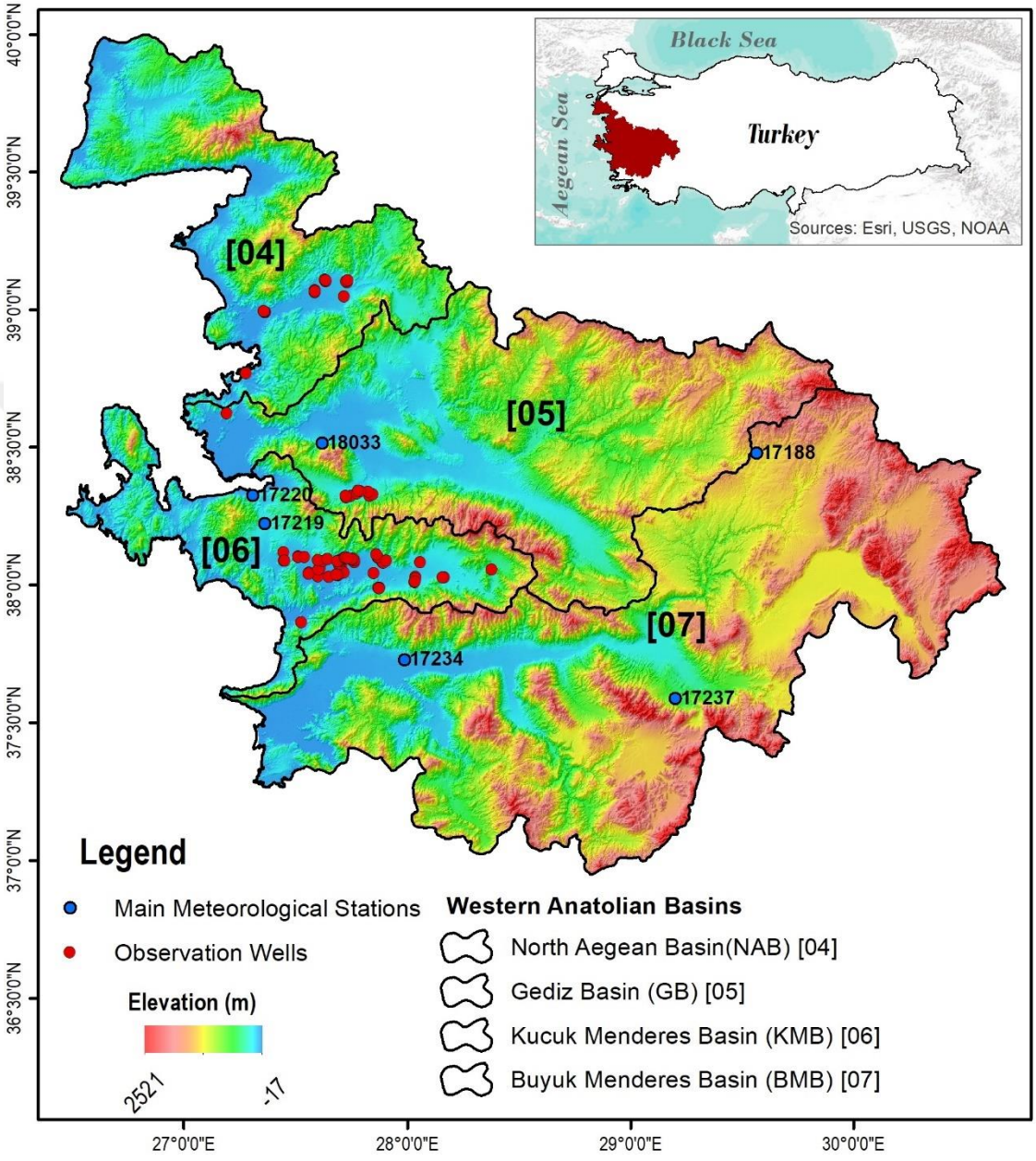


Figure 4.7 Geographic position of the Western Anatolian Basin (WAB), west of Turkey

4.2.1 North Aegean Basin (NAB)

The North Aegean Basin is located in the west of the Anatolian peninsula between 38-40° N and 26-28° E and encompasses İzmir, Balıkesir, Çanakkale and Manisa provinces. The NAB is encircled by the Marmara Basin and Gediz Basin in the south, the Aegean Sea in the west and Susurluk Basin in the east (Yılmaz et al., 2019). There are 3 sub-basins in the NAB: Upper North Aegean, Mid-North Aegean and Lower North Aegean. As of 2016, the total irrigated area of the NAB reaches 110374 ha, from which, 78767 ha is irrigated by surface water and 31607 ha by groundwater. It is estimated that the surface water and groundwater resources supply 487.5 Mm^3/year and 169 Mm^3/year of the agricultural water need of the basin. Groundwater also accounts for about 41 Mm^3 of water used by the industry of the region in 2016 (WMP, 2020).

4.2.2 Gediz Basin (GB)

The Gediz basin has experienced a critical shift from water-rich into a water-poor basin during the past decades mainly in the aftermath of the severe drought from 1989 to 1994 as well as the partial forces imposed on the basin water resources from the increased water demand of population growth and industrial expansion (Harmancioglu et al., 2008). There is no balance between the input and output water in the basin. While the estimated safe yield of the aquifer reaches 160 million m^3/year, the annual extraction of the groundwater aquifers of the basin is 219 million m^3/year from which, 61 million m^3/year belongs to the irrigation sector and 158 million m^3/year for urban use. As the industry expands in the region, it is expected to have increased pressure on the groundwater aquifers of the basin.

4.2.3 Kucuk Menderes Basin (KMB)

The Kucuk Menderes basin is a one of the most fruitful agricultural areas of the Aegean region. Almost all the water demand for agricultural and industrial usages is met by groundwater aquifers (Yagbasan, 2016). While the total groundwater recharge of the basin

is about 716.5 hm^3 (38%), the total abstraction from groundwater aquifers of the basin reaches 1145.5 hm^3 (62%). There has been a severe decline in the groundwater level during recent years mainly because of the overexploitation of groundwater by irrigation wells (Sakiyan and Yazicigil, 2004). There are more than 20,000 unregistered private wells within the basin, which are operated mostly for irrigation purposes (Yagbasan, 2016). The majority of water use in the area appertains to the agricultural sectors. The water consumption share of the domestic and industrial sectors is about 13% (Yagbasan, 2016). Although there is no certainty on the exact amount of the extracted groundwater over the basin, it is estimated that 335.6 million m^3/year of groundwater is extracted from the basin, of which 279.5 million m^3/year is for irrigation use, 35.1 million m^3/year is used for drinking and domestic needs and 21 million m^3/year is consumed by the industry (Yagbasan, 2016). The groundwater resources of the basin are directly influenced by both overexploitation and climate change. The declining trend in the groundwater wells of the basin was started after 1981 as a result of the harsh drought impacts between 1981 to 1995(Yagbasan, 2016).

4.2.4 Buyuk Menderes Basin (BMB)

The Buyuk Menderes basin is one of the agricultural hubs of the country whose economy is highly dependent on agricultural activities. The long-term average groundwater extraction of the basin is about 479 hm^3/yr which is mainly used for irrigation which makes use of about 79% of water from the basin. With an estimated length of 584 km, the Buyuk Menderes is the longest river in the Aegean region (Yilmaz et al., 2009). The river valley hosts the majority of the cultivation practices in the basin with an area of 907,000 ha that corresponds to 87% of its total agricultural area (Yilmaz et al., 2009). The majority of the water used in the basin is irrigation water. The groundwater aquifers of the region provide the majority of the water needs for the cultivation sector whose intense application of water-demanding crops has led to a significant water demand increase. The hydrological water balance of the basin was destructed by the overuse of the groundwater

particularly during dry seasons (Durdu, 2010). Table 4.3 illustrates the groundwater potential of each basin.

Table 4.3 Groundwater potential reported for each subbasin of WAB (Yazicigil and Ekmekci, 2020).

ID	**Name**	**Area (km^2)**	**Groundwater Recharge (Mm^3/year)**
04	North Aegean	9,974	289.4
05	Gediz	17,034	1155.9
06	Kucuk Menderes	7,060	179.2
07	Buyuk Menderes	26,133	1045.4

CHAPTER 5

RESULTS AND DISCUSSION

5.1 Fluctuations of the Simulated SMS and SWE over Turkey

Soil moisture and snow water are two effective compartments of the hydrological cycle whose variations impact the terrestrial water storage particularly over the areas with arid and semi-arid climate. The monthly simulations of SMS and SWE from three different hydrological models (the GLDAS, the FLDAS and the WGHM) were extracted over the study area. The anomalies of the monthly estimates were calculated by using the GRACE baseline (2004-2009) (Moghim, 2020) and the time-series graphs were generated (Figure 5.1 and 5.2). The simulated SMS and SWE show harmony in catching the hydrometeorological extremes of drought events from 2003 to 2020. Especially the drought events experienced in 2007, 2008, 2014 and 2020 are detected by taking the temporal variability of SMS and SWE into account. Further details on the drought analysis will be given in the following sections.

According to the resulted graphs for SMS and SWE over Turkey, areal means of soil moisture over the country manifests a decreasing trend from Jan 2003 to Dec 2020. The moisture storage of the soil profile reaches 17.57 cm of equivalent water height (EWH) in January 2019, while the minimum storage is -14.74 cm of EWH in Feb 2014. The soil moisture storage time series also reveals the minimum soil moisture storage in 2004, 2016 and 2020. The SWE, on the other hand, shows almost no trend through the same period. The variations of the SWE reveal that excluding 4 points in the time series graph, the monthly variations in the snow storage are not so dramatic. At these 4 dramatic points, the moisture storage shows its maximum values of 4.82 cm, 2.74 cm and 2.64 cm in January 2019, March 2003 and March 2012, respectively. The minimum soil moisture storage, on the other hand, was recorded in Feb 2014 with a decrease of -3.44 cm of EWH.

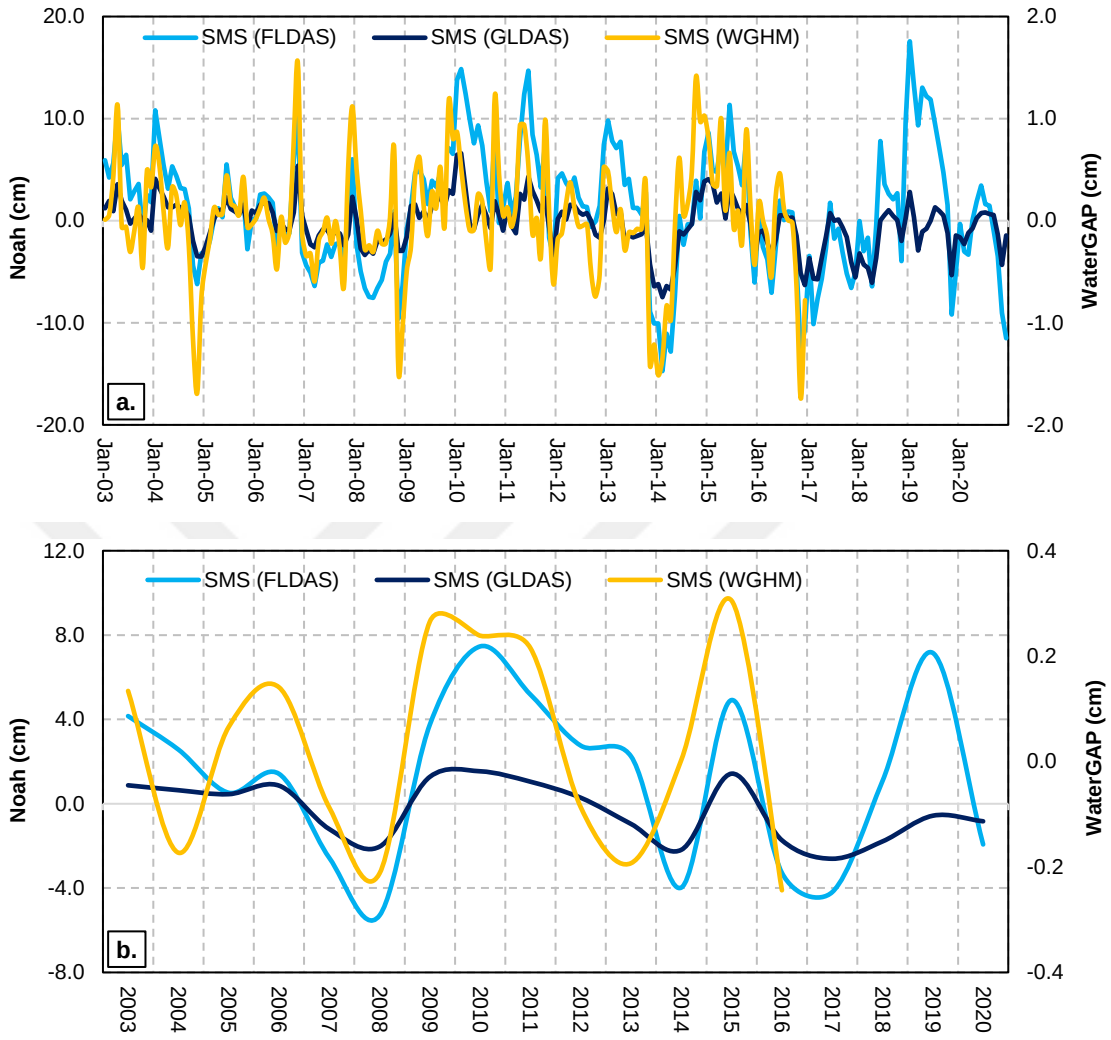


Figure 5.1 Temporal variations of the simulated soil moisture storage (SMS) over Turkey at monthly (a) and annual (b) time scales. Soil moisture simulation is done at 0.1-degree (FLDAS), 0.25- degree (GLDAS) and 0.5- degree (WGHM) spatial resolutions.

According to Figure 5.1, the time series graphs also suggest that the GLDAS- and WGHM-based simulation of SMS seem to suffer from a bit of underestimation with shorter peak and trough point values. The differences in the ranges of the SMS and SWE values stem from the different resolutions of the simulated products. While the FLDAS gives fine-resolution simulations (10 km), the GLDAS and WGHM simulate hydrometeorological variables with coarser spatial resolutions of 25 km and 50 km, respectively. The enhanced resolution of the FLDAS simulations improves its temporal

sampling of soil moisture (Lu et al., 2019) simulations. Furthermore, although both the GLDAS and FLDAS missions make use of the same land surface model (Noah LSM), the FLDAS model makes better and more accurate simulations due to the fact that it is forced by CHIRPS (Agutu et al., 2017; Shahzaman et al., 2021).

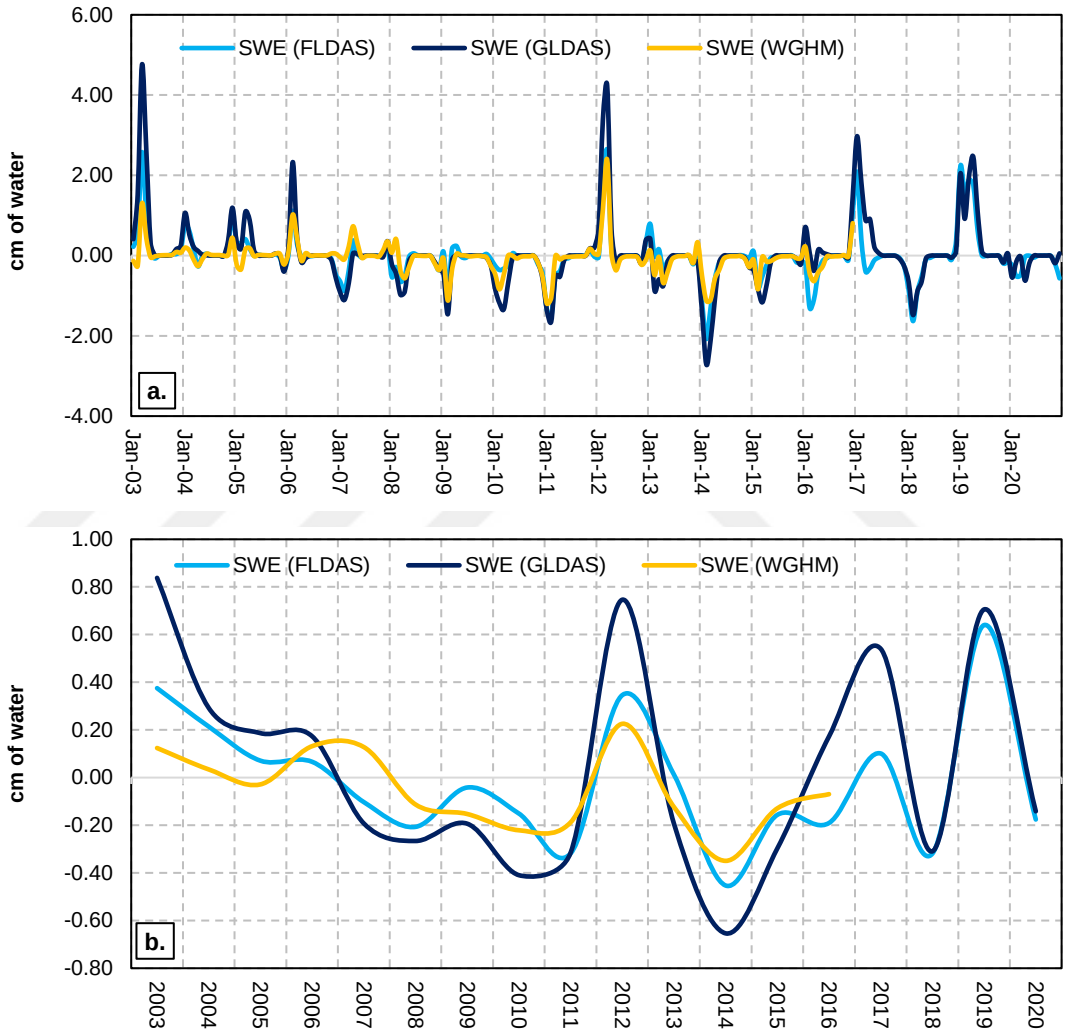


Figure 5.2 Temporal variations of the simulated snow water equivalent over Turkey at monthly (a) and annual (b) time scales. Snow water simulation is done at 0.1-degree (FLDAS), 0.25- degree (GLDAS) and 0.5- degree (WGHM) spatial resolutions.

5.2 Fluctuations of the GRACE-derived TWS over Turkey

GRACE gridded data provides Terrestrial Water Storage Anomalies estimated directly from the space based on the variations in the gravitational pull of the earth. There are some individual gaps in GRACE records, which hamper the continual evaluation of the values. In this study, the linear interpolation technique (Long et al., 2015; Yang et al., 2017) was applied to fill in the gaps in TWS values. The temporal variability of the TWS was investigated based on the areal-mean time series at different time scales including monthly, climatology, annual and seasonal time scales (Figure 5.3).

The variations of the GRACE-derived TWS show a descending trend from 2003 to 2020 over Turkey. The decreasing TWS can be ascribed to the impacts of the both droughts and groundwater abstraction (Lenk, 2013; Okay Ahi and Jin, 2019). The monthly TWS time series show outstanding descending patterns in 2007, 2008, 2009, 2014 and through 2018 to 2020 with the maximum decline (-19.70 cm of EWH) occurring in Oct 2020. The findings for the period of 2003 to 2016 agree with that of Okay Ahi and Jin (2019).

According to the annual variations, the variations of the GRACE-derived TWS are in agreement with the experienced dry periods in 2008 and 2014, in which, the TWS for the country was at the minimum amount. This is in utter agreement with the literature, which states country-wide dry periods between 2007-2008 and in 2014 over Turkey (Türkeş et al., 2009; Kurnaz, 2014; Okay Ahi and Jin, 2019). The annual time series also indicates that from 2018 to 2020, Turkey has suffered from another dry period where the total water storage deficit has reached -11.91 cm of water in 2018 signaling a severe drought over the country. This finding is in complete accordance with the newly published news from the NASA regarding the observed dryness in Turkey (NASA, 2021). The report says that Turkey is experiencing harsh soil drought conditions as a result of consecutive dry conditions experienced in 2019 and 2020. In Figure 5.4, the soil moisture drought condition is given for the January of 2021 over Turkey.

The climatological time series also indicate that the volume of water storage for TWS is increasing for the first half of the year (from January to June), while, over the second half (from July to December), it decreases (Okay Ahi and Jin, 2019). The maximum and minimum anomalies of TWS over Turkey have been recorded by GRACE in April and October, respectively.

The seasonal values were estimated by averaging the monthly values over Turkey: Spring (March, April, May), Summer (June, July, August), Autumn (September, October, November) and Winter (December, January, February). The seasonal variability of TWS implies that the anomalies are positive only in Spring (Okay ahi & Jin, 2019) while they have negative anomalies during the rest of the seasons from 2003 to 2020. It is found that, in Spring and Autumn, Turkey experiences extreme situations regarding the variations of the terrestrial water storage.

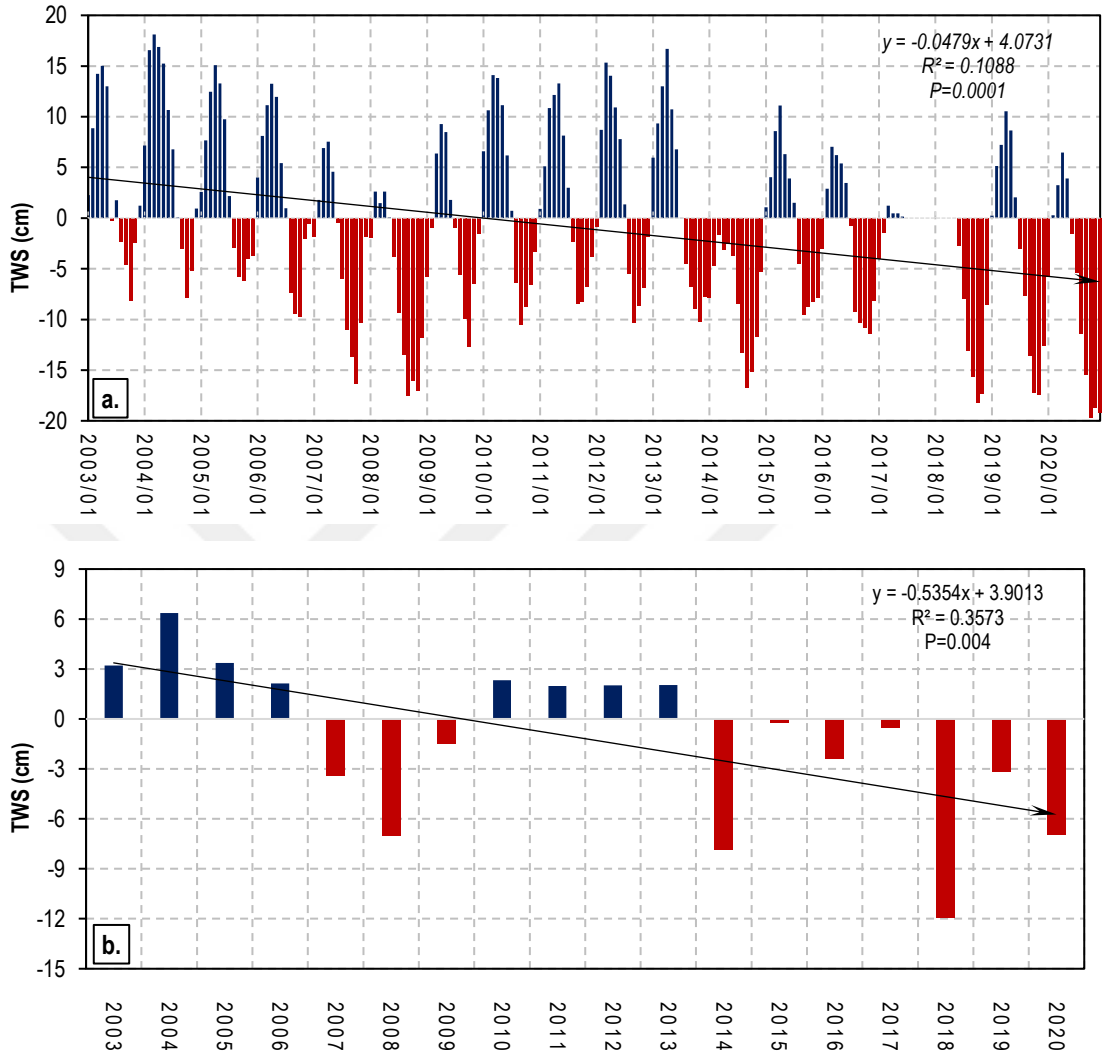


Figure 5.3 Temporal variations of the GRACE-driven TWS over Turkey at monthly (a), annual (b), climatology (c) and seasonal (d) time scales

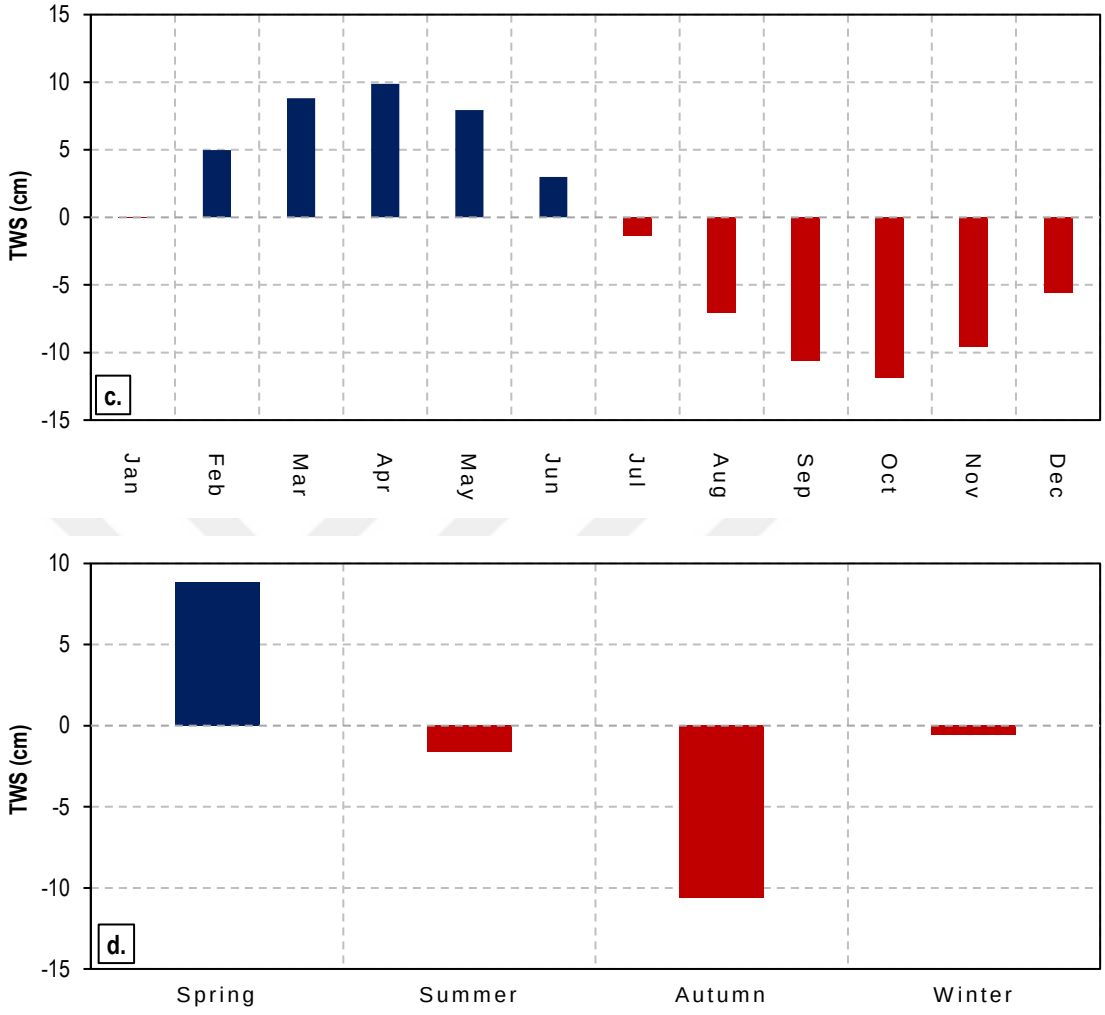


Figure 5.3 Continues.

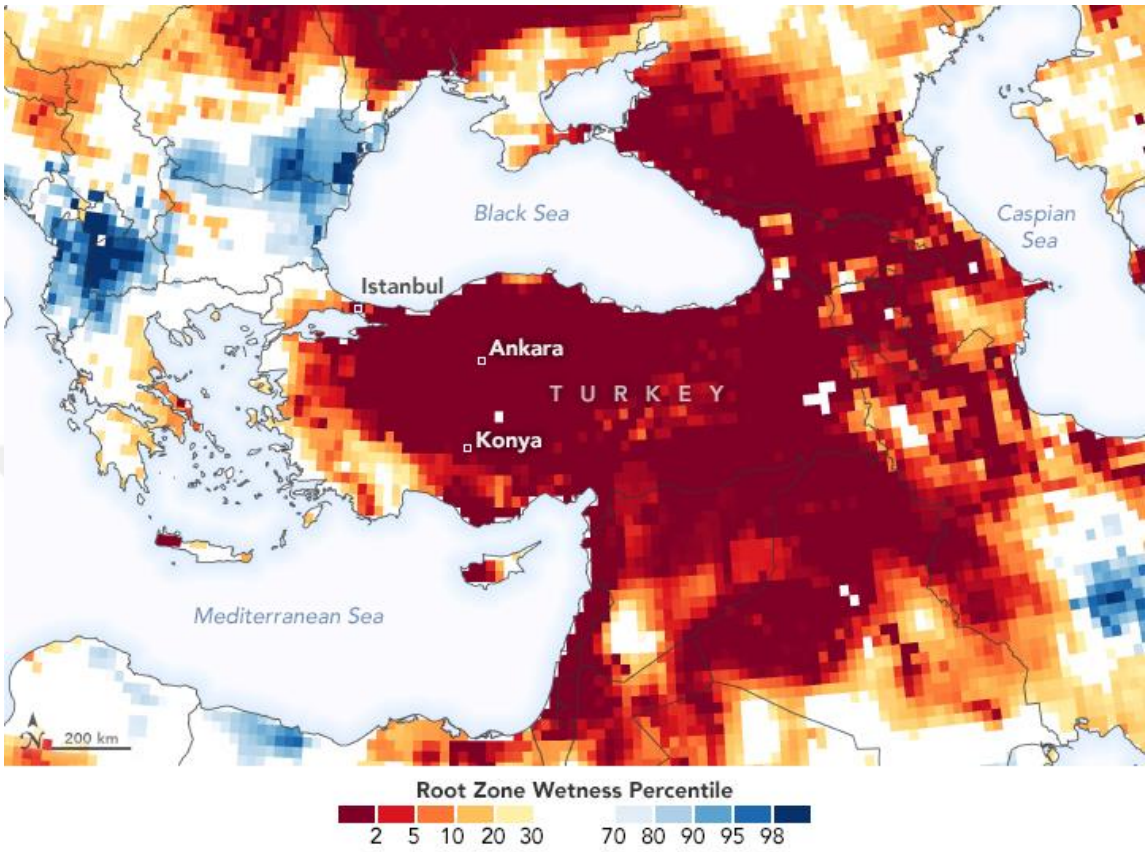


Figure 5.4 The detected soil moisture deficit in January 2021 by the GRACE satellite harbingers a severe drought over Turkey.

5.3 Fluctuations of the GRACE-derived GWS over Turkey

The global hydrological models provide a range of hydrometeorological parameters with different spatio-temporal characteristics that allow wide applications in environmental studies. Integration of the simulated hydrometeorological variables into the GRACE estimates is a well-established and tested manner of vertical disintegration of the GRACE-TWS values to extract the GWS over a given area of interest. Different models provide different data with varying spatio-temporal characteristics and also different levels of uncertainty. In this study, the GRACE-TWS were also integrated with the simulated hydrological water cycle components (including SMS and SWE) from the GLDAS and the WGHM models to investigate the temporal associations between them.

According to Figure 5.5, the GRACE-derived GWS through the TWS isolation based on different hydrological models manifest the same fluctuation patterns with differences in the range of values that stem from the differences in the characteristics of the simulated SMS and SWE from different models. Although the GLDAS and the FLDAS simulations are based on the same LSM (Noah), the spatial resolution of these two models differs. The varied characteristics of these two models result in the different temporal variations of the isolated GWS. While the GRACE-GLDAS derived GWS shows the highest correlation (0.96) with the GRACE-WGHM derived GWS over the country, the temporal correlation between the GRACE-FLDAS- and GRACE-WGHM-based GWS values is 0.77. The correlation between the GRACE-GLDAS and the GRACE-FLDAS derived GWS is 0.88. The discrepancies in the temporal correlation of the model-based isolated GWS over Turkey are associated with their different characteristics. While the WGHM and the GLDAS models give their simulated variables at 0.5- and 0.25-degree resolution, the FLDAS model simulates at a finer resolution (0.1-degree) and as a result, the detailed information of the simulated soil moisture and snow water results in the various fluctuations of the GWS over the study area.

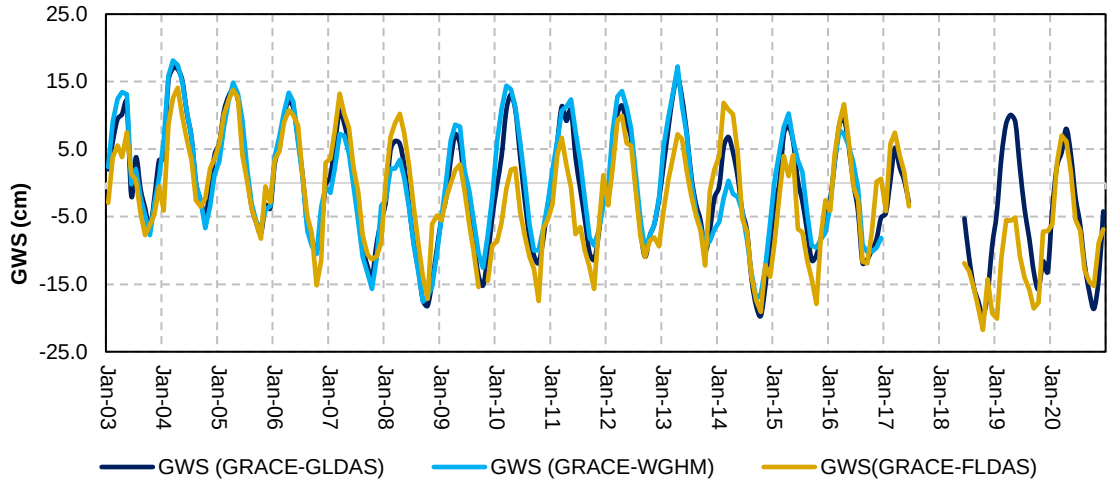


Figure 5.5 Temporal associations of the GRACE-derived GWS by integrating different hydrological model outputs into the TWS estimates over Turkey

In light of the fact that the finer resolution outputs of the FLDAS model are considered more accurate than those of the available hydrological models (Shahzaman et al., 2021), the temporal fluctuations of the GRACE-GWS are given from the FLDAS integrated results.

The monthly time series suggests that, like the TWS variations, the GWS has also a descending trend (Khorrami and Gunduz, 2021b) at all time scales from 2003 to 2020. The monthly variations of the GWS (Figure 5.6) manifest decreased values over different months through 2003 to 2020. Its variations through 2018 to 2020 seem to be more condensed temporally, which stress a severer drought period compared to the reported events in 2007, 2008 and 2014 over Turkey (Türkeş et al., 2009; Kurnaz, 2014; Ahi and Jin, 2019). The declined water storage of the county from 2018 to 2020 is also confirmed by the NASA's report (NASA, 2021).

According to the annual variations of the GWS over Turkey, through 2009 to 2011 and through 2018 to 2020, the GWS of the country has experienced severe declines. Unlike the TWS variations with the maximum annual storage loss in 2014 and 2018, the GWS shows its maximum annual storage loss in 2010 and 2018.

The climatological and seasonal variations of the GWS are akin to those of the TWS. The climatology GWS exhibit positive and negative values through the first and the second half of the year, respectively. The maximum storage loss of the groundwater of Turkey happens in October with the detected depletion of -13.33 cm. The seasonal fluctuations of the GWS suggest that while in Spring the groundwater of the country benefits from a relatively large water storage surplus, it suffers from decreased values through the following seasons with the maximum storage loss (-8.7 cm) in Autumn. The severe decrease observed in the seasonal variations of both the TWS and GWS over Turkey can be ascribed to the commence of extensive agricultural activities all over the country where the majority of the needed irrigation water is supplied from groundwater (Harmancioglu and Altinbilek, 2020).

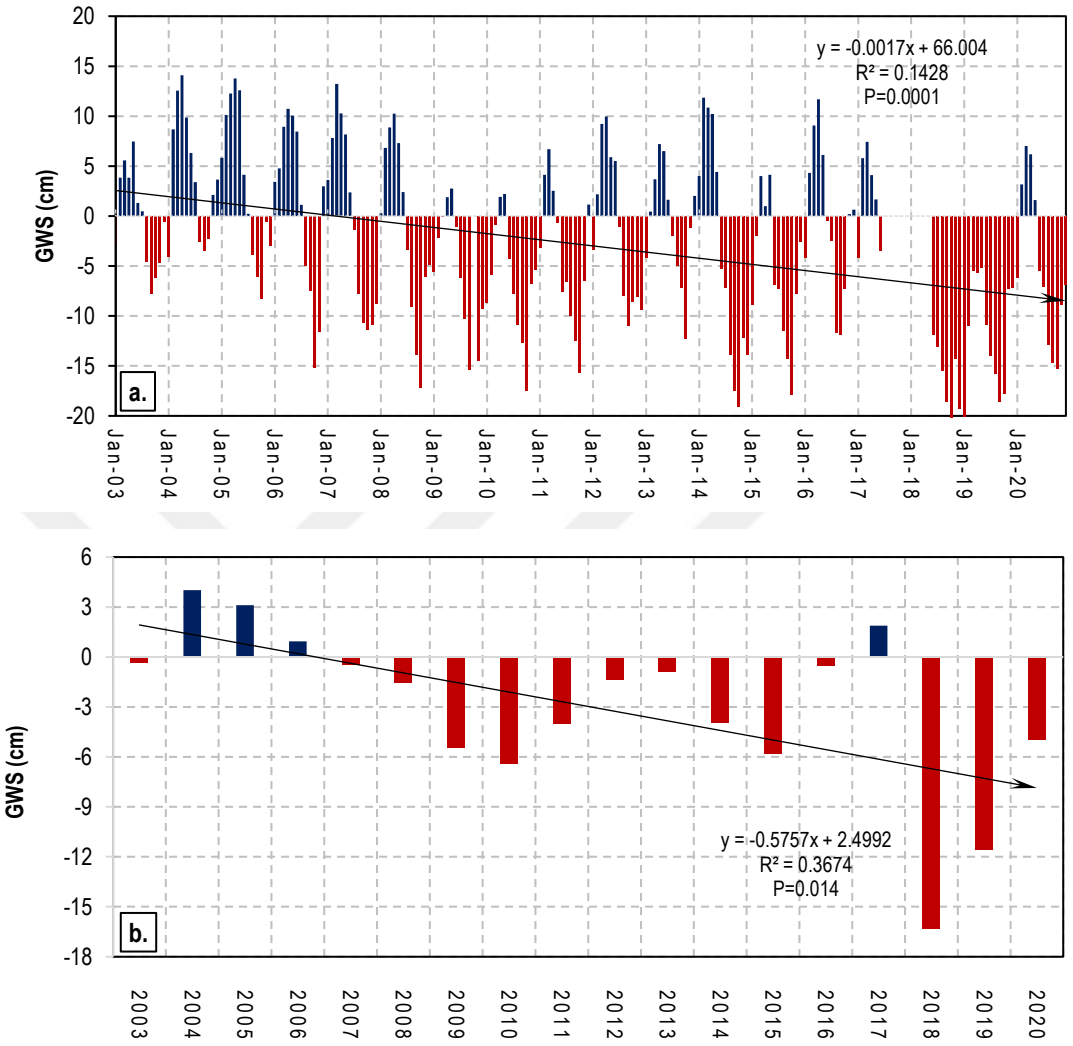


Figure 5.6 Temporal variations of the GRACE-driven GWS over Turkey at monthly (a), annual (b), climatology (c) and seasonal (d) time scales

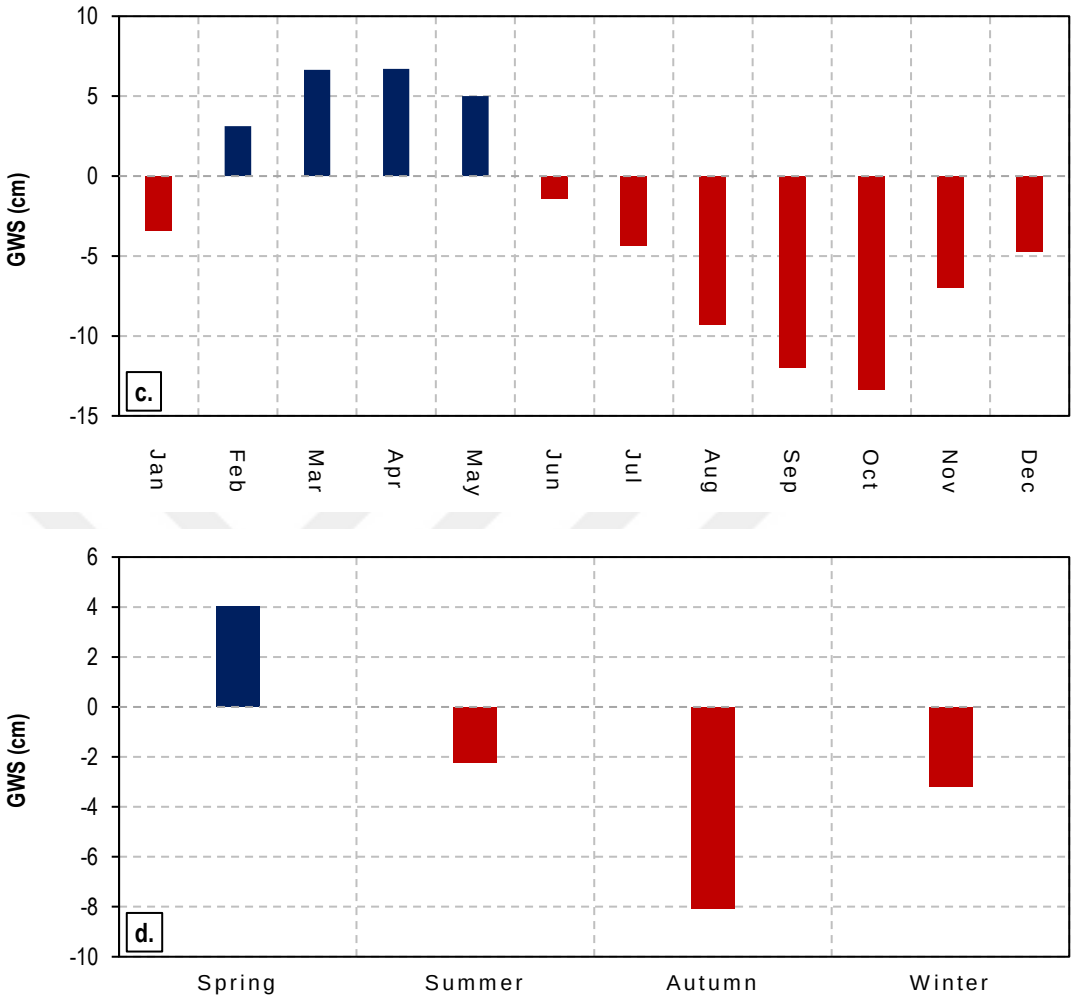


Figure 5.6 Continues.

5.4 Associations Between the GRACE- and Model-based TWS and GWS over Turkey

Although the available models simulate a wide range of parameters, a handful of them simulates TWS and GWS. In light of their high precision, the GRACE data are used for the calibration of these global models. The WGHM and the GLDAS-CLSM model are among those few models to provide large-scale simulations of the TWS and GWS together. The variations of the model-derived TWS and GWS were cross-validated against those of the GRACE-derived estimates to come up with an idea regarding the feasibility and accuracy level of the WGHM and CLSM models for Turkey applications.

The associations between the GRACE-derived and the simulated TWS and GWS were investigated through their correlation in space and time. The temporal variations of TWS and GWS are given in Figure 5.7. The temporal interactions suggest that the calibrated CLSM shows a perfect correlation with the GRACE TWS and GWS estimates with correlation values of 0.95 and 0.91, respectively. The correlation values for the WGHM based TWS and GWS with the GRACE-derived TWS and GWS are 0.76 and 0.84, respectively. The close relationship between the CLSM model estimates and the GRACE estimates refers to the fact that the CLSM is calibrated with the GRACE data, therefore its quality has been increased through data assimilation process.

According to the graphs, although it seems that the WGHM-derived TWS is in a good value range compared to the GRACE estimates, the simulated GWS range from -2 cm to 2 cm of EWH, which falls far below the range of the GRACE-derived and CLSM-based GWS over Turkey. The WGHM underestimates the annual amplitude of the simulations by 10% over the majority of the world watersheds (Müller Schmied et al., 2021). Notwithstanding this value mismatch, the overall correlation between the GRACE and the WGHM is high.

The spatial correlation maps (Figures 5.8 & 5.9) demonstrate higher correlated values for the majority of the country. The spatial correlation of the GRACE and the modelled TWS ranges from -0.9 to +1 and -0.6 to +0.8 for the CLSM and WGHM, respectively. The correlation of the GWS, on the other hand, ranges from -0.2 to +0.8 and -0.5 to +1 for the CLSM and WGHM, respectively. Almost the same correlation pattern for the GRACE and the model values over small areas in the Marmara, the Mediterranean and the Black Sea regions is observed where the lower correlation values happen. For the spatial associations between the GRACE- and the WGHM-derived GWS over the central Anatolia, there seems a negative correlation to be exist while for the same area the correlation for the TWS values is positive. This can be justified by taking the fact that the WGHM do also simulate the groundwater extraction and integrate it into its GWS estimations which is not the case for the GRACE-derived values. Overall, the spatio-temporal consistency between the GRACE-driven and the simulated TWS and GWS over Turkey is high stressing the feasibility of the modelled variables for detecting and monitoring of the spatio-temporal variations of both the TWS and GWS (Syed et al., 2008) over the country.

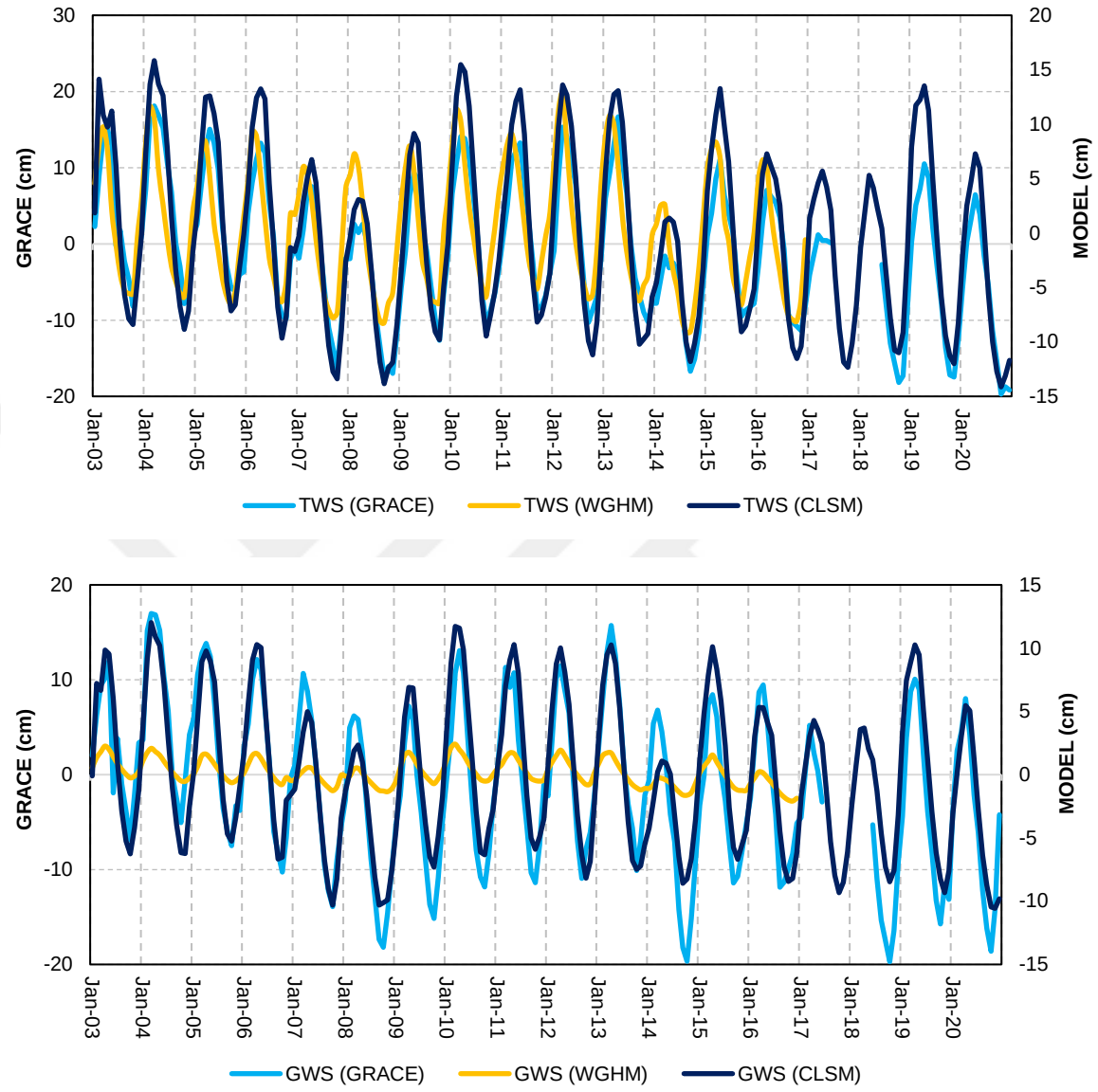


Figure 5.7 Temporal interactions between the GRACE-derived and simulated TWS and GWS over Turkey. The GRACE-GWS is derived based on the GLDAS outputs

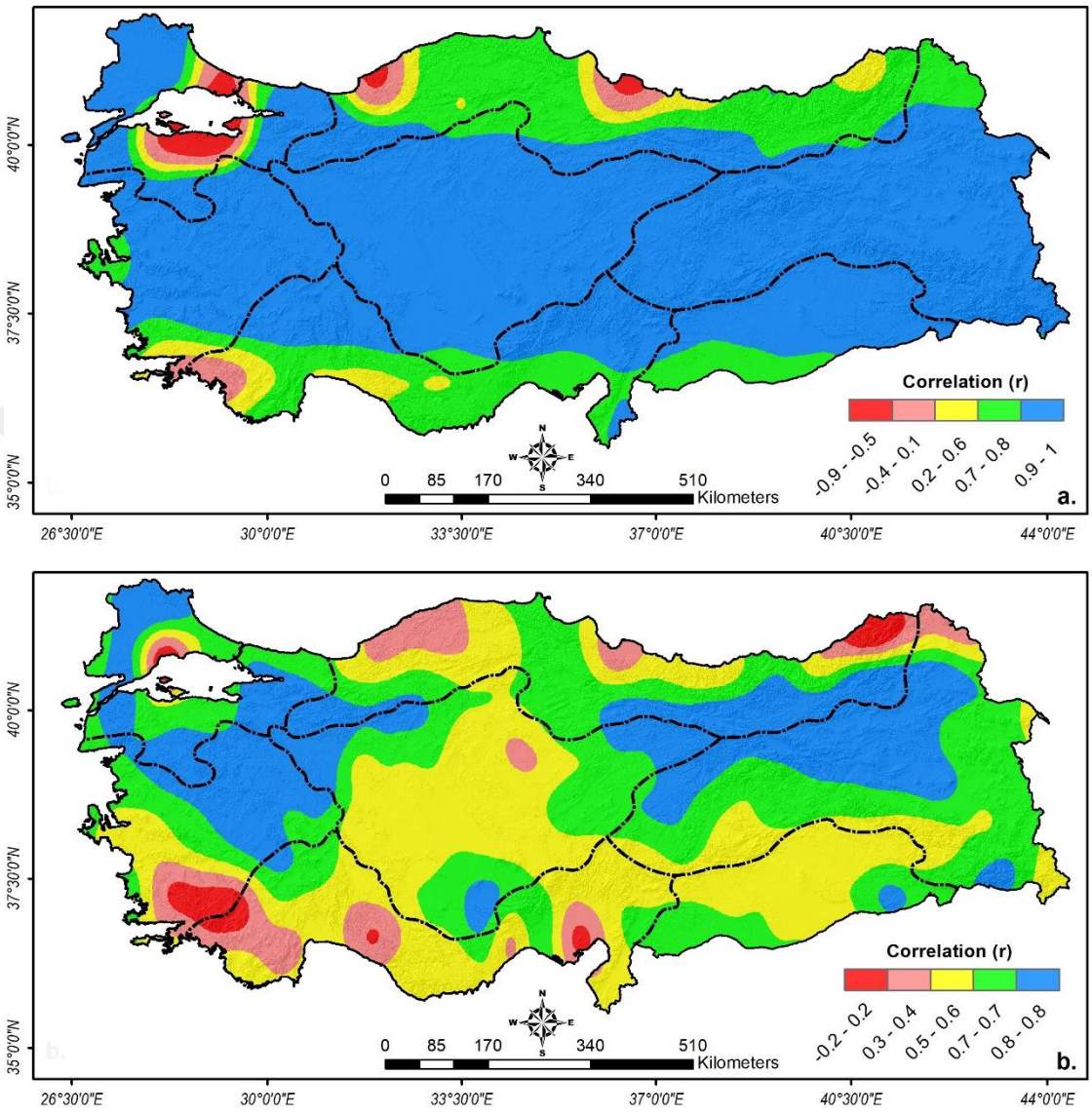


Figure 5.8 Spatial associations between the GRACE-derived and the CLSM-derived TWS (a) and GWS (b) over Turkey

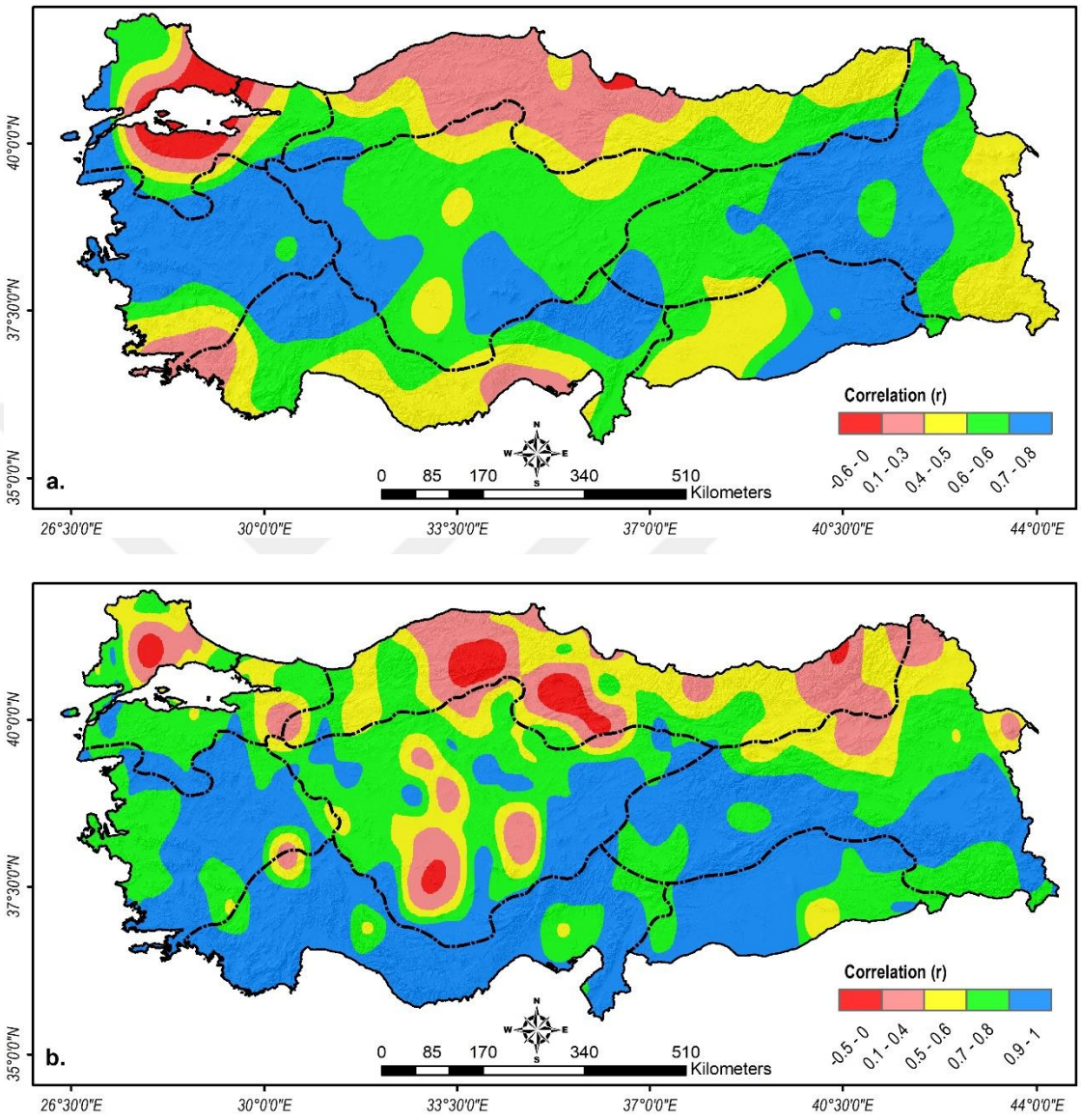


Figure 5.9 Spatial associations between the GRACE-derived and the WGHM-derived TWS (a) and GWS (b) over Turkey

5.5 Fluctuations of GWS in Response to the Variations in the Meteorological Variables

The temporal associations between the variations of the climatic parameters of precipitation (P) and temperature (T) were investigated to unravel the interactions between them and to see the impacts of the climatic parameters on the variations of the GRACE-derived GWS over Turkey. To this end, the monthly anomalies of P and T variables were extracted from the CHELSA and FLDAS models based on the same timeline as the GRACE estimates. The temporal interactions graphs are given in Figure 5.10.

Looking at the variations of the GWS and the climatic parameters, it can be deduced that Turkey's groundwater storage responds to the variations in the climatic situation of the country within a 2-month lag. The results reveal that the GWS over Turkey is best correlated with the monthly variations of meteorological variables of P and T in a 2-month-lag, for which the correlation coefficient is 0.47 and -0.81, respectively (Figure 5.11). The max variations of P and T conform to the peaks and troughs of the GWS time series emphasizing the important role of the received precipitation, as a major input of the hydrological cycle and experienced temperature anomalies, in the monthly fluctuations of GWS over Turkey. Precipitation anomalies manifest more than 40 mm of monthly deficit in three-time points: October 2006, October 2010 and September 2015. The monthly variations of precipitation over Turkey from 2006 to 2008 have been below the long-term normals (Okay Ahi and Jin, 2019). The huge precipitation deficit in September 2008 (-39.5 mm) corresponds exactly to the maximum loss of TWS (17.54 cm) in the study area.

The results also indicate that the fluctuations of the GWS in the study area interact more strongly with temperature. Therefore, it can be said that temperature decrease plays a dominant role in the variations of groundwater storage over Turkey (Khorrami and Gunduz, 2021a). According to the climatology graphs, the GWS demonstrate its least storage (-11.75 cm of EWH) in October, the time which correspond to minimum amount of precipitation (-32.15 mm). The overall correlation values for the climatological variations are 0.92 and -0.97 for P-GWS and T-GWS, respectively.

The annual variations, however, do not show good associations for the GWS and the climatic parameters over the study area. The annual correlations between the GWS and P and T are 0.12 and -0.45 respectively. According to the annual variations of the climatic variables, the decreased P and increased T in 2007 signify the commence of a dry period whose impacts are observed on the decreased GWS during the following years. In 2010, there is a sharp increase in the T and P variations. However, the GWS shows a decreasing trend stressing the fact that the impact of the T anomalies on the GWS is more than that of P over the country.

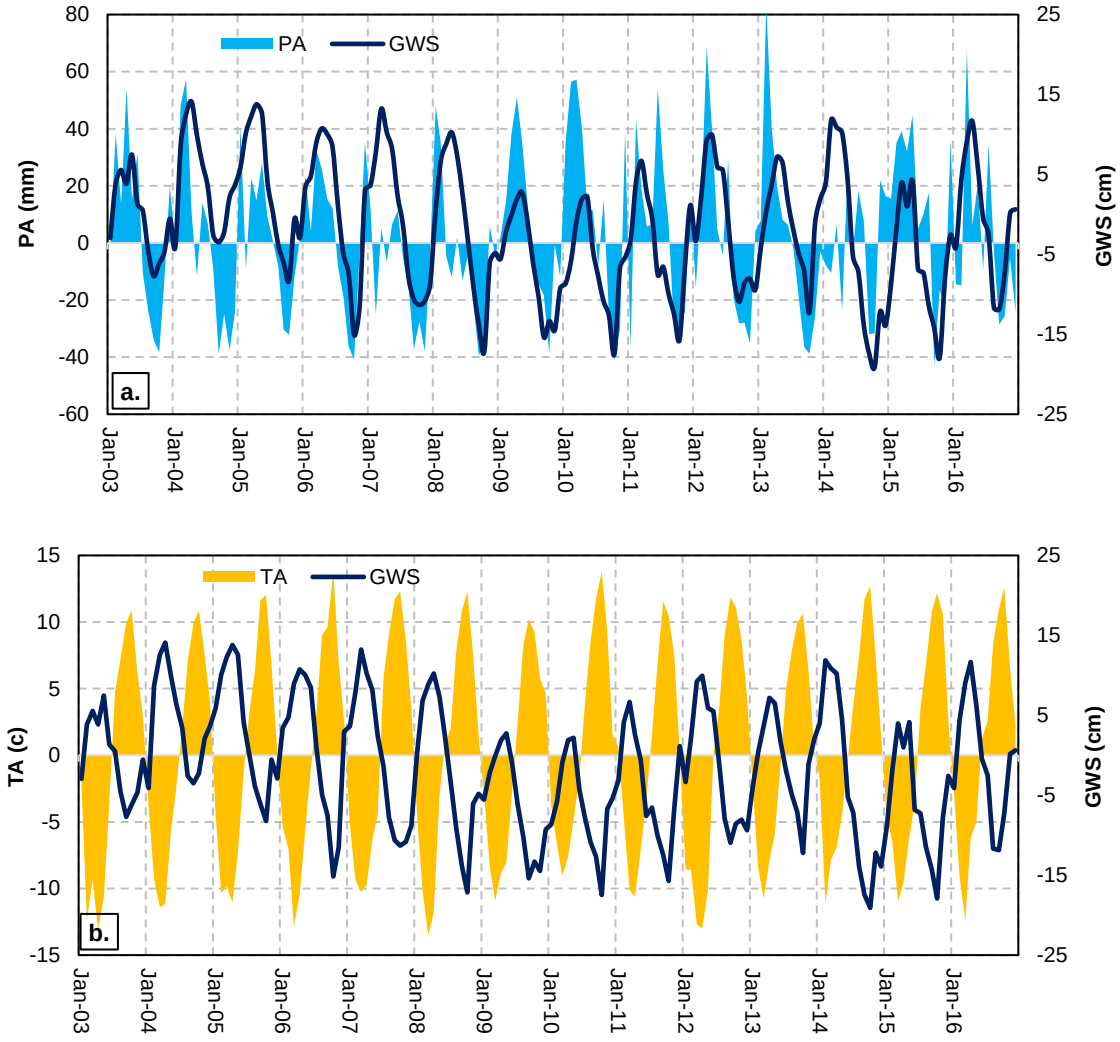


Figure 5.10 The monthly associations of GWS with PA (a) and TA (b) over Turkey.

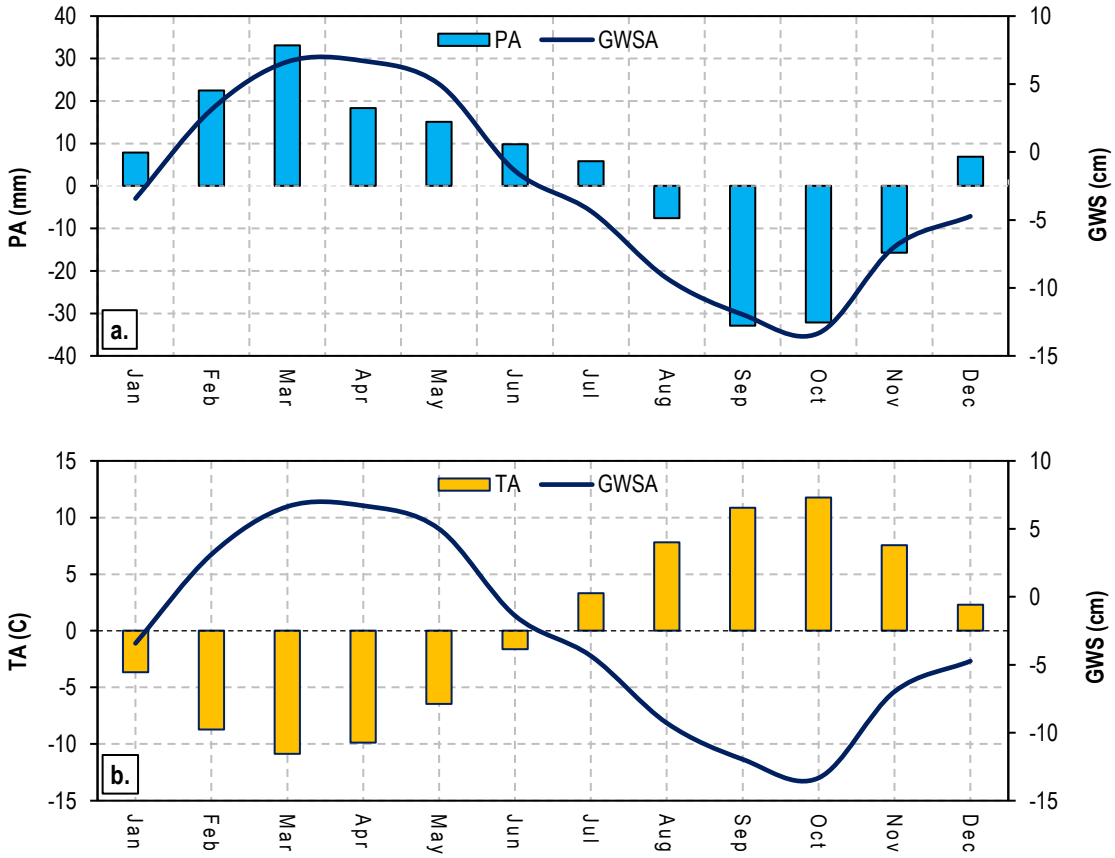


Figure 5.11 Climatological associations between GWS and PA(a) and TA(b).

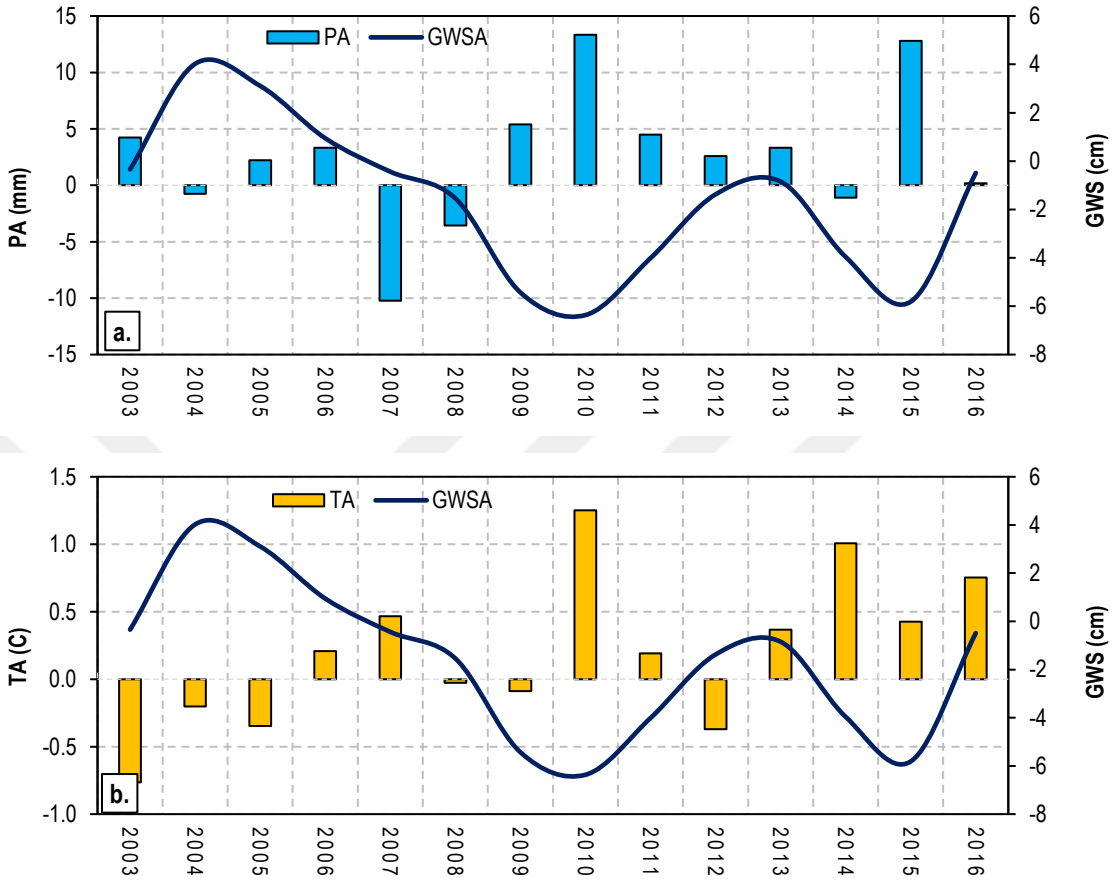


Figure 5.12 Annual associations between GWS and PA(a) and TA(b).

5.6 Groundwater Response to the Hydrometeorological Extremes

To investigate the responsive behavior of the groundwater storage against the hydrometeorological extremes over Turkey, different hydrometeorological indicators including the GRACE-based, in-situ SPI and model-based indices were applied. According to Khorrami and Gunduz (2021b), the GRACE-derived EWSDI gives the best characterization of the drought events in Turkey when calculated based on the decomposed GRACE TWS values. Therefore, to derive the EWSDI, first of all, the time series decomposition of the GRACE-TWS values was implemented.

5.6.1 TWS Decomposition

The GRACE-derived TWS time series was disintegrated into its compartments by trying both the additive and multiplicative techniques. Then, the best technique was opted for taking the accuracy-test results (Table 5.1) into account. As a result of the accuracy assessment, the multiplicative decomposition model turned out to be more accurate than the additive one with lower MSD and MAPE values. Therefore, the decomposition results based on the multiplicative model were used.

Table 5.1 Results of the accuracy assessment of the tried decomposition models. Mean absolute deviation (MAD), Mean Absolute Percentage Error (MAPE) and Mean Squared Deviation (MSD) metrics were used to determine the best decomposition model.

Model	**Metric**		
	MAPE	**MAD**	**MSD**
Additive	378.8	3.25	17.34
Multiplicative	316.8	4.63	3.06

Using the multiplicative model, the GRACE monthly TWS estimates were dissolved into different seasonal, trend and residual ingredients. The estimated trends were subtracted from the original TWS to compute the de-trended TWS. The de-seasoned TWS was also calculated using seasonal factors. The seasonal factor is a specific seasonal value received by fitting the best model. Table 5.2 depicts the seasonal factors for each month. De-seasoned TWS refers to the time series of TWS, for which the seasonality impacts have been removed. At the final stage and by subtracting the trend and seasonality from the original TWS, residuals are computed. In Figures 5.13 and 5.14, the results of the time series decomposition are shown.

The seasonal decomposition was done by using the mean value of each season over the study area. The seasonal TWS values were calculated as accumulative monthly values of each season. The results of the GRACE seasonal disintegration for Turkey suggest that its groundwater storage suffer from the maximum and minimum storage variations in spring and fall (Figure 5.15). The seasonal patterns found for Turkey agree precisely with the seasonal cycles of TWS reported by Humphrey et al. (2016) for the temperate regions in the Northern hemisphere.

Table 5.2 Scale factor revealed for each season through the seasonal disintegration of the GRACE-TWS

Month	**Seasonal Factor**	**Month**	**Seasonal Factor**
Jan	1.54	**Jul**	0.89
Feb	2.57	**Aug**	-1.08
Mar	3.61	**Sep**	-1.36
Apr	3.32	**Oct**	-2.28
May	3.04	**Nov**	-0.65
Jun	2.17	**Dec**	0.30

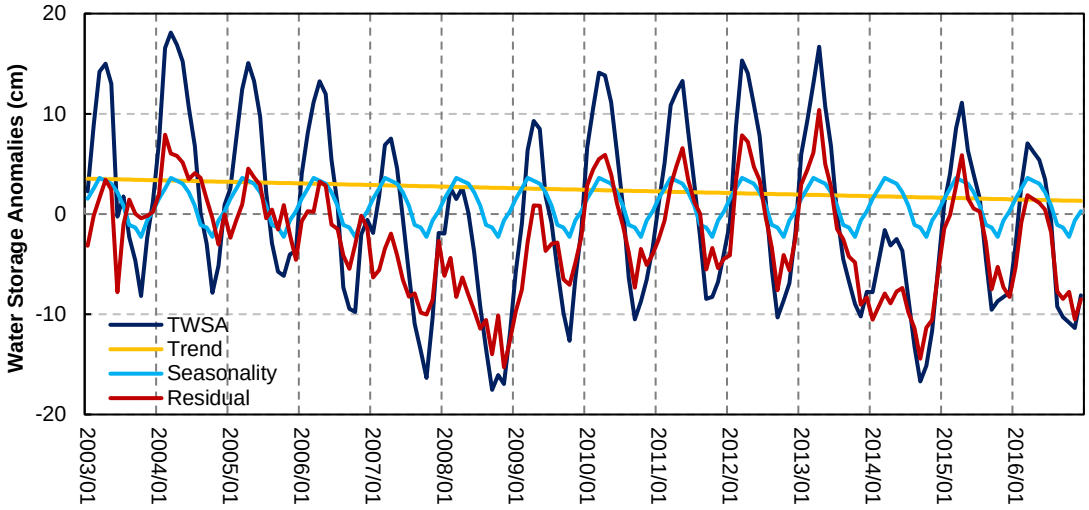


Figure 5.13 Decomposed GRACE-TWS over Turkey

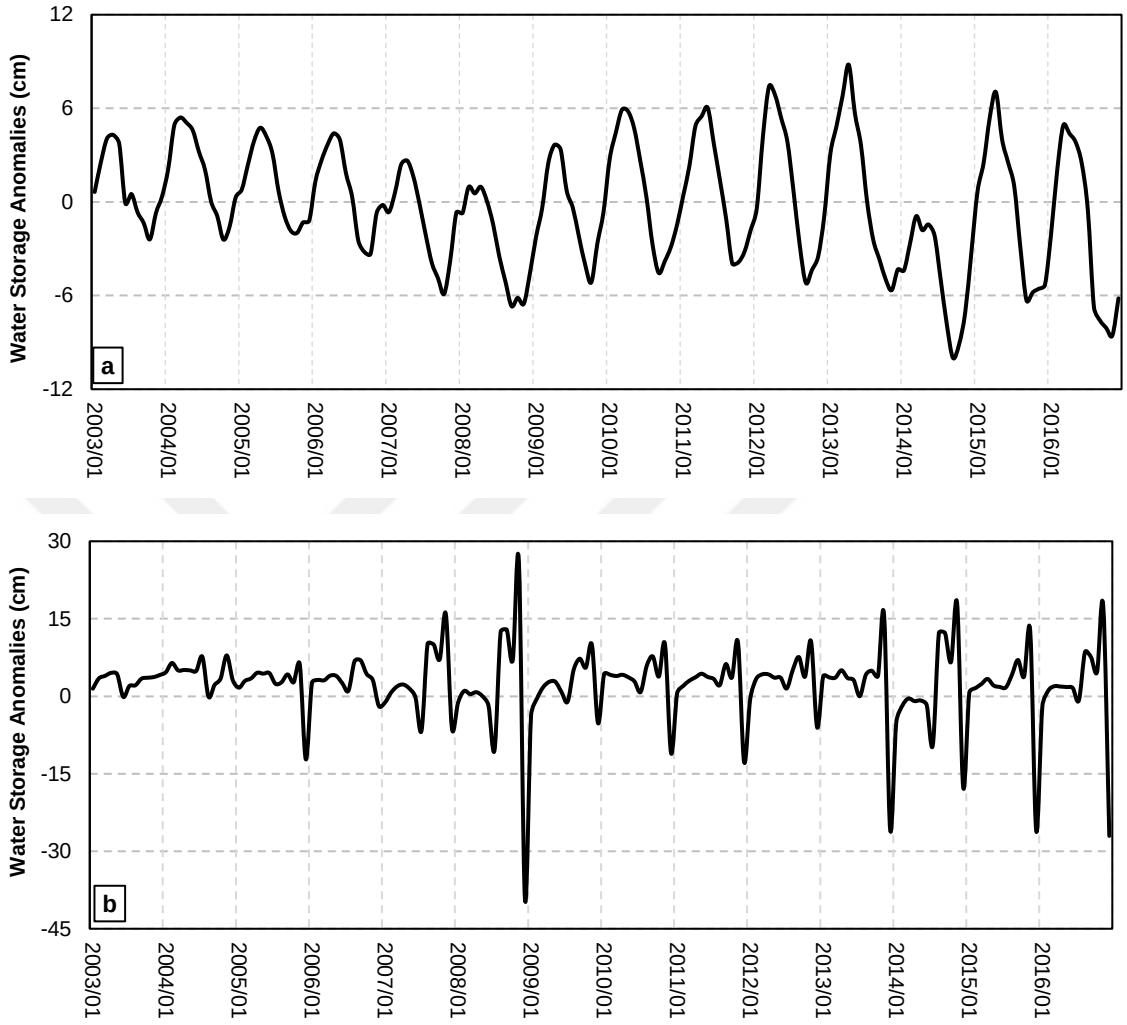


Figure 5.14 Time series of de-trended (a) and de-seasoned (b) TWS

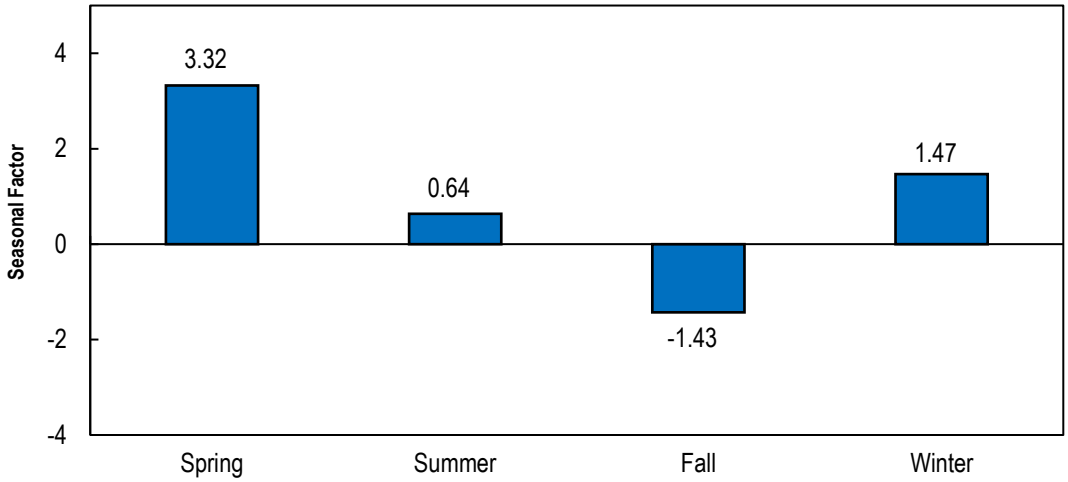


Figure 5.15 Seasonal variations of the water storage over Turkey

The overall variance of the TWS time series is determined through the accumulative values of individual decomposed components (Shamsudduha and Taylor, 2020). Figure 5.16 demonstrates that the trend with 42% of contribution accounts for the majority of the TWS time-series variance over Turkey. Seasonality, on the other hand, has the minimum share of 17%. By getting rid of the trend and seasonality, residual TWS contributes to 41% of the variance.

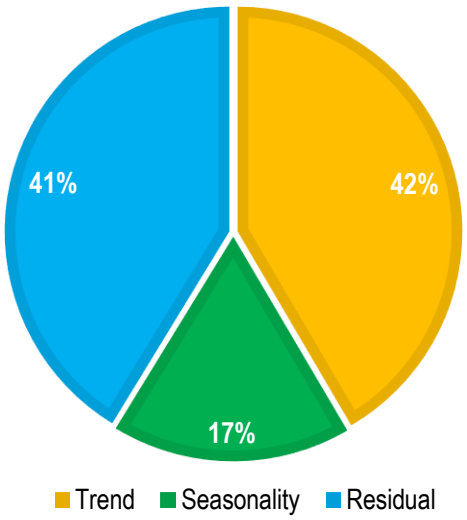


Figure 5.16 The contribution of the GRACE-TWS timeseries components to its total variance

5.6.2 Investigating the Extreme Hydrometeorological Events over Turkey

In an attempt to reveal the interactions between the extreme hydrometeorological events and the fluctuations of groundwater storage over Turkey, the recent history in terms of dry and wet periods was investigated. As the first step, different indices including the GRACE-derived EWSDI as well as the traditional drought indicators of SPI, SPEI and PDSI were utilized to unravel the recent hydrometeorological status of the country. The GRACE-driven EWSDI was calculated based on the detrended TWS resulting from the time series decomposition task. SPI was computed using the real observations of monthly precipitation received from meteorological stations over the country. SPEI and scPDSI were extracted from global models.

The time series of the used drought indices (Figure 5.17) were drawn using the areal mean values of each corresponding index over Turkey. According to the resulted graphs, although the variations of the used indices differ slightly over the study period (2003-2016), they all have a common ground in detecting the main droughts over the country. The graphs clearly manifest that Turkey has experienced droughts during 2007-2008 and 2014, which is in accordance with the previously published paper results (e.g., Marim et al. 2008; Türkeş et al. 2009; Kurnaz, 2014; Okay Ahi and Jin, 2019). Since the SPI is based on real field-based records, the performance of the other indices can be quantified in terms of correlation coefficient. According to the results, the GRACE-derived EWSDI shows a good agreement with the field-based SPI with a correlation of 0.7. The model-based indices of SPEI and scPDSI, on the other hand, show even more correlation values. The SPEI and PDSI are highly correlated with the SPI with correlation coefficients of 0.85 and 0.72 over Turkey, respectively.

Taking the nature of the used indices into account, the variations in the temporal situation of the used indices can be justified. Although the EWSDI gives a relatively high correlation against the SPI over Turkey, its performance seems a bit low with regard to the simulated SPEI. This is mainly because of two factors. First, the GRACE measures

the variations of large-scale water storage. Therefore, the GRACE-based indices suffer from some uncertainties, which may hinder their performance in the exact detection of the hydrometeorological incidents especially over regional to local scale areas (Khorrami and Gunduz, 2021b). Furthermore, the TWS-deficit-oriented drought studies based on the GRACE records are generally lame in detecting minor drought incidents (Chen and Rodell, 2021). The integration of the air temperature in terms of evapotranspiration into the SPEI through Penman-Monteit methods (Zhang et al., 2020) culminates in its better performance. The annual time-series graph (Figure 5.17b) of the used indices reveal even more the dry years of 2008 and 2014 over Turkey, from which the year 2008 shows the most critical situation where all the used indices show their maximum trough. The variations of the annual values also suggest that in 2010 and 2015, Turkey has experienced relatively wet periods in comparison to other years.

The interpolated surfaces of the GRACE-EWSDI, SPI, SPEI and scPDSI were generated to better illustrate the variability of the used indices over Turkey. Since the year 2008 is nominated as the harshest year in terms of drought impacts in the country, the thematic maps of drought indices (Figure 5.18) were drawn for the year 2008 to have a visualistic perspective of the spatial footprint of the 2008-drought event over Turkey. According to the drought maps, the 2008-drought has been felt almost all over Turkey excluding small areas in the coastal area of the Black Seas region, over which the positive values of the SPI, SPEI and scPDSI are observed. On the other hand, over eastern Turkey, especially the Southeast Anatolian region, the SPI manifests a more intense situation with the concentration of large negative values. This situation can be also seen in the SPEI and PDSI maps. The SPEI and PDSI maps seem to better catch the spatial extension of the drought event, from which the evolution of the dryness in the eastern regions, particularly the Aegean and Marmara regions, can be observed clearly.

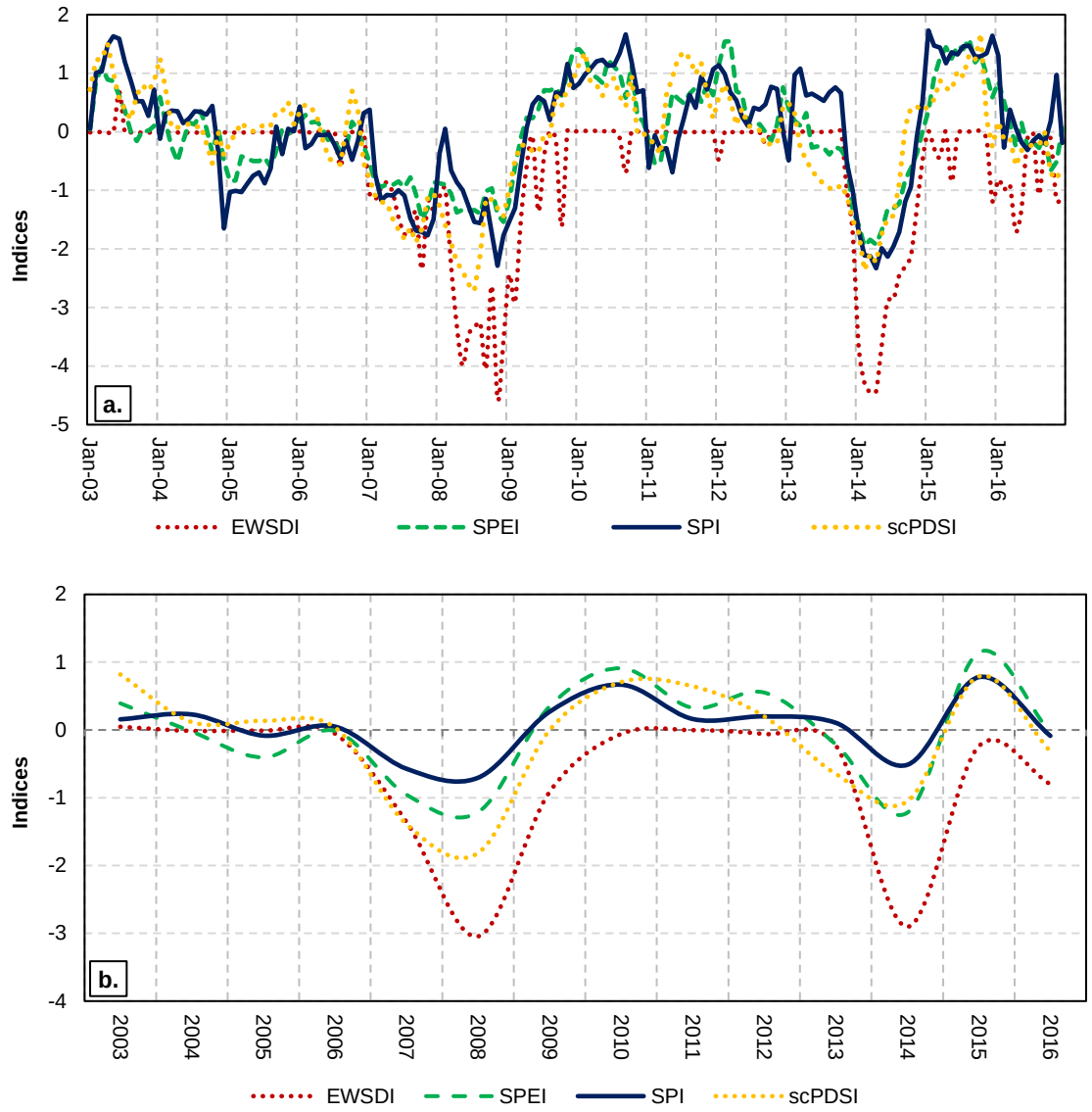


Figure 5.17 The recent monthly (a.) and annual (b) hydrometeorological status of Turkey according to the GRACE-based EWSI, SPI, SPEI and scPDSI indicators

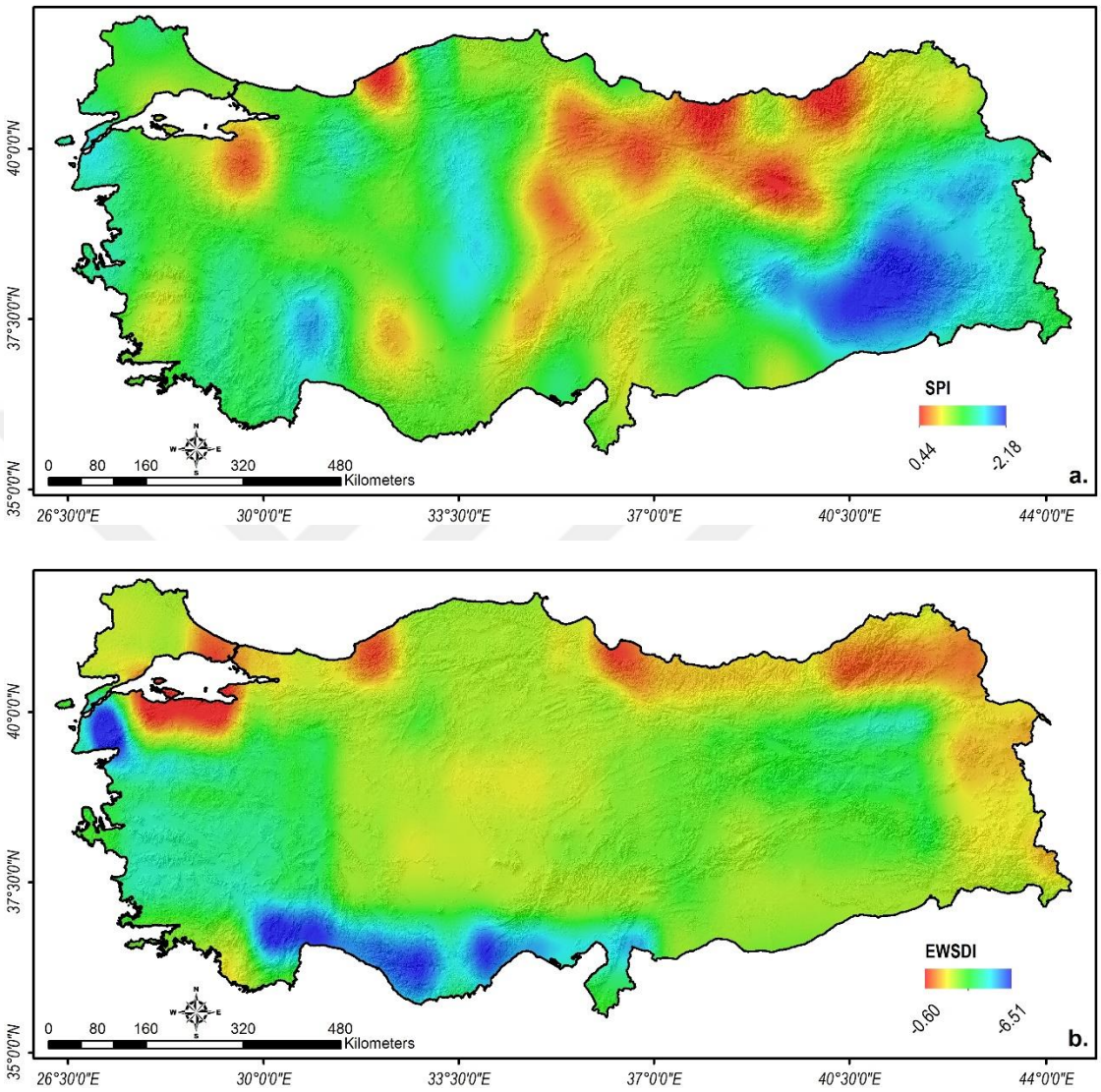


Figure 5.18 Thematic maps of the spatial distribution of drought indices over Turkey: SPI (a.), EWSDI (b.), SPEI (c.) and scPDSI (d) for the year 2008.

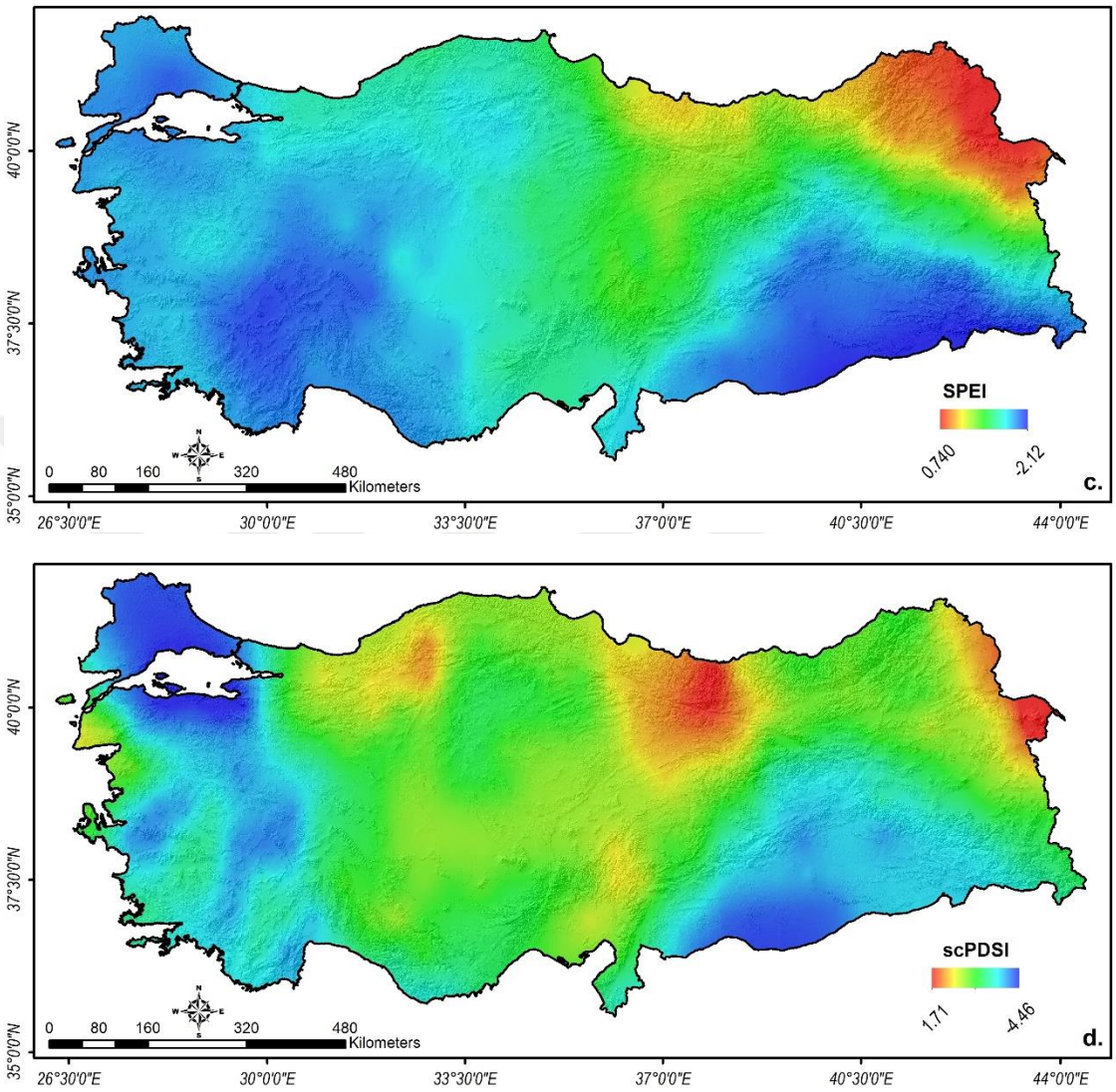


Figure 5.18 Continues.

5.6.3 Associations Between the Drought Indices and GWS

The spatio-temporal associations between drought events and the fluctuations of groundwater storage over Turkey were investigated by means of interactive time-series graphs and spatial correlation maps. Figure 5.19 shows the temporal interactions between the used drought indices and GWS from 2003 to 2016 at monthly and annual time scales. The variations peaks and troughs of the GWS show seasonality. However, the extreme groundwater storage loss observed in 2008 and 2014 demonstrate the impacts of dry periods on the excessive demand for groundwater thus depleting groundwater storage over the country. To get the seasonality effect rid of the GWS variations, the climatology GWS values were subtracted from the original GWS to come up with the residual GWS called groundwater storage deficit (GSD) (Thomas et al., 2017; Nigatu et al., 2021). By using the GSD in the time-series graph, the groundwater associations with drought indices are better apprehended. While the GRACE-derived EWSDI shows the correlation of 0.37 with the GWS, the SPEI, SPI and PDSI demonstrate lower correlation values of 0.13, 0.12 and 0.12, respectively. The overall correlation values between the GWS and drought indices seem low, which results from the fact that the groundwater aquifer responds to the variations of hydrometeorological parameters with monthly lags. This monthly lag is apparent in the monthly and annual graphs especially in 2014.

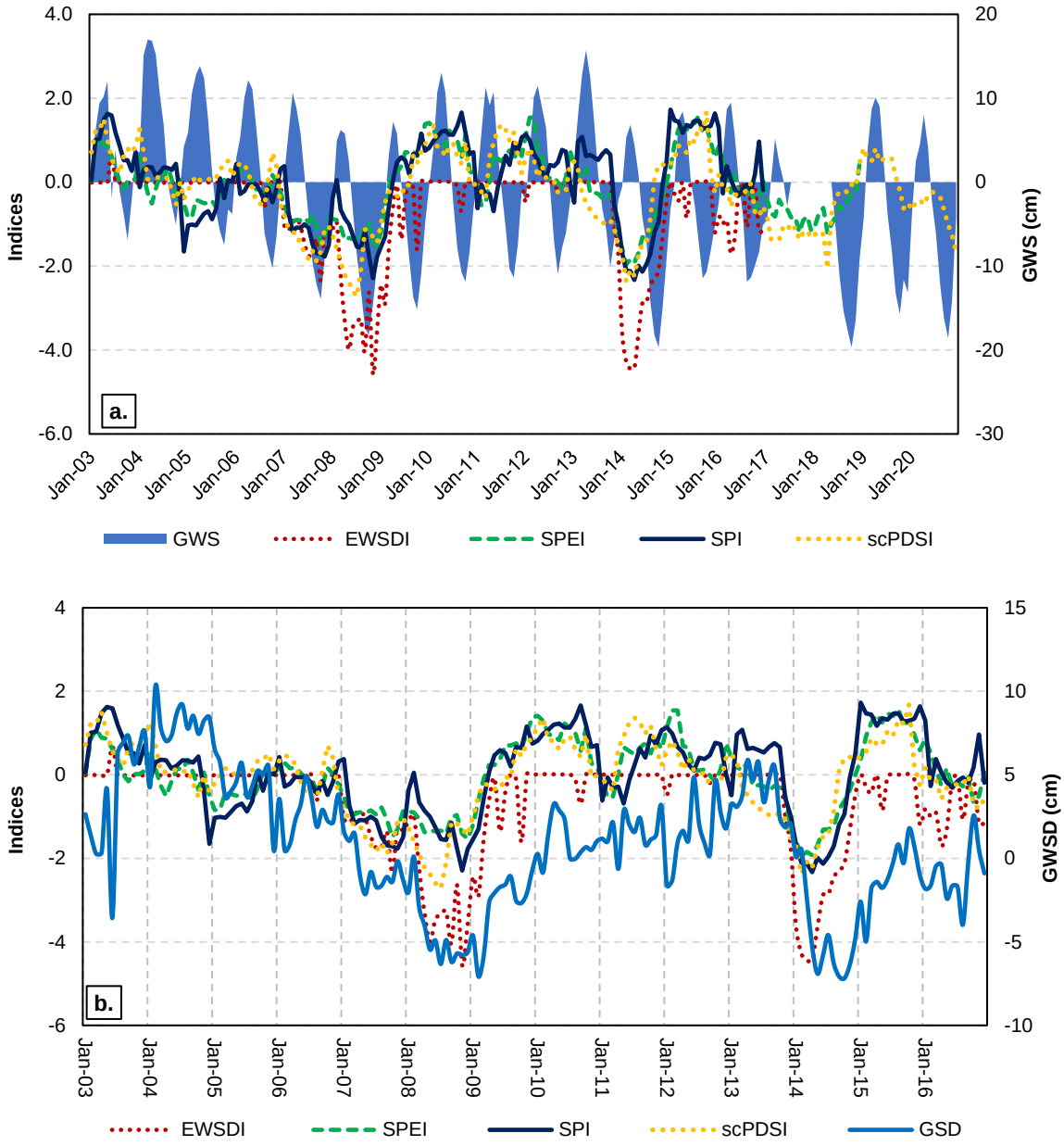


Figure 5.19 Illustration of the temporal associations between the hydrometeorological indicators and monthly groundwater storage (a), monthly groundwater storage deficit (b) and annual groundwater storage (c).

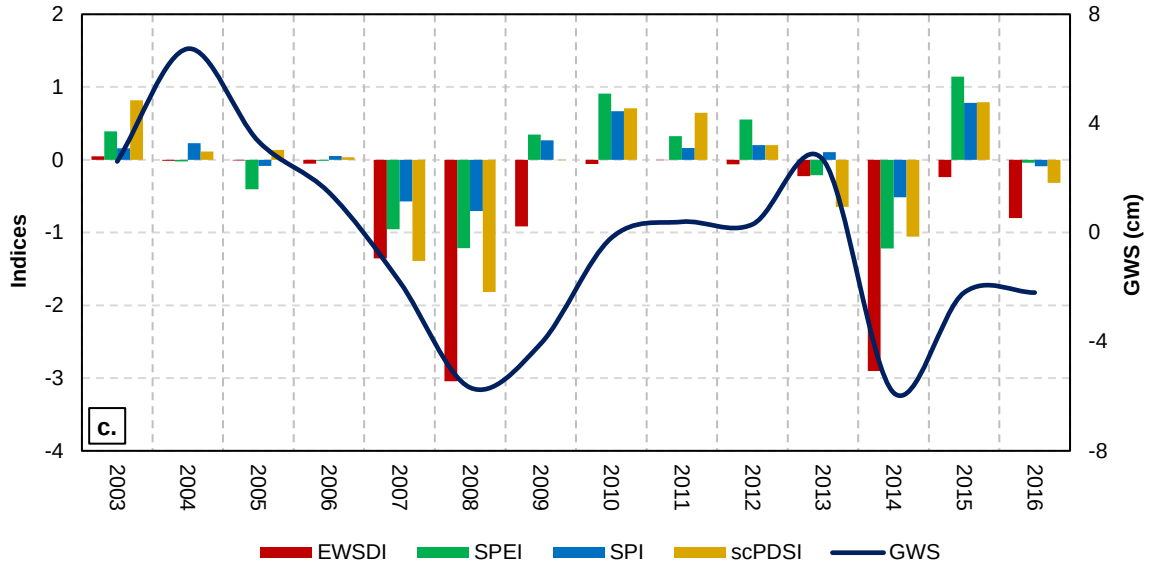


Figure 5.19 Continues.

The spatial associations between the drought indices and the groundwater storage variations over Turkey were further investigated utilizing spatial correlation maps (Figure 5.20). The spatial correlation maps generated here delegate the correlation of the time series values of corresponding indices and the variations of the groundwater storage. Therefore, by using these maps, one can better understand the spatial scale of the associations between the hydrometeorological events and their impacts on the fluctuations of groundwater storage. The spatial distribution of the correlation values indicates that there is a central- and west-wise positive correlation pattern between the used indices and GWS, which implies that the groundwater aquifers in the central and western Anatolian regions suffer more from the drought events. On the other hand, the lowest impacts can be inferred for the Black Sea regions where negative or low correlations are observed.

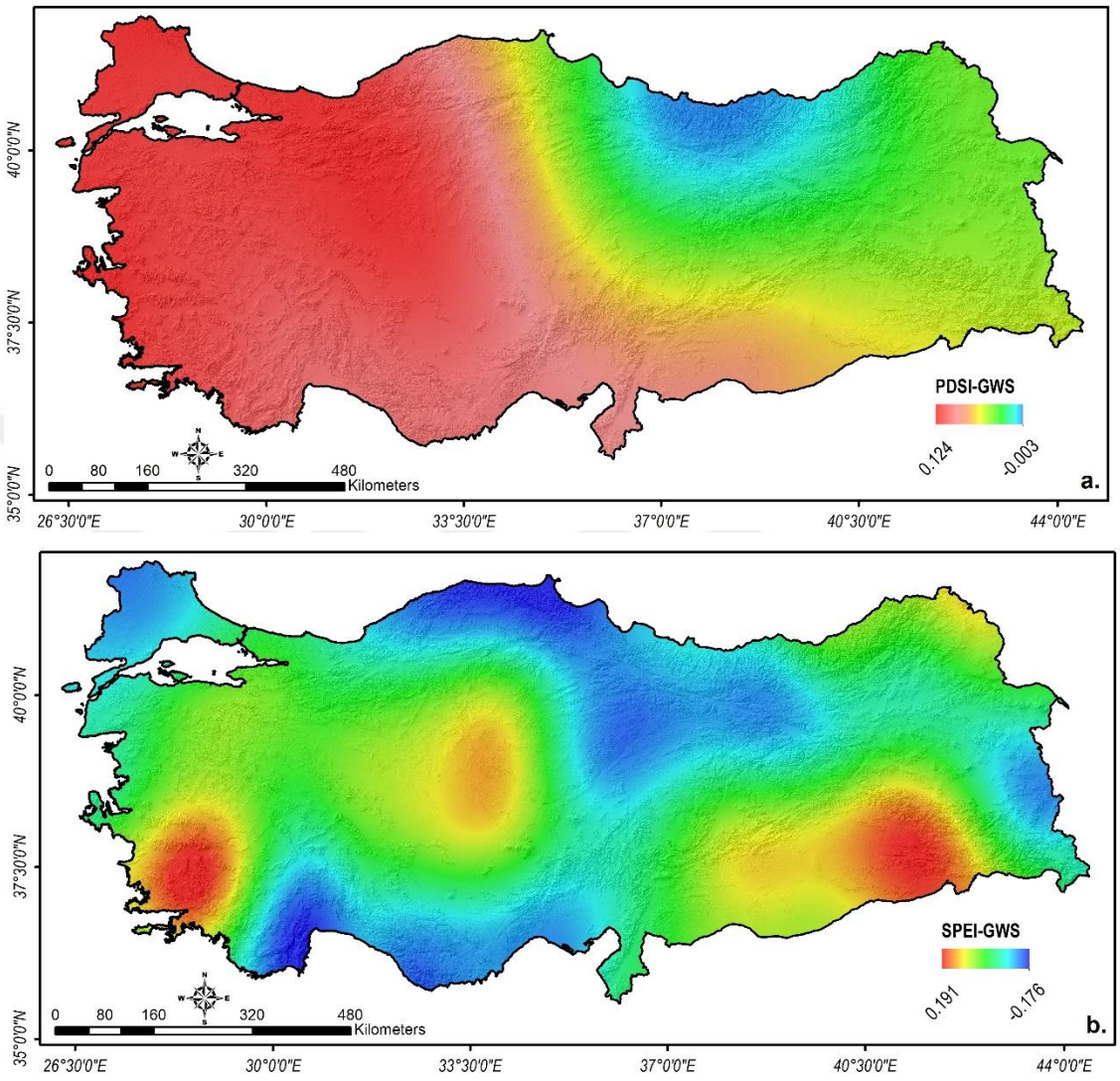


Figure 5.20 Spatial correlation of the GRACE-derived GWS and hydrometeorological indices of PDSI (a.), SPEI (b.), SPI (c.) and EWSDI (d.)

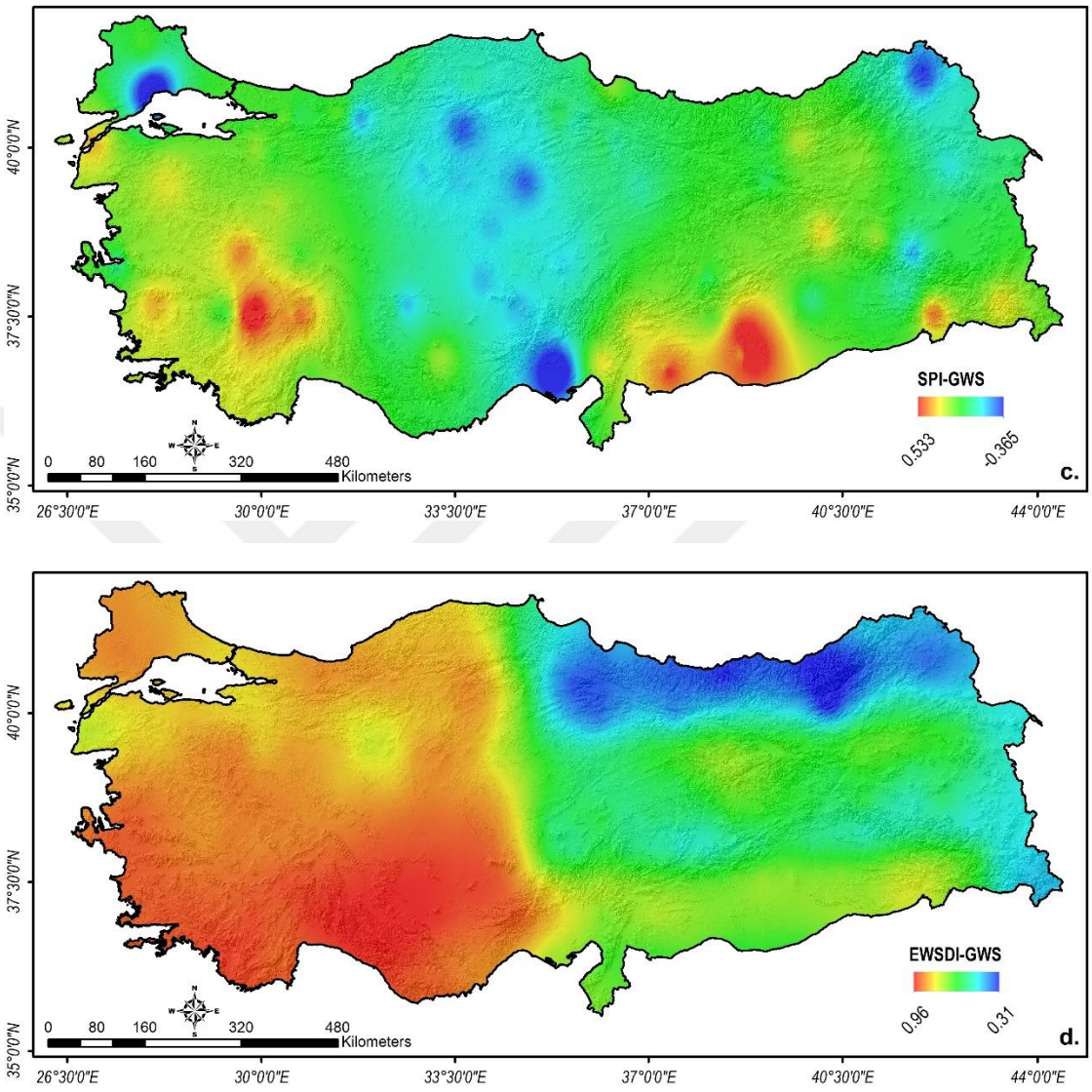


Figure 5.20 Continues

5.7 Assessment of the Agricultural Activities over Turkey

Turkey is a rapidly developing country and agriculture is still the main economic activity of the majority of its population. The extent of this economic practice differs according to the different geographic regions of Turkey. While the agricultural practices in the Western and Southern regions include competitive and capital-intensive cultivation of export productions, they are limited to subsidized and trade-protection crops over the Northern and Northeastern Turkey (Aerni, 2007). With an estimated cultivated area of 23.14 million hectares, Turkey is known as one of the richest countries of the world regarding its land under cultivation (Ministry of Agriculture and Forestry, 2020). Since a considerable volume of water is consumed for irrigation purposes in Turkey, variations in the agricultural activities play a determining impact on those of the groundwater storage. Increased irrigation results in increased water abstraction from either the surface water or the groundwater resources. To investigate the impacts of the agricultural practices on the variations of the groundwater storage and water consumption over Turkey, the NDVI time series from MODIS and consumptive water time series from the WGHM model were used.

The time series of the NDVI were generated using the country-mean values of the NDVI retrieved from the monthly MODIS dataset. The variations of the retrieved NDVI (Figure 5.21) demonstrate a statistically significant ($P < 0.5$) ascending trend from 2002 to 2020. The ascending trend in the variations of the NDVI over Turkey is confirmed by the findings of Evrendilek and Gulbeyaz (2008). In light of the fact that the variations of the satellite-based NDVI can be suitably utilized for the monitoring of the agricultural crop densities at global to regional scales (Rasmussen, 1997; Granados-Ramírez et al., 2004), the variations of the NDVI are deemed to represent the changes in the extent of the agricultural activities over Turkey. Hence, its variations were used in combination with the model-based water consumption values to investigate the interactions between agricultural activities, water use and consequently GWS over Turkey.

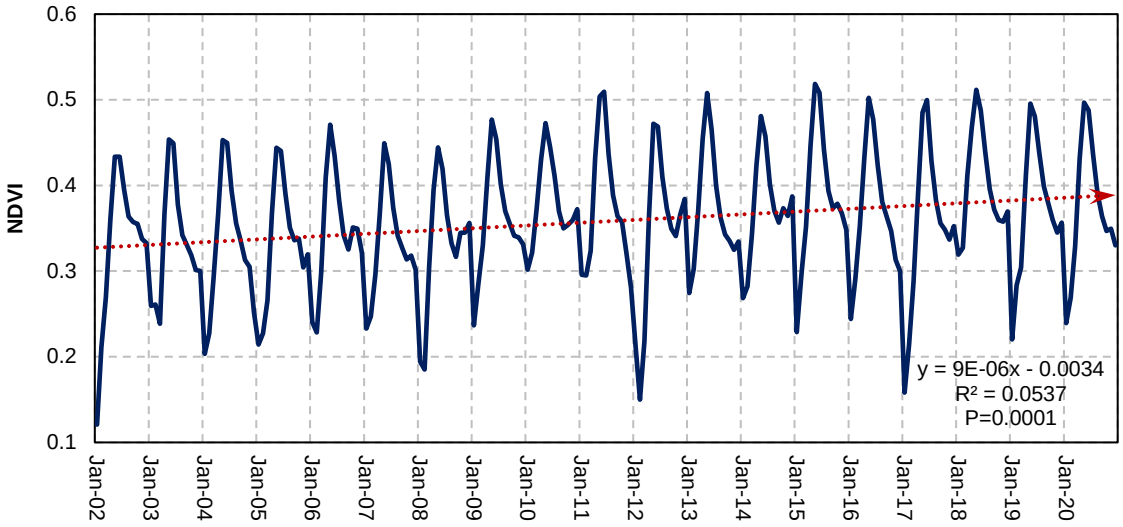


Figure 5.21 Time series variations of the MODIS-derived Normalized Difference Vegetation Index (NDVI) over Turkey.

The time series of the surface water and groundwater consumption over Turkey were generated based on the actual net abstraction from surface water (ANAS) and actual net abstraction from groundwater (ANAG) simulated by the WGHM model. The variations in the surface and groundwater use do not show any trend over Turkey. Instead, these model-driven values manifest strong seasonality. The associations between the country-mean variations of the NDVI with the water consumption are shown in Figure 5.22. The associations reveal that over the country, the NDVI impacts the surface water use directly with a correlation value of 0.73. It shows that the increased NDVI brings about augmented water consumption from the surface water sources over Turkey. The association between the NDVI and groundwater use, on the other hand, show a time lag. The groundwater use values are highly correlated (0.7) with the lagged NDVI with a 6-month temporal lag. It demonstrates that the response of groundwater consumption to the variations in the magnitude of the agricultural activities takes time compared to that of the surface water.

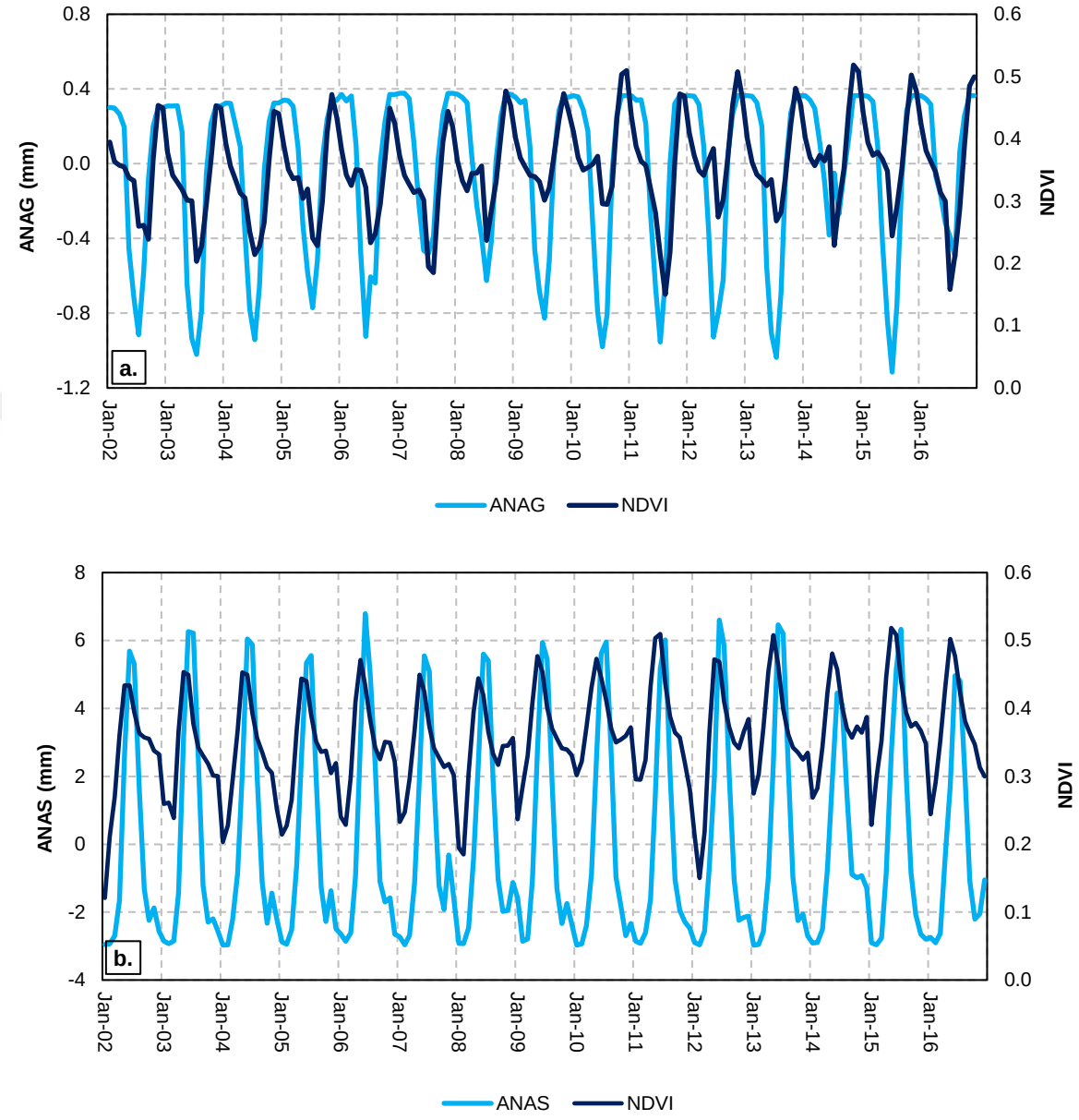


Figure 5.22 Temporal associations between the variations of the NDVI and the simulated abstracted water from groundwater water (a.) and surface water (b.) over Turkey

The associations between the NDVI and GWS were also investigated through their temporal time series (Figure 5.23). It indicates that the fluctuations of the groundwater storage over Turkey react to the variations of the NDVI within 3 months that is there is a temporal lag between them. The correlation of coefficient between the GWS and the

NDVI is -0.72. This pattern is also rational because the increased NDVI prompts increased water extraction from the groundwater aquifer and as a result, the groundwater storage decreases. The high interactions between the NDVI and GWS variations has also been reported by Seeyan et al., (2014) and Bhanja et al., (2019). The increased and sustained NDVI variations over Turkey especially during the dry periods stem are ascribed to the overexploitation form the groundwater aquifers (Yilmaz, et al., 2016).

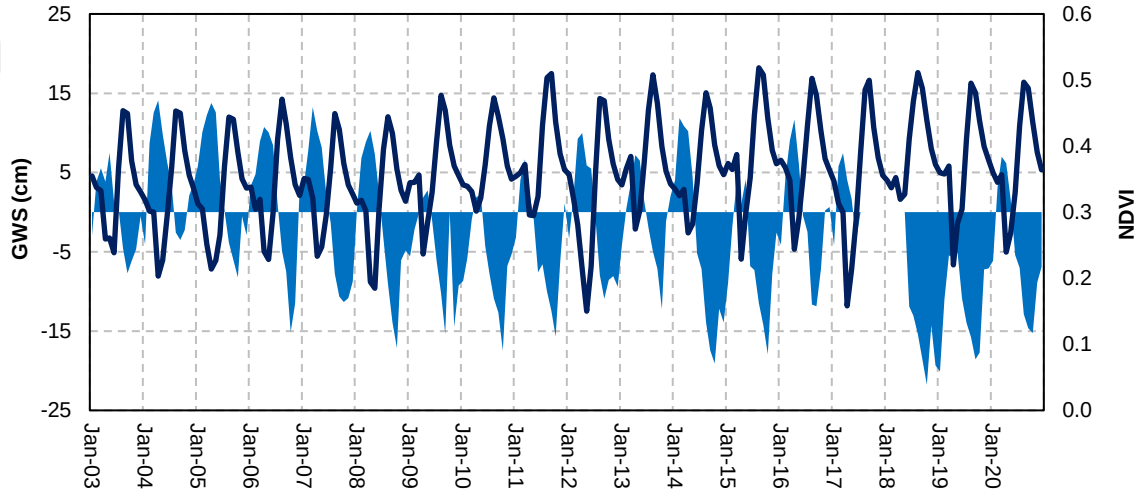


Figure 5.23 Temporal associations between the fluctuations of the GRACE-derived GWS and the MODIS-derived NDVI over Turkey.

5.8 Downscaling Results

Within the scope of the current study, the small-scale variations of the GRACE-observed GWS were investigated through downscaling technique.

5.8.1 Model Sensitivity

The Random Forest model provides the relative contribution of each input variable in the process of downscaling to determine their importance. The importance of each variable is given in terms of %IncMSE, which demonstrates the possible increase in MSE by randomly permuted variables (Zhao et al., 2018). The sensitivity result is interpreted as follows; The larger the %IncMSE, the more important the variable to the model. Associations between the model inputs impact the model performance. In this study, different values such as precipitation, soil moisture, snow water, surface runoff, evapotranspiration and surface elevation were integrated into the GRACE-TWS to develop the RF model. The predictability of the inputs of the developed model for the study area was investigated based on the variable importance measures predictive (VIMP) test. The VIMP calculates the variations of the prediction error of each input variable before and after permutation (Rahaman et al., 2019b; Ali et al., 2021).

The sensitivity results for the harsh climatic situation of Oct 2020 are given in Figure 5.24. It reveals that precipitation and surface elevation (DEM) were the most crucial variables in developing the RF model. Precipitation is the main input water for the hydrological water cycle (Khorrami and Gunduz, 2021a) therefore, its variations have a dominating impact on the variations of different hydrological components, especially the total water storage. The highest weight of precipitation in the process of the GRACE-TWS downscaling has also been reported by Ali et al., (2021).

The surface elevation (DEM) is the second most effective parameter for the RF model. This can be ascribed to the role that the diverse surface topography of the country plays in the variations of different hydrometeorological variables over Turkey. Especially the orographic effects (Ding et al., 2014) of the surface elevation on the climatic parameters such as precipitation and temperature are probably a controlling factor for the RF-based model downscaling of the GRACE TWS over Turkey. Rahaman et al (2019b) also reported a significant role of the surface elevation for downscaling of the GRACE data over the United States.

The anomalies of the snow water storage, on the other hand, turned out to be the least effective parameter for the RF-based downscaling of the GRACE TWS. This is rational because the variations of the snow water are restricted to a small spatial fraction of the country in the Eastern regions. Therefore, with its least impact on the variations of Turkey's TWS, snow water manifests the least importance among the used variables. In light of the fact that all the used input parameters revealed above-zero values, they were considered skillful in the downscaling of the GRACE-TWS.

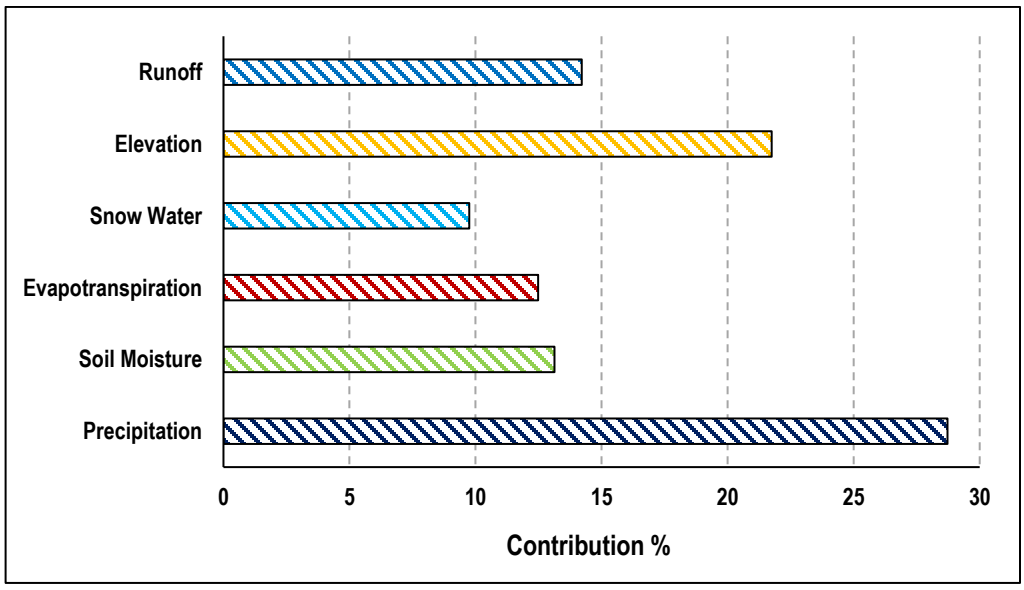


Figure 5.24 Importance Measure Predictive (VIMP) test results for the model inputs

5.8.2 Investigating the Predictive Precision of the RF Model

The performance of the RF model was tested using the original and modeled (downscaled) TWS and GWS values. Five statistical metrics (R, R^2, RMSE, MAE and D) were applied to show the accuracy of the downscaling technique. According to the results (Figure 5.25), with a correlation of coefficient of more than 0.98, coefficient of determination of more than 0.91 and NSE value of more than 0.92, the RF model turned out to be highly successful in modeling the finer resolution TWS and GWS over the study area. Higher associations between the RF-based downscaled TWS and the GRACE-TWS have been found by several researchers over different study areas. For example, Ali et al. (2021), Milewski et al. (2019), Chen et al. (2019-b) and Rahaman et al. (2019b) reported correlation values of 0.97, 0.97, 0.96 and 0.94 for the RF- and GRACE-based TWS.

To check the spatial consistency of the pre-and post-downscaling TWS and GWS over Turkey, the variations of 2020 were mapped as an example. As observed in Figure 5.26 and Figure 5.27, the original and downscaled distribution of the TWS and GWS are consistent from the perspective of spatial distribution. The figures manifest a good performance for the RF model in filling in the spatial gaps of the TWS and GWS values and simulating the exact spatial dispersion of the fine resolution GRACE estimates over Turkey, which overall correspond with the trends of the original values.

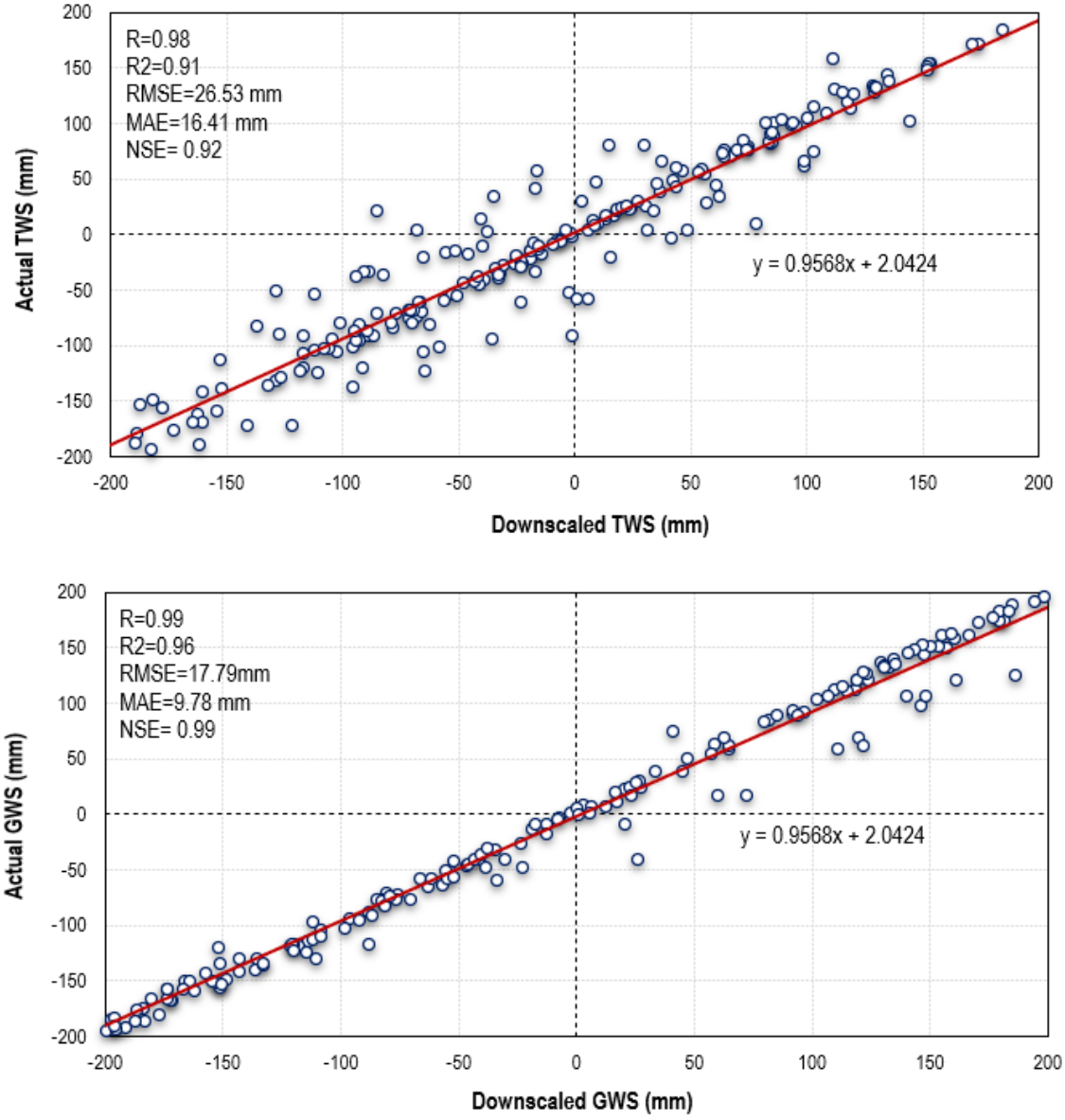


Figure 5.25 Scatter plots and regression fits of the RF-based and GRACE-based TWS and GWS over Turkey

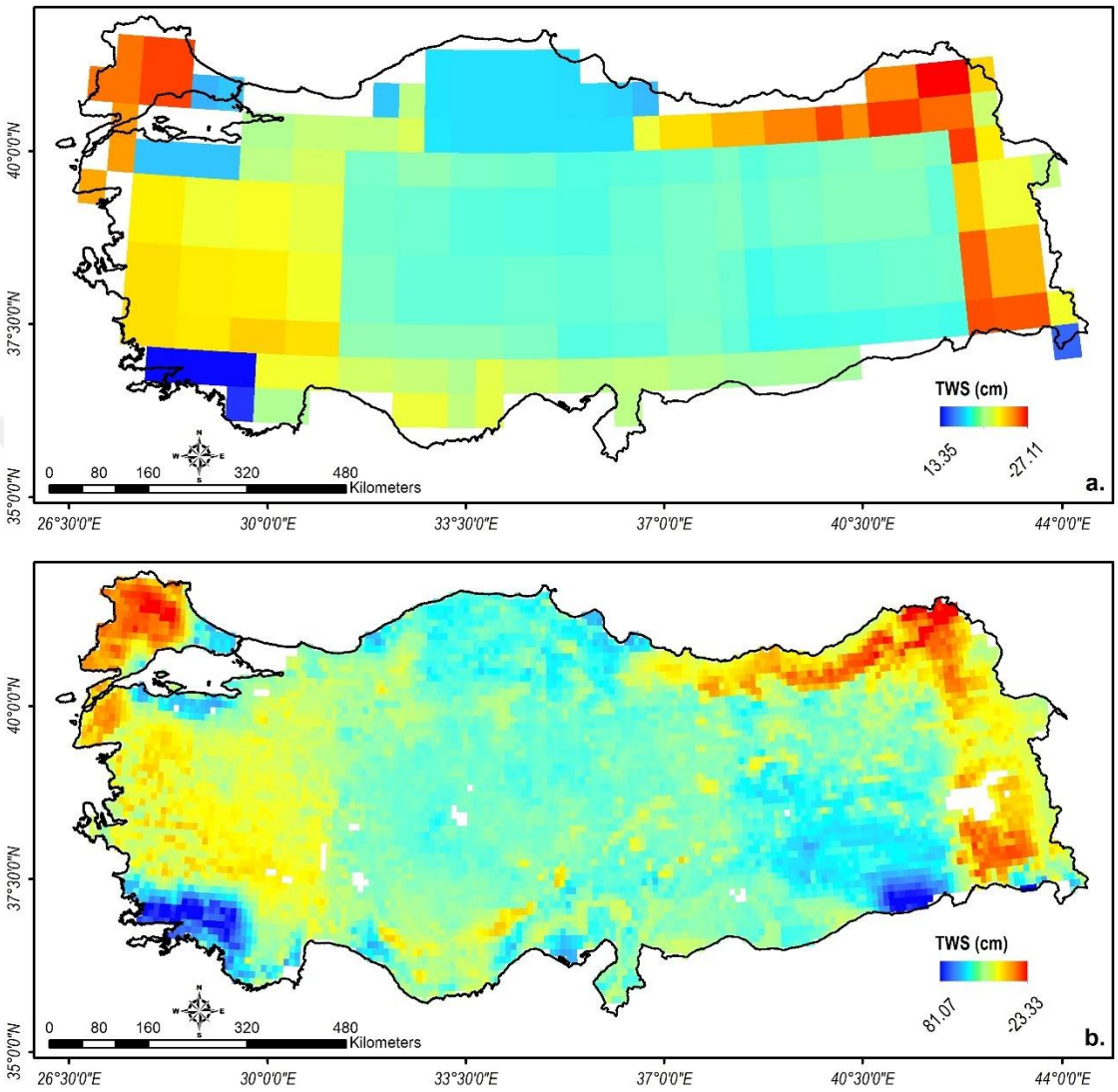


Figure 5.26 Illustration of the annual spatial fluctuations of the GRACE-derived TWS for the year 2020 before (a.) and after downscaling (b.) practice. The spatial resolution of the GRACE-JPL estimates (50-km) over Turkey was enhanced up to 10-km based on the machine learning RF model.

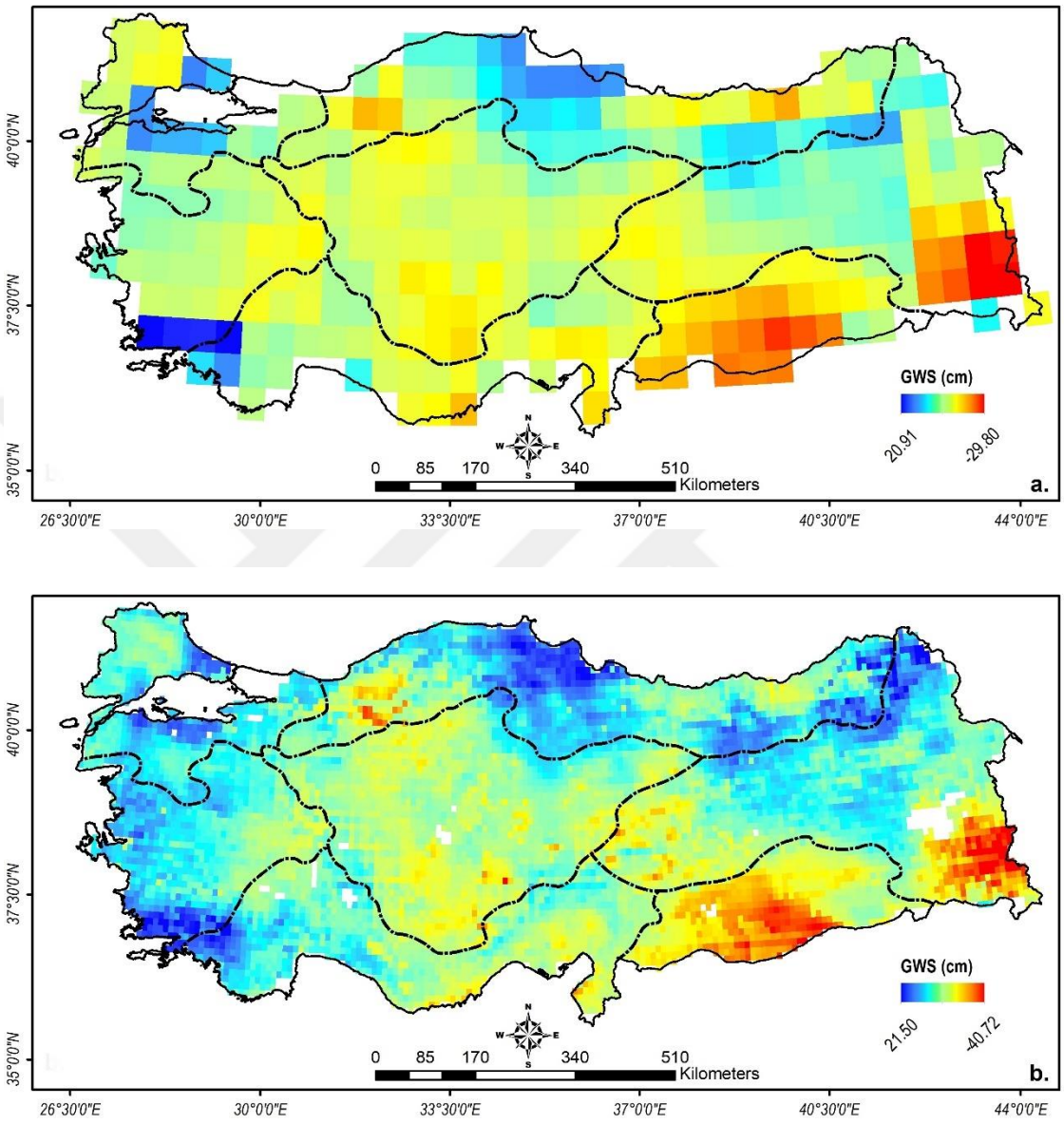


Figure 5.27 Illustration of the annual spatial fluctuations of the GRACE-derived GWS for the year 2020 before (a.) and after downscaling (b.) practice. The spatial resolution of the GRACE-JPL estimates (50-km) over Turkey was enhanced up to 10-km based on the machine learning RF model.

5.8.3 The Basin-Scale Variations of The TWS and GWS

The time series of the downscaled TWS and GWS over the WAB is shown in Figure 5-28. The monthly variations of the terrestrial and groundwater storage over the WAB show descending trends that stress the diminishing water storage of the basin over time. According to the graphs, the annual depletion rates for the TWS and GWS over the WAB are about 2.3 mm/yr and 1.12 mm/yr respectively. The fluctuations of the TWS and GWS imply that extreme situations were experienced in 2007 and 2020. The TWS shows its minimum values of 216.17 mm and 180.35 mm on Oct 2020 and Oct 2007, respectively. GWS, on the other hand, manifests the maximum storage loss of 220 mm and 187.2 mm in Nov 2007 and Oct 2020, respectively. These troughs in the time series of the TWS and GWS are under the drought analysis results for Turkey (Khorrami and Gunduz, 2021b).

The fluctuations of SMS and SWE show seasonality like that of the GRACE-derived TWS and GWS. The seasonal variations for SMS are more tangible than that of SWE. While the variations of SMS are in harmony with the drought analysis results (Khorrami and Gunduz, 2021b), SWE changes do not seem to catch the impacts of the dry periods over the basin which results from the fact that there is no considerable snowpack over this region. The associations of the soil moisture and snow water with the TWS and GWS demonstrate the existence of a lagged relationship in their temporal variations over the basin. The lagged association is more apparent between SMS and GWS.

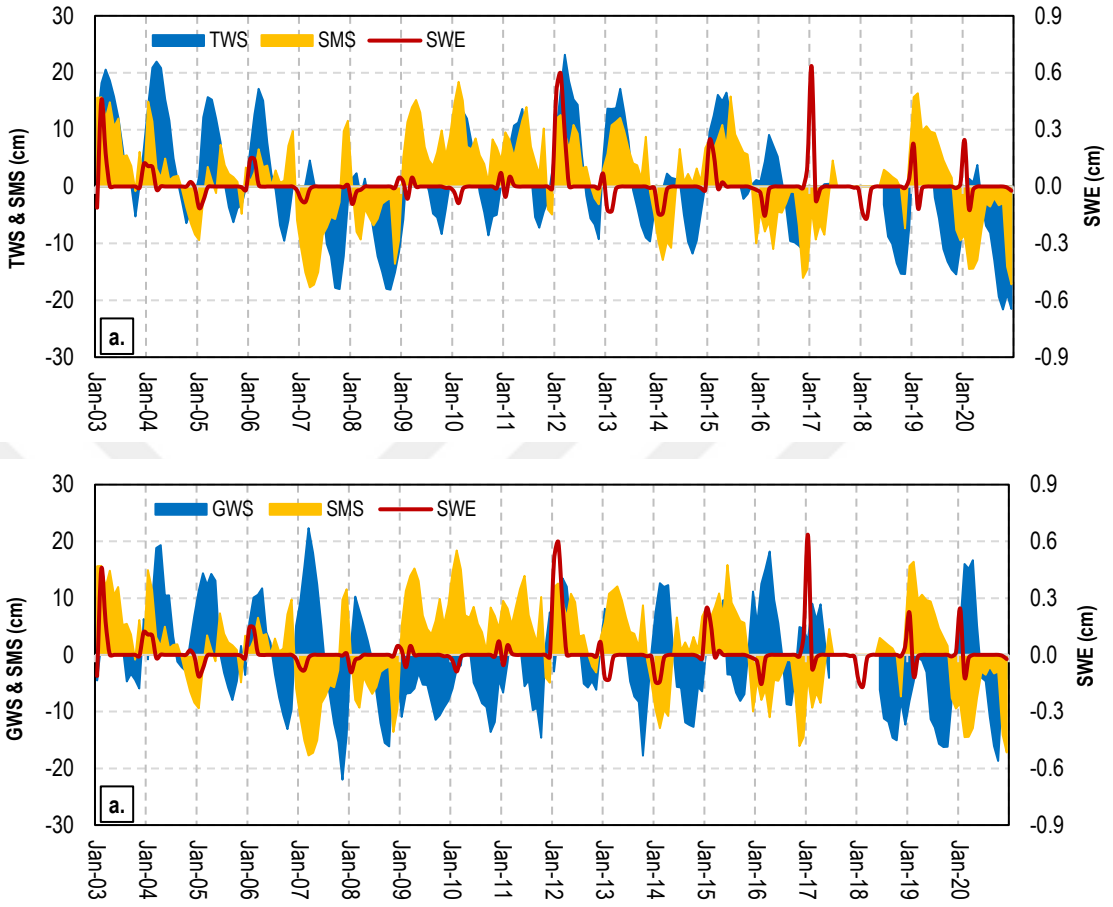


Figure 5.28 Local-scale fluctuations of terrestrial (a) and groundwater (b) storage and their interactions with soil moisture and snow water variations over the WAB.

5.9 Validation

For the validation purpose of the results, three different data including the modeled groundwater consumption and depth to groundwater records were utilized. The coarse resolution simulated groundwater use was used to check the accuracy of the coarse GRACE data over Turkey. The in-situ estimates of stream discharge were also used to evaluate the GRACE-derived TWS. Finally, the accuracy of the local scale estimates of the GRACE mission was investigated by using the depth to groundwater observations.

5.9.1 Temporal Validation Against the Simulated Groundwater Use

The monthly net abstraction of water from underground and surface water resources is simulated by the WGHM. Net abstraction refers to the deviation of total water abstraction from either groundwater or surface water resources and the return flow to the respective source (Döll et al. 2012). Cumulative groundwater and surface water abstraction are called potential consumptive water use (CWU). To validate the variations of GWS over Turkey, CWU was calculated using the WGHM outputs. The associations between GWS and CWU (Figure 5.29) are highly strong at 3-month of time lag, at which the correlation coefficient reaches -0.77. The seasonal associations between the GWS and CWU turned out to be even stronger with a correlation of -0.81.

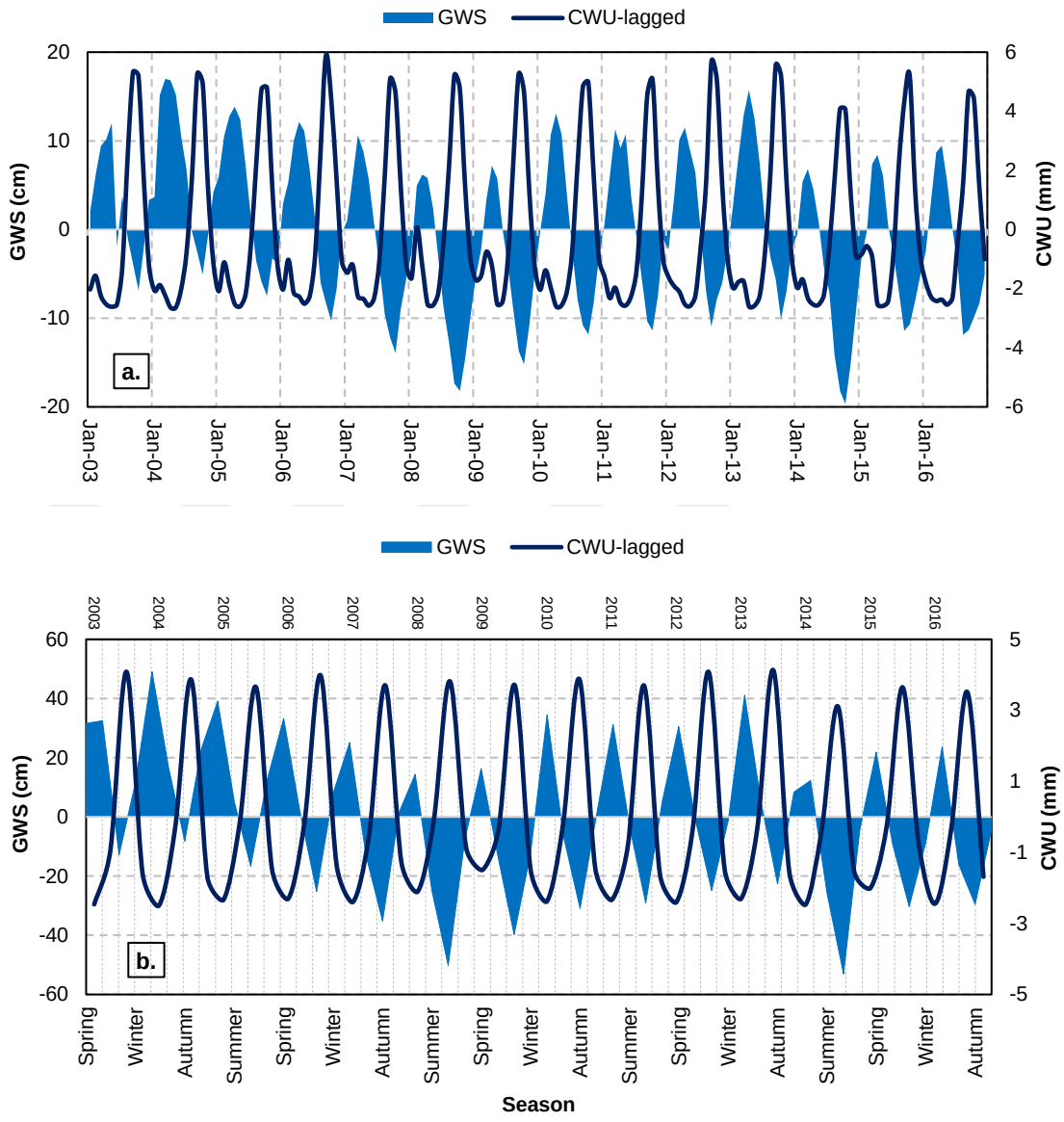


Figure 5.29 illustration of the monthly (a.) and seasonal (b.) interactions between the potential consumptive water use (from WGHM) and groundwater storage variations. The GRACE-derived GWS responds to the variations in the total water use within a 3-month lag.

5.9.2 Validation Against the Monthly Groundwater Level Observations

For the validation of the GRACE-derived and model-derived GWS values, in-situ values of depth to groundwater (DTG) were used. The seasonal DTG data received from

82 observation wells was converted into groundwater level (GWL) data based on the surface elevation of each well. The GWL values were later converted into groundwater storages by using the estimated Sy value for the individual wells. A point-wise approach was followed for validation purpose and the GRACE-derived and in-situ values of GWS were cross-validated. The validation results (Figure 5.30) show that while the correlation coefficients between the original GRACE-GWS and the in-situ GWS is 0.54 at the seasonal scale, the downscaled GWS has a higher correlation of 0.60. The improvement of the correlation indicates that the RFML model was successful in modeling the finer resolution (10 km) GWS. The graph also demonstrates improved seasonal trend for the downscaled GRACE, which is in harmony with the decreasing trend of the in-situ GWS.

To check the spatial consistency of the pre-and post-downscaling TWS and GWS over the WAB, the variations of Oct 2020 were mapped as an example. As observed in Figure 5.31, the original and downscaled distribution of the TWS and GWS is consistent from the perspective of spatial distribution. The figures manifest the good performance of the RFML model in filling in the spatial gaps of the TWS and GWS values in the basin, which overall correspond with the trends of the original values. The spatial variations of the original and the downscaled TWS and GWS are consistent throughout the WAB with increased values towards the north and the south and concentrated decreasing values inside the basin. The thematic maps for the TWS and GWS before and after downscaling process suggest that, by using the downscaled products, the area texture information can be better retrieved than by using the original data (Zhang et al., 2021b).

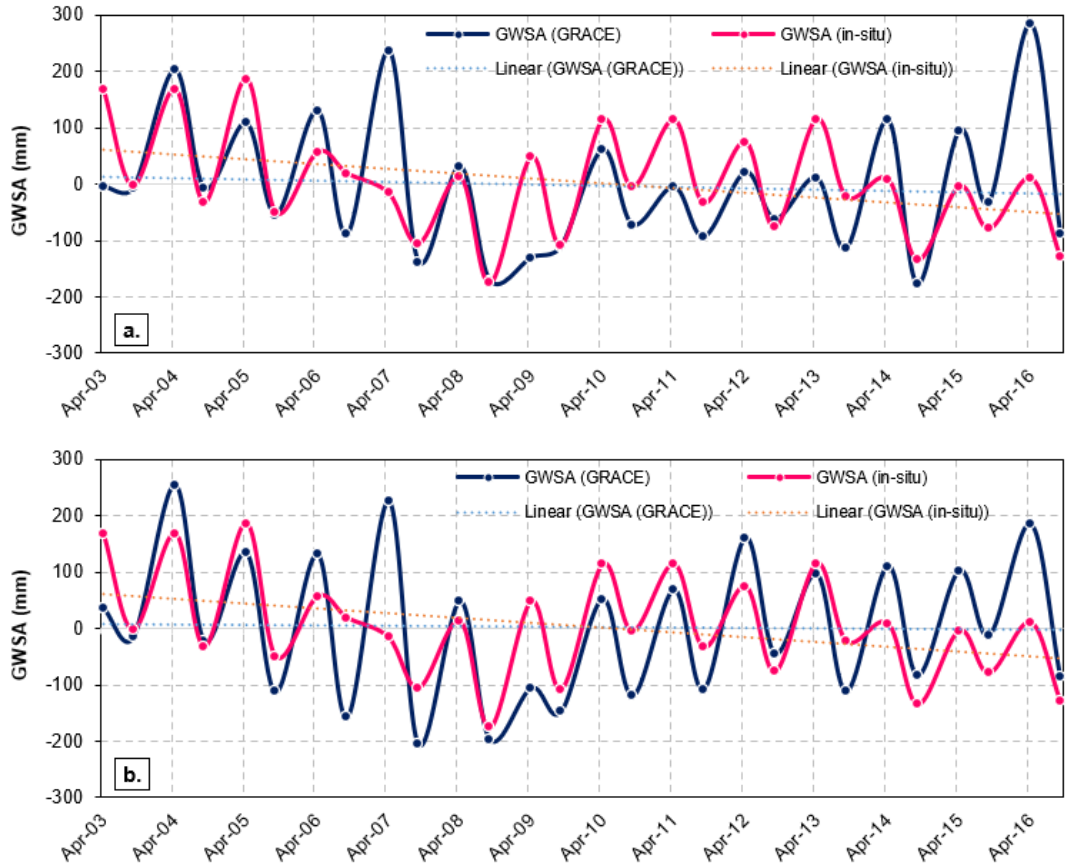


Figure 5.30 Validation of the original (50 km) (a) and downscaled (10 km) GWS (b) against in-situ GWS.

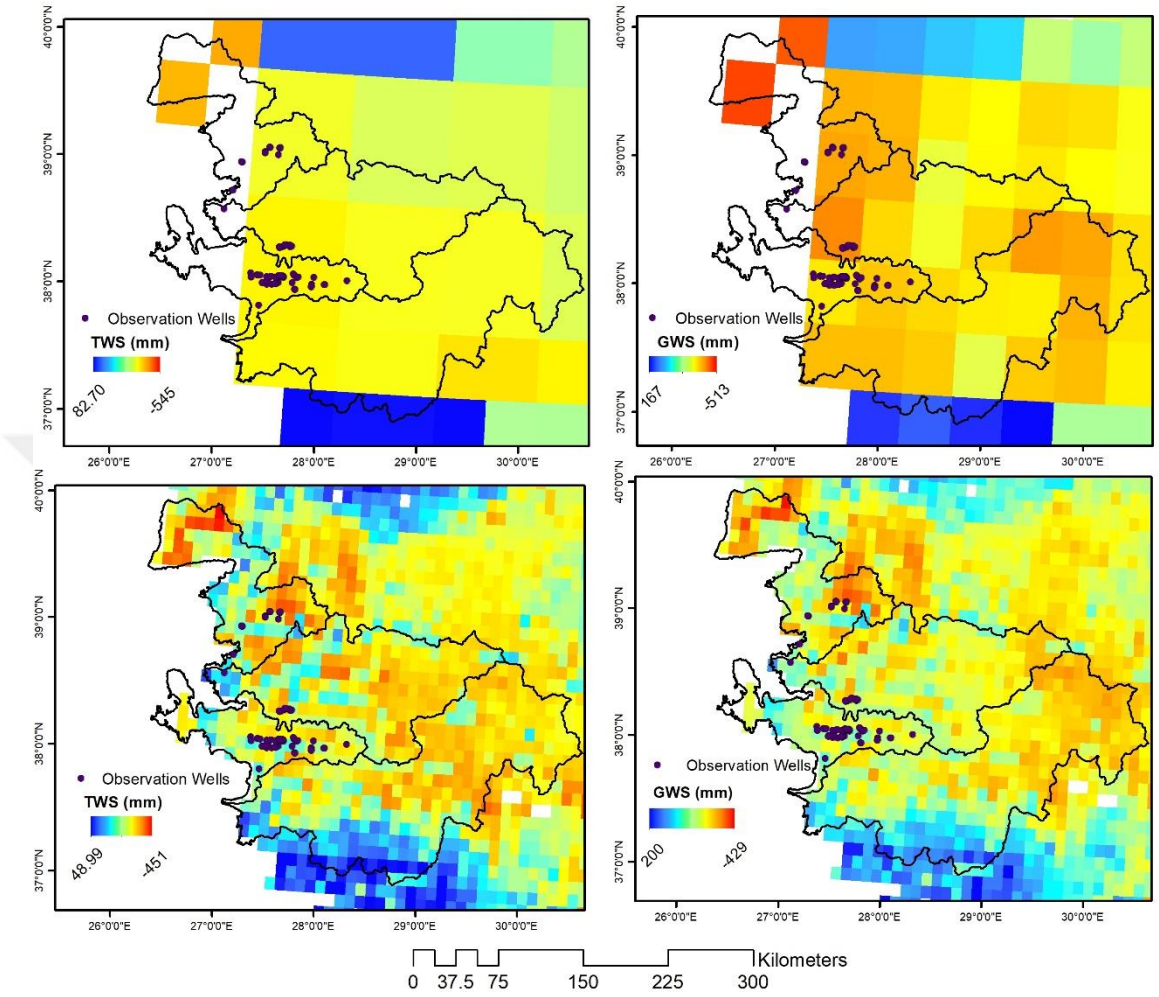


Figure 5.31 Illustration of the original and downscaled TWS and GWS over the WAB.

5.10 Trend and Uncertainty Estimation

The trend values of the time series of each component of the hydrological water cycle over Turkey were computed based on the MK test at 0.05 of significance level. For uncertainty estimation of the modeled soil moisture and snow water values, standard deviation between the land surface models (the GLDAS-Noah, the FLDAS-Noah and the ERA-5) were applied. Consequently, the uncertainty of GWS was estimated based on error propagation theory. The estimated trends and associated uncertainties are reported in Table 5.3.

The results reveal that, from 2003 to 2020, the TWS and GWS over Turkey have suffered from an approximated yearly water storage loss of 0.68 cm/yr and 0.53 cm/yr of water, respectively. The annual rate of TWS found in this study is very close to the findings of the previously implemented studies. Atayer (2012), Yıldırım (2015) and Okay Ahi and Jin (2019) reported an annual TWS loss of 0.7 cm/yr , 0,64 cm/yr and 0.77 cm/yr, respectively. The variations of the soil moisture and snow water variables, on the other hand, show 0.13 cm/yr and 0.02 cm/yr of annual depletion, respectively.

Table 5.3 The secular trend and uncertainty estimates of the hydrological water cycle components over Turkey.

TWS (cm/year)	**SMS (cm/year)**	**SWE (cm/year)**	**GWS (cm/year)**
0.68 ± 0.16	0.13 ± 0.12	0.02± 0.00	0.53 ± 0.28

The volumetric trend values (Table 5.4) were derived based on the underlain area of the total of 7918 pixels (0.1 degrees in spatial resolution) over Turkey for each parameter. Consequently, the depletion rate and total depletion of each hydrological cycle compartment were estimated. Accordingly, it is found that during the last 18 years (2003-2020), Turkey has lost an estimated volume of 92.83 km^3, 17.88 km^3, 2.75 km^3 and 72.34 km^3 from its storage of the TWS, SMS, SWE and GWS, respectively. Over the same period, the mean annual volume of the water received through precipitation for the country reaches 450 km^3. With annual groundwater and surface water potential of 18 km^3 and 94 km^3, the annual water consumption of Turkey reaches 57 km^3 (TSHW, 2021). Considering the 18-year study span of this study, it is estimated that from 2003 to 2020, about 1026 km^3 of water resources of the country have been consumed. According to the findings of this study, this huge water consumption has culminated in the severe depletion of the GWS with an annual rate of -4.02 km^3/yr.

Table 5.4 Volumetric trends of the hydrological water cycle components over Turkey.

Parameter	Mean Depletion Rate (cm/yr)	Number of Pixels	Depletion Rate (km^3/yr)	Total Storage Loss (km^3)
TWS	-0.68	7918	-5.16	-92.83
SMS	-0.13	7918	-0.99	-17.88
SWE	-0.02	7918	-0.15	-2.75
GWS	-0.53	7918	-4.02	-72.34

5.11 Spatial Variability of Trends

To investigate the spatial variability of the annual trends, the trend maps were generated based on the Sen's slope trend analysis parameter (Zhang et al., 2021). The annual trend maps (Figure 5.32) demonstrate different spatial patterns for the study's hydrological parameters of the GRACE TWS and GWS and the simulated Noah-derived SWE and SMS over Turkey. The spatial trend of the TWS suggest that excluding a tiny area in the southeastern part of the country, whole Turkey experienced decreased TWS through the last 18 years from 2003 to 2020. The situation is worse in terms of the lost TWS over the Mediterranean coasts, the southern parts of the Central Anatolia, South Eastern Anatolia as well as the boundaries of the Eastern Anatolian region. Almost the same pattern is observed for the variations of GWS over the Mediterranean and Eastern Anatolian regions. The severe decrease in the storage of terrestrial water over the southern Central Anatolian region has also been reported by Lenk (2013).

The annual trend of the GWS also imply severe storage deficit over the Central Anatolian region, which is rational taking its groundwater status into account where has been the most critical region of the country in terms of the decreased groundwater table during the recent decades (Caló et al., 2017; Khorrami et al., 2021). The trend of the simulated SWE indicates considerable decrease for the SWE over the mountainous Northeastern and Eastern Anatolia regions over, which the most year-round storage of the

accumulated snow and ice are reserved. The simulated SMS, on the other hand, shows decreasing soil moisture pattern all over the country with more exacerbated situation over the Black Sea region, Eastern and the Western regions as well. Also, the SMS over the Central Anatolian region is decreasing, its situation seems better than the mentioned regions in terms of the annual soil moisture storage loss. Overall, the spatial variations of the annual trends of the SMS and the TWS over Turkey seem to be akin especially the extreme variations over the Marmara, Aegean, Mediterranean and the Eastern Anatolia Regions. The close spatial associations in the variations of the TWS and SMS can be ascribed to the fact that the SMS changes play the most prominent role in the variations of the TWS over Turkey (Okay Ahi and Jin, 2019).

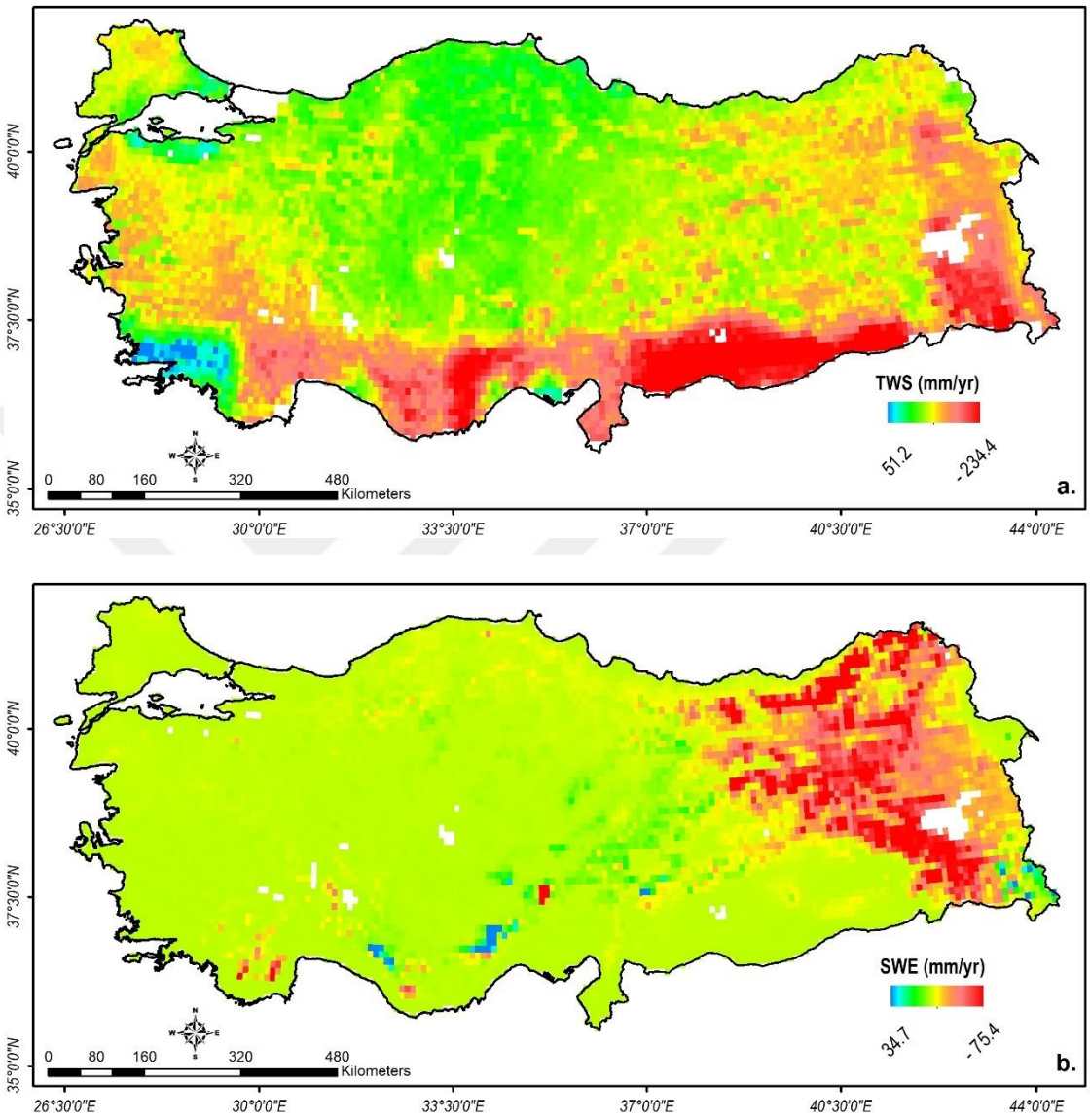
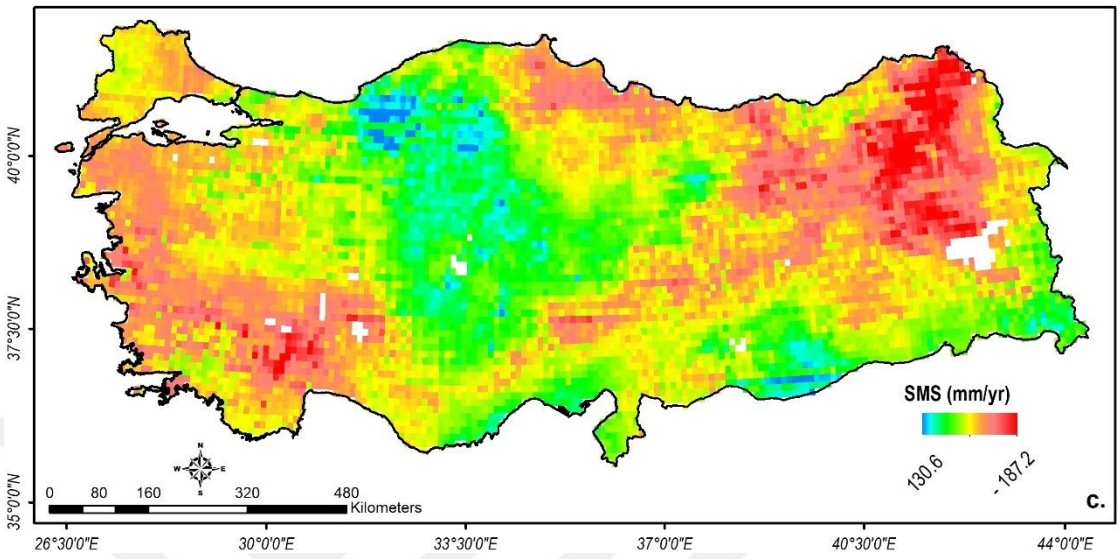


Figure 5.32 Illustration of the spatial pattern of the annual trends of TWS (a), SWE (b), SMS (c) and GWS (d) from 2003 to 2020 over Turkey



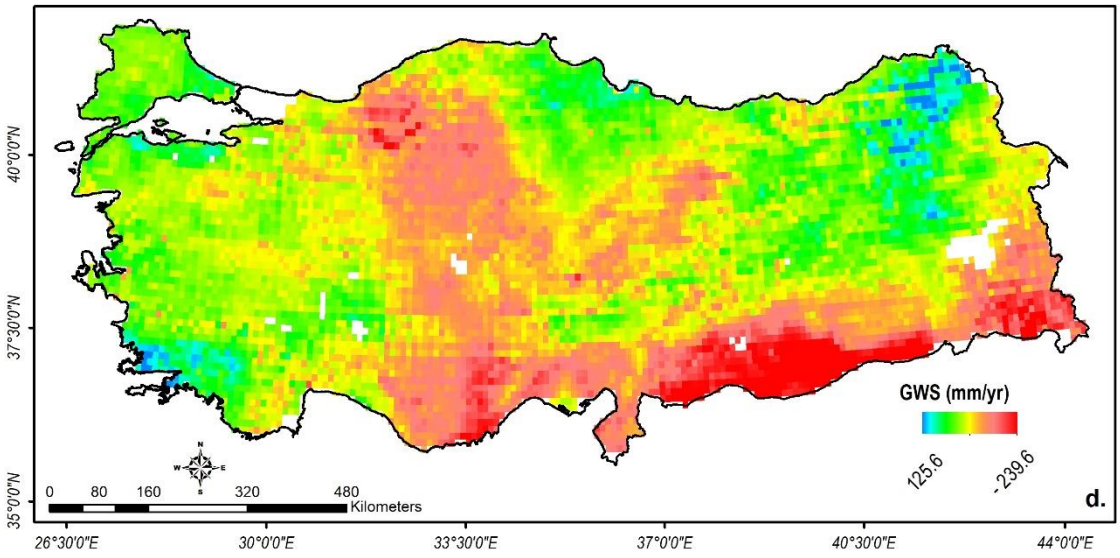


Figure 5.32 Continues

5.12 Spatial Variability of TWS and GWS over Turkey

To have an overview of the spatial characteristics of the variations of the terrestrial and groundwater over Turkey, the mean annual maps of the spatial variability of the downscaled TWS and GWS are given in Figures 5.33 and 5.34, respectively. The annual maps give insights into the status of the TWS and GWS regarding their spatial variability over different regions of the country. These annual maps also manifest the impacts of the dry and wet periods on the TWS and GWS changes throughout Turkey. According to the annual TWS maps, the coastal areas of the country in the black Sea, Mediterranean, Marmara, Southeast Anatolia and Aegean regions have so far suffered from decreased TWS in comparison with the inland areas. For instance, from 2003 to 2006, the coastal Black Sea areas show the maximum loss of TWS while from 2008 to 2018, the maximum loss of TWS is observed over the Southeast Anatolian coasts. The annual maps of the GWS, on the other hand, imply a different pattern where the inland areas show the most decline in the GWS over Turkey. The GWS situation is dire over central Turkey and the Southeast Anatolia.

The hydrometeorological dry periods can be also inferred by looking at these annual maps. For example, the spatial dispersion of the TWS is in accordance with the drought incidents experienced in 2008, 2009, 2014, partially in 2018, 2019 and 2020. The spatial variations of the GWS in 2009 show the harshest groundwater decline when the whole country has experienced groundwater depletion due to the impacts of the dry years of 2007 and 2008 over Turkey. The situation in 2018 and 2019 is also critical with the maximum decline recorded for the groundwater depletion with the 491 and 451 mm of storage loss, respectively.

Based on the entire analysis of this study, the spatio-temporal fluctuations of the main hydrological water cycle components including terrestrial water storage, soil moisture, snow water, groundwater as well as precipitation were scrutinized over Turkey based on remote sensing data and techniques. As an overall assessment, the results indicate that by

using the GRACE data and integrating it into hydrological model outputs, the variations of different hydrometeorological parameters can be estimated with an acceptable accuracy.

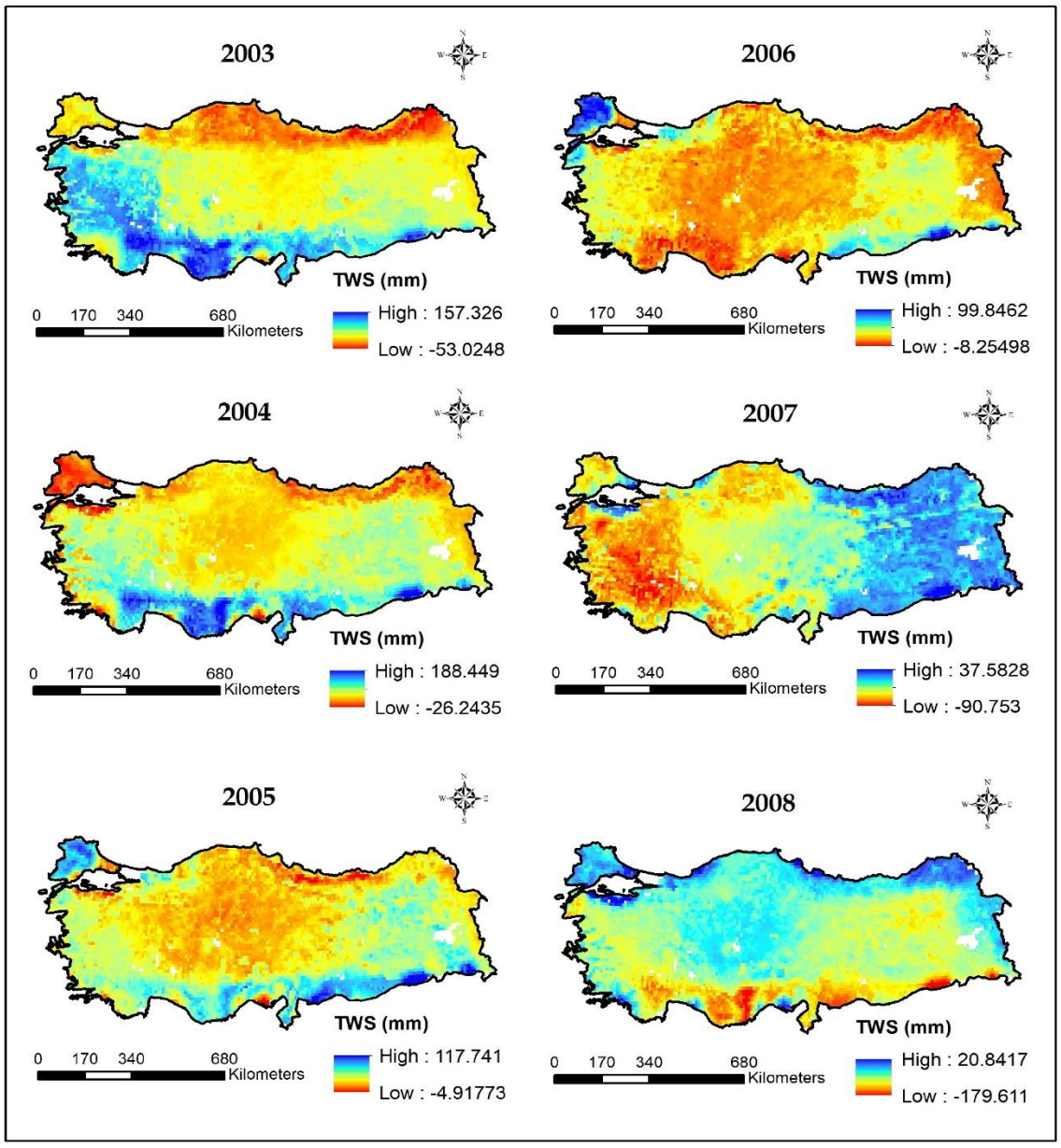


Figure 5.33 Spatial illustration of the annual distribution of the downscaled GRACE TWS over Turkey

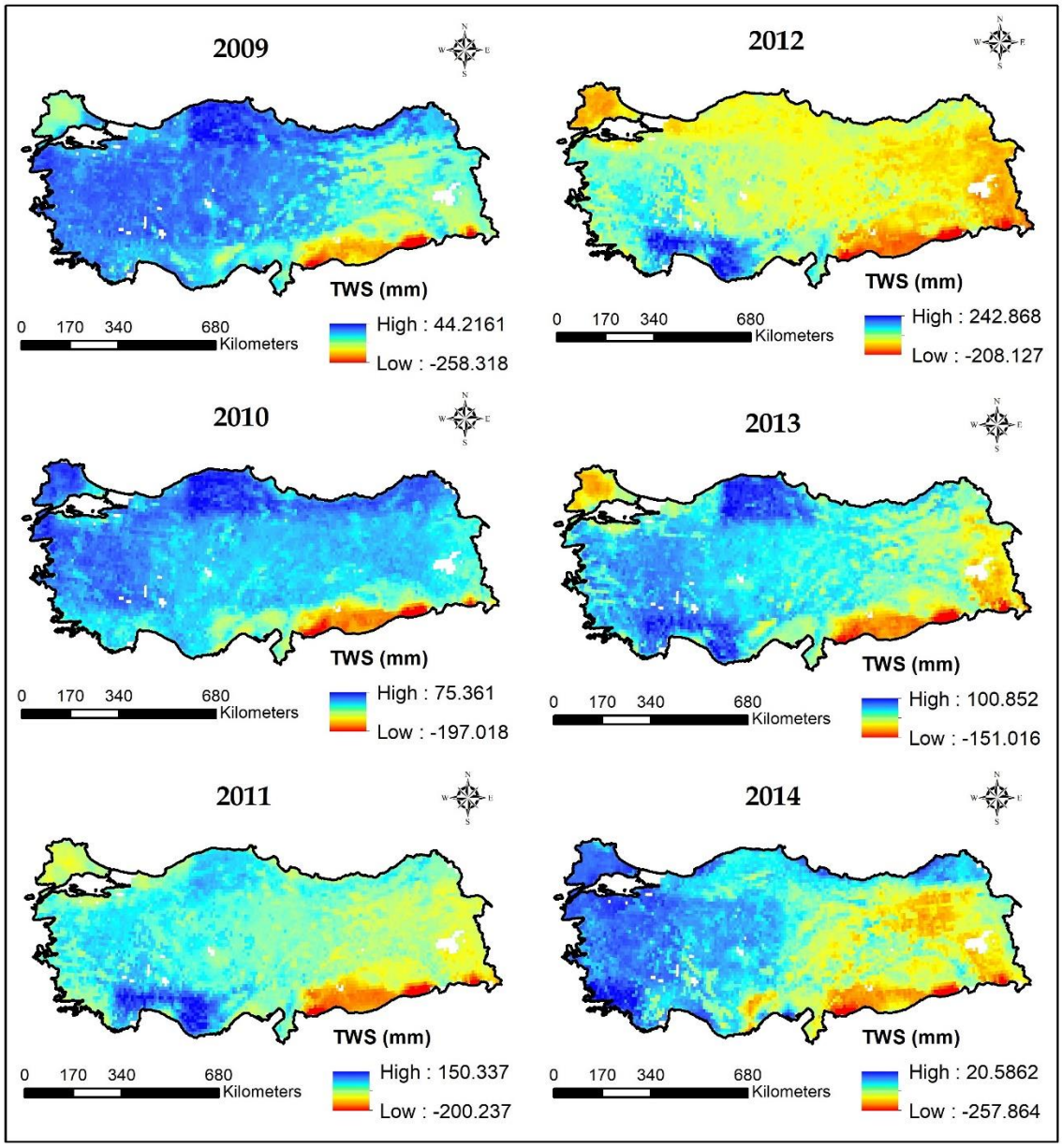


Figure 5.33 Continues

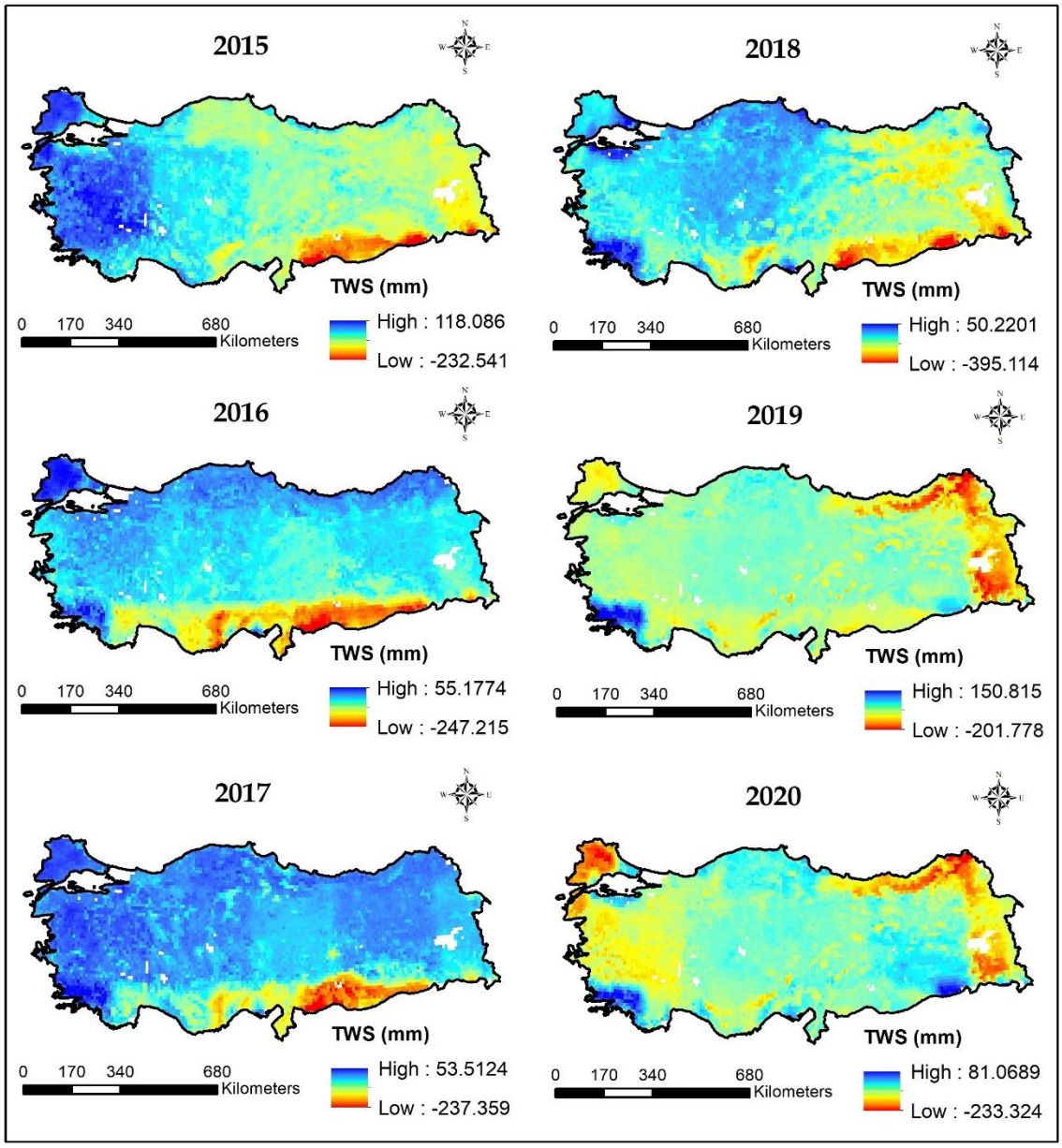


Figure 5.33 Continues.

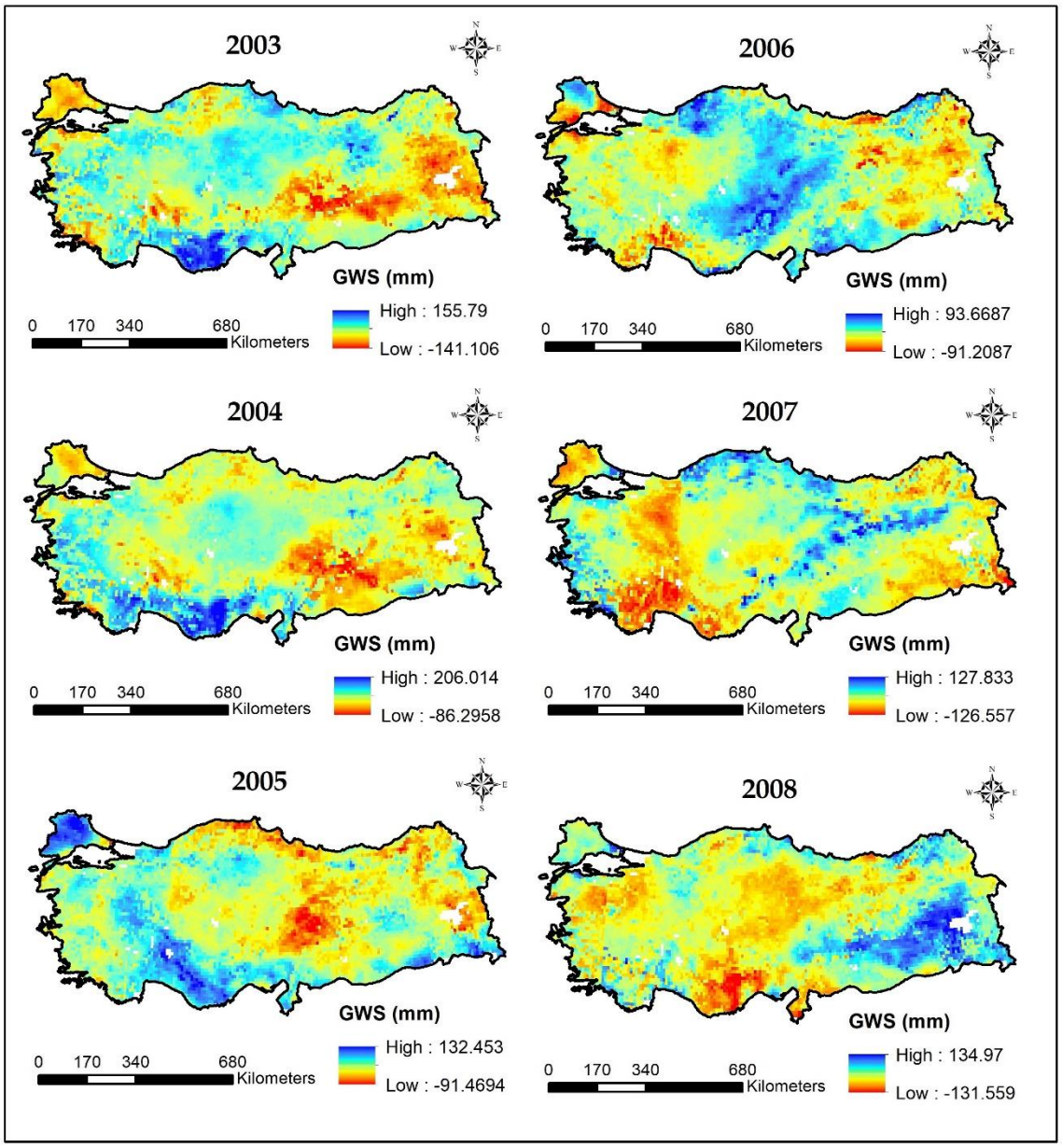


Figure 5.34 Spatial illustration of the annual distribution of the downscaled GRACE GWS over Turkey. The GWS values were extracted from the TWS by integrating the fine resolution FLDAS parameters.

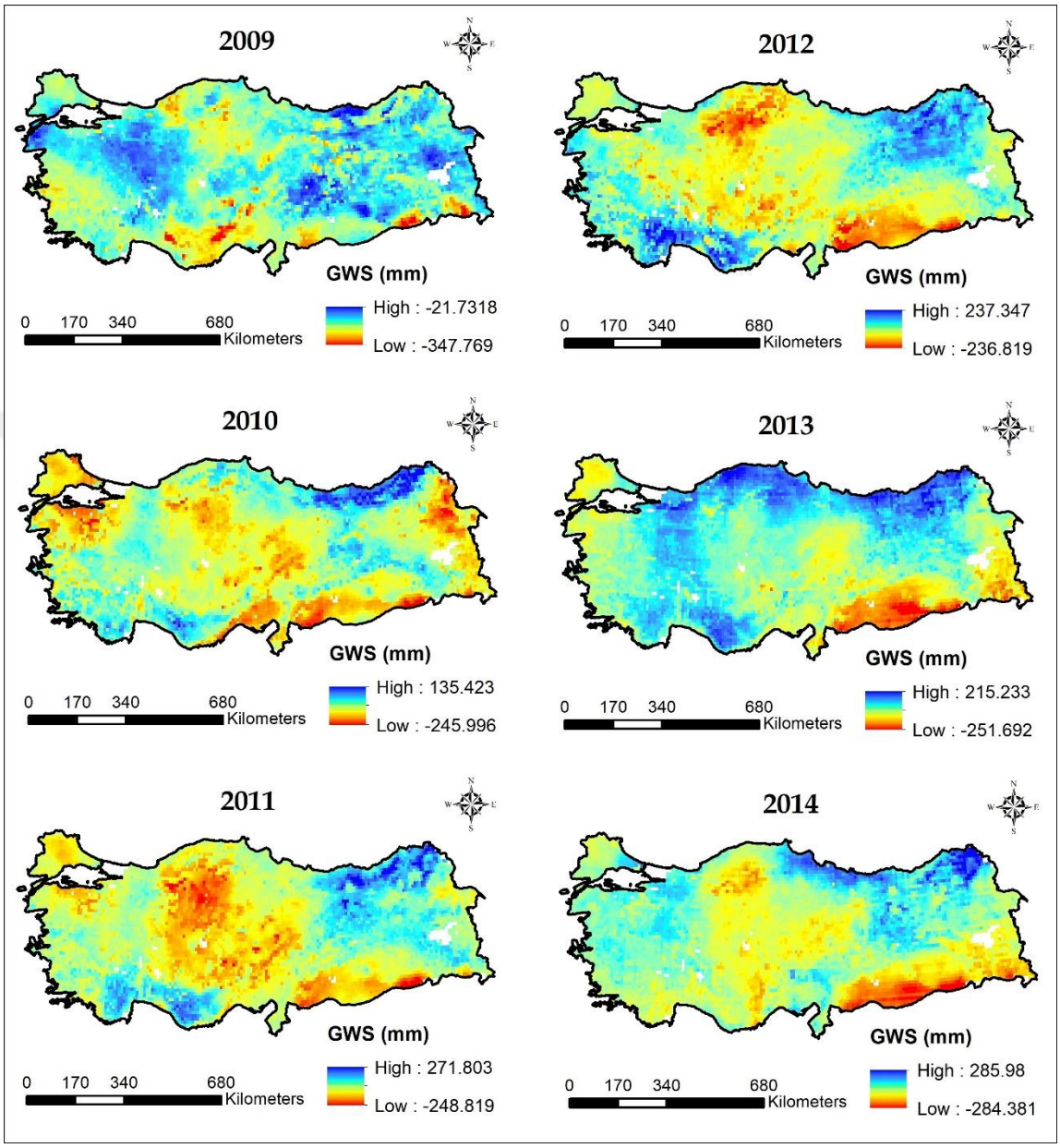


Figure 5.34 Continues

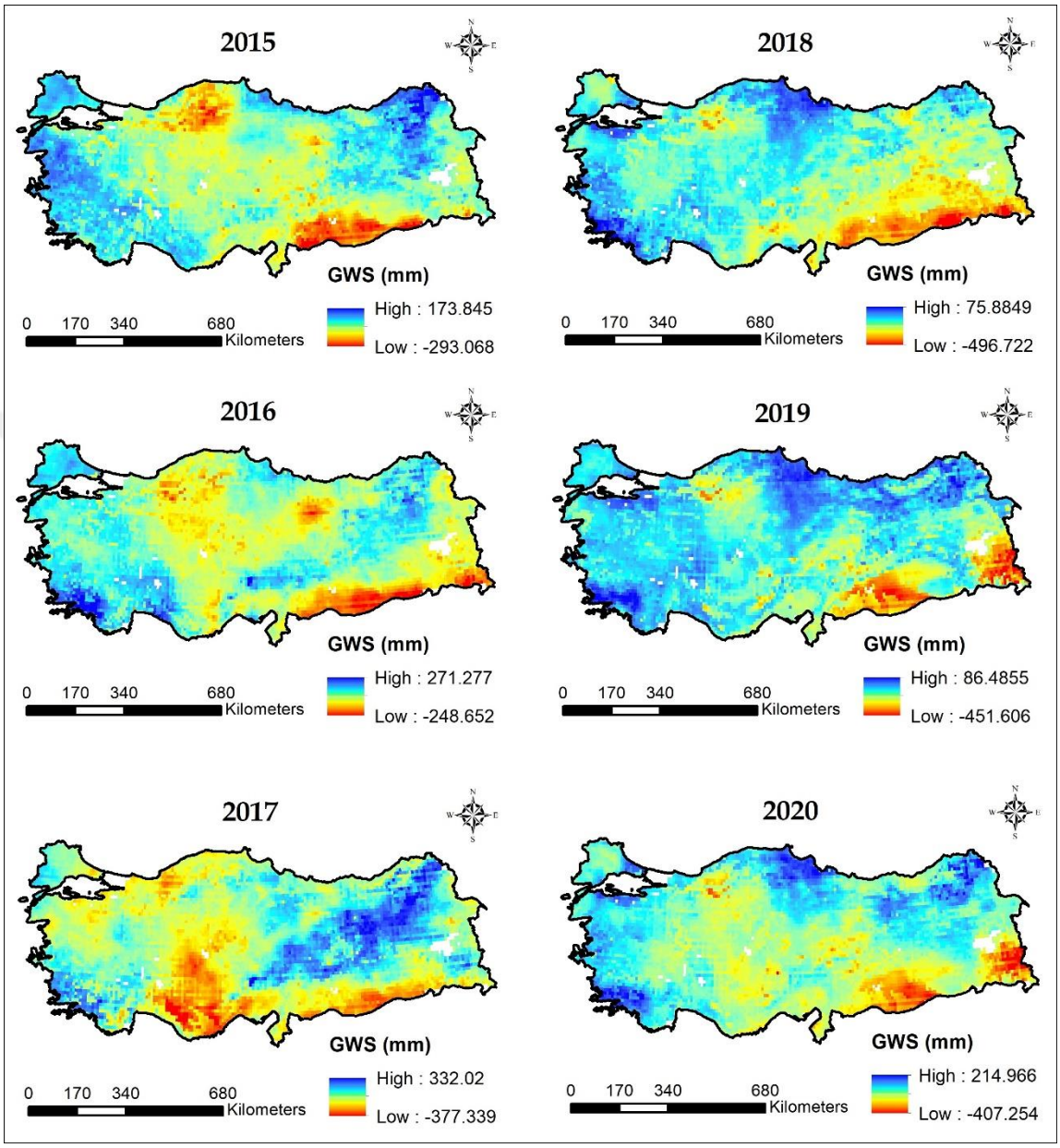


Figure 5.34 Continues

CHAPTER 6

CONCLUSIONS AND RECOMMENDATIONS

6.1 The Main Outcomes of the Study

Natural resources especially water resources play a predominant and indispensable role in sustaining all forms of life on the planet. These precious resources have been subjected to intemperate utilization throughout human history. The importance of water especially subsurface water resources is even more due to their substantial impacts on the continuation and stabilizing the natural environment and human societies as well. Although surface water resources provide an easy-to-reach and convenient water source for different sectors worldwide, they have been considered unreliable and unprotected towards pollution for years. Surface waters react swiftly to the external forces either natural or anthropogenic forces, which alter their spatio-temporal status culminating in their poor position regarding the water sustenance over different regions of the world.

Groundwater aquifers have been one of the main victims of human ignorance, mismanagement and overexploitation. Anthropogenic pressure in the companionship of the harsh climatic impacts in terms of the surging temperatures and evapotranspiration and diminishing precipitation and humidity, have so far contributed to a severe decline in the groundwater storage over different areas in many regions around the world. This condition resulted in considerable losses, the extent of which has been very broad in some cases with irreversible ramifications. The problem is even more crucial over the regions located on the arid belts of the world where groundwater aquifers are subjected to overwhelming pressure. Intemperate exploitation of groundwater is associated with some socio-economic and environmental consequences. The socio-economic losses can be in the forms of increased water harvesting costs, environmental rehabilitation costs, costs incurred through environmental asylum seekers, etc. The environmental costs cover a variety of harsh environmental impacts such as groundwater depletion, which may finally

culminate into the land deformation and increased land subsidence activities, groundwater quality degradation, desiccation of groundwater wells and springs, etc.

Turkey is crippled with the crucial situation of its water resources, a situation that is projected to be more exacerbated in the upcoming years. The geo-climatic characteristics of Turkey pose the country with great challenges regarding the spatio-temporal distribution of water, which threatens the stability of water-dependent economic activities over different regions of the country. The Aegean and Central Anatolian regions have been facing with even more critical situation concerning the ramifications associated with the recent severe groundwater depletion. Remote sensing throws off the shackles of the known traditionally applied field-based data and techniques by taking the unique benefit of its high accuracy and low-cost data and tools. Considering these wonderful properties, the RS approaches and data are being more and more alluring to both the scientific community and the policy-makers at governmental levels especially the emergence of GRACE satellites and the development of data modeling and assimilation systems have expedited this shift from the in-situ data to the remote sensing observation.

In this premise, the fluctuations of terrestrial and groundwater storage as well as some important hydrometeorological variables were investigated over Turkey by utilizing different remotely sensed data and remote sensing techniques. The findings, for the time span of 2003 to 2020, suggest that the variations of TWS and GWS over Turkey are statistically descending with annual shrinkage rates of 0.68± 0.16 cm/yr and 0.53 ± 0.28 cm/yr, respectively. As other compartments of the hydrological cycle, the SMS and SWE, on the other hand, show annual variations of 0.13 ± 0.12 cm/yr and 0.02± 0.00 cm/yr, respectively. The findings also indicate that the recent hydrometeorological extreme events over the country have had a determining impact on the variations of the water cycle components especially during the 2007-2008, 2014 and 2018-2020 dry periods when the troughs of TWS, GWS, SMS and SWE correspond exactly with the drought indicators. The analysis of the impacts of the anthropogenic parameter of cumulative water consumption on groundwater storage of the country unravels a significant association

between the monthly and seasonal variations of the GWS and those of water consumption with the correlation of -0.70 and -0.81 over Turkey. The results also indicated a good association between the GWS and climatic parameters of P and T with monthly correlation values of 0.47 and -0.81 respectively.

To better characterize the situation on a regional or local scales, GRACE-based data has been downscaled to increase its resolution. The downscaling results suggest a good performance of the used RFML algorithm for statistical downscaling of the GRACE data over Turkey. The correlation between the actual and the downscaled TWS and GWS time-series turn out to be 0.98 and 0.99 respectively, which signals a very good accuracy for the simulated finer resolution values over the study area.

6.2 Recommendations

Considering the results obtained through the spatio-temporal analysis of various hydrometeorological parameters over Turkey, it can be stated that, by using the coarse resolution RS data, the variations of these variables particularly the fluctuations of TWS and GWS can be monitored at an acceptable accuracy level. Notwithstanding the good achievements of the large-scale satellite and hydrological modeling missions, a perfect application of these datasets is shackled by some drawbacks associated with both the remotely sensed estimates and their processing techniques. Taking the findings of this study and the mentioned technical considerations into account, the following can be expressed as the final recommendations for this thesis:

- The GRACE mission has been a very promising space project with its accurate estimates of the variations of TWS over the globe. However, the GRACE-derived TWS is a vertically composite parameter that cannot be used without disintegration. For the GRACE disintegration process, the global hydrological models are generally applied, through which, some additional uncertainties are added to the final disintegrated parameters. To overcome this problem especially

over regional scales, it is highly recommended to apply the area-specific hydrological models, for which, the level of uncertainty is thought to be low.

- The GRACE disintegration can also be executed by using in-situ measurements of the hydrological water cycle components of soil moisture, snow water and surface water. However, since these measurements are point-wise values, a better illustration of the spatial status of the results is not possible without using interpolation techniques, which also have their uncertainties. Therefore, it is recommended to take the benefit of high accuracy RADAR estimates of soil moisture and snow water for better integration of the GRACE estimates.

- The statistical downscaling results suggest that by using the RFML algorithm, the spatially enhanced GRACE estimates yield a better depiction of the variations of the TWS and GWS over a small scale (basin-scale), through which, fine resolution fluctuations can be deducted with almost the same and even better temporal accuracy as the actual GRACE. However, the temporal enhancement of the GRACE estimates is not possible by using the RFML method. It is recommended to apply more sophisticated techniques such as data assimilation algorithms to downscale the monthly estimates of the TWS to daily and even hourly resolution estimates, which are more preferred in hydrological modeling practices.

REFERENCES

Abbaspour, K. C., Faramarzi, M., Ghasemi, S. S., & Yang, H. (2009). Assessing the impact of climate change on water resources in Iran. *Water Resources Research*, *45*(10),1-16.

Abeysingha, N. S., & Rajapaksha, U. R. L. N. (2020). SPI-based spatiotemporal drought over Sri Lanka. *Advances in Meteorology, 2020*,1-10.

Abiye, T., Masindi, K., Mengistu, H., & Demlie, M. (2018). Understanding the groundwater-level fluctuations for better management of groundwater resource: A case in the Johannesburg region. *Groundwater for Sustainable Development*, *7*, 1-7.

Adenomon, M.O. & Ojehomon, V.E.T. (2014). Comparison of decomposition time series method and winters' seasonal exponential smoothing in forecasting seasonal temperature in Niger state, Nigeria. *International Journal of Mathematics and Statistics Research*, *1*,10-16.

Aerni, P. (2007). Agriculture in Turkey–structural change, sustainability and EU-compatibility. International Journal of Agricultural Resources, *Governance and Ecology*, *6*(4/5), 429-439.

Aeschbach-Hertig, W., & Gleeson, T. (2012). Regional strategies for the accelerating global problem of groundwater depletion. *Nature Geoscience, 5*(12), 853-861.

Agutu, N. O., Awange, J. L., Zerihun, A., Ndehedehe, C. E., Kuhn, M., & Fukuda, Y. (2017). Assessing multi-satellite remote sensing, reanalysis and land surface models' products in characterizing agricultural drought in East Africa. *Remote Sensing of Environment*, *194*, 287-302.

Alcamo, J., Döll, P., Henrichs, T., Kaspar, F., Lehner, B., Rösch, et al (2003). Development and testing of the WaterGAP 2 global model of water use and availability. *Hydrological Sciences Journal*. *48*, 317–338.

Alhaji, U. U., Yusuf, A. S., Edet, C. O., Oche, C. O., & Agbo, E. P. (2018). Trend analysis of temperature in Gombe state using Mann Kendall trend test. *Journal of Scientific Research & Reports*, *20* (3), 1-9.

Ali, S., Liu, D., Fu, Q., Cheema, M. J. M., Pham, Q. B., Rahaman, M., et al. (2021). Improving the resolution of GRACE data for spatio-temporal groundwater storage assessment. *Remote Sensing*, *13*(17), 3513.

Alley, W. M. (2006). Tracking US groundwater: reserves for the future?.*Environment: Science and Policy for Sustainable Development*, *48*(3), 10-25.

Altinbilek, D., & Hatipoglu, M. A. (2020). Water resources development. In: Harmancioglu N., Altinbilek D. (eds) *Water Resources of Turkey. World Water Resources* (pp. 61-84). Springer, Cham.

Andersen, O. B., Seneviratne, S. I., Hinderer, J., & Viterbo, P. (2005). GRACE-derived terrestrial water storage depletion associated with the 2003 European heat wave. *Geophysical Research Letters*, *32*(18), L18405.

Apaydin, A. (2011). Groundwater legislation in Turkey: problems of conception and application. *Water International*, *36*(3), 314-327.

Argus, D. F., Fu, Y., & Landerer, F. W. (2014). Seasonal variation in total water storage in California inferred from GPS observations of vertical land motion. *Geophysical Research Letters*, *41*(6), 1971-1980.

Argus, D. F., Ratliff, B., DeMets, C., Borsa, A. A., Wiese, D. N., Blewitt, G, et al. (2020). Rise of Great Lakes surface water, sinking of the upper Midwest of the United States and viscous collapse of the forebulge of the former Laurentide ice sheet. *Journal of Geophysical Research: Solid Earth*, *125*(9), 1-16.

Asikoglu, O. L., & Benzeden, E. (2014). Simple generalization approach for intensity–duration–frequency relationships. *Hydrological Processes*, *28*(3), 1114-1123.

Atayer, E. S. (2012). *Yeryuvarı gravite alanının aylık GRACE çözümleri ile izlenmesi ve duyarlılığı üzerine bir inceleme* [Master's Thesis]. Yildiz Teknik University.

Awad, M., Khawlie, M., & Darwich, T. (2009). Web based meta-database and its role in improving water resources management in the Mediterranean basin. *Water Resources Management*, *23*(13), 2669-2680.

Ay, M. (2021). Trend tests on maximum rainfall series by a novel approach in the Aegean region, Turkey. *Meteorology and Atmospheric Physics*, *133*(4),1041-1055.

Baboo, S. S., & Devi, M. R. (2010). An analysis of different resampling methods in Coimbatore, District. *Global Journal of Computer Science and Technology*, *10* (15), 61-66.

Bai, P., Liu, X., & Liu, C. (2018). Improving hydrological simulations by incorporating GRACE data for model calibration. *Journal of Hydrology*, *557*, 291-304.

Bhanja, S. N., Malakar, P., Mukherjee, A., Rodell, M., Mitra, P., & Sarkar, S. (2019). Using satellite-based vegetation cover as indicator of groundwater storage in natural vegetation areas. *Geophysical Research Letters*, *46*(14), 8082-8092.

Barletta V, Bordoni A, Aoudia A, Sabadini R (2012). Squeezing more information out of time variable gravity data with a temporal decomposition approach. *Global Planet Change 82*, 51–64.

Becker, M., Meyssignac, B., Xavier, L., Cazenave, A., Alkama, R., & Decharme, B. (2011). Past terrestrial water storage (1980–2008) in the Amazon Basin reconstructed from GRACE and in situ river gauging data. *Hydrology and Earth System Sciences*, *15*(2), 533-546.

Beguería, S., Vicente-Serrano, S. M., & Angulo-Martínez, M. (2010). A multiscalar global drought dataset: the SPEIbase: a new gridded product for the analysis of drought variability and impacts. *Bulletin of the American Meteorological Society*, *91*(10), 1351-1354.

Bettadpur, S. (2012). CSR Level-2 Processing Standards Document for Product Release 05, GRACE 327-742, The GRACE Project, Cent. for Space Res., Univ. of Tex., Austin, Tex. Retrieved December 25, 2020, from: http://icgem.gfz-potsdam.de/GRACE_CSR_L2_Processing_Standards_Document_for_RL06.pdf

Bhanja, S. N., Mukherjee, A., & Rodell, M. (2020). Groundwater storage change detection from in situ and GRACE-based estimates in major river basins across India. *Hydrological Sciences Journal*, *65*(4), 650-659.

Bi, H., Ma, J., Zheng, W., & Zeng, J. (2016). Comparison of soil moisture in GLDAS model simulations and in situ observations over the Tibetan Plateau. *Journal of Geophysical Research: Atmospheres*, *121*(6), 2658-2678.

Bierkens, M. F., & Wada, Y. (2019). Non-renewable groundwater use and groundwater depletion: a review. *Environmental Research Letters*, *14*(6), 1-43.

Blain, G. C. (2013). The modified Mann-Kendall test: on the performance of three variance correction approaches. *Agrometeorology*, *72* (4), 416-425.

Boergens, E., Dobslaw, H., Dill, R., Thomas, M., Dahle, C., Murböck, M., et al. (2020). Modelling spatial covariances for terrestrial water storage variations verified with synthetic GRACE-FO data. *GEM-International Journal on Geomathematics*, *11*(1), 1-25.

Botai, C. M., & Combrinck, L. (2012). Global geopotential models from Satellite Laser Ranging data with geophysical applications: A review. *South African Journal of Science*, *108*(3), 1-10.

Breiman, L. (2001). Random forests. *Machine Learning*, *45*(1), 5-32.

Breña-Naranjo, J. A., Kendall, A. D., & Hyndman, D. W. (2014). Improved methods for satellite-based groundwater storage estimates: A decade of monitoring the high plains aquifer from space and ground observations. *Geophysical Research Letters*, *41*(17), 6167-6173.

Briffa, K. R., van der Schrier, G., & Jones, P. D. (2009). Wet and dry summers in Europe since 1750: evidence of increasing drought. *International Journal of Climatology: A Journal of the Royal Meteorological Society*, *29*(13), 1894-1905.

Caffrey, P., & Farmer, A. (2014). A review of Downscaling methods for climate change projections. Tetra Tech ARD. Retrieved December 20, 2020, from: http://www.ciesin.org/documents/Downscaling_CLEARED_000.pdf

Cakmak, E. H. (1997). Water resources in Turkey: Availability, use and management. In: Parker D.D., Tsur Y. (eds) *Decentralization and Coordination of Water Resource*

Management. *Natural Resource Management and Policy* (pp. 33-44). Springer, Boston, MA.

Caló, F., Notti, D., Galve, J. P., Abdikan, S., Görüm, T., Pepe, A., et al. (2017). Dinsar-Based detection of land subsidence and correlation with groundwater depletion in Konya Plain, Turkey. *Remote Sensing, 9*(1), *83.*

Cao, B., Gruber, S., Zheng, D., & Li, X. (2020). The ERA5-Land soil temperature bias in permafrost regions. *The Cryosphere, 14*(8), 2581-2595.

Castellazzi, P., Longuevergne, L., Martel, R., Rivera, A., Brouard, C., & Chaussard, E. (2018). Quantitative mapping of groundwater depletion at the water management scale using a combined GRACE/InSAR approach. *Remote Sensing of Environment, 205*, 408-418.

Castellazzi, P., Martel, R., Galloway, D. L., Longuevergne, L., & Rivera, A. (2016). Assessing groundwater depletion and dynamics using GRACE and InSAR: Potential and limitations. *Groundwater, 54*(6), 768-780.

Castellazzi, P., Martel, R., Rivera, A., Huang, J., Pavlic, G., Calderhead, A. I., et al. et al. (2016). Groundwater depletion in Central Mexico: Use of GRACE and InSAR to support water resources management. *Water Resources Research*, *52*(8), 5985-6003.

Castle, S. L., Thomas, B. F., Reager, J. T., Rodell, M., Swenson, S. C., & Famiglietti, J. S. (2014). Groundwater depletion during drought threatens future water security of the Colorado River Basin. *Geophysical Research Letters*, *41*(16), 5904-5911.

Chambers, D. P., & Bonin, J. A. (2012). Evaluation of Release-05 GRACE time-variable gravity coefficients over the ocean. *Ocean Science*, *8*(5), 859-868.

Chen, H., Zhang, W., Nie, N., & Guo, Y. (2019-a). Long-term groundwater storage variations estimated in the Songhua River Basin by using GRACE products, land surface models and in-situ observations. *Science of the Total Environment*, *649*, 372-387.

Chen, J. L., Wilson, C. R., & Tapley, B. D. (2006). Satellite gravity measurements confirm accelerated melting of Greenland ice sheet. *Science*, *313*(5795), 1958-1960.

Chen, J. L., Wilson, C. R., Tapley, B. D., & Ries, J. C. (2004). Low degree gravitational changes from GRACE: validation and interpretation. *Geophysical Research Letters*, *31*(22), 1-5.

Chen, J., & Rodell, M. (2021). Applications of Gravity Recovery and Climate Experiment (GRACE) in global groundwater study. In: Mukherjee, A., Scanlon, B. R., Aureli, A., Langan, S., Guo, H., & McKenzie, A. A. (Eds.) *Global Groundwater: Source, Scarcity, Sustainability, Security, and Solutions* (pp.531-543). Elsevier.

Chen, J., Famigliett, J. S., Scanlon, B. R., & Rodell, M. (2016). Groundwater storage changes: present status from GRACE observations. *Surveys in Geophysics*, *37*(2), 397-417.

Chen, J., Tapley, B., Tamisiea, M. E., Save, H., Wilson, C., Bettadpur, S., et al. (2021). Error Assessment of GRACE and GRACE Follow-On Mass Change. *Journal of Geophysical Research: Solid Earth*, *126*(9), 1-18.

Chen, L., He, Q., Liu, K., Li, J., & Jing, C. (2019-b). Downscaling of grace-derived groundwater storage based on the random forest model. *Remote Sensing*, *11*(24), 1-19.

Chen, N., Li, R., Zhang, X., Yang, C., Wang, X., Zeng, L., et al. et al. (2020). Drought propagation in Northern China Plain: A comparative analysis of GLDAS and MERRA-2 datasets. *Journal of Hydrology*, *588*, 125026.

Chen, S., Ouyang, W., Hao, F., & Zhao, X. (2013). Combined impacts of freeze–thaw processes on paddy land and dry land in Northeast China. *Science of the Total Environment*, *456*, 24-33.

Chen, S., She, D., Zhang, L., Guo, M., & Liu, X. (2019-a). Spatial downscaling methods of soil moisture based on multisource remote sensing data and its application. *Water*, *11*(7), 1401.

Chen, X., Long, D., Hong, Y., Zeng, C., & Yan, D. (2017). Improved modeling of snow and glacier melting by a progressive two-stage calibration strategy with GRACE and multisource data: How snow and glacier meltwater contributes to the runoff of the Upper Brahmaputra River basin?. *Water Resources Research*, *53*(3), 2431-2466.

Chinnasamy, P., Hubbart, J. A., & Agoramoorthy, G. (2013). Using remote sensing data to improve groundwater supply estimations in Gujarat, India. *Earth Interactions*, *17*(1), 1-17.

Cooray, T.M.J.A. (2008). Applied Time Series Analysis and Forecasting Nerosa Publishing House. Retrieved January 2, 2022 from: http://bogonefexi.files.wordpress.com/2014/07/applied-time-series-analysis-and-forecasting.pdf

Croteau, M. J., Nerem, R. S., Loomis, B. D., & Sabaka, T. J. (2020). Development of a daily GRACE Mascon solution for terrestrial water storage. *Journal of Geophysical Research: Solid Earth*, *125*(3). e2019JB018468.

Crow, W. T., Ryu, D., & Famiglietti, J. S. (2005). Upscaling of field-scale soil moisture measurements using distributed land surface modeling. *Advances in Water Resources*, *28*(1), 1-14.

Cui, L., Zhang, C., Luo, Z., Wang, X., Li, Q., & Liu, L. (2021). Using the Local Drought Data and GRACE/GRACE-FO Data to Characterize the Drought Events in Mainland China from 2002 to 2020. *Applied Sciences*, *11*(20), 9594.

Dalin, C., Wada, Y., Kastner, T., & Puma, M. J. (2017). Groundwater depletion embedded in international food trade. *Nature*, *543*(7647), 700-704.

Dangar, S., Asoka, A., & Mishra, V. (2021). Causes and implications of groundwater depletion in India: A review. *Journal of Hydrology*, *596*, 126103.

Davis, J. L., Elósegui, P., Mitrovica, J. X., & Tamisiea, M. E. (2004). Climate-driven deformation of the solid Earth from GRACE and GPS. *Geophysical Research Letters*, *31*(24),1-4.

Dawood, M. (2017). Spatio-statistical analysis of temperature fluctuation using Mann–Kendall and Sen's slope approach. *Climate Dynamics*, *48*(3-4), 783-797.

De Graaf, I. E. M., Van Beek, L. P. H., Wada, Y., & Bierkens, M. F. P. (2014). Dynamic attribution of global water demand to surface water and groundwater resources: Effects of abstractions and return flows on river discharges. *Advances in Water Resources*, *64*, 21-33.

De Graaf, I. E., van Beek, R. L., Gleeson, T., Moosdorf, N., Schmitz, O., Sutanudjaja, E. H., et al. (2017). A global-scale two-layer transient groundwater model: Development and application to groundwater depletion. *Advances in Water Resources*, *102*, 53-67.

Deng, H., & Chen, Y. (2017). Influences of recent climate change and human activities on water storage variations in Central Asia. *Journal of Hydrology, 544*, 46-57.

Deng, H., Pepin, N. C., Liu, Q., & Chen, Y. (2018). Understanding the spatial differences in terrestrial water storage variations in the Tibetan Plateau from 2002 to 2016. *Climatic Change*, *151*(3), 379-393.

Devia, G. K., Ganasri, B. P., & Dwarakish, G. S. (2015). A review on hydrological models. *Aquatic Procedia, 4*, 1001-1007.

Dikici, M. & Aksel, M. (2021). Comparison of Drought Indices in the Case of the Ceyhan Basin. *International Journal of Environment and Geoinformatics (IJEGEO), 8*(2),113-125.

Ding, B., Yang, K., Qin, J., Wang, L., Chen, Y., & He, X. (2014). The dependence of precipitation types on surface elevation and meteorological conditions and its parameterization. *Journal of Hydrology, 513*, 154-163.

Dokumentov, A. and Hyndman, R.J. (2020). STR: *A seasonal-trend decomposition procedure based on regression.* Retrieved January 1, 2022 from: https://arxiv.org/pdf/2009.05894.pdf

Döll, P., Hoffmann-Dobrev, H., Portmann, F. T., Siebert, S., Eicker, A., Rodell, M., et al. (2012). Impact of water withdrawals from groundwater and surface water on continental water storage variations. *Journal of Geodynamics, 59*, 143-156.

Döll, P., Mueller Schmied, H., Schuh, C., Portmann, F. T., & Eicker, A. (2014). Global-scale assessment of groundwater depletion and related groundwater abstractions: Combining hydrological modeling with information from well observations and GRACE satellites. *Water Resources Research, 50*(7), 5698-5720.

Döll, P., Siebert, S. (2002). Global modeling of irrigation water requirements. *Water Resources Research*. *38* (8), 1–18.

Dong, Y., Jiang, C., Suri, M. R., Pee, D., Meng, L., & Goldstein, R. E. R. (2019). Groundwater level changes with a focus on agricultural areas in the Mid-Atlantic region of the United States, 2002–2016. *Environmental Research*, *171*, 193-203.

TSHW (2020). *TSHW 2020 yılı faalıyet raporu*. Retrieved January, 1, 2022 from: https://cdniys.tarimorman.gov.tr/api/File/GetFile/425/KonuIcerik/759/1107/DosyaGaleri/DS%C4%B0%202020-yili-faaliyet-raporu.pdf.

TSHW (2021). *Toprak Su Kaynaklari*. Retrieved January 1, 2022 from: https://www.dsi.gov.tr/Sayfa/Detay/754

Dunn, C., Bertiger, W., Bar-Sever, Y., Desai, S., Haines, B., Kuang, D., et al. (2003). Instrument of GRACE GPS augments gravity measurements. *GPS World*, *14*(2), 16-29.

Durdu, O. F. (2010). Effects of climate change on water resources of the Büyük Menderes river basin, western Turkey. *Turkish Journal of Agriculture and Forestry*, *34*(4), 319-332.

Dutt Vishwakarma, B., Devaraju, B., & Sneeuw, N. (2016). Minimizing the effects of filtering on catchment scale GRACE solutions. *Water Resources Research*, *52*(8), 5868-5890.

Eicker, A., Schumacher, M., Kusche, J., Döll, P., & Schmied, H. M. (2014). Calibration/data assimilation approach for integrating GRACE data into the WaterGAP Global Hydrology Model (WGHM) using an ensemble Kalman filter: First results. *Surveys in Geophysics*, *35*(6), 1285-1309.

Erban, L. E., Gorelick, S. M., Zebker, H. A., & Fendorf, S. (2013). Release of arsenic to deep groundwater in the Mekong Delta, Vietnam, linked to pumping-induced land subsidence. *Proceedings of the National Academy of Sciences*, *110*(34), 13751-13756.

Evrendilek, F., & Gulbeyaz, O. (2008). Deriving vegetation dynamics of natural terrestrial ecosystems from MODIS NDVI/EVI data over Turkey. *Sensors*, *8*(9), 5270-5302.

Famiglietti, J. S. (2004). Remote sensing of terrestrial water storage, soil moisture and surface waters. *Washington DC American Geophysical Union Geophysical Monograph Series*, *150*, 197-207.

Famiglietti, J. S. (2014). The global groundwater crisis. *Nature Climate Change*, *4*(11), 945-948.

Famiglietti, J. S. and M. Rodell (2013), Water in the balance. *Science*, *340*(6138), 1300–1301.

Famiglietti, J. S., Lo, M., Ho, S. L., Bethune, J., Anderson, K. J., Syed, T. H., et al. (2011). Satellites measure recent rates of groundwater depletion in California's Central Valley. *Geophysical Research Letters*, *38*(3), 1-4.

FAO (2016). *Turkey Water Along the Food Chain* [2016]. Retreived in May,1, 2020 from:http://www.fao.org/3/a-i5991e.pdf

Fatolazadeh, F., & Goïta, K. (2021). Mapping terrestrial water storage changes in Canada using GRACE and GRACE-FO. *Science of the Total Environment*, *779*, 146435.

Fatolazadeh, F., Eshagh, M., & Goïta, K. (2020). A new approach for generating optimal GLDAS hydrological products and uncertainties. *Science of the Total Environment*, *730*, 138932.

Feng, W. (2018). GRAMAT: A comprehensive Matlab toolbox for estimating global mass variations from GRACE satellite data. *Earth Science Informatics*,*12*, 389–404.

Feng, W., Lemoine, J. M., Zhong, M., & Hsu, T. T. (2012). Terrestrial water storage changes in the Amazon basin measured by GRACE during 2002—2010. *Chinese Journal of Geophysics*, *55*(3), 814-821.

Feng, W., Zhong, M., Lemoine, J.M., Biancale, R., Hsu, H.T.,& Xia, J., (2013). Evaluation of groundwater depletion in North China using the Gravity Recovery and Climate Experiment [GRACE] data and ground-based measurements. *Water Resources Research*, *49*, 2110–2118.

Flörke, M., Kynast, E., Bärlund, I., Eisner, S., Wimmer, F., & Alcamo, J. (2013). Domestic and industrial water uses of the past 60 years as a mirror of socio-economic development: A global simulation study. *Global Environmental Change*, *23*(1), 144-156.

Foster, S. S. D., & Chilton, P. J. (2003). Groundwater: the processes and global significance of aquifer degradation. Philosophical Transactions of the Royal Society of London. Series B: *Biological Sciences*, *358*(1440), 1957-1972.

Frappart, F., & Ramillien, G. (2018). Monitoring groundwater storage changes using the Gravity Recovery and Climate Experiment (GRACE) satellite mission: A review. *Remote Sensing*, *10*(6), 829.

Frappart, F., Seoane, L., & Ramillien, G. (2013). Validation of GRACE-derived terrestrial water storage from a regional approach over South America. *Remote Sensing of Environment*, *137*, 69-83.

Galloway, D. L., & Burbey, T. J. (2011). Regional land subsidence accompanying groundwater extraction. *Hydrogeology Journal*, *19*(8), 1459-1486.

Gaur, S., Chahar, B. R., & Graillot, D. (2011). Combined use of groundwater modeling and potential zone analysis for management of groundwater. *International Journal of Applied Earth Observation and Geoinformation*, *13*(1), 127-139.

Getirana, A., Kumar, S., Girotto, M., & Rodell, M. (2017-a). Rivers and floodplains as key components of global terrestrial water storage variability. *Geophysical Research Letters*, *44*(20), 10-359.

Getirana, A., Peters-Lidard, C., Rodell, M., & Bates, P. D. (2017-b). Trade-off between cost and accuracy in large-scale surface water dynamic modeling. *Water Resources Research*, *53*(6), 4942-4955.

Ghasemian D (2018). *Groundwater management using remotely sensed data in High Plains aquifer*. [PhD Thesis]. the University of Arizona, Arizona, USA.

Gilfedder, M., Rassam, D. W., Stenson, M. P., Jolly, I. D., Walker, G. R., & Littleboy, M. (2012). Incorporating land-use changes and surface–groundwater interactions in a simple catchment water yield model. *Environmental Modelling & Software*, *38*, 62-73.

Girotto, M., De Lannoy, G. J., Reichle, R. H., Rodell, M., Draper, C., Bhanja, S. N., et al. (2017). Benefits and pitfalls of GRACE data assimilation: A case study of terrestrial water storage depletion in India. *Geophysical Research Letters*, *44*(9), 4107-4115.

Gleeson, T., Alley, W. M., Allen, D. M., Sophocleous, M. A., Zhou, Y., Taniguchi, M., et al. (2012). Towards sustainable groundwater use: Setting long-term goals, backcasting and managing adaptively. *Groundwater*, *50*(1), 19-26.

Gleeson, T., VanderSteen, J., Sophocleous, M. A., Taniguchi, M., Alley, W. M., Allen, D. M., et al. (2010). Groundwater sustainability strategies. *Nature Geoscience*, *3*(6), 378-379.

Gocic, M., & Trajkovic, S. (2013). Analysis of changes in meteorological variables using Mann-Kendall and Sen's slope estimator statistical tests in Serbia. *Global and Planetary Change*, *100*, 172-182.

Goetz, S. J., Bunn, A. G., Fiske, G. J., & Houghton, R. A. (2005). Satellite-observed photosynthetic trends across boreal North America associated with climate and fire disturbance. *Proceedings of the National Academy of Sciences*, *102*(38), 13521-13525.

Gómez, L., Haesevoets, S., Kuijpers, B., & Vaisman, A. A. (2009). Spatial aggregation: Data model and implementation. *Information Systems*, *34*(6), 551-576.

GRACE Missions Applications Plan, (2016). Retrieved Oct, 1, 2021 from: https://grace.jpl.nasa.gov/internal_resources/114/.

Granados-Ramírez, R., Reyna-Trujillo, T., Gómez-Rodríguez, G., & Soria-Ruiz, J. (2004). Analysis of NOAA-AVHRR-NDVI images for crops monitoring. *International Journal of Remote Sensing*, *25*(9), 1615-1627.

Gumidyala, S., Ruess, P. J., Konar, M., Marston, L., Dalin, C., & Wada, Y. (2020). Groundwater depletion embedded in domestic transfers and international exports of the United States. *Water Resources Research*, *56*(2), e2019WR024986.

Hallet, B., & Allard, M. (1998, June). *Measurement of soil motion in sorted circles, western Spitsbergen. In Permafrost*. Retrieved January 1, 2022 from: https://www.arlis.org/docs/vol1/ICOP/40770716/CDOM/Proceedings/PDF001189/064299.pdf

Han, S. C., Shum, C. K., Jekeli, C., & Alsdorf, D. (2005). Improved estimation of terrestrial water storage changes from GRACE. *Geophysical Research Letters*, *32*(7), 1-5.

Hao, Z., AghaKouchak, A., Nakhjiri, N., & Farahmand, A. (2014). Global integrated drought monitoring and prediction system. *Scientific Data*, *1*(1), 1-10.

Harmancioglu, N. B., & Altinbilek, D. (Eds.). (2020). *Water Resources of Turkey*. Springer International Publishing.

Harmancioglu, N. B., Fedra, K., & Barbaros, F. (2008). Analysis for sustainability in management of water scarce basins: the case of the Gediz River Basin in Turkey. *Desalination*, *226*(1-3), 175-182.

He, X., Chaney, N. W., Schleiss, M., & Sheffield, J. (2016). Spatial downscaling of precipitation using adaptable random forests. *Water Resources Research*, *52*(10), 8217-8237.

Heath, R.C., (1983). *Basic ground-water hydrology, U.S. Geological Survey Water-Supply Paper 2220*. Retrieved January 2, 2022 from: https://pubs.usgs.gov/wsp/2220/report.pdf

Hersbach, H., Bell, B., Berrisford, P., Hirahara, S., Horányi, A., Muñoz-Sabater, J., et al. (2020). The ERA5 global reanalysis. *Quarterly Journal of the Royal Meteorological Society*, *146*(730), 1999-2049.

Hosseini-Moghari, S.M., Araghinejad, S., Ebrahimi, K. & Tourian, M. J. (2019). Introducing modified total storage deficit index (MTSDI) for drought monitoring using GRACE observations. *Ecological Indicators*, *101*: 465-475.

Hou, Y. K., Chen, H., Xu, C. Y., Chen, J., & Guo, S. L. (2017). Coupling a Markov chain and support vector machine for at-site downscaling of daily precipitation. *Journal of Hydrometeorology, 18*(9), 2385-2406.

Houborg, R., Rodell, M., Li, B., Reichle, R., & Zaitchik, B. F. (2012). Drought indicators based on model-assimilated Gravity Recovery and Climate Experiment (GRACE) terrestrial water storage observations. *Water Resources Research, 48*(7), W07525.

Hu, Z., Zhou, Q., Chen, X., Chen, D., Li, J., Guo, M., et al. (2019). Groundwater depletion estimated from GRACE: A challenge of sustainable development in an arid region of Central Asia. *Remote Sensing, 11*(16), 1908.

Hua, J. W., Zhu, S. Y., & Zhang, G. X. (2018). Downscaling land surface temperature based on random forest algorithm. *Remote Sensing for Land & Resources, 30*(1), 78-86.

Huang, Y., Salama, M. S., Krol, M. S., Su, Z., Hoekstra, A. Y., Zeng, Y., et al. (2015-a). Estimation of human-induced changes in terrestrial water storage through integration of GRACE satellite detection and hydrological modeling: A case study of the Y angtze R iver basin. *Water Resources Research, 51*(10), 8494-8516.

Huang, Y., Salama, M. S., Krol, M. S., Velde, R., Hoekstra, A. Y., Zhou, Y., et al. (2013). Analysis of long-term terrestrial water storage variations in the Yangtze River basin. *Hydrology and Earth System Sciences, 17*(5), 1985-2000.

Huang, Z., Jiao, J. J., Luo, X., Pan, Y., & Jin, T. (2021). Drought and flood characterization and connection to climate variability in the Pearl river basin in southern China using long-term GRACE and reanalysis data. *Journal of Climate, 34*(6), 2053-2078.

Huang, Z., Pan, Y., Gong, H., Yeh, P. J. F., Li, X., Zhou, D., et al. (2015-b). Subregional-scale groundwater depletion detected by GRACE for both shallow and deep aquifers in North China Plain. *Geophysical Research Letters*, *42*(6), 1791-1799.

Humphrey, V., Gudmundsson, L., & Seneviratne, S. I. (2016). Assessing global water storage variability from GRACE: Trends, seasonal cycle, subseasonal anomalies and extremes. *Surveys in Geophysics*, *37*(2), 357-395.

Ivanova, Y., Kovalev, A., & Soukhovolsky, V. (2021). Modeling the radial stem growth of the pine (pinus sylvestris l.) forests using the satellite-derived NDVI and LST (MODIS/AQUA) data. *Atmosphere*, *12*(12), 1-15.

Jekeli, C. (1981), *Alternative methods to smooth the Earth's gravity field*. Retrieved January 3, 2022 from: https://earthsciences.osu.edu/sites/earthsciences.osu.edu/files/report-327.pdf

Jia, X., Hou, D., Wang, L., O'Connor, D., & Luo, J. (2020). The development of groundwater research in the past 40 years: A burgeoning trend in groundwater depletion and sustainable management. *Journal of Hydrology*, *587*, 125006.

Jia, X., O'Connor, D., Hou, D., Jin, Y., Li, G., Zheng, C., et al. (2019). Groundwater depletion and contamination: Spatial distribution of groundwater resources sustainability in China. *Science of the Total Environment*, *672*, 551-562.

Jiang, D., Wang, J., Huang, Y., Zhou, K., Ding, X., & Fu, J. (2014). The review of GRACE data applications in terrestrial hydrology monitoring. *Advances in Meteorology*, *2014*, 1-9.

Jin, Q., Wei, J., Yang, Z. L., & Lin, P. (2017). Irrigation-induced environmental changes around the Aral Sea: An integrated view from multiple satellite observations. *Remote Sensing*, *9*(9), 900.

Jin, S. G., Hassan, A. A., & Feng, G. P. (2012). Assessment of terrestrial water contributions to polar motion from GRACE and hydrological models. *Journal of Geodynamics*, *62*, 40-48.

Jin, S., & Feng, G. (2013). Large-scale variations of global groundwater from satellite gravimetry and hydrological models, 2002–2012. *Global and Planetary Change*, *106*, 20-30.

Jin, Y., Ge, Y., Wang, J., Heuvelink, G., & Wang, L. (2018). Geographically weighted area-to-point regression kriging for spatial downscaling in remote sensing. *Remote Sensing*, *10*(4), 579.

Jing, W., Zhao, X., Yao, L., Jiang, H., Xu, J., Yang, J., et al. (2020). Variations in terrestrial water storage in the Lancang-Mekong river basin from GRACE solutions and land surface model. *Journal of Hydrology*, *580*, 124258.

Johnson, AI. (1967). Specific yield – *compilation of specific yield for various materials, geological survey water* – Supply Paper 1662-D. United States Government Printing Office, Washington.

Joodaki, G., Wahr, J., & Swenson, S. (2014). Estimating the human contribution to groundwater depletion in the Middle East, from GRACE data, land surface models and well observations. *Water Resources Research*, *50*(3), 2679-2692.

Jury, W. A., & Vaux Jr, H. J. (2007). The emerging global water crisis: managing scarcity and conflict between water users. *Advances in Agronomy*, *95*, 1-76.

Justice, C. O., Townshend, J. R. G., Vermote, E. F., Masuoka, E., Wolfe, R. E., Saleous, N., et al. (2002). An overview of MODIS Land data processing and product status. *Remote sensing of Environment*, *83*(1-2), 3-15.

Jyolsna, P. J., Kambhammettu, B. V. N. P., & Gorugantula, S. (2021). Application of random forest and multi-linear regression methods in downscaling GRACE-derived groundwater storage changes. *Hydrological Sciences Journal*, *66*(5), 874-887.

Kamran, K. V., & Khorrami, B. (2018). Change detection and prediction of urmia lake and its surrounding environment during the past 60 years applying geobased remote sensing analysis. *International Archives of the Photogrammetry, Remote Sensing and Spatial Information Sciences*, *42*(3/W4).

Karasu, İ. G. (2019). *Intercomparison of grace-based groundwater level change and in-situ measurements over Central Anatolia basins, Turkey* [Master's thesis]. Middle East Technical University, Ankara.

Karger, D. N., & Zimmermann, N. E. (2019). *Climatologies at High Resolution for the Earth Land Surface Areas CHELSA V1. 2: Technical Specificatin*. Retrieved December 10, 2021 from https://www.stevenphipps.com/publications/karger2017_sci_data_v1p2.pdf

Karger, D. N., Conrad, O., Böhner, J., Kawohl, T., Kreft, H., Soria-Auza, R. W., et al. (2017). Climatologies at high resolution for the earth's land surface areas. *Scientific Data*, *4*(1), 1-20.

Karmaker, C. L., Halder, P. K. and Sarker, E. (2017). A study of time series model for predicting jute yarn demand: case study. *Journal of Industrial Engineering*, *2017*, 2061260.

Karunakalage, A. A., Kannaujiya, S., Chatterjee, R. S., Taloor, A. K., Pranjal, P., Chauhan, P., et al. (2021). Groundwater storage assessment using effective downscaling GRACE data in water-stressed regions of India. In: Taloor A.K., Kotlia B.S., Kumar K. (eds) *water, cryosphere, and climate change in the Himalayas. geography of the physical environment*. (pp. 233-245). Springer, Cham.

Katpatal, Y. B., Rishma, C., & Singh, C. K. (2018). Sensitivity of the Gravity Recovery and Climate Experiment (GRACE) to the complexity of aquifer systems for monitoring of groundwater. *Hydrogeology Journal*, *26*(3), 933-943.

Kendall, M.G., (1975). *Rank Correlation Methods*. Griffin, London.

Khaki, M., & Hoteit, I. (2021). Monitoring water storage decline over the Middle East. *Journal of Hydrology,603*, 127166.

Forootan, E., Schumacher, M., Awange, J. L., & Müller Schmied, H. (2016). Exploring the influence of precipitation extremes and human water use on total water storage (TWS) changes in the G anges-B rahmaputra-M eghna River Basin. *Water Resources Research*, *52*(3), 2240-2258.

Khorrami, B. & Gunduz, O. (2019). Analyses of meteorological drought and its impacts on groundwater fluctuations, a case study: Marand plain (Iran). *Pamukkale University Journal of Engineering Sciences 25* (6): 711–717.

Khorrami, B., & Gunduz, O. (2021a). Evaluation of the temporal variations of groundwater storage and its interactions with climatic variables using GRACE data and hydrological models: A study from Turkey. *Hydrological Processes*, *35*(3), e14076.

Khorrami, B., & Gunduz, O. (2021b). En enhanced water storage deficit index (EWSDI) for drought detection using GRACE gravity estimates. *Journal of Hydrology, 603*, 126812.

Khorrami, B., Arik, F., & Gunduz, O. (2021). Land deformation and sinkhole occurrence in response to the fluctuations of groundwater storage: an integrated assessment of GRACE gravity measurements, ICESat/ICESat-2 altimetry data and hydrologic models. *GIScience & Remote Sensing*, *58*(8), 1-25.

Khorrami, B., Gunduz, O., Patel, N., Ghouzlane, S., & Najjar, M. (2019). Land surface temperature anomalies in response to changes in forest cover. *International Journal of Engineering and Geosciences, 4*(3), 149-156.

Kibaroglu, A., Scheumann, W., & Kramer, A. (Eds.). (2011). *Turkey's water policy: national frameworks and international cooperation.* Springer Science & Business Media.

Kim, H., Yeh, P. J. F., Oki, T., & Kanae, S. (2009). Role of rivers in the seasonal variations of terrestrial water storage over global basins. *Geophysical Research Letters*, *36*(17), L17402.

Konikow, L. F., & Kendy, E. (2005). Groundwater depletion: A global problem. *Hydrogeology Journal*, *13*(1), 317-320.

Konikow, L. F., & Leake, S. A. (2014). Depletion and capture: revisiting the source of water derived from wells. *Groundwater*, *52*(S1), 100-111.

Kornelsen, K. C., & Coulibaly, P. (2013). Advances in soil moisture retrieval from synthetic aperture radar and hydrological applications. *Journal of Hydrology*, *476*, 460-489.

Koster, R. D., Suarez, M. J., Ducharne, A., Stieglitz, M., & Kumar, P. (2000). A catchment-based approach to modeling land surface processes in a general circulation model: 1. Model structure. *Journal of Geophysical Research: Atmospheres*, *105*(D20), 24809-24822.

Kumar, S. V., Zaitchik, B. F., Peters-Lidard, C. D., Rodell, M., Reichle, R., Li, B., et al. (2016). Assimilation of gridded GRACE terrestrial water storage estimates in the North American Land Data Assimilation System. *Journal of Hydrometeorology*, *17*(7), 1951-1972.

Kundzewicz, Z. W., & Doell, P. (2009). Will groundwater ease freshwater stress under climate change? *Hydrological Sciences Journal*, *54*(4), 665-675.

Kuzucuoğlu, C. (2019). The physical geography of Turkey: an outline. In: Kuzucuoğlu C., Çiner A., Kazancı N. (eds) *Landscapes and Landforms of Turkey. World Geomorphological Landscapes.* (pp. 7-15). Springer, Cham.

Landerer, F. W., & Swenson, S. C. (2012). Accuracy of scaled GRACE terrestrial water storage estimates. *Water Resources Research*, *48*(4), W04531.

Le Roux, R., Katurji, M., Zawar-Reza, P., Quénol, H., & Sturman, A. (2018). Comparison of statistical and dynamical downscaling results from the WRF model. *Environmental Modelling & Software*, *100*, 67-73.

Leblanc, M., Tweed, S., Van Dijk, A., & Timbal, B. (2012). A review of historic and future hydrological changes in the Murray-Darling Basin. *Global and Planetary Change*, *80*, 226-246.

Leblanc, M.J., Tregoning, P., Ramillien, G., Tweed, S.O., Fakes, A., (2009). Basin-scale, integrated observations of the early 21st century multiyear drought in southeast Australia, *Water Resources Research*. *45*, W04408.

Lenk, O. (2013). Satellite based estimates of terrestrial water storage variations in Turkey. *Journal of Geodynamics*, *67*, 106-110.

Li, B., Rodell, M., Zaitchik, B. F., Reichle, R. H., Koster, R. D., & van Dam, T. M. (2012). Assimilation of GRACE terrestrial water storage into a land surface model: Evaluation and potential value for drought monitoring in western and central Europe. *Journal of Hydrology*, *446*, 103-115.

Li, W., Ni, L., Li, Z. L., Duan, S. B., & Wu, H. (2019). Evaluation of machine learning algorithms in spatial downscaling of MODIS land surface temperature. *IEEE Journal of Selected Topics in Applied Earth Observations and Remote Sensing*, *12*(7), 2299-2307.

Lin, M., Biswas, A., & Bennett, E. M. (2019). Spatio-temporal dynamics of groundwater storage changes in the Yellow River Basin. *Journal of Environmental Management*, *235*, 84-95.

Liu, F., Kang, P., Zhu, H., Han, J., & Huang, Y. (2021-b). Analysis of spatiotemporal groundwater-storage variations in China from GRACE. *Water*, *13*(17), 2378.

Liu, X., Hu, L., Sun, K., Yang, Z., Sun, J., & Yin, W. (2021-a). Improved Understanding of Groundwater Storage Changes under the Influence of River Basin Governance in Northwestern China Using GRACE Data. *Remote Sensing*, *13*(14), 2672.

Liu, Y., Guo, W., Feng, J., & Zhang, K. (2011). A summary of methods for statistical downscaling of meteorological data. *Advances in Earth Science*, *26*(8), 837-847.

Ljungqvist, F. C., Seim, A., Krusic, P. J., González-Rouco, J. F., Werner, J. P., Cook, E. R., et al. E. (2019). European warm-season temperature and hydroclimate since 850 CE. *Environmental Research Letters*, *14*(8), 084015.

Lombard, A., Garcia, D., Ramillien, G., Cazenave, A., Biancale, R., Lemoine, J. M., et al. (2007). Estimation of steric sea level variations from combined GRACE and Jason-1 data. *Earth and Planetary Science Letters*, *254*(1-2), 194-202.

Long, D., Scanlon, B. R., Longuevergne, L., Sun, A. Y., Fernando, D. N., & Save, H. (2013). GRACE satellite monitoring of large depletion in water storage in response to the 2011 drought in Texas. *Geophysical Research Letters*, *40*(13), 3395-3401.

Long, D., Chen, X., Scanlon, B. R., Wada, Y., Hong, Y., Singh, V. P., et al. (2016). Have GRACE satellites overestimated groundwater depletion in the Northwest India Aquifer?. *Scientific Reports*, *6*(1), 1-11.

Long, D., Longuevergne, L., & Scanlon, B. R. (2015). Global analysis of approaches for deriving total water storage changes from GRACE satellites. *Water Resources Research*, *51*(4), 2574-2594.

Long, D., Pan, Y., Zhou, J., Chen, Y., Hou, X., Hong, Y., et al. (2017). Global analysis of spatiotemporal variability in merged total water storage changes using multiple GRACE products and global hydrological models. *Remote Sensing of Environment*, *192*, 198-216.

Longuevergne, L., Wilson, C. R., Scanlon, B. R., & Crétaux, J. F. (2013). GRACE water storage estimates for the Middle East and other regions with significant reservoir and lake storage. *Hydrology and Earth System Sciences*, *17*(12), 4817-4830.

Loomis, B. D., Felikson, D., Sabaka, T. J., & Medley, B. (2021). High-spatial-resolution mass rates from GRACE and GRACE-FO: Global and ice sheet analyses. *Journal of Geophysical Research: Solid Earth*, *126* (12), e2021JB023024.

Lu, Y., Dong, J., & Steele-Dunne, S. C. (2019). Impact of soil moisture data resolution on soil moisture and surface heat flux estimates through data assimilation: a case study in the southern Great Plains. *Journal of Hydrometeorology*, *20*(4), 715-730.

Luthcke, S. B., Sabaka, T. J., Loomis, B. D., Arendt, A. A., McCarthy, J. J., & Camp, J. (2013). Antarctica, Greenland and Gulf of Alaska land-ice evolution from an iterated GRACE global mascon solution. *Journal of Glaciology*, 59(216), 613-631.

Ma, S., Wu, Q., Wang, J., & Zhang, S. (2017). Temporal evolution of regional drought detected from GRACE TWSA and CCI SM in Yunnan Province, China. *Remote Sensing*, *9*(11), 1124.

MacDonald, A. M., Bonsor, H. C., Ahmed, K. M., Burgess, W. G., Basharat, M., Calow, R. C., et al. (2016). Groundwater quality and depletion in the Indo-Gangetic Basin mapped from in situ observations. *Nature Geoscience*, *9*(10), 762-766.

Mann, H. B. (1945). Nonparametric tests against trend. Econometrica: *Journal of the Econometric Society, 13* (3), 245-259.

McNally, A., Arsenault, K., Kumar, S., Shukla, S., Peterson, P., Wang, S., et al. (2017). A land data assimilation system for sub-Saharan Africa food and water security applications. *Scientific Data*, *4*(1), 1-19.

MGM (2014). *Havza bazinda yağişin el nino ve la nina ile ilişkisi*. Retrieved January 1, 2020 from: https://www.mgm.gov.tr/FILES/genel/kitaplar/havze-el.pdf.

MGM (2020). *Official Statistics*. Received in 3 April, 2020 from: https://www.mgm.gov.tr/veridegerlendirme/il-ve-ilceler-istatistik.aspx.

Milewski, A. M., Thomas, M. B., Seyoum, W. M., & Rasmussen, T. C. (2019). Spatial downscaling of GRACE TWSA data to identify spatiotemporal groundwater level trends in the Upper Floridan Aquifer, Georgia, USA. *Remote Sensing*, *11*(23), 2756.

Minderhoud, P. S. J., Erkens, G., Pham, V. H., Bui, V. T., Erban, L., Kooi, H., et al. (2017). Impacts of 25 years of groundwater extraction on subsidence in the Mekong delta, Vietnam. *Environmental Research Letters*, *12*(6), 064006.

Ministry Of Agriculture And Forestry (2020). *Herbal Production data*. Retrieved September 12, 2019 from https://www.tarimorman.gov.tr/sgb/Belgeler/SagMenuVeriler/BUGEM.pdf

Ministry of Agriculture and Forestry (2020). *The General directorate of water management. Water Management Plan (WMP) of the North Aegean River basin*. Retrieved 1 January 2020, from: https://www.tarimorman.gov.tr/SYGM/Belgeler/Kuzey%20Ege%20NHYP%20Taslak%20Raporu/Kuzey%20Ege%20NHYP%20Taslak%20Raporu.pdf

Miro, M., & Famiglietti, J. (2018). Downscaling GRACE remote sensing datasets to high-resolution groundwater storage change maps of California's Central Valley. *Remote Sensing*, *10*(1), 143.

Modarres, R., & da Silva, V. D. P. R. (2007). Rainfall trends in arid and semi-arid regions of Iran. *Journal of Arid Environments*, *70*(2), 344-355.

Moghim, S. (2020). Assessment of water storage changes using GRACE and GLDAS. *Water Resources Management*, *34*(2), 685-697.

Mohamed, A. (2019). Hydro-geophysical study of the groundwater storage variations over the Libyan area and its connection to the Dakhla basin in Egypt. *Journal of African Earth Sciences, 157,* 103508.

Mohamed, A. (2020). Gravity applications to groundwater storage variations of the Nile Delta Aquifer. *Journal of Applied Geophysics, 182*, 104177.

Moore, P., & Williams, S. D. P. (2014). Integration of altimetric lake levels and GRACE gravimetry over A frica: Inferences for terrestrial water storage change 2003–2011. *Water Resources Research*, *50*(12), 9696-9720.

Morris, B.L., Lawrence, A.R., Chilton, P.J.C., Adams, B., Calow, R.C. & Klinck, BA. (2003). *Groundwater and its susceptibility to degradation: a global assessment of the problem and options for management*. Retrieved December 30, 2021 from: http://nora.nerc.ac.uk/id/eprint/19395/1/Groundwater_INC_cover.pdf.

Morris, D.A. and A.I. Johnson, (1967). Summary of hydrologic and physical properties of rock and soil materials as analyzed by the Hydrologic Laboratory of the U.S. Geological Survey, U.S. *Geological Survey Water-Supply Paper* 1839-D, 42p.

Mohsin, S., & Lone, M. A. (2021). Trend analysis of reference evapotranspiration and identification of responsible factors in the Jhelum River Basin, Western Himalayas. *Modeling Earth Systems and Environment*, *7*(1), 523-535.

Mu, Q., Zhao, M., & Running, S. W. (2011). Improvements to a MODIS global terrestrial evapotranspiration algorithm. *Remote Sensing of Environment*, *115*(8), 1781-1800.

Müller Schmied, H., Cáceres, D., Eisner, S., Flörke, M., Herbert, C., Niemann, C., et al. (2021). The global water resources and use model WaterGAP v2. 2d: model description and evaluation. *Geoscientific Model Development*, *14*(2), 1037-1079.

Naghibi, S. A., Pourghasemi, H. R., & Dixon, B. (2016). GIS-based groundwater potential mapping using boosted regression tree, classification and regression tree and random forest machine learning models in Iran. *Environmental Monitoring and Assessment*, *188*(1), 1-27.

NASA (2002). *GRACE Launch Press Kit [Press release]*. Retrieved January 1, 2022 from: https://grace.jpl.nasa.gov/mission/grace.

NASA (2021). *NASA Earth Observatory images by Lauren Dauphin, using GRACE data from the National Drought Mitigation Center. Story by Kasha Patel.* Retrieved December 30, 2021 from: https://earthobservatory.nasa.gov/images/147811/turkey-experiences-intense-drought.

NASA Facts (2003). *Studying the Earth's Gravity from Space: The Gravity Recovery and Climate Experiment [GRACE]*. Retrieved January 18, 2020 from: https://eospso.nasa.gov/sites/default/files/publications/GRACE_Fact_Sh_Final.pdf

Ndehedehe, C., Awange, J., Agutu, N., Kuhn, M., & Heck, B. (2016). Understanding changes in terrestrial water storage over West Africa between 2002 and 2014. *Advances in Water Resources*, *88*, 211-230.

Neves, M. C., Nunes, L. M., & Monteiro, J. P. (2020). Evaluation of GRACE data for water resource management in Iberia: a case study of groundwater storage monitoring in the Algarve region. *Journal of Hydrology: Regional Studies*, *32*, 100734.

Ni, S., Chen, J., Wilson, C. R., Li, J., Hu, X., & Fu, R. (2018). Global terrestrial water storage changes and connections to ENSO events. *Surveys in Geophysics*, *39*(1), 1-22.

Nie, N., Zhang, W., Zhang, Z., Guo, H., & Ishwaran, N. (2016). Reconstructed terrestrial water storage change (ΔTWS) from 1948 to 2012 over the Amazon Basin with the latest GRACE and GLDAS products. *Water Resources Management*, *30*(1), 279-294.

Nigatu, Z. M., Fan, D., You, W., & Melesse, A. M. (2021). Hydroclimatic Extremes Evaluation Using GRACE/GRACE-FO and Multidecadal Climatic Variables over the Nile River Basin. *Remote Sensing*, *13*(4), 651.

Ning, S., Ishidaira, H., & Wang, J. (2014). Statistical downscaling of GRACE-derived terrestrial water storage using satellite and GLDAS products. *Journal of Japan Society of Civil Engineers*.*70* (4), 133-138.

Nistor, M. M., & Man, T. C. (2019). Water availability variation under climate change in Turkey during 21 St century. *Carpathian Journal of Earth and Environmental Sciences*, *14*, 19-28.

Okay Ahi, G., & Jin, S. (2019). Hydrologic mass changes and their implications in Mediterranean-climate Turkey from GRACE measurements. *Remote Sensing*, *11*(2), 120.

Oke, S. A., & Fourie, F. (2017). Guidelines to groundwater vulnerability mapping for Sub-Saharan Africa. *Groundwater for Sustainable Development*, *5*, 168-177.

Oyebande, L. (2001). Water problems in Africa—how can the sciences help?. *Hydrological Sciences Journal*, *46*(6), 947-962.

Ozturk, S., & Ozturk, F. (2018). Forecasting energy consumption of Turkey by Arima model. *Journal of Asian Scientific Research*, *8*(2), 52.

Palmer, W. C., (1965). *Meteorlogical drought, Tech. Rep*. Weather Bureau Research Paper No. 45, US Department of Commerce, Washington DC.

Pan, Y., Zhang, C., Gong, H., Yeh, P. J. F., Shen, Y., Guo, Y., ... & Li, X. (2017). Detection of human-induced evapotranspiration using GRACE satellite observations in the Haihe River basin of China. *Geophysical Research Letters*, *44*(1), 190-199.

Partal, T., & Kahya, E. (2006). Trend analysis in Turkish precipitation data. *Hydrological Processes*. *20*(9), 2011-2026.

Parker, J. A., Kenyon, R. V., & Troxel, D. E. (1983). Comparison of interpolating methods for image resampling. *IEEE Transactions on medical imaging*, *2*(1), 31-39.

Paul, P., Tenaiji, A., Kulaib, A., & Braimah, N. (2016). A review of the water and energy sectors and the use of a nexus approach in Abu Dhabi. *International Journal of Environmental Research and Public Health*, *13*(4), 364.

Phillips, T., Nerem, R. S., Fox-Kemper, B., Famiglietti, J. S., & Rajagopalan, B. (2012). The influence of ENSO on global terrestrial water storage using GRACE. *Geophysical Research Letters*, *39*(16), L16705.

Pimentel, D., & Burgess, M. (2013). Soil erosion threatens food production. *Agriculture*, *3*(3), 443-463.

Portmann, F. (2017). *Global irrigation in the 20th century: extension of the WaterGAP Global Irrigation Model (GIM) with the spatially explicit Historical Irrigation Data set (HID).* Retrieved Oct 2, 2021 from: http://publikationen.ub.uni-frankfurt.de/frontdoor/index/index/docId/44410

Postel, S. L. (2000). Water and world population growth. *Journal-American Water Works Association*, *92*(4), 131-138.

Rahaman, M. M., Thakur, B., Kalra, A., & Ahmad, S. (2019-a). Modeling of GRACE-derived groundwater information in the Colorado River Basin. *Hydrology*, *6*(1), 19.

Rahaman, M. M., Thakur, B., Kalra, A., Li, R., & Maheshwari, P. (2019-b). Estimating high-resolution groundwater storage from GRACE: A random forest approach. *Environments*, *6*(6), 63.

Rateb, A., Scanlon, B. R., Pool, D. R., Sun, A., Zhang, Z., Chen, J., et al. (2020). Comparison of groundwater storage changes from GRACE satellites with monitoring and modeling of major US aquifers. *Water Resources Research*, *56*(12), e2020WR027556.

Richey, A. S. (2014). *Stress and resilience in the world's largest aquifer systems: A GRACE-based methodology*. [PhD Thesis]. University of California, Irvine.

Richey, A. S., Thomas, B. F., Lo, M. H., Reager, J. T., Famiglietti, J. S., Voss, K., et al. (2015). Quantifying renewable groundwater stress with GRACE. *Water Resources Research*, *51*(7), 5217-5238.

Richey, J. E., Melack, J. M., Aufdenkampe, A. K., Ballester, V. M., & Hess, L. L. (2002). Outgassing from Amazonian rivers and wetlands as a large tropical source of atmospheric CO 2. *Nature*, *416*(6881), 617-620.

Riley, P and Klemann, V. (2021). *GRACE and GRACE-FO related publications*. Accessed from http://www-app2.gfz-potsdam.de/pb1/op/grace/references/sort_date.html.

Rodell, M., & Famiglietti, J. S. (2001). An analysis of terrestrial water storage variations in Illinois with implications for the Gravity Recovery and Climate Experiment (GRACE). *Water Resources Research*, *37*(5), 1327-1339.

Rodell, M., & Famiglietti, J. S. (2002). The potential for satellite-based monitoring of groundwater storage changes using GRACE: the High Plains aquifer, Central US. *Journal of Hydrology*, *263*(1-4), 245-256.

Rodell, M., Chen, J., Kato, H., Famiglietti, J. S., Nigro, J., & Wilson, C. R. (2007). Estimating groundwater storage changes in the Mississippi River basin (USA) using GRACE. *Hydrogeology Journal*, *15*(1), 159-166.

Rodell, M., Chen, J., Kato, H., Famiglietti, J. S., Nigro, J., & Wilson, C. R. (2008). Estimating groundwater storage changes in the Mississippi River basin (USA) using GRACE. *Hydrogeology Journal*, *15*(1), 159-166.

Rodell, M., Famiglietti, J. S., Wiese, D. N., Reager, J. T., Beaudoing, H. K., Landerer, F. W., et al. (2018). Emerging trends in global freshwater availability. *Nature*, *557*(7707), 651-659.

Rodell, M., Houborg,R., Li,B., Zaitchik,B.F., Reichle,R., Bolten,J., et al. (2019). *Practical Applications of GRACE and Future Satellite Gravity Missions. NASA GFCS.* Retrieved October 5, 2021 from: www.igcp565.org/.../P1_03_Rodell_FGW09_plenary.pdf.

Rodell, M., Velicogna, I., & Famiglietti, J. S. (2009). Satellite-based estimates of groundwater depletion in India. *Nature*, *460*(7258), 999-1002.

Rowlands, D. D., Luthcke, S. B., Klosko, S. M., Lemoine, F. G., Chinn, D. S., McCarthy, J. J., et al. (2005). Resolving mass flux at high spatial and temporal resolution using GRACE intersatellite measurements. *Geophysical Research Letters*, *32*(4),1-4.

Sachindra, D. A., Ahmed, K., Rashid, M. M., Shahid, S., & Perera, B. J. C. (2018). Statistical downscaling of precipitation using machine learning techniques. *Atmospheric Research*, *212*, 240-258.

Sahin, S., & Cigizoglu, H. K. (2012). The sub-climate regions and the sub-precipitation regime regions in Turkey. *Journal of Hydrology*, *450*, 180-189.

Sahour, H., Sultan, M., Vazifedan, M., Abdelmohsen, K., Karki, S., Yellich, J. A., et al. (2020). Statistical applications to downscale GRACE-derived terrestrial water storage data and to fill temporal gaps. *Remote Sensing*, *12*(3), 533.

Sakiyan, J., & Yazicigil, H. (2004). Sustainable development of an aquifer system in western Turkey. *Hydrogeology Journal*, *12*, 66–80.

Salomonson, V. V., Barnes, W. L., Maymon, P. W., Montgomery, H. E., & Ostrow, H. (1989). MODIS: Advanced facility instrument for studies of the Earth as a system. *IEEE Transactions on Geoscience and Remote Sensing*, *27*(2), 145-153.

Sarkar, T., Kannaujiya, S., Taloor, A. K., Ray, P. K. C., & Chauhan, P. (2020). Integrated study of GRACE data derived interannual groundwater storage variability over water stressed Indian regions. *Groundwater for Sustainable Development*, *10*, 100376.

Save, H., Bettadpur, S., & Tapley, B. D. (2016). High-resolution CSR GRACE RL05 mascons. *Journal of Geophysical Research: Solid Earth*, *121*(10), 7547-7569.

Seeyan, S., Merkel, B., & Abo, R. (2014). Investigation of the relationship between groundwater level fluctuation and vegetation cover by using NDVI for Shaqlawa Basin, Kurdistan Region-Iraq. *Journal of Geography and Geology*, *6*(3), 187.

Scanlon, B. R., Faunt, C. C., Longuevergne, L., Reedy, R. C., Alley, W. M., McGuire, V. L., et al. (2012b). Groundwater depletion and sustainability of irrigation in the US High Plains and Central Valley. *Proceedings of the National Academy of Sciences*, *109*(24), 9320-9325.

Scanlon, B. R., Longuevergne, L., & Long, D. (2012a). Ground referencing GRACE satellite estimates of groundwater storage changes in the California Central Valley, USA. *Water Resources Research*, *48*(4), 1-9.

Scanlon, B. R., Z. Zhang, R. C. Reedy, D. R. Pool, H. Save, D. Long, J., et al. (2015), Hydrologic implications of GRACE satellite data in the Colorado River basin, *Water Resources Research*., *51*, 9891–9903.

Scanlon, B. R., Zhang, Z., Save, H., Wiese, D. N., Landerer, F. W., Long, D., et al. (2016). Global evaluation of new GRACE mascon products for hydrologic applications *Water Resources Research*, *52*(12), 9412-9429.

Schmidt, R., Schwintzer, P., Flechtner, F., Reigber, C., Güntner, A., Döll, P., et al. (2006). GRACE observations of changes in continental water storage. *Global and Planetary Change*, *50*(1-2), 112-126.

Schrama, E. J., & Wouters, B. (2011). Revisiting Greenland ice sheet mass loss observed by GRACE. *Journal of Geophysical Research: Solid Earth*, *116*(B2),1-10.

Schrama, E. J., Wouters, B., & Rietbroek, R. (2014). A mascon approach to assess ice sheet and glacier mass balances and their uncertainties from GRACE data. *Journal of Geophysical Research: Solid Earth, 119*(7), 6048-6066.

Schumacher, M. (2012). *Assimilation of GRACE data into a global hydrological model using an ensemble Kalman filter*. [Master Thesis]. University of Bonn.

Sensoy, S., Demircan, M., Ulupınar, U., & Balta, İ., (2008). *Türkiye İklimi*. Retrieved December 20, 2021 from: Url: http://www.mgm.gov.tr/FILES/iklim/turkiye_iklimi.pdf

Sensoy, S., (2012). *İklim sınıflandırmaları*. Retrieved December 20, 2021 from: http://www.mgm.gov.tr/FILES/iklim/iklim_siniflandirmalari.pdf

Seyoum, W. M., & Milewski, A. M. (2016). Monitoring and comparison of terrestrial water storage changes in the northern high plains using GRACE and in-situ based integrated hydrologic model estimates. *Advances in Water Resources, 94*, 31-44.

Seyoum, W. M., Kwon, D., & Milewski, A. M. (2019). Downscaling GRACE TWSA data into high-resolution groundwater level anomaly using machine learning-based models in a glacial aquifer system. *Remote Sensing, 11*(7), 824.

Shahzaman, M., Zhu, W., Ullah, I., Mustafa, F., Bilal, M., Ishfaq, S., et al. (2021). Comparison of multi-year reanalysis, models and satellite remote sensing products for agricultural drought monitoring over South Asian countries. *Remote Sensing, 13*(16), 3294.

Shamsudduha, M., & Taylor, R. G. (2020). Groundwater storage dynamics in the world's large aquifer systems from GRACE: uncertainty and role of extreme precipitation. *Earth System Dynamics, 11*(3), 755-774.

Shen, H., Leblanc, M., Tweed, S., & Liu, W. (2015). Groundwater depletion in the Hai River Basin, China, from in situ and GRACE observations. *Hydrological Sciences Journal*, *60*(4), 671-687.

Shi, L., & Jiao, J. J. (2014). Seawater intrusion and coastal aquifer management in China: a review. *Environmental Earth Sciences*, *72*(8), 2811-2819.

Shokri, A., Walker, J. P., van Dijk, A. I., & Pauwels, V. R. (2018). Performance of different ensemble Kalman filter structures to assimilate GRACE terrestrial water storage estimates into a high-resolution hydrological model: A synthetic study. *Water Resources Research*, *54*(11), 8931-8951.

Shokri, A., Walker, J. P., van Dijk, A. I., & Pauwels, V. R. (2019). On the use of adaptive ensemble Kalman filtering to mitigate error misspecifications in GRACE data assimilation. *Water Resources Research*, *55*(9), 7622-7637.

Sidhu, B. S., Sharda, R., & Singh, S. (2021). Spatio-temporal assessment of groundwater depletion in Punjab, India. *Groundwater for Sustainable Development*, *12*, 100498.

Singh, A. (1989). Review article digital change detection techniques using remotely-sensed data. *International Journal of Remote Sensing*, *10*(6), 989-1003.

Singh, A., Seitz, F., & Schwatke, C. (2012). Inter-annual water storage changes in the Aral Sea from multi-mission satellite altimetry, optical remote sensing and GRACE satellite gravimetry. *Remote Sensing of Environment*, *123*, 187-195.

Sinha, D, Syed, T.H. and Reager, J.T. (2019). Utilizing combined deviations of precipitation and GRACE-based terrestrial water storage as a metric for drought characterization: a case study over major Indian river basins. *Journal of Hydrology*. *572*, 294–307.

Sinha, D., Syed, T.H., Famiglietti, J.S., Reager, J.T. & Thomas, R.C. (2017). Characterizing drought in India using GRACE observations of terrestrial water storage deficit. *Journal of Hydrometeorology, 18*(2), 381-396.

Sliwinska, J., Birylo, M., Rzepecka, Z., & Nastula, J. (2019). Analysis of Groundwater and Total Water Storage Changes in Poland Using GRACE Observations, In-situ Data and Various Assimilation and Climate Models. *Remote Sensing*, *11*(24), 29-49.

So, B. J., Kim, J. Y., Kwon, H. H., & Lima, C. H. (2017). Stochastic extreme downscaling model for an assessment of changes in rainfall intensity-duration-frequency curves over South Korea using multiple regional climate models. *Journal of Hydrology*, *553*, 321-337.

Stagge, J. H., Tallaksen, L. M., Gudmundsson, L., Van Loon, A. F., & Stahl, K. (2015). Candidate distributions for climatological drought indices (SPI and SPEI). *International Journal of Climatology*, *35*(13), 4027-4040.

Stöckle, C. O., Kjelgaard, J., & Bellocchi, G. (2004). Evaluation of estimated weather data for calculating Penman-Monteith reference crop evapotranspiration. *Irrigation Science, 23*(1), 39-46.

Strassberg, G., Scanlon, B. R., & Chambers, D. (2009). Evaluation of groundwater storage monitoring with the GRACE satellite: Case study of the High Plains aquifer, central United States. *Water Resources Research, 45*(5).

Su, Y., Guo, B., Zhou, Z., Zhong, Y., & Min, L. (2020). Spatio-temporal variations in groundwater revealed by GRACE and its driving factors in the Huang-Huai-Hai Plain, China. *Sensors, 20*(3), 922.

Sun, A. Y. (2013). Predicting groundwater level changes using GRACE data. *Water Resources Research, 49*(9), 5900-5912.

Sun, Z., Zhu, X., Pan, Y., Zhang, J., & Liu, X. (2018). Drought evaluation using the GRACE terrestrial water storage deficit over the Yangtze River Basin, China. *Science of the Total Environment*, *634*, 727-738.

Sutanudjaja, E. H., Van Beek, R., Wanders, N., Wada, Y., Bosmans, J. H., Drost, N., et al. (2018). PCR-GLOBWB 2: a 5 arcmin global hydrological and water resources model. *Geoscientific Model Development*, *11*(6), 2429-2453.

Swenson, S., & Wahr, J. (2006). Post-processing removal of correlated errors in GRACE data. *Geophysical Research Letters*, *33*(8),1-4.

Swenson, S. and J. Wahr (2002). Methods for inferring regional surface-mass anomalies from Gravity Recovery and Climate Experiment (GRACE) measurements of time-variable gravity. *Journal of Geophysical Research: Solid Earth.107*(B9), 2193.

Swenson, S., Yeh, P. J. F., Wahr, J., & Famiglietti, J. (2006). A comparison of terrestrial water storage variations from GRACE with in situ measurements from Illinois. *Geophysical Research Letters*, *33*(16),1-5.

Syed, T. H., Famiglietti, J. S., Rodell, M., Chen, J., & Wilson, C. R. (2008). Analysis of terrestrial water storage changes from GRACE and GLDAS. *Water Resources Research*, *44*(2),1-15.

Tabari, H., Marofi, S., Aeini, A., Talaee, P. H., & Mohammadi, K. (2011). Trend analysis of reference evapotranspiration in the western half of Iran. *Agricultural and Forest Meteorology*, *151*(2), 128-136.

Tangdamrongsub, N., & Šprlák, M. (2021). The assessment of hydrologic-and flood-induced land deformation in data-sparse regions using GRACE/GRACE-FO data assimilation. *Remote Sensing*, *13*(2), 235.

Tangdamrongsub, N., Han, S. C., Yeo, I. Y., Dong, J., Steele-Dunne, S. C., Willgoose, G., et al. (2020). Multivariate data assimilation of GRACE, SMOS, SMAP measurements for improved regional soil moisture and groundwater storage estimates. *Advances in Water Resources*, *135*, 103477.

Tapley, B. D., Bettadpur, S., Ries, J. C., Thompson, P. F., & Watkins, M. M. (2004a). GRACE measurements of mass variability in the Earth system. *Science*, *305*(5683), 503–505.

Tapley, B. D., Bettadpur, S., Watkins, M., & Reigber, C. (2004b). The gravity recovery and climate experiment: Mission overview and early results. *Geophysical Research Letters*, *31*(9).

Taylor, R. G., Scanlon, B., Döll, P., Rodell, M., Van Beek, R., Wada, Y., et al. (2013). Ground water and climate change. *Nature Climate Change*, *3*(4), 322-329.

Theis, C. V. (1940). The source of water derived from wells. *Civil Engineering*, *10*(5), 277-280.

Thomas, A. C., Reager, J. T., Famiglietti, J. S., & Rodell, M. (2014). A GRACE-based water storage deficit approach for hydrological drought characterization. *Geophysical Research Letters*, *41*(5), 1537-1545.

Thomas, B. F., & Famiglietti, J. S. (2019). Identifying climate-induced groundwater depletion in GRACE observations. *Scientific Reports*, *9*(1), 1-9.

Thomas, B. F., Famiglietti, J. S., Landerer, F. W., Wiese, D. N., Molotch, N. P., & Argus, D. F. (2017). GRACE groundwater drought index: Evaluation of California Central Valley groundwater drought. *Remote Sensing of Environment*, *198*, 384-392.

Tigkas, D., Vangelis, H., & Tsakiris, G. (2015). DrinC: a software for drought analysis based on drought indices. *Earth Science Informatics*, *8*(3), 697-709.

Tiwari, V. M., Wahr, J., & Swenson, S. (2009). Dwindling groundwater resources in northern India, from satellite gravity observations. *Geophysical Research Letters*, *36*(18).

Türkeş, M., & Erlat, E. (2003). Precipitation changes and variability in Turkey linked to the North Atlantic Oscillation during the period 1930–2000. *International Journal of Climatology: A Journal of the Royal Meteorological Society*, *23*(14), 1771-1796.

Türkeş, M., & Tatlı, H. (2009). Use of the standardized precipitation index (SPI) and a modified SPI for shaping the drought probabilities over Turkey. *International Journal of Climatology: A Journal of the Royal Meteorological Society*, *29*(15), 2270-2282.

Ülker, D., Ergüven, O. & Gazioğlu, C. (2018). Socio-economic impacts in a Changing Climate: Case Study Syria, *International Journal of Environment and Geoinformatics*. *5*(1), 84-93.

Vallee, D., Margat, J., Eliasson, A., & Hoogeveen, J. (2003). *Review of world water resources by country. Food and Agricultural Organization of the United Nations.* Retrieved December 30, 2021 from : https://www.fao.org/3/Y4473E/y4473e.pdf

Van der Schrier, G., Barichivich, J., Briffa, K. R., & Jones, P. D. (2013). A scPDSI-based global data set of dry and wet spells for 1901–2009. *Journal of Geophysical Research: Atmospheres*, *118*(10), 4025-4048.

Vasco, D. W., Farr, T. G., Jeanne, P., Doughty, C., & Nico, P. (2019). Satellite-based monitoring of groundwater depletion in California's Central Valley. *Scientific Reports, 9*(1), 1-14.

Vaux, H. (2011). Groundwater under stress: the importance of management. *Environmental Earth Sciences, 62*(1), 19-23.

Velicogna, I., & Wahr, J. (2013). Time-variable gravity observations of ice sheet mass balance: Precision and limitations of the GRACE satellite data. *Geophysical Research Letters*, *40*(12), 3055-3063.

Velicogna, I., Mohajerani, Y., Landerer, F., Mouginot, J., Noel, B., Rignot, E., et al. (2020). Continuity of ice sheet mass loss in Greenland and Antarctica from the GRACE and GRACE Follow-On missions. *Geophysical Research Letters, 47*(8), e2020GL087291.

Verma, K., & Katpatal, Y. B. (2020). Groundwater monitoring using GRACE and GLDAS data after downscaling within basaltic aquifer system. *Groundwater, 58*(1), 143-151.

Vishwakarma, B. D., Zhang, J., & Sneeuw, N. (2021). Downscaling GRACE total water storage change using partial least squares regression. *Scientific Data*, *8*(1), 1-13.

Voss, K. A., Famiglietti, J. S., Lo, M., De Linage, C., Rodell, M., & Swenson, S. C. (2013). Groundwater depletion in the Middle East from GRACE with implications for transboundary water management in the Tigris-Euphrates-Western Iran region. *Water Resources Research, 49*(2), 904-914.

Wada, Y. (2016). Modeling groundwater depletion at regional and global scales: Present state and future prospects. *Surveys in Geophysics*, *37*(2), 419-451.

Wada, Y., Van Beek, L. P., Van Kempen, C. M., Reckman, J. W., Vasak, S., & Bierkens, M. F. (2010). Global depletion of groundwater resources. *Geophysical Research Letters*, *37*(20), L20402.

Wahr, J., M. Molenaar and F. Bryan (1998), Time variability of the Earth's gravity field: Hydrological and oceanic effects and their possible detection using GRACE. *Geophysical Research Letters*, *103*(B12), 30,205–30,229.

Wang, F., Shao, W., Yu, H., Kan, G., He, X., Zhang, D., et al. (2020). Re-evaluation of the power of the mann-kendall test for detecting monotonic trends in hydrometeorological time series. *Frontiers in Earth Science*, *8* (14), 1-12.

Wang, L., Davis, J. L., & Howat, I. M. (2021). Complex patterns of antarctic ice sheet mass change resolved by time-dependent rate modeling of GRACE and GRACE Follow-On observations. *Geophysical Research Letters*, *48*(1), e2020GL090961.

Wang, L., Kaban, M. K., Thomas, M., Chen, C., & Ma, X. (2019). The challenge of spatial resolutions for GRACE-based estimates volume changes of larger man-made lake: the case of China's Three Gorges reservoir in the Yangtze river. *Remote Sensing*, *11*(1), 99.

Wang, S., & Li, J. (2016). Terrestrial water storage climatology for Canada from GRACE satellite observations in 2002–2014. *Canadian Journal of Remote Sensing*, *42*(3), 190-202.

Wang, W., Cui, W., Wang, X., & Chen, X. (2016). Evaluation of GLDAS-1 and GLDAS-2 forcing data and Noah model simulations over China at the monthly scale. *Journal of Hydrometeorology*, *17*(11), 2815-2833.

Watkins, M. M., Wiese, D. N., Yuan, D. N., Boening, C., & Landerer, F. W. (2015). Improved methods for observing Earth's time variable mass distribution with GRACE

using spherical cap mascons. Journal of Geophysical Research: *Solid Earth*, *120*(4), 2648-2671.

Wei, Z., Hou-Ze, X., Min, Z., & Mei-Juan, Y. (2008). Physical explanation on designing three axes as different resolution indexes from GRACE satellite-borne accelerometer. *Chinese Physics Letters*, *25*(12), 4482.

Wei, L., Jiang, S., Ren, L., Tan, H., Ta, W., Liu, Y., et al. (2021). Spatiotemporal changes of terrestrial water storage and possible causes in the closed Qaidam Basin, China using GRACE and GRACE Follow-On data. *Journal of Hydrology*, *598*, 126274.

Wells, N., Goddard, S., & Hayes, M. J. (2004). A self-calibrating Palmer drought severity index. *Journal of Climate*, *17*(12), 2335-2351.

Wiese, D. N., Landerer, F. W., & Watkins, M. M. (2016). Quantifying and reducing leakage errors in the JPL RL05M GRACE mascon solution. *Water Resources Research*, *52*(9), 7490-7502.

Wilby, R. L., & Wigley, T. M. L. (1997). Downscaling general circulation model output: a review of methods and limitations. Progress in Physical Geography: *Earth and Environment, 21*(4), 530–548.

Xia, Y., Mocko, D., Huang, M., Li, B., Rodell, M., Mitchell, K. E., et al. (2017). Comparison and assessment of three advanced land surface models in simulating terrestrial water storage components over the United States. *Journal of Hydrometeorology*, *18*(3), 625-649.

Xie, Y., Huang, S., Liu, S., Leng, G., Peng, J., Huang, Q., & Li, P. (2018). GRACE-based terrestrial water storage in northwest China: changes and causes. *Remote Sensing*, *10*(7), 1163.

Xiong, J., Guo, S., Yin, J., Gu, L., & Xiong, F. (2021). Using the global hydrodynamic model and GRACE Follow-on data to access the 2020 catastrophic flood in Yangtze river basin. *Remote Sensing, 13*(15), 3023.

Xu, L., Chen, N., Zhang, X., & Chen, Z. (2019). Spatiotemporal changes in China's terrestrial water storage from GRACE satellites and its possible drivers. *Journal of Geophysical Research: Atmospheres, 124*(22), 11976-11993.

Yagbasan, O. (2016). Impacts of climate change on groundwater recharge in Küçük Menderes River Basin in Western Turkey. *Geodinamica Acta*, *28*(3), 209-222.

Yan, S., Liu, J., Gu, X., & Kong, D. (2021). Global runoff signatures changes and their response to atmospheric environment, GRACE water storage and dams. *Remote Sensing*, *13*(20), 4084.

Yang, P., & Chen, Y. (2015). An analysis of terrestrial water storage variations from GRACE and GLDAS: The Tianshan mountains and its adjacent areas, central Asia. *Quaternary International*, *358*, 106-112.

Yang, P., Xia, J., Zhan, C., & Wang, T. (2018). Reconstruction of terrestrial water storage anomalies in Northwest China during 1948–2002 using GRACE and GLDAS products. *Hydrology Research*, *49*(5), 1594-1607.

Yang, P., Xia, J., Zhan, C., Qiao, Y., & Wang, Y. (2017). Monitoring the spatio-temporal changes of terrestrial water storage using GRACE data in the Tarim River basin between 2002 and 2015. *Science of the Total Environment*, *595*, 218-228.

Yang, T., Wang, C., Yu, Z., & Xu, F. (2013). Characterization of spatio-temporal patterns for various GRACE-and GLDAS-born estimates for changes of global terrestrial water storage. *Global and Planetary Change*, *109*, 30-37.

Yazicigil, H., & Ekmekci, M. (2020). Groundwater. In: Harmancioglu N., Altinbilek D. (eds) *Water Resources of Turkey. World Water Resources* (pp. 159-201). Springer, Cham.

Yeh PJ-F, Swenson SC, Famiglietti JS, & Rodell M (2006). Remote sensing of groundwater storage changes in Illinois using the gravity recovery and climate experiment (GRACE). *Water Resources Research 42*, W12203.

Yeh, P. J.-F. and J. Famiglietti (2009). Regional groundwater evapotranspiration in Illinois, J. *Hydrometeorology*, *10*(2), 464-478.

Yi, H. & Wen, L. (2016). Satellite gravity measurement monitoring terrestrial water storage change and drought in the continental United States. *Scientific Reports, 6*(1): 19909.

Yi, H., & Wen, L. (2016). Satellite gravity measurement monitoring terrestrial water storage change and drought in the continental United States. *Scientific Reports, 6*(1), 1-9.

Yilmaz, B., Yurdusev, M. A., & Harmancioglu, N. B. (2009). The assessment of irrigation efficiency in Buyuk Menderes Basin. *Water Resources Management*, *23*(6), 1081-1095.

Yilmaz, K. K., Saber, M., & Yilmaz, M. T. (2016, December 12-16). *Evaluation of GRACE-based groundwater storage change information at Konya Closed Basin, Turkey, using remote sensing and in-situ measurements*. [Conference presentation abstract]. American Geophysical Union Fall Meeting 2016. https://open.metu.edu.tr/handle/11511/77971

Yıldırım, Y.Ö. (2015). *GRACE uydu verileri ile Türkiye'nin uzun dönemli su kütle değişiminin incelenmesi* [Doktora Tezi]. Gebze Teknik University.

Yılmaz, M. T., Bulut, B., Afshar, M., Yücel, İ., Aras, M., Ozaltin, A. M., et al. (2019). *İklim Değişikliğinin Kuzey Ege Havzası Su Potansiyeline Olan Etkisinin Araştırılması*. [Bildiei Özeti] 10. Ulusal Hidroloji Kongresi, Muğla, Türkiye. https://open.metu.edu.tr/handle/11511/79646

Yirdaw, S (2011). *Implications of grace satellite gravity measures for diverse hydrological applications.* [PhD Thesis]. University of Manitoba, Manitoba.

Yirdaw, S.Z., Snelgrove, K.R. and Agboma, C.O. (2008). Grace satellite observations of terrestrial moisture changes for drought characterization in the Canadian prairie. *Journal of Hydrology*. *356,* 84–92.

Yue, S., Pilon, P., & Cavadias, G. (2002). Power of the Mann–Kendall and Spearman's rho tests for detecting monotonic trends in hydrological series. *Journal of Hydrology*, *259*(1-4), 254-271.

Yue, S., & Hashino, M. (2003). Temperature trends in Japan: 1900–1996. *Theoretical and Applied Climatology*, *75*(1), 15-27.

Yunling, H., & Yiping, Z. (2005). Climate change from 1960 to 2000 in the Lancang River Valley, China. *Mountain Research and Development*, *25*(4), 341-348.

Zaitchik, B. F., Rodell, M., & Reichle, R. H. (2008). Assimilation of GRACE terrestrial water storage data into a land surface model: Results for the Mississippi River basin. *Journal of Hydrometeorology*, *9*(3), 535-548.

Zawadzki, J., & Kędzior, M. (2014). Statistical analysis of soil moisture content changes in Central Europe using GLDAS database over three past decades. *Open Geosciences*, *6*(3), 344-353.

Zehe, E., Becker, R., Bárdossy, A., & Plate, E. (2005). Uncertainty of simulated catchment runoff response in the presence of threshold processes: Role of initial soil moisture and precipitation. *Journal of Hydrology*, *315*(1-4), 183-202.

Zhang, G., Su, X., Ayantobo, O. O., & Feng, K. (2021-a). Drought monitoring and evaluation using ESA CCI and GLDAS-Noah soil moisture datasets across China. *Theoretical and Applied Climatology*, *144*(3), 1407-1418.

Zhang, J., Liu, K., & Wang, M. (2021-b). Downscaling groundwater storage data in China to a 1-km resolution using machine learning methods. *Remote Sensing*, *13*(3), 523.

Zhang, L., Dobslaw, H., Stacke, T., Güntner, A., Dill, R., & Thomas, M. (2017). Validation of terrestrial water storage variations as simulated by different global numerical models with GRACE satellite observations. *Hydrology and Earth System Sciences*, *21*(2), 821-837.

Zhang, M., & Burbey, T. J. (2016). Inverse modelling using PS-InSAR data for improved land subsidence simulation in Las Vegas Valley, Nevada. *Hydrological Processes*, *30*(24), 4494-4516.

Zhang, R., Chen, T., & Chi, D. (2020). Global sensitivity analysis of the standardized precipitation evapotranspiration index at different time scales in Jilin province, China. *Sustainability*, *12*(5), 1713.

Zhao, M., Velicogna, I. and Kimball, J.S. (2017). Satellite observations of regional drought severity in the continental United States using GRACE-based terrestrial water storage changes. *Journal of Climate*, *30*(16): 6297-6308.

Zhao, Q., Wu, W., & Wu, Y. (2015). Variations in China's terrestrial water storage over the past decade using GRACE data. *Geodesy and Geodynamics*, *6*(3), 187-193.

Zhao, Q., Zhang, B., Yao, Y., Wu, W., Meng, G., & Chen, Q. (2019). Geodetic and hydrological measurements reveal the recent acceleration of groundwater depletion in North China Plain. *Journal of Hydrology*, *575*, 1065-1072.

Zhao, W., Sánchez, N., Lu, H., & Li, A. (2018). A spatial downscaling approach for the SMAP passive surface soil moisture product using random forest regression. *Journal of Hydrology*, *563*, 1009-1024.

Zhong, Y., Zhong, M., Feng, W., Zhang, Z., Shen, Y., & Wu, D. (2018). Groundwater depletion in the West Liaohe River Basin, China and its implications revealed by GRACE and in situ measurements. *Remote Sensing*, *10*(4), 493.

Zounemat-Kermani, M., Batelaan, O., Fadaee, M., & Hinkelmann, R. (2021). Ensemble machine learning paradigms in hydrology: A review. *Journal of Hydrology*, *598*, 126266.

APPENDIX

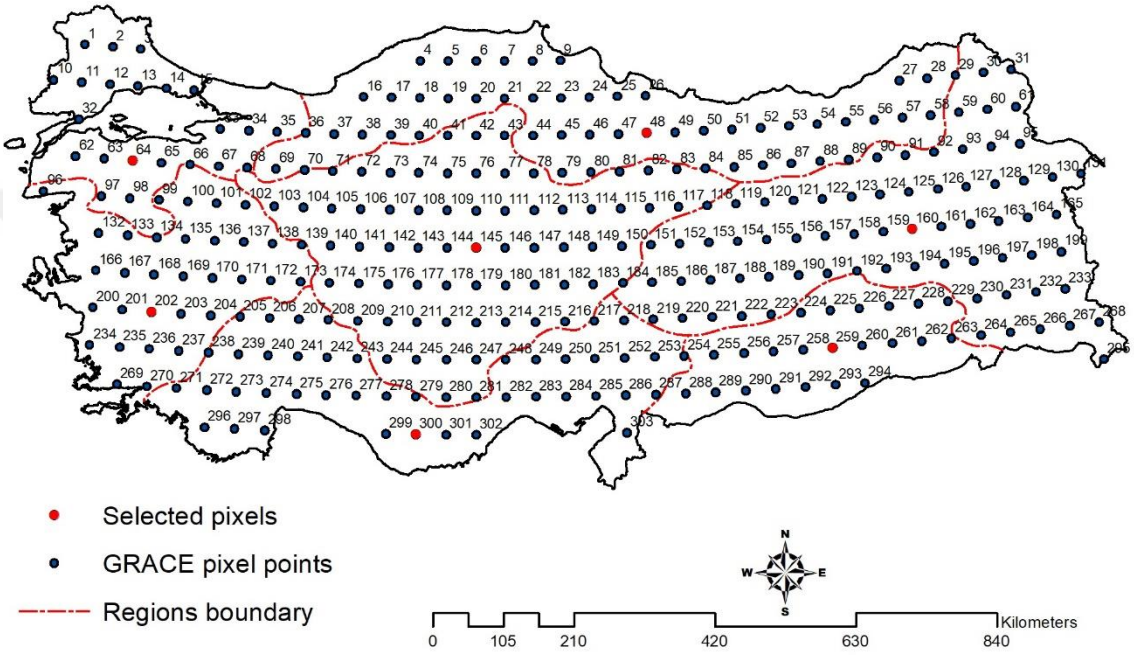


Figure A1. Illustration of the spatial distribution of GRACE pixels over Turkey

Table A.1 The GRACE observed TWS values in cm of equivalent water height

Date	Area mean	Pixel ID						
		48	64	145	160	202	259	300
Jan-03	2.26	-9.43	-0.81	3.15	-4.46	15.20	-2.39	16.94
Feb-03	8.88	-4.77	-1.45	6.50	4.29	27.30	2.30	23.19
Mar-03	14.22	0.98	-1.53	9.52	17.62	28.66	9.45	28.11
Apr-03	15.01	9.30	-1.23	6.67	31.13	22.99	16.70	27.52
May-03	13.00	5.38	-1.21	6.45	25.23	22.66	13.54	24.58
Jun-03	-0.27	-5.82	-0.27	-0.62	0.25	5.09	0.14	13.89
Jul-03	1.76	-5.31	-0.47	0.80	3.14	8.74	1.69	15.78
Aug-03	-2.30	-6.33	-0.08	-2.04	-2.64	1.44	-1.41	11.99
Sep-03	-4.62	-15.82	-0.08	-0.75	-13.36	1.44	-7.17	14.38
Oct-03	-8.18	-13.42	0.32	-4.12	-15.12	-5.97	-8.11	9.98
Nov-03	-2.41	-8.66	-0.08	-0.85	-8.55	1.41	-4.59	10.65
Dec-03	1.23	-6.04	-0.46	0.25	1.22	8.72	0.65	12.82
Jan-04	7.17	-4.13	-0.89	5.50	7.03	16.75	3.77	23.14
Feb-04	16.55	2.78	-1.45	10.01	26.92	27.23	14.45	36.65
Mar-04	18.11	13.19	-1.45	9.09	31.83	27.28	17.08	39.18
Apr-04	16.89	10.51	-1.38	9.73	27.91	25.87	14.98	29.73
May-04	15.23	8.09	-0.98	8.42	26.18	18.38	14.05	26.90
Jun-04	10.66	3.99	-0.80	5.09	19.77	15.09	10.61	21.01
Jul-04	6.79	-1.32	-0.35	4.19	8.95	6.48	4.80	20.09
Aug-04	0.07	-2.75	-0.01	-0.52	-0.65	0.16	-0.35	12.08
Sep-04	-2.97	-8.40	0.23	-0.91	-10.20	-4.34	-5.47	10.09
Oct-04	-7.84	-13.76	0.45	-3.84	-17.53	-8.49	-9.41	3.23
Nov-04	-5.14	-12.43	0.39	-3.21	-8.11	-7.41	-4.35	7.75
Dec-04	0.93	-0.87	0.13	-0.49	3.76	-2.49	2.02	13.39

Table A.1 Continues.

Date	Area mean	Pixel ID						
		48	64	145	160	202	259	300
Jan-05	2.57	0.12	-0.02	0.57	7.23	0.36	3.88	9.48
Feb-05	7.65	-2.81	-0.78	4.24	11.66	14.72	6.26	18.12
Mar-05	12.45	3.30	-0.94	7.47	19.20	17.64	10.30	18.26
Apr-05	15.07	15.61	-0.82	6.53	31.25	15.40	16.77	16.02
May-05	13.29	11.35	-0.77	6.59	23.43	14.50	12.57	11.78
Jun-05	9.75	11.66	-0.43	3.75	19.67	8.02	10.55	7.63
Jul-05	2.16	-0.95	0.02	0.67	3.47	-0.31	1.86	4.15
Aug-05	-2.92	-6.40	0.32	-2.47	-4.31	-5.96	-2.31	-3.70
Sep-05	-5.74	-11.32	0.51	-3.57	-10.88	-9.51	-5.84	-3.71
Oct-05	-6.15	-15.52	0.25	-2.98	-14.51	-4.76	-7.78	-4.79
Nov-05	-4.03	-4.76	0.33	-2.96	-6.27	-6.21	-3.37	-1.05
Dec-05	-3.66	-8.03	0.02	-2.05	-9.04	-0.38	-4.85	2.22
Jan-06	3.99	-0.81	-0.45	2.43	2.52	8.44	1.35	3.29
Feb-06	8.10	0.76	-0.86	4.86	12.82	16.09	6.88	8.55
Mar-06	11.13	3.78	-0.99	6.61	16.05	18.53	8.61	10.92
Apr-06	13.24	11.23	-0.93	5.84	25.22	17.42	13.53	11.56
May-06	11.95	16.63	-0.36	3.30	28.40	6.78	15.24	6.38
Jun-06	5.44	5.31	-0.08	1.59	12.09	1.46	6.49	0.56
Jul-06	0.96	-1.65	0.15	-0.14	2.18	-2.87	1.17	-5.64
Aug-06	-7.32	-7.50	0.63	-4.66	-10.96	-11.85	-5.88	-11.39
Sep-06	-9.45	-10.48	0.77	-4.90	-17.36	-14.39	-9.32	-11.70
Oct-06	-9.77	-16.96	0.31	-3.93	-19.91	-5.82	-10.68	-13.45
Nov-06	-2.04	-5.75	0.02	-0.70	-0.97	-0.38	-0.52	-5.29
Dec-06	-0.57	1.49	-0.04	-0.21	0.79	0.72	0.42	-2.47

Table A.1 Continues.

Date	Area mean	Pixel ID						
		48	64	145	160	202	259	300
Jan-07	-1.87	0.61	0.20	-1.77	1.14	-3.71	0.61	-2.74
Feb-07	1.80	7.32	0.05	0.07	6.91	-0.98	3.71	-1.14
Mar-07	6.90	11.85	-0.19	2.75	17.79	3.54	9.55	-0.73
Apr-07	7.54	19.50	-0.09	0.80	23.69	1.77	12.71	1.84
May-07	4.56	15.42	0.24	-0.48	20.84	-4.51	11.18	-3.24
Jun-07	-0.42	4.73	0.27	-2.38	8.80	-5.05	4.72	-8.74
Jul-07	-5.94	0.56	0.80	-5.27	-1.79	-15.07	-0.96	-10.00
Aug-07	-10.96	-9.00	0.86	-7.01	-13.36	-16.15	-7.17	-13.99
Sep-07	-13.62	-8.12	1.35	-8.11	-19.87	-25.39	-10.66	-13.18
Oct-07	-16.34	-11.64	1.27	-10.09	-22.96	-23.90	-12.32	-21.75
Nov-07	-10.35	-5.43	0.92	-6.83	-12.66	-17.21	-6.79	-15.43
Dec-07	-1.87	3.91	0.17	-2.27	-1.23	-3.10	-0.66	-13.42
Jan-08	-1.95	-4.33	-0.15	-0.15	-7.44	2.90	-3.99	-11.13
Feb-08	2.60	6.23	-0.27	1.46	5.25	5.00	2.82	-8.23
Mar-08	1.49	10.09	0.11	-0.57	10.58	-1.98	5.68	0.67
Apr-08	2.61	8.35	-0.03	0.96	7.44	0.58	3.99	-7.87
May-08	0.09	5.30	0.04	-0.18	1.82	-0.80	0.98	-8.58
Jun-08	-3.85	4.04	0.39	-2.90	-4.45	-7.35	-2.39	-14.64
Jul-08	-9.27	0.33	0.76	-6.06	-13.93	-14.33	-7.48	-22.53
Aug-08	-13.45	-7.89	0.98	-7.24	-22.35	-18.47	-12.00	-23.53
Sep-08	-17.54	-15.59	1.12	-8.19	-32.56	-21.01	-17.47	-25.71
Oct-08	-16.07	-10.85	1.12	-8.49	-28.66	-20.96	-15.38	-24.56
Nov-08	-16.97	-16.22	0.93	-8.23	-30.23	-17.41	-16.22	-24.03
Dec-08	-11.81	-8.72	0.77	-5.05	-23.81	-14.42	-12.77	-16.38

Table A.1 Continues.

Date	Area mean	Pixel ID						
		48	64	145	160	202	259	300
Jan-09	-5.75	-2.16	0.23	-0.90	-15.97	-4.34	-8.57	-5.20
Feb-09	-0.97	-0.60	-0.40	2.33	-10.25	7.50	-5.50	-3.38
Mar-09	6.38	6.46	-0.72	6.88	2.28	13.43	1.22	7.19
Apr-09	9.28	11.64	-0.72	7.52	9.81	13.43	5.26	7.36
May-09	8.49	9.61	-0.71	8.33	4.80	13.34	2.57	10.24
Jun-09	1.78	8.30	-0.17	2.23	-0.36	3.28	-0.19	-0.64
Jul-09	-0.94	2.59	-0.01	1.71	-7.27	0.13	-3.90	0.00
Aug-09	-5.54	-3.65	0.13	-0.65	-17.56	-2.35	-9.42	-6.31
Sep-09	-9.88	-9.65	0.30	-3.04	-25.84	-5.68	-13.86	-8.90
Oct-09	-12.66	-11.09	0.48	-5.00	-28.77	-9.00	-15.44	-8.69
Nov-09	-6.48	1.28	0.25	-3.51	-11.82	-4.68	-6.35	-9.19
Dec-09	-1.56	3.65	-0.04	0.39	-5.64	0.82	-3.03	-2.37
Jan-10	6.60	6.11	-0.64	4.91	7.73	11.97	4.15	3.06
Feb-10	10.64	7.79	-1.15	7.77	13.53	21.55	7.26	6.27
Mar-10	14.10	15.20	-1.31	8.56	20.30	24.65	10.89	3.78
Apr-10	13.81	19.20	-0.93	7.61	21.49	17.47	11.53	12.50
May-10	11.15	18.01	-0.53	5.21	23.23	9.87	12.47	10.65
Jun-10	6.19	11.68	-0.25	2.50	12.52	4.62	6.72	3.73
Jul-10	0.73	0.17	-0.03	0.66	-1.38	0.51	-0.74	-0.49
Aug-10	-6.34	-11.03	0.18	-2.50	-14.76	-3.45	-7.92	-7.76
Sep-10	-10.49	-8.77	0.51	-6.17	-16.47	-9.63	-8.84	-10.33
Oct-10	-8.71	-10.97	0.35	-3.30	-19.83	-6.63	-10.64	-4.18
Nov-10	-6.55	-0.50	0.28	-3.27	-12.79	-5.30	-6.86	3.55
Dec-10	-3.30	-1.76	-0.10	-0.71	-11.85	1.91	-6.36	1.55

Table A.1 Continues.

Date	Area mean	Pixel ID						
		48	64	145	160	202	259	300
Jan-11	0.91	1.49	-0.33	2.21	-6.36	6.17	-3.41	9.63
Feb-11	5.11	4.74	-0.56	5.12	-0.86	10.43	-0.46	17.70
Mar-11	10.87	4.63	-1.01	9.53	6.41	18.90	3.44	26.42
Apr-11	12.16	7.52	-0.88	9.72	13.12	16.53	7.04	32.91
May-11	13.27	12.96	-1.03	7.55	24.39	19.37	13.09	26.80
Jun-11	8.13	8.71	-0.59	5.24	12.79	10.99	6.87	21.98
Jul-11	2.99	4.47	-0.14	2.93	1.20	2.60	0.64	17.17
Aug-11	-2.32	-2.36	0.27	0.59	-9.54	-5.15	-5.12	15.76
Sep-11	-8.46	-8.16	0.49	-3.71	-16.72	-9.26	-8.97	9.93
Oct-11	-8.26	-8.36	0.20	-4.01	-18.03	-3.68	-9.68	13.66
Nov-11	-6.76	-7.17	0.06	-2.96	-17.56	-1.11	-9.42	13.89
Dec-11	-3.82	-4.72	-0.18	-0.83	-12.86	3.32	-6.90	21.46
Jan-12	-0.88	-2.27	-0.41	1.30	-8.16	7.75	-4.38	29.02
Feb-12	8.69	5.58	-1.08	6.11	6.41	20.29	3.44	40.55
Mar-12	15.33	13.74	-1.50	9.16	22.32	28.07	11.98	38.28
Apr-12	14.05	15.73	-1.24	8.66	21.02	23.18	11.28	43.88
May-12	10.93	8.52	-1.14	7.67	12.11	21.36	6.50	41.57
Jun-12	7.80	1.30	-1.04	6.69	3.21	19.54	1.72	39.27
Jul-12	1.34	2.26	-0.42	2.42	-6.95	7.92	-3.73	27.30
Aug-12	-5.51	-7.92	-0.04	-0.61	-18.24	0.81	-9.79	22.13
Sep-12	-10.31	-11.84	0.23	-4.03	-24.55	-4.23	-13.17	13.90
Oct-12	-8.61	-7.43	0.33	-2.97	-21.57	-6.27	-11.58	15.32
Nov-12	-6.90	-3.03	0.44	-1.92	-18.60	-8.31	-9.98	16.74
Dec-12	-1.81	-4.09	-0.52	0.44	-6.03	9.76	-3.24	12.87

Table A.1 Continues.

Date	Area mean	Pixel ID						
		48	64	145	160	202	259	300
Jan-13	5.96	0.98	-0.92	5.60	7.69	17.26	4.13	25.34
Feb-13	9.33	0.03	-1.08	8.08	10.21	20.26	5.48	24.38
Mar-13	13.01	5.33	-1.23	10.00	16.17	23.05	8.68	26.54
Apr-13	16.69	10.63	-1.38	11.92	22.13	25.83	11.87	28.70
May-13	10.72	8.74	-0.89	7.53	16.15	16.76	8.66	21.71
Jun-13	6.77	2.74	-0.61	5.91	6.76	11.50	3.63	14.01
Jul-13	0.01	-2.40	-0.02	1.03	-1.08	0.33	-0.58	6.65
Aug-13	-4.48	-4.09	0.29	-1.26	-10.06	-5.49	-5.40	1.60
Sep-13	-6.72	-4.93	0.45	-2.41	-14.55	-8.40	-7.81	-0.92
Oct-13	-8.96	-5.78	0.60	-3.56	-19.04	-11.30	-10.22	-3.44
Nov-13	-10.21	-5.80	0.58	-3.65	-23.03	-10.82	-12.36	-6.65
Dec-13	-7.76	-5.76	0.24	-2.63	-19.86	-4.59	-10.66	-4.49
Jan-14	-7.80	-6.49	0.19	-2.82	-17.67	-3.47	-9.48	-5.58
Feb-14	-4.70	-4.49	-0.08	-1.04	-12.98	1.58	-6.97	0.87
Mar-14	-1.60	-2.49	-0.35	0.74	-8.29	6.63	-4.45	7.33
Apr-14	-3.14	-3.11	-0.17	0.01	-8.66	3.14	-4.65	1.89
May-14	-2.49	3.01	-0.25	-0.31	-9.58	4.68	-5.14	-0.62
Jun-14	-3.67	-0.09	-0.22	-0.70	-11.21	4.11	-6.02	-7.77
Jul-14	-8.45	-4.68	0.11	-3.58	-19.82	-2.06	-10.63	-13.42
Aug-14	-13.22	-9.28	0.44	-6.46	-28.42	-8.22	-15.25	-19.07
Sep-14	-16.71	-13.84	0.56	-7.58	-36.06	-10.60	-19.35	-20.40
Oct-14	-15.13	-13.81	0.49	-7.04	-31.21	-9.13	-16.74	-16.52
Nov-14	-11.64	-10.94	0.15	-4.99	-25.39	-2.77	-13.62	-13.07
Dec-14	-5.29	-10.02	-0.37	0.08	-17.15	7.02	-9.21	-0.35

Table A.1 Continues.

Date	Area mean	Pixel ID						
		48	64	145	160	202	259	300
Jan-15	1.06	-9.09	-0.89	5.16	-8.92	16.80	-4.79	12.37
Feb-15	4.02	-3.14	-1.13	4.97	-0.78	21.20	-0.42	6.19
Mar-15	8.59	1.43	-1.31	5.83	10.90	24.55	5.85	23.43
Apr-15	11.11	2.84	-1.36	8.20	18.87	25.52	10.12	21.25
May-15	6.32	1.03	-0.97	6.44	5.81	18.21	3.12	10.36
Jun-15	3.92	0.13	-0.78	5.56	-0.71	14.56	-0.38	4.92
Jul-15	1.52	-0.78	-0.58	4.68	-7.24	10.91	-3.88	-0.53
Aug-15	-4.47	-9.67	-0.26	1.03	-14.43	4.82	-7.74	-1.68
Sep-15	-9.55	-9.65	-0.04	-3.08	-20.96	0.79	-11.24	-5.83
Oct-15	-8.69	-8.83	-0.09	-3.12	-18.40	1.67	-9.87	-13.47
Nov-15	-8.26	-8.42	-0.11	-3.14	-17.12	2.11	-9.19	-17.29
Dec-15	-7.83	-8.01	-0.14	-3.16	-15.84	2.55	-8.50	-21.12
Jan-16	-3.03	0.40	-0.37	-3.46	8.80	6.86	4.72	-15.14
Feb-16	2.91	-3.92	-0.79	3.57	4.92	14.87	2.64	-1.84
Mar-16	7.04	4.78	-1.06	4.99	14.02	19.92	7.52	-5.89
Apr-16	6.22	6.67	-0.77	4.81	11.37	14.48	6.10	-6.99
May-16	5.40	8.56	-0.48	4.63	8.71	9.04	4.67	-8.09
Jun-16	3.46	12.14	-0.25	2.06	6.83	4.75	3.67	-16.89
Jul-16	-0.71	5.92	0.14	0.68	-3.08	-2.58	-1.65	-20.06
Aug-16	-9.22	-4.62	0.47	-3.56	-18.47	-8.82	-9.91	-24.65
Sep-16	-10.29	-4.53	0.65	-4.48	-19.62	-12.11	-10.53	-25.01
Oct-16	-10.82	-4.48	0.73	-4.95	-20.19	-13.76	-10.83	-25.19
Nov-16	-11.35	-4.43	0.82	-5.41	-20.77	-15.41	-11.14	-25.37
Dec-16	-8.11	3.34	0.67	-5.86	-7.48	-12.59	-4.01	-24.88

Table A.1 Continues.

Date	Area mean	Pixel ID						
		48	64	145	160	202	259	300
Jan-17	-4.03	-0.45	-0.08	-1.32	-6.48	1.58	-3.48	-12.79
Feb-17	-1.41	1.43	-0.11	0.57	-1.83	2.00	-0.98	-9.05
Mar-17	1.21	3.32	-0.13	2.47	2.83	2.42	1.52	-5.32
Apr-17	0.46	0.90	-0.25	2.01	0.13	4.65	0.07	-5.94
May-17	0.45	4.85	-0.06	1.41	1.53	1.07	0.82	-9.51
Jun-17	0.15	5.15	-0.16	1.85	-2.48	3.00	-1.33	-10.99
Jul-17	-	-	-	-	-	-	-	-
Aug-17	-	-	-	-	-	-	-	-
Sep-17	-	-	-	-	-	-	-	-
Oct-17	-	-	-	-	-	-	-	-
Nov-17	-	-	-	-	-	-	-	-
Dec-17	-	-	-	-	-	-	-	-
Jan-18	-	-	-	-	-	-	-	-
Feb-18	-	-	-	-	-	-	-	-
Mar-18	-	-	-	-	-	-	-	-
Apr-18	-	-	-	-	-	-	-	-
May-18	-	-	-	-	-	-	-	-
Jun-18	-2.68	0.07	0.13	0.11	-6.85	-2.47	-3.67	-17.06
Jul-18	-7.93	-5.27	0.51	-2.11	-19.69	-9.59	-10.57	-19.39
Aug-18	-13.06	-13.66	0.72	-3.55	-30.48	-13.46	-16.36	-18.89
Sep-18	-15.62	-17.85	0.82	-4.27	-35.87	-15.39	-19.25	-18.64
Oct-18	-18.19	-22.04	0.92	-4.99	-41.27	-17.33	-22.14	-18.39
Nov-18	-17.30	-19.76	0.87	-6.53	-32.79	-16.33	-17.59	-21.34
Dec-18	-8.58	-8.59	0.45	-3.04	-13.07	-8.44	-7.01	-15.80

Table A.1 Continues.

Date	Area mean	Pixel ID						
		48	64	145	160	202	259	300
Jan-19	0.24	-7.75	-0.60	3.30	0.97	11.18	0.52	-5.57
Feb-19	5.12	-3.61	-0.93	6.93	4.03	17.51	2.16	-0.15
Mar-19	7.24	-3.61	-0.69	8.07	9.51	12.90	5.10	3.93
Apr-19	10.54	6.86	-0.60	6.26	27.43	11.25	14.72	-2.19
May-19	8.65	5.24	-0.30	6.64	19.62	5.60	10.53	-0.27
Jun-19	2.05	0.46	0.25	1.91	9.25	-4.77	4.96	-5.14
Jul-19	-2.99	-5.03	0.47	0.64	-3.85	-8.75	-2.07	-9.39
Aug-19	-7.68	-8.18	0.86	-2.30	-11.51	-16.06	-6.18	-14.77
Sep-19	-13.56	-19.35	0.92	-4.75	-24.92	-17.30	-13.37	-17.73
Oct-19	-17.20	-21.39	1.09	-8.67	-23.93	-20.39	-12.84	-19.02
Nov-19	-17.44	-17.94	1.06	-9.01	-25.27	-19.90	-13.56	-22.62
Dec-19	-12.57	-13.81	0.88	-6.15	-16.90	-16.52	-9.07	-18.38
Jan-20	-5.81	-14.13	0.17	-0.64	-10.62	-3.28	-5.70	-4.54
Feb-20	0.27	-11.00	-0.12	4.13	0.21	2.20	0.11	4.93
Mar-20	3.23	-7.96	-0.02	4.34	9.92	0.31	5.32	4.26
Apr-20	6.47	1.36	-0.17	4.16	20.48	3.18	10.99	3.02
May-20	3.92	4.59	0.32	1.27	22.17	-5.96	11.90	-2.02
Jun-20	-1.54	1.01	0.55	-1.83	11.03	-10.30	5.92	-10.32
Jul-20	-5.39	-5.82	0.70	-4.12	2.40	-13.21	1.29	-19.91
Aug-20	-11.41	-14.04	0.97	-6.47	-11.63	-18.21	-6.24	-20.17
Sep-20	-15.45	-16.49	1.42	-7.99	-20.85	-26.58	-11.19	-18.55
Oct-20	-19.70	-27.83	1.48	-9.11	-29.55	-27.85	-15.86	-18.09
Nov-20	-18.72	-19.22	1.44	-10.53	-26.01	-27.00	-13.96	-25.70
Dec-20	-19.18	-17.85	1.47	-11.40	-23.41	-27.58	-12.56	-20.43

Table A.2 Basic statistics of the area-mean GRACE observed TWS in cm of equivalent water height.

Stats	**TWS**
Mean	-0.94
Max	18.11
Min	-19.70
StD	8.99
Percentile 80th	7.56
Percentile 90th	11.14
Percentile 95th	14.00
Percentile 99th	16.68

Table A.3 List of the Main Meteorological Stations of Turkey used in the Study

ID	X	Y	Station Name	District	Geographic Region	Z (m)
17352	35.298	36.984	Adana Airport	Adana	MED	20
17265	38.278	37.755	Adıyaman	Adıyaman	SEA	672
17190	30.560	38.738	Afyonkarahisar	Afyonkarahisar	AEG	1034
17099	43.052	39.725	Ağrı	Ağrı	EAR	1646
17192	33.999	38.371	Aksaray	Aksaray	CAR	970
17085	35.835	40.667	Amasya	Amasya	BSR	409
17130	32.864	39.973	Ankara	Ankara	CAR	891
17300	30.799	36.906	Antalya Airport	Antalya	MED	64
17046	42.705	41.106	Ardahan	Ardahan	EAR	1827
17045	41.819	41.175	Artvin	Artvin	BSR	613
17234	27.838	37.840	Aydın	Aydın	AEG	56
17150	27.920	39.633	Balıkesir Airport	Balıkesir	MAR	102
17020	32.357	41.625	Bartın	Bartın	BSR	33
17282	41.156	37.864	Batman	Batman	SEA	610
17089	40.221	40.255	Bayburt	Bayburt	BSR	1584
17120	29.977	40.141	Bilecik	Bilecik	MAR	539
17203	40.501	38.885	Bingöl	Bingöl	EAR	1139
17207	42.100	38.366	Bitlis	Bitlis	EAR	1573
17070	31.602	40.733	Bolu	Bolu	BSR	743
17238	30.294	37.722	Burdur	Burdur	MED	957
17116	29.013	40.231	Bursa	Bursa	MAR	100
17112	26.399	40.141	Çanakkale	Çanakkale	MAR	6
17080	33.610	40.608	Çankırı	Çankırı	CAR	755
17084	34.936	40.546	Çorum	Çorum	BSR	776
17237	29.092	37.762	Denizli	Denizli	AEG	425
17280	40.203	37.897	Diyarbakır Airport	Diyarbakır	SEA	674
17072	31.149	40.844	Düzce	Düzce	BSR	146
17050	26.551	41.677	Edirne	Edirne	MAR	51
17201	39.256	38.644	Elazığ	Elazığ	EAR	989

Table A.3 Continues.

ID	X	Y	Station Name	District	Geographic Region	Z (m)
17094	39.487	39.752	Erzincan	Erzincan	EAR	1216
17096	41.190	39.953	Erzurum Airport	Erzurum	EAR	1758
17124	30.580	39.781	Eskişehir Airport	Eskişehir	CAR	786
17261	37.351	37.059	Gaziantep	Gaziantep	SEA	854
17034	38.388	40.923	Giresun	Giresun	BSR	38
17088	39.465	40.460	Gümüşhane	Gümüşhane	BSR	1216
17285	43.739	37.575	Hakkari	Hakkari	EAR	1727
17372	36.205	36.151	Antakya	Hatay	MED	104
17100	44.052	39.923	Iğdır	ığdır	EAR	856
17240	30.568	37.785	Isparta	ısparta	MED	997
17638	29.160	40.910	Kartal	İstanbul	MAR	27
17220	27.082	38.395	Izmir	İzmir	AEG	29
17255	36.915	37.576	Kahramanmaras	Kahramanmaraş	MED	572
17077	32.629	41.233	Karabük kapullu	Karabük	BSR	485
17246	33.220	37.193	Karaman	Karaman	CAR	1018
17097	43.107	40.604	Kars	Kars	EAR	1777
17074	33.776	41.371	Kastamonu	Kastamonu	BSR	800
17196	35.500	38.687	Kayseri	Kayseri	CAR	1094
17135	33.518	39.843	Kırıkkale	Kırıkkale	CAR	751
17052	27.218	41.738	Kırklareli	Kırklareli	MAR	232
17160	34.156	39.164	Kırşehir	Kırşehir	CAR	1007
17262	37.112	36.709	Kilis	Kilis	SEA	640
17066	29.917	40.766	Kocaeli	Kocaeli	MAR	74
17244	32.574	37.984	Konya Airport	Konya	CAR	1031
17155	29.989	39.417	Kütahya	Kütahya	AEG	969
17199	38.217	38.337	Malatya	Malatya	EAR	950
17186	27.405	38.615	Manisa	Manisa	AEG	71
17275	40.728	37.310	Mardin	Mardin	SEA	1040
17340	34.603	36.781	Mersin	Mersin	MED	7
17292	28.367	37.210	Muğla	Muğla	AEG	646
17204	41.502	38.751	Muş	Muş	EAR	1322
17193	34.703	38.616	Nevşehir	Nevşehir	CAR	1260
17250	34.680	37.959	Niğde	Niğde	CAR	1211

Table A.3 Continues.

ID	X	Y	Station Name	District	Geographic Region	Z (m)
17033	37.886	40.984	Ordu	Ordu	BSR	5
17355	36.254	37.102	Osmaniye	Osmaniye	MED	94
17040	40.501	41.040	Rize	Rize	BSR	3
17069	30.393	40.768	Sakarya	Sakarya	MAR	30
17030	36.256	41.344	Samsun	Samsun	BSR	4
17210	41.935	37.932	Siirt	Siirt	SEA	895
17026	35.155	42.030	Sinop	Sinop	BSR	32
17090	37.002	39.744	Sivas	Sivas	CAR	1294
17270	38.786	37.161	Şanlıurfa	Şanlıurfa	SEA	550
17287	42.452	37.521	Şırnak	Şırnak	EAR	1350
17056	27.497	40.959	Tekirdağ	Tekirdağ	MAR	4
17086	36.558	40.331	Tokat	Tokat	BSR	611
17037	39.765	40.998	Trabzon	Trabzon	BSR	25
17165	39.541	39.106	Tunceli	Tunceli	EAR	981
17188	29.404	38.671	Uşak	Uşak	AEG	919
17172	43.346	38.469	Van bölge	Van	EAR	1675
17119	29.280	40.659	Yalova	Yalova	MAR	4
17140	34.816	39.824	Yozgat	Yozgat	CAR	1301
17022	31.778	41.449	Zonguldak	Zonguldak	BSR	135